Advances in Stochastic Geometry for Cellular Networks

by

Chiranjib Saha

Dissertation submitted to the Faculty of the
Virginia Polytechnic Institute and State University
in partial fulfillment of the requirements for the degree of

Doctor of Philosophy
in
Electrical Engineering

Harpreet S. Dhillon, Chair
R. Michael Buehrer
Walid Saad
Vassilis Kekatos
Shyam Ranganathan

July 27, 2020
Blacksburg, Virginia

Keywords: Stochastic geometry, Poisson cluster process (PCP), Poisson point process (PPP), coverage probability, Integrated access and backhaul (IAB), determinantal point process (DPP).

Advances in Stochastic Geometry for Cellular Networks

Chiranjib Saha

ABSTRACT

The mathematical modeling and performance analysis of cellular networks have seen a major paradigm shift with the application of stochastic geometry. The main purpose of stochastic geometry is to endow probability distributions on the locations of the base stations (BSs) and users in a network, which, in turn, provides an analytical handle on the performance evaluation of cellular networks. To preserve the tractability of analysis, the common practice is to assume *complete spatial randomness* of the network topology. In other words, the locations of users and BSs are modeled as independent homogeneous Poisson point processes (PPPs). Despite its usefulness, the PPP-based network models fail to capture any spatial coupling between the users and BSs which is dominant in a multi-tier cellular network (also known as the heterogeneous cellular networks (HetNets)) consisting of macro and small cells. For instance, the users tend to form *hotspots* or clusters at certain locations and the small cell BSs (SBSs) are deployed at higher densities at these locations of the hotspots in order to cater to the high data demand. Such user-centric deployments naturally couple the locations of the users and SBSs. On the other hand, these spatial couplings are at the heart of the spatial models used in industry for the system-level simulations and standardization purposes. This dissertation proposes fundamentally new spatial models based on stochastic geometry which closely emulate these spatial couplings and are conductive for a more realistic and fine-tuned performance analysis, optimization, and design of cellular networks.

The first contribution of this dissertation is a new class of spatial models for HetNets where the locations of the BSs and users are assumed to be distributed as Poisson cluster process (PCP). From the modeling perspective, the proposed models can capture different spatial couplings in a network topology such as the user hotspots and user BS coupling occurring due to the user-centric deployment of the SBSs. The PCP-based model is a generalization of the state-of-the-art PPP-based HetNet model. This is because the model reduces to the PPP-based model once all spatial couplings in the network are ignored. From the stochastic geometry perspective, we have made contributions in deriving the fundamental distributional properties of PCP, such as the distance distributions and sum-product functionals, which are instrumental for the performance characterization of the HetNets, such as coverage and rate.

The focus on more refined spatial models for small cells and users brings to the second direction of the dissertation, which is modeling and analysis of HetNets with millimeter wave (mm-wave) integrated access and backhaul (IAB), an emerging design concept of the fifth generation (5G) cellular networks. While the concepts of network densification with small cells have emerged in the fourth generation (4G) era, the small cells can be realistically deployed with IAB since it avoids the need for providing high capacity wired backhaul to each SBS by replacing the *last-mile fibers* with mm-wave links. We have proposed new stochastic geometry-based models for the performance analysis of IAB-enabled HetNets. Our

analysis reveals some interesting system-design insights: (1) the IAB HetNets can support a maximum number of users beyond which the data rate drops below the rate of a single-tier macro-only network, and (2) there exists a saturation point of SBS density beyond which no rate gain is observed with the addition of more SBSs.

The third and final direction of this dissertation is the combination of machine learning and stochastic geometry to construct a new class of *data driven* network models which can be used in the performance optimization and design of a network. As a concrete example, we investigate the classical problem of wireless link scheduling where the objective is to choose an optimal subset of simultaneously active transmitters (Tx-s) from a ground set of Tx-s which will maximize the network-wide sum-rate. Since the optimization problem is NP-hard, we replace the computationally expensive heuristic by inferring the point patterns of the active Tx-s in the optimal subset after training a determinantal point process (DPP). Our investigations demonstrate that the DPP is able to learn the spatial interactions of the Tx-s in the optimal subset and gives a reasonably accurate estimate of the optimal subset for any new ground set of Tx-s.

Advances in Stochastic Geometry for Cellular Networks

Chiranjib Saha

GENERAL AUDIENCE ABSTRACT

The high speed global cellular communication network is one of the most important technologies, and it continues to evolve rapidly with every new generation. This evolution greatly depends on observing performance-trends of the emerging technologies on the network models through extensive system-level simulations. Since these simulation models are extremely time-consuming and error prone, the complementary analytical models of cellular networks have been an area of active research for a long time. These analytical models are intended to provide crisp insights on the network behavior such as the dependence of network performance metrics (such as coverage or rate) on key system-level parameters (such as transmission powers, base station (BS) density) which serve as the *prior* knowledge for more *fine-tuned* simulations. Over the last decade, the analytical modeling of the cellular networks has been driven by *stochastic geometry*. The main purpose of stochastic geometry is to endow the locations of the base stations (BSs) and users with probability distributions and then leverage the properties of these distributions to average out the spatial randomness. This process of spatial averaging allows us to derive the analytical expressions of the system-level performance metrics despite the presence of a large number of random variables (such as BS and user locations, channel gains) under some reasonable assumptions.

The simplest stochastic geometry based model of cellular networks, which is also the most tractable, is the so-called Poisson point process (PPP) based network model. In this model, users and BSs are assumed to be distributed as independent homogeneous PPPs. This is equivalent to saying that the users and BSs independently and uniformly *at random* over a plane. The PPP-based model turned out to be a reasonably accurate representation of the yesteryear's cellular networks which consisted of a single tier of macro BSs (MBSs) intended to provide a uniform coverage blanket over the region. However, as the data-hungry devices like smart-phones, tablets, and application like online gaming continue to flood the consumer market, the network configuration is rapidly deviating from this *baseline* setup with different spatial interactions between BSs and users (also termed *spatial coupling*) becoming dominant. For instance, the user locations are far from being homogeneous as they are concentrated in specific areas like residential and commercial zones (also known as *hotspots*). Further, the network, previously consisting of a single tier of macro BSs (MBSs), is becoming increasingly *heterogeneous* with the deployment of small cell BSs (SBSs) with small coverage footprints and targeted to serve the user hotspots. It is not difficult to see that the network topology with these spatial couplings is quite far from complete spatial randomness which is the basis of the PPP-based models. The key contribution of this dissertation is to enrich the stochastic geometry-based mathematical models so that they can capture the fine-grained spatial couplings between the BSs and users. More specifically, this dissertation contributes in the following three research directions.

Direction-I: Modeling Spatial Clustering. We model the locations of users and SBSs forming hotspots as *Poisson cluster processes* (PCPs). A PCP is a collection of *o spring* points which are located around the *parent* points which belong to a PPP. The coupling between the locations of users and SBSs (due to their *user-centric* deployment) can be introduced by assuming that the user and SBS PCPs share the same parent PPP. The key contribution in this direction is the construction of a general HetNet model with a *mixture* of PPP and PCP-distributed BSs and user distributions. Note that the baseline PPP-based HetNet model appears as one of the many configurations supported by this general model. For this general model, we derive the analytical expressions of the performance metrics like coverage probability, BS load, and rate as functions of the coupling parameters (e.g. BS and user cluster size).

Direction-II: Modeling Coupling in Wireless Backhaul Networks. While the deployment of SBSs clearly enhances the network performance in terms of coverage, one might wonder: *how long network densification with tens of thousands of SBSs can meet the ever-increasing data demand?* It turns out that in the current network setting, where the backhaul links (i.e. the links between the BSs and core network) are still wired, it is not feasible to densify the network beyond some limit. This *backhaul bottleneck* can be overcome if the backhaul links also become wireless and the backhaul and access links (link between user and BS) are jointly managed by an *integrated access and backhaul* (IAB) network. In this direction, we develop the analytical models of IAB-enabled HetNets where the key challenge is to tackle new types of couplings which exist between the rates on the wireless access and backhaul links. Such couplings exist due to the spatial correlation of the signal qualities of the two links and the number of users served by different BSs. Two fundamental insights obtained from this work are as follows: (1) the IAB HetNets can support a maximum number of users beyond which the network performance drops below that of a single-tier macro-only network, and (2) there exists a saturation point of SBS density beyond which no performance gain is observed with the addition of more SBSs.

Direction-III: Modeling Repulsion. In this direction, we focus on modeling another aspect of spatial coupling imposed by the intra-point repulsion. Consider a device-to-device (D2D) communication scenario, where some users are transmitting some on-demand content locally cached in their devices using a common channel. Any reasonable multiple access scheme will ensure that two nearly users are never simultaneously active as they will cause severe mutual interference and thereby reducing the *network-wide* sum rate. Thus the active users in the network will have some spatial repulsion. The locations of these users can be modeled as determinantal point processes (DPPs). The key property of DPP is that it forms a bridge between stochastic geometry and *machine learning*, two otherwise non-overlapping paradigms for wireless network modeling and design. The main focus in this direction is to explore the learning framework of DPP and bring together advantages of stochastic geometry and machine learning to construct a new class of *data-driven analytical* network models.

To my parents and the city of my heart which was once called 'Calcutta'.

Acknowledgments

I would like to begin with acknowledging some very special people who are the integral parts of my journey this far. Here it goes.

Thank you Dr. Dhillon[1]. I cannot express in words how fortunate I am to have an advisor like you. The last five years in Virginia Tech have really been a roller-coster ride. Thank you for introducing me to this wonderful field called stochastic geometry and providing me the necessary guidance to explore this intricate field beyond the application to cellular networks. Our conversations in countless in-person and over-the-phone meetings have always helped me to find a clear path out of any stagnation. You have profoundly influenced my ideas and shaped the way I approach research. Thank you for believing in me from the first day when I joined in the PhD program right after completing my undergrad. I never would have imagined that the small problem of modeling user hotspots in a network will evolve to become a full-fledged book[2] in these five years. Thank you for the hand-holdings I desperately needed in the earlier days of my PhD and the utmost freedom of working on multiple problems of my interest during the later years. Your style of advising will be a role model for me during the professional life that awaits for me after my graduation.

Thank you Mehrnaz[3] for being the best mentor. I will always cherish our endless discussions in Durham 470 and your office those went way beyond the particulars of our research problems. I wish I had penned down excerpts of our conversations on the differences and similarities between Indian and Persian cultures. Had you stayed longer, I would have learned a bit of Farsi and you have become fluent in Bengali.

I am indebted to the wonderful professors in Virginia Tech. I sincerely thank Prof. Mike Buehrer for the amazing courses on digital communication and MIMO. I am grateful to Prof. Scotland Leeman for teaching the course of Bayesian statistics in the most interesting way. I am also thankful to Prof. Allen MacKenzie for his lectures on stochastic signals and information theory. These courses have been very helpful in building my background during the formative years in grad school. I would also like to thank my professors at Jadavpur University (JU), India, where I completed my bachelors in engineering. I couldn't have thanked enough Joydip-Da[4] for introducing me to the field of mathematical analysis during my undergrad days.

My colleagues at Wireless@VT have enriched my graduate life in many ways and deserve a special mention. My interactions with Priyabrata[5] and Vishnu[6] have been very fruitful. Thank you Praful[7] for illuminating me with your deep insights on stochastic geometry. I wish we had started collaborating earlier. I am very fortunate to have shared the lab space with

[1] Dr. Harpreet S. Dhillon [2] Dhillon et al. *Poisson cluster process: Theory and Application to Wireless Networks*, under preparation, Cambridge University Press, 2021. [3] Dr. Mehrnaz Afshang [4] Dr. Joydip Saha [5] Priyabrata Parida [6] Dr. Vishnu Vardhan Chetlur [7] Dr. Praful Mankar

some wonderful people: Morteza Banagar, Mohamed A. Abd-Elmagid, Anish Pradhan, Dr. Mustafa Kishk, Dr. Raghunandan M. Rao, and J. Kartheek Devineni. A special mention to Keerthana[8] who has been working with me from last year on a very challenging problem of topological manifolds. I sincerely wish her a productive career ahead.

It would be an injustice not to acknowledge the assistance I received from Hilda and Nancy from the office of Wireless@VT. They diligently kept the administrative process running so that I never had to worry about my pay-cheques and paper-works.

I sincerely acknowledge Aditya[9] and Boon[10] for providing me an intriguing problem during my internship in Samsung research America in the summer of 2019. Also, Raghu, thanks for being the most amazing teammate during the internship. It has been a great pleasure working with you. Thank you Dr. Amitabha Ghosh for hosting me as an intern in Nokia Bell labs in the summer of 2018.

Well, now it is time to thank all my friends and family in Blacksburg, College Park and Calcutta. It is going to be a long list and I sincerely hope I don't miss out any names. Shantanab-da[11], a big thanks for informing me about Wireless@VT while I was applying for the grad school. Also, thank you for being there as a responsible senior and taking the time for teaching me the essential skills such as driving and cooking. Nath-da[12], our conversations in the hallways of Norris Hall and the premises of Chasewood Downs did help me to be inquisitive about everything which is the most fundamental attribute of a researcher. I believe you will be renowned for your works on fluid mechanics and I will be proud to be a part of your tenure at Virginia Tech. Thank you Ranit-da[13], Shuchishmita[14], Arit[15], Paul[16], Sreeya-di[17], and Anindya[18] for being the most amazing roommates. I will miss our weekend hangouts, movie nights, and holiday trips. Thank you Abhijit-Da[19], Shreya-Di[20], Gupta-Da[21], Poorna-Di[22], Srijan-Da[23], and Swarnali-Di[24] for being the elders of my extended family in Blacksburg. Niharika, you have been the center of all the happiness since the day you were born. The Blacksburg chapter of my life will be incomplete without mentioning Esha Dwibedi, Lekha Chowdhuri, Debasmita Biswas, Harsh Sharma, Aniket Jana, and Abinash Padhi. Thank you.

Debdipta[25], I am very fortunate to have you as the best friend, philosopher, and guide. I have always thought your place at College Park as my second home in United States. I wish you will shine as an academician at Princeton University. And yes, we will accomplish our long due plan of the cross country road trip. Speaking of College Park, I must mention the names of two wonderful people: Prithviraj[26] and Soumojit[27]. I wish good luck for your careers ahead.

Thank you Ma (Mum)[28] and Baba (Dad)[29] for your unwavering support throughout

[8] Keerthana Bhogi [9] Dr. Aditya Padaki [10] Dr. Boon Loong Ng [11] Dr. Shantanab Debchoudhury [12] Saurabh Nath [13] Ranit Mukherjee [14] Shuchismita Biswas [15] Arit Das [16] Arnab Paul [17] Sreeya Brahma [18] Sheikh Shadab Towqir [19] Dr. Abhijit Sarkar [20] Dr. Shreya Mitra [21] Dr. Arnab Gupta [22] Poorna Goswami [23] Dr. Srijan Sengupta [24] Dr. Swarnali Sanyal [25] Dr. Debdipta Goswami [26] Prithviraj Dhar [27] Soumojit Das [28] Krishna Saha [29] Chitta Ranjan Saha

the long road until this day and days to come. I am here only because of you. Any word of thanks or gratitude will fall short for you two being my supportive pillars during my highs and lows, and trusting me with my decisions and accepting my successes and failures wholeheartedly. Your visit to Blacksburg is perhaps the most happiest moment during my grad school. I wish you were here beside me during this special moment of graduation. Thank you Mani[30], Mehson[31], and Suvrajit[32] and the other wonderful members of my family for making this journey possible. A person is incomplete without memories and you are the part of my memories. And Anisha[33], I wish we had met earlier.

As I am writing this dissertation, the world is obscured by the dark clouds of a global pandemic (COVID 19). A special mention to all the public heath professionals and medical researchers who are fighting at the forefront. Thanks to everyone who, in the midst of a pandemic, are risking their lives to keep the essential services up and running.

I would like to acknowledge financial support from the National Science Foundation (NSF Grants CNS-1617896 and CNS- 1923807) for all the projects discussed herein.

[30] Kanta Saha [31] Pradip Saha [32] Suvrajit Podder [33] Anisha Sahu

Contents

List of Figures

List of Tables

1

Introduction

All models are wrong, but some are useful.

– George Box

With the unprecedented increase in the demand of mobile data, wireless cellular networks are evolving at a rapid pace. What started as a *small step* of extending the telephony to the mobile environment has transformed into a *giant leap* towards ushering global connectivity–the access of information *anytime, anywhere*, and the rise of a multi-trillion dollar industry. Today, cellular networks have become an integral part of the social infrastructure, that have mobilized our daily life and facilitated digital economy. We are at a very exciting phase in the evolution of cellular networks, with the roll-out of the fifth generation (5G) technologies and the initiation of research on the sixth generation (6G). Every year, the mobile handsets (e.g. smart-phones, tablets) are getting major refresh and newer applications requiring mobile data (such as navigation, streaming, augmented and virtual reality etc.) continue to flood the app-stores. These developments are setting new performance standards for the existing cellular network to meet. In order to design efficient networks that meet the service requirements, it is important to evaluate the system-level performance of the networks under different operational scenarios. The common methodology to evaluate the performance of a cellular network is extensive computer simulations. As one can expect, network simulations with multiple base stations (BSs) and users can easily become complicated with the increase in the complexity of the cellular networks. Hence it is important to develop complimentary analytical methods which will reduce the burden of the simulations.

Over the last decade, stochastic geometry has emerged as a key component in the mathematical modeling and analysis of cellular networks. The main purpose of stochastic geometry is to endow probability distributions on the locations of the base stations (BSs) and users in a network. In order to ensure the tractability of analysis, the BSs and users in the network are commonly modeled as independent homogeneous Poisson point processes (PPPs) which means that the users and BSs are placed independently and uniformly *at random* over the plane. While this assumption of *complete spatial independence* might have been sufficient for yesteryear's cellular networks, the state-of-the-art spatial models are quickly becoming outdated as the networks are becoming increasingly complex. A critical missing piece in these models is the *spatial coupling* between the locations of the BS and users. For instance, the user hotspots in a network and user-centric deployment of BSs are very common factors to be considered in today's network design and deployment. Clearly, the analytical models

of cellular networks based on PPP are not equipped to handle these spatial couplings. On the other hand, the simulation-driven models have been continuously updated, thanks to the standardization efforts lead by the third generation partnership project (3GPP). In an attempt to close the gap between the simulation-driven and analytical models of cellular network, this dissertation develops fundamentally new stochastic geometry-based models for a more realistic and fine-tuned performance analysis, optimization and design of cellular networks. We will follow three different directions for the development of these models: *first*, general spatial models incorporating user and BS clustering and user-BS coupling, *second*, spatial models for the analysis of integrated access and backhaul (IAB) networks which is an emerging network architecture in 5G, and *third*, a new class of machine learning inspired stochastic geometry based models which can *learn* the spatial distribution of the network from the actual locations of its nodes. In order to put the key contributions of this dissertation in perspective, we provide some background on the existing modeling approaches and the analytical methods.

1.1 Performance Characterization of Cellular Networks

An integral part of the development and standardization of the cellular networks is the performance evaluation of the network under a given setting. The performance evaluation methods of cellular networks can be broadly classified into two types. (1) *Link-level evaluation*, where the performance of an individual link is evaluated, such as the variation of the bit error rate with signal-to-interference-and-noise-ratio (SINR) for some modulation and coding scheme, antenna setting, and channel conditions and (2) *System-level evaluation,* where the entire network is taken into account and the performance of an arbitrarily selected user is evaluated, such as, the cumulative distribution function of the SINR at the location of an arbitrary user. The distribution of SINR (also known as the coverage of a network) is the fundamental metric of interest in the system-level since many other performance metrics like rate and area spectral efficiency can be derived from the SINR distribution. In the system level, more attention is paid to the spatial layout of the network (such as the user and BS locations) with many link-level details (e.g. the modulation and coding schemes, channel estimation techniques etc.) being abstracted for the sake of simplicity. The performance characterization in the link-level has traditionally been backed up by the analytical models providing accurate estimates of the performance metrics [4, 5]. On the other hand, the system-level evaluations almost entirely rely on simulations because of the lack of analytical tools that can handle realistic placements users and BSs in the network.

The basis of the simulation-driven models till date is the hexagonal macrocells on the hexagonal lattice, which was originally proposed in MacDonald's paper on the cellular concept [6]. However, the propagation characteristics of wireless signals greatly reduces the burden of simulating a large network to the "19-cell wraparound region" [7] around the cell of interest. Here the term "wraparound" means that the boundaries of the simulation region are assumed to be contiguous (see Fig. 1.1 for an illustration), so that any edge effects do

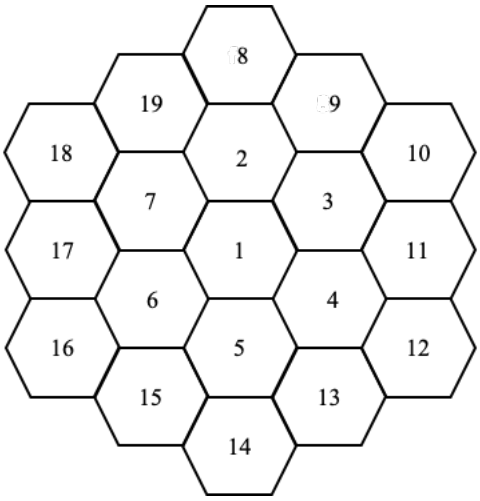

Figure 1.1: 19-cell wraparound region used to simulate macrocellular network.

not affect the simulation.

As the networks are becoming more heterogeneous with different types of BSs like macro and small cell BSs, system-level simulations are becoming more complicated. Moreover, with increasing number of network parameters in play, the comparison between the simulations performed by different entities is becoming next to impossible. In order to harmonize the simulations, the standardization bodies like 3GPP define detailed simulation scenarios including the methods for BS and user placements. These simulation settings are available in publicly available technical reports and standards[1]. Despite their popularity in standardization activities, there are a few fundamental problems with the simulation-driven investigations. The first problem is the number of total scenarios to evaluate via simulation with will yield spatial averaging with reasonable accuracy is often very large. This may require several person-weeks of effort to code, debug, and run the simulations before every standards meeting. Second, even if the networks are simulated, the total set of all possible scenarios can be quite large with the number of network parameters, for instance, antenna heights, cell density, base station transmit power, user density etc. Hence the simulation-driven evaluations are not the most effective means to obtain some useful insight or trend of the network performance.

Analytical Models. The increasing complexity of the simulation models has inspired a lot of work focusing on developing analytical models of cellular networks. The key objective of these models is to enable the performance characterization by deriving easy-to-compute mathematical expressions of the performance metrics without the need for running extensive Monte Carlo simulations. As noted earlier, the hexagonal grid structure or in general any of the regular placement of BSs is not amenable to mathematical analysis. Interestingly, if the regular spatial models are *perturbed* with random displacement, the network model gains

[1] The reader can visit https://www.3gpp.org/specifications to access the specification documents.

significant analytical tractability by inheriting the properties of random spatial model [8, Chapter 1],[9].

1.2 Stochastic Geometry-based Network Models

Stochastic geometry deals with the probability distributions related to the random spatial models or random topology [10–13]. In a wireless network setting, the main theme of the stochastic geometry-based model is to endow probability distributions on the locations of transmitters and receivers in a network. In other words, the transmitter and receiver locations are assumed to be the realizations of point processes or random processes in Euclidean space (such as R^2). The point process based models of wireless nodes have been a standard approach for the performance analysis of wireless ad hoc networks for a long time (see [14–17] for a rich history of the random spatial modeling of wireless networks). In the context of cellular networks, in [18, 19], Baccelli et al. used PPP as the spatial distribution of BSs for the traffic and economic models of the networks. In [20], Andrews et al. characterized the fundamental performance metrics like coverage and rate of a single tier cellular network with PPP-distributed BSs. In [8, 21], Dhillon et al. formulated a PPP-based analytical model for a general multi-tier cellular network consisting of macro and small cell BSs (SBSs).

In a stochastic geometry based cellular network model, the BSs and user locations are treated as realizations of some random point pattern, also known as a point processes. Then the performance metrics of the network (such as the coverage and rate of an arbitrary user) are evaluated as functionals[2] of these point processes. The key role of stochastic geometry is to transform these point process functionals (which are sum, product or the combination of sum and product over the points) to easy-to-compute expressions which are often times integrals over R^2. The most common practice is to use the homogeneous PPP as the spatial model for the BSs and users. This assumption is equivalent to saying that the users and BSs are placed independently and uniformly *at random* over a plane. The PPP-based models have gained significant popularity in cellular network modeling because of the following reasons.

Tractability. It is possible to obtain easy-to-compute expressions (which often times reduces to closed forms) of the key performance metrics like the coverage and rate [20]. It is also possible to generalize the network models to a K-tier HetNet model with different types of BSs (such as macro, pico and femto cells) [8, 21]. As a result, a wide set of network deployment scenarios can be studied using this model [22–24].

Flexibility. These models are very flexible to be used for the performance evaluation of different technologies, such as self-powered energy harvesting BSs [25], multiple input multiple output (MIMO) enabled networks [26, 27], localization [28] and millimeter wave (mm-wave) communication [29], and many more. The PPP-based modeling and analysis of cellular networks is quite mature by now. We refer to [23, 30–32] for more pedagogical treatment of the topic as well as extensive surveys of the prior art. Over the last decade

[2] *functionals* are higher order functions which takes the usual functions as arguments.

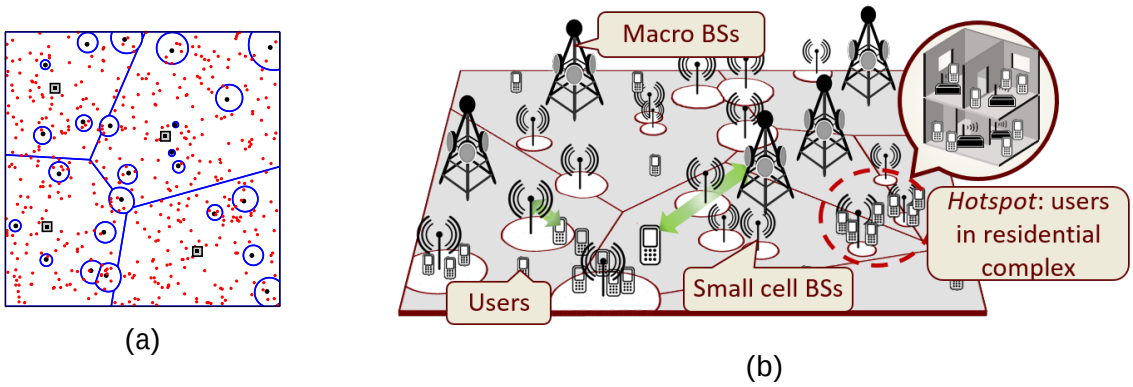

Figure 1.2: Illustration of the shortcoming of the PPP-based HetNet model: (a) relization of a two-tier PPP-based HetNet. The macro BSs, SBSs, and users are indicated by squares, black dots and red dots, respectively, (b) layout of an HetNet with user hotspots and user-SBS coupling.

PPP has remained the foundation of the stochastic geometry based cellular network models. However, as the performance analysis of the cellular networks are becoming more intertwined with the complex topology of the network, the PPP-based models are becoming significantly inaccurate. For instance, the PPP-based models are based on the assumption of *complete spatial independence* of the points and hence cannot capture any kind of spatial coupling between the network nodes (such as the BSs and users). See Fig 1.2 for an illustration. These spatial couplings are quite central to some network deployments (such as the heterogeneous cellular networks or HetNets) and hence can significantly impact the system-level evaluations. After describing the shortcomings of the baseline PPP-based cellular network models, we are now in a position to discuss three directions along which we will be developing new stochastic geometry based models.

1.3 New Stochastic Geometry-based Network Models

Direction I: 3GPP-inspired HetNet Models (3GPP-HetNets). For the standardization purposes, 3GPP has recommended different spatial configurations for the system-level simulations of the cellular networks. These spatial configurations of users and BSs used in the 3GPP-compliant simulation models are fundamentally different from the PPP-based model. In order to highlight this difference, we first provide a brief overview of the relevant spatial setups used in the 3GPP simulation models.

For modeling macrocells, 3GPP simulation scenarios rely on either a single macrocell setup or the hexagonal grid based models. On the contrary, as discussed next, several different configurations corresponding to a variety of real-life deployment scenarios are considered for modeling the locations of users and SBSs [1, Section A.2.1.1.2]. In order to be consistent with the 3GPP documents, we will put *keywords* reserved for referring to the configurations

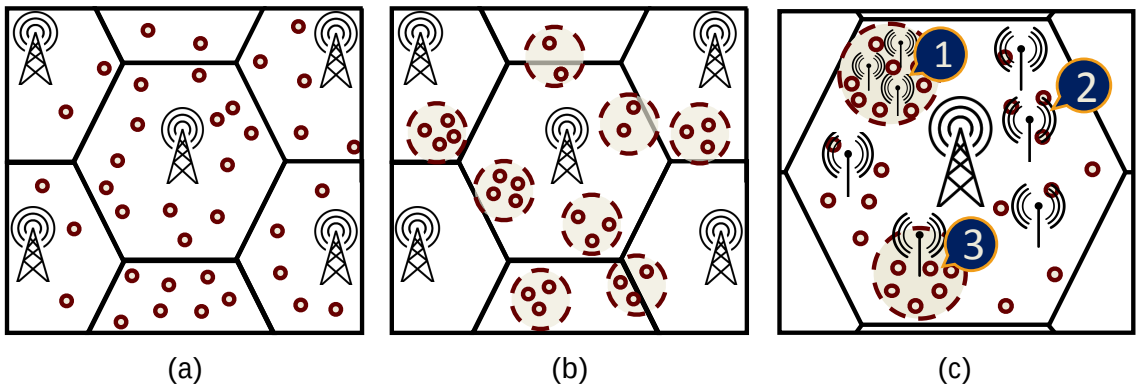

Figure 1.3: User and SBS configurations considered in 3GPP HetNet models. Figs. (a) and (b) illustrate two different user configurations: (a) "uniform" within a macrocell, and (b) "clustered" within a macrocell. Fig. (c) illustrates SBS configurations: (1) Dense deployment of SBSs at certain areas (usually within user hotspots or indoors), (2) SBSs deployed uniformly at random within a macrocell, and (3) a single SBS deployed within a user hotspot.

of users (uniform and clustered) and SBSs ('correlated' and 'uncorrelated') in the 3GPP documents in quotation marks.

Users. As illustrated in Figs. 1.3a and 1.3b, there are two main user configurations considered in 3GPP simulation models: (i) 'uniform' and (ii) 'clustered'. In the 'uniform' configuration, the users are assumed to be distributed uniformly at random within each macrocell. Given the coverage-centric nature of macrocellular deployments, this configuration has been the default choice for system-level simulations of cellular networks since their inception. However, with the focus quickly shifting towards capacity-driven deployments of SBSs, the 'clustered' user configuration has become at least as much (if not more) important. In this configuration, the users are assumed to be distributed uniformly at random within circular regions of a constant radius (modeling user hotspots). As discussed next, SBSs are often deployed in these user hotspots, which couples their locations with those of the users.

SBSs. Roughly speaking, there are two different classes of configurations considered for SBSs: (i) 'uncorrelated' and (ii) 'correlated'. In the 'uncorrelated' configuration, the SBSs are assumed to be distributed uniformly at random inside a macrocell. This corresponds to configuration 2 in Fig. 1.3c. The complete description of 'correlated' configurations is a bit more tedious due to their context-specific nature. Therefore, we will first summarize the factors that introduce correlation or coupling in the SBS locations and then describe the configurations that are most relevant to our work. *Intra-tier* coupling in the SBS locations is introduced when SBSs are deployed according to some site-planning optimization strategies to maximize coverage over the macrocell. *Inter-tier* coupling in the SBS and MBS locations is introduced when more SBSs are deployed at the cell-edge to boost cell-edge coverage. Similarly, *SBS-user* coupling results from the user-centric deployment of small cells in the user hotspots. Interested readers are advised to refer to [1–3] for more details about how

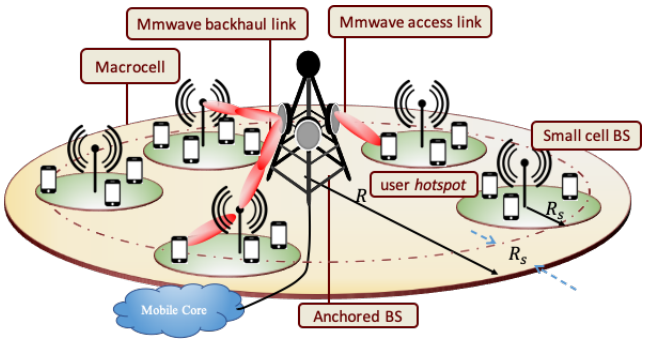

Figure 1.4: Illustration of a two tier mm-wave HetNet with IAB.

these sources of correlation manifest into the 3GPP simulation models. In this direction, we will focus on the SBS-user coupling. Please refer to Fig. 1.3c (configurations 1 and 3) for illustrative examples.

It is quite obvious by now that the simulation models discussed so far are quite different than the PPP-based model for the multi-tier network, originally proposed in [21, 22], where the users and BSs of different tiers are distributed independently and uniformly at random over a plane. For a concrete example, we illustrate a realization of a two-tier PPP-based HetNet model in Fig. 1.2a.

Since the fundamental assumption in this PPP-based K-tier HetNet model is the mutual independence of all the BS and user locations, it is not rich enough to model spatial couplings which are extensively captured in the spatial configurations in the 3GPP-compliant simulation settings (see Fig. 1.3c for example). In order to model intra-tier, inter-tier and SBS-user couplings in HetNets, we need to consider spatial models beyond PPP. We defer a more detailed discussion on these non-Poisson point processes and their applications in cellular network modeling to Section 3.1.2. While there are infinite ways of constructing random spatial models of cellular networks (note that even the spatial configurations proposed by 3GPP can be interpreted as realizations of some point processes), the main challenge is to guarantee the analytical tractability of these models for system-level performance evaluations. A key contribution of this dissertation is to identify *Poisson cluster process* (PCP) as a suitable candidate spatial model which offers a balance between the realistic modeling of the spatial couplings and preserving the mathematical tractability of the models. Thus, in the first part of this dissertation (Chapters 2-6), we develop a new class of stochastic geometry based HetNet models based on PCPs which encompass a wide set of the aforementioned instances of spatial coupling.

Direction-II: Millimeter-wave Integrated access and Backhaul Network Models (mm-wave IAB). While the development of the PCP-based HetNet models in Direction-I (3GPP-HetNets) was intended to emphasize on the spatial couplings between the locations of

the users and SBSs, we now move to another important aspect of the deployment of the SBSs. It is well-known that the denser deployment of SBSs enables more aggressive frequency reuse. However, the efforts towards network densification face a fundamental challenge because of the structure of the current cellular networks, where the backhaul network (BN) connecting the BSs to the network core is predominantly wired and hence is designed separately from the radio access network (RAN). Hence, although the SBSs can be deployed ubiquitously, it is not feasible to reach these tens of thousands of SBSs with wired backhaul connections. This backhaul bottleneck (also known as the complexity of *last-mile fiber*) can potentially be removed by adding wireless self-backhaling capabilities to the RAN. In this case, the wireless BN will be integrated with the RAN and will share the same resources and infrastructure which are used for the RAN. This will reduce the reliability on the fiber BN which will only need to provide backhaul to a few BSs (called the anchored BSs (ABSs)) and the ABSs will provide wireless backhaul to the other BSs in the network. See Fig. 1.4 for an illustration. This IAB design is not feasible in the current networks operating in sub-6 GHz because of the scarcity of bandwidth to be shared between the RANs and the BNs. This challenge can be mitigated in mm-wave frequencies where it is possible to achieve fiber-like performance of the backhaul links due to the large BW and beamforming gain using large antenna arrays. While the IAB architecture can enable the ultra-densification of the network in 5G, it will also introduce new design challenges which were not present in the traditional networks, such as the resource management at the BSs between the RAN and BN. These type of questions cannot be answered with the traditional stochastic geometry-based models of HetNets since these models completely ignore the BN by assuming infinite capacity backhaul for all the BSs in the network. Thus, the second direction (Chapters 7 and 8) of this dissertation is to build generative models for the IAB-enabled HetNets.

Direction-III: Machine Learning-inspired stochastic geometry models (MLSG). In the third direction of this dissertation (Chapter 9), our objective is to explore a completely new modeling technique of wireless networks by combining machine learning and stochastic geometry, two powerful tools used in wireless network analysis and design. While the stochastic geometry-based models are quite indispensable for the performance analysis of the network, their role in the network optimization and design has been quite limited. Unlike the traditional stochastic geometry-based analyses that assumes some distributions of the random spatial model of the network (such as PPP or PCP with known parameters), our objective is to *learn* the spatial distributions from the layouts of the actual networks using a machine learning framework. The key enabling tool for this learning-based approach is the determinantal point process (DPP), which lies at the intersection of machine learning and stochastic geometry.

1.4 Contributions

The specific contributions in the three directions are highlighted next.

1.4. Contributions

New HetNet model considering user-centric small cell deployments. One of the principal underlying assumptions of current approaches to the analysis of HetNets with random spatial models is the uniform distribution of users independent of the BS locations. This assumption is not quite accurate, especially for user-centric capacity-driven small cell deployments where low-power BSs are deployed in the areas of high user density, thus inducing a natural correlation in the BS and user locations. In order to capture this correlation, in Chapter 2 we enrich the existing K-tier PPP-based HetNet model by considering user locations as PCPs with the BSs at the cluster centers. We provide the formal analysis of the downlink coverage probability in terms of a general density function describing the locations of users around the BSs. The derived results are specialized for two cases of interest: 1) Thomas cluster process (TCP) and 2) Matérn cluster process (MCP). Tight closed-form bounds for the coverage probability in these two cases are also derived.

General HetNet models: Coverage analysis for max-SIR based association. While Chapter 2 focused on modeling one particular instance of user BS coupling, there are many other configurations of users and BSs that exhibit spatial coupling in the simulation models of HetNets proposed by 3GPP. In Chapter 3, we unify all these configurations and construct a more general HetNet model by modeling a fraction of users and arbitrary number of BS tiers with PCP and PPP. We derive the downlink coverage probability of a typical user under maximum SIR-based association. We further show that the proposed model converges to the PPP-based HetNet model as the cluster size of the PCPs tends to infinity. Finally, we specialize our analysis based on general PCPs for TCP and MCP.

General HetNet models: Coverage analysis for max-power based association. In Chapter 4, we develop an analytical framework for the evaluation of the coverage probability, or equivalently the CCDF of SINR, of a typical user in a K-tier HetNet under maximum average received power-based association strategy, where the BS locations of each tier follow either a PPP or a PCP. The key enabling step involves conditioning on the parent PPPs of all the PCPs which allows us to express the coverage probability as a product of sum-products and PGFLs of the parent PPPs. In addition to several useful insights, our analysis provides a rigorous way for studying the impact of the cluster size on the SINR distribution, which was not possible using existing PPP-based models.

Meta distribution of downlink SIR in the general HetNet Model. In the previous chapters, we have constructed a general HetNet model with a combination of PPP and PCP and presented the downlink coverage analysis . In Chapter 5, we focus on a more fine grained analysis in terms of the meta distribution of SINR. In particular, we derive the distribution of the conditional success probability of the typical user (probability that the received SINR exceeds some threshold conditioned on the BS locations) averaged over small scale fading assuming that the user connects to the BS providing the maximum received power.

Load on the typical Poisson Voronoi cell with clustered user distribution. In Chapter 6, we characterize the distribution of the number of users associating with the typical base station (BS), termed the *typical cell load*, in a cellular network where the BSs are distributed as a homogeneous PPP and the users are distributed as an independent PCP. In this setting, we derive the exact expressions for the first two moments of the typical cell load. Given the computational complexity of evaluating the higher moments, we derive easy-to-use approximations for the probability generating function (PGF) of the typical cell load, which can be inverted to obtain the probability mass function (PMF).

Bandwidth partitioning and downlink analysis in mm-wave IAB. In Chapter 7, we develop an analytical framework for mm-wave cellular network with IAB using which its downlink rate coverage probability is accurately characterized. Using this framework, we study the performance of three backhaul bandwidth (BW) partition strategies: 1) equal partition: when all SBSs obtain equal share of the backhaul BW; 2) instantaneous load-based partition: when the backhaul BW share of an SBS is proportional to its instantaneous load; and 3) average load-based partition: when the backhaul BW share of an SBS is proportional to its average load. Our analysis shows that depending on the choice of the partitioning strategy, there exists an optimal split of access and backhaul BW for which the rate coverage is maximized. Further, there exists a critical volume of cell-load (total number of users) beyond which the gains provided by the IAB-enabled network disappear and its performance converges to that of the traditional macro-only network with no SBSs.

Load balancing in 5G HetNets with mm-wave IAB. While extending the PCP-based HetNet models for mm-wave IAB networks, we found that it is not straightforward to perform the rate analysis in the standard multi-cell setting analogous to the system models considered in Chapters 2-5. In Chapter 8, we resort to the baseline PPP-based model and develop an analytical framework for a two-tier HetNet with IAB. For this network, we derive the downlink rate coverage probability for two types of resource allocations at the MBS: 1) integrated resource allocation (IRA): where the total bandwidth is dynamically split between access and backhaul, and 2) orthogonal resource allocation (ORA): where a static partition is defined for the access and backhaul communications. Our analysis concretely demonstrates that offloading users from the MBSs to SBSs may not provide similar rate improvements in an IAB setting as it would in a HetNet with fiber-backhauled SBS. Our analysis also shows that it is not possible to improve the user rate in an IAB setting by simply densifying the SBSs due to the bottleneck on the rate of wireless backhaul links between MBS and SBS.

Determinantal subset selection for wireless networks. In wireless networks, many problems can be formulated as *subset selection problems* where the goal is to select a subset from the ground set with the objective of maximizing some objective function. These problems are typically NP-hard and hence solved through carefully constructed heuristics,

which are themselves mostly NP-complete and thus not easily applicable to large networks. On the other hand, subset selection problems occur in slightly different context in machine learning where the goal is to select a subset of high *quality* yet *diverse* items from a ground set. This balance in quality and diversity is often maintained in the ML problems by using DPP, which endows distributions on the subsets such that the probability of selecting two *similar* items is negatively correlated. While DPPs have been explored more generally in stochastic geometry to model inter-point repulsion, they are particularly conducive for machine learning applications because the parameters of their distributions can be efficiently learnt from a training set. In Chapter 9, we introduce a novel DPP-based learning (DPPL) framework for efficiently solving subset selection problems in wireless networks. The DPPL is intended to replace the traditional optimization algorithms for subset selection by *learning* the quality-diversity trade-off in the optimal subsets selected by an optimization routine. As a case study, we apply DPPL to the wireless link scheduling problem, where the goal is to determine the subset of simultaneously active links which maximizes the network-wide sum-rate. We demonstrate that the proposed DPPL approaches the optimal solution with significantly lower computational complexity than the popular optimization algorithms used for this problem in the literature.

1.5 List of Publications

This dissertation had led to a book and several journal and conference papers as listed below.

Book

[**B1**] H. S. Dhillon, C. Saha, and M. Afshang, *Poisson Cluster Processes: Theory and Application to Wireless Networks*, under preparation. Cambridge University Press, 2021.

Journal

[**J10**] **C. Saha**, M. Afshang, and H. S. Dhillon, "Meta Distribution of Downlink SIR in a Poisson Cluster Process-based HetNet Model", *IEEE Wireless Commun. Letters*, to appear.

[**J9**] **C. Saha**, H. S. Dhillon, "Load on the Typical Poisson Voronoi Cell with Clustered User Distribution", *IEEE Wireless Commun. Letters*, to appear.

[**J8**] **C. Saha**, H. S. Dhillon, "Millimeter Wave Integrated Access and Backhaul in 5G: Performance Analysis and Design Insights ", *IEEE Journal on Sel. Areas in Commun.*, vol. 37, no. 12, pp. 2669-2684, Dec. 2019.

[**J7**] **C. Saha**, H. S. Dhillon, N. Miyoshi, and J. G. Andrews, "Unified Analysis of HetNets using Poisson Cluster Process under Max-Power Association", *IEEE Trans. on Wireless Commun.*, vol. 18, no. 8, pp. 3797-3812, Aug. 2019.

[**J6**] **C. Saha**, M. Afshang, and H. S. Dhillon, "Bandwidth Partitioning and Downlink Analysis in Millimeter Wave Integrated Access and Backhaul for 5G", *IEEE Trans. Wireless Commun.*, vol. 17, no. 12, pp. 8195-8210, Dec. 2018.

[**J5**] M. Afshang, **C. Saha**, and H. S. Dhillon, "Equi-Coverage Contours in Cellular Networks", *IEEE Wireless Commun. Letters*, vol. 7, no. 5, pp. 700-703, Oct. 2018.

[**J4**] **C. Saha**, M. Afshang, and H. S. Dhillon, "3GPP-inspired HetNet Model using Poisson Cluster Process: Sum-product Functionals and Downlink Coverage", *IEEE Trans. on Commun.*, vol. 66, no. 5, pp. 2219-2234, May 2018.

[**J3**] M. Afshang, **C. Saha**, and H. S. Dhillon, "Nearest-Neighbor and Contact Distance Distributions for Matérn Cluster Process", *IEEE Commun. Letters*, vol. 21, no. 12, pp. 2686-2689, Dec. 2017.

[**J2**] **C. Saha**, M. Afshang, and H. S. Dhillon, "Enriched K-Tier HetNet Model to Enable the Analysis of User-Centric Small Cell Deployments", *IEEE Trans. on Wireless Commun.*, vol. 16, no. 3, pp. 1593-1608, Mar. 2017.

[**J1**] M. Afshang, **C. Saha**, and H. S. Dhillon, "Nearest-Neighbor and Contact Distance Distributions for Thomas Cluster Process", *IEEE Wireless Commun. Letters*, vol. 6, no. 1, pp. 130-133, Feb. 2017.

Conference Proceedings

[**C9**] **C. Saha**, P. D. Mankar, H. S. Dhillon, "Rate Coverage of a Cellular Network with Users distributed as Poisson Cluster Process", in *Proc. Asilomar*, Pacific Grove, CA, Nov. 2020.

[**C8**] S. Mulleti, **C. Saha**, H. S. Dhillon, Y. Elder, "A Fast-Learning Sparse Antenna Array", in *Proc. IEEE Radar Conference*, Florence, Italy, Sept. 2020.

[**C7**] **C. Saha** and H. S. Dhillon, "Interference Characterization in Wireless Networks: A Determinantal Learning Approach", in *Proc. IEEE Int. Workshop in Machine Learning for Sig. Processing*, Pittsburgh, PA, Oct. 2019.

[**C6**] **C. Saha** and H. S. Dhillon, "Machine Learning meets Stochastic Geometry: Determinantal Subset Selection for Wireless Networks", in *Proc. IEEE Globecom*, Waikoloa, HI, Dec. 2019.

[**C5**] **C. Saha** and H. S. Dhillon, "On Load Balancing in Millimeter Wave HetNets with Integrated Access and Backhaul", in *Proc. IEEE Globecom*, Waikoloa, HI, Dec. 2019.

[**C4**] **C. Saha**, M. Afshang and H. S. Dhillon, "Integrated mmWave Access and Backhaul in 5G: Bandwidth Partitioning and Downlink Analysis", in *Proc. IEEE ICC*, Kansas City, MO, May 2018.

1.5. List of Publications

[**C3**] **C. Saha**, M. Afshang and H. S. Dhillon, "Poisson Cluster Process: Bridging the Gap Between PPP and 3GPP HetNet Models", in *Proc. ITA*, San Diego, CA, Feb. 2017.

[**C2**] **C. Saha** and H. S. Dhillon, "D2D Underlaid Cellular Networks with User Clusters: Load Balancing and Downlink Rate Analysis", in *Proc. IEEE WCNC*, San Francisco, CA, March 2017.

[**C1**] **C. Saha** and H. S. Dhillon, "Downlink Coverage Probability of K-Tier HetNets with General Non-Uniform User Distributions", in *Proc. IEEE ICC*, Kuala Lumpur, Malaysia, May 2016.

2

Modeling and Analysis of K-tier HetNet with Clustered User Distribution

2.1 Introduction

The increasing popularity of Internet-enabled mobile devices, such as smartphones and tablets, has led to an unprecendented increase in the global mobile data traffic, which has in turn necessitated the need to dramatically increase the capacity of cellular networks. Not surprisingly, a key enabler towards increasing network capacity at such a rate is to reuse spectral resources over space and time more aggressively. This is already underway in the form of capacity-driven deployment of several types of low-power BSs in the areas of high user density, such as coffee shops, airport terminals, and downtowns of large cities [2, 3]. Due to the coexistence of the various types of low-power BSs, collectively called *small cells*, with the conventional high-power macrocells, the resulting network is often termed as a heterogeneous cellular network (HetNet). Because of the increasing irregularity of BS locations in HetNets, random spatial models have become preferred choice for the accurate modeling and tractable analysis of these networks. The most popular approach is to model the locations of different classes of BSs by independent PPPs and perform the downlink analysis at a typical user chosen independent of the BS locations; see [23, 32, 33] and the references therein. However, none of the prior works has focused on developing tools for the more realistic case of user-centric deployments in which the user and BS locations are correlated. Developing new tools to fill this gap is the main goal of this chapter.

2.1.1 Related works

Stochastic geometry has recently emerged as a useful tool for the analysis of cellular networks. Building on the single-tier cellular model developed in [20], a multi-tier HetNet model was first developed in[21, 34], which was then extended in [22, 35, 36]. While the initial works were mainly focused on the downlink coverage and rate analyses, the models have since been extended in multiple ways, such as for load aware modeling of HetNets in [37], traffic offloading in [24], and throughput optimization in [38]. Please refer to [22, 23, 31, 32] for more pedagogical treatment of the topic as well as extensive surveys of the prior art. While PPP remains a popular abstraction of spatial distribution of cellular BSs

randomly and independently coexisting over a finite but large area, a common assumption of the aforementioned analysis, as noted above, is that the users are uniformly distributed independent of the BS locations. However, in reality, the users form hotspots, which are where some types of small cells, such as picocells are deployed to enhance coverage and capacity [39]. As a result, the user-centric deployment of small cells is one of the dominant themes in future wireless architectures [40]. In such architectures, one can envision small cells being deployed to serve *clusters* of users. Such models are also being used by the standardization bodies, such as 3GPP [2, 3]. While there have been attempts to model such clusters of small cells by using PCP, e.g., see [41–45], the user distribution is usually still assumed to be independent of the BS locations.

As noted above, modeling and performance analysis of user-centric capacity-driven deployment of small cells require accurate characterization of not only the spatial distribution of users but also correlation between the BS and user locations. Existing works, however sparse, on the analysis of correlated non-uniform user distributions can be classified into two main directions. The first is to characterize the performance through detailed system-level simulations [46–49]. As expected, the general philosophy is to capture the capacity-centric deployments by assuming higher user densities in the vicinity of small cell BSs, e.g., see [46]. In [47], the authors proposed non-uniform correlated traffic pattern generation over space and time based on log-normal or Weibull distribution. On similar lines, [48] has introduced a low complexity PPP simulation approach for HetNets with correlated user and BS locations. System level simulation shows that network performance significantly deteriorates with increased heterogeneity of users if there exists no correlation among the users and the small cell BS locations. But the HetNet performance improves if the small cell BSs are placed at the cluster centers which are determined by means of clustering algorithms from a given user distribution [49].

The second direction, in which the contributions are even sparser, is to use analytic tools from stochastic geometry to characterize the performance of HetNets with non-uniform user distributions. One notable contribution in this direction is the generative model proposed in [50], where non-uniform user distribution is generated from the homogeneous PPP by thinning the BS field independently, conditional on the active link from a typical user to its serving BS. While the resulting model is tractable, it suffers from two shortcomings: (i) it is restricted to single-tier networks and extension to HetNet is not straightforward, and (ii) even for single-tier networks, it does not allow the inclusion of any general non-uniform distribution of users in the model. In [51], the authors proposed a mixture of correlated and uncorrelated user distribution with respect to small cell BS deployment and evaluated the enhancement in coverage probability as a function of correlation coefficient. Correlation has been introduced by generating users initially as an independent PPP and later shifting them towards the BSs with some probability. In [38], the authors have considered clustered users around femto-BSs as uniformly distributed on the circumference of a circle with fixed radius. Besides, some other attempts have been made at including non-uniform user distributions using simple models, especially in the context of indoor communications, e.g., see [52]. Over-

all, we are still somewhat short-handed when it comes to handling the analysis of user-centric deployments, which is the main focus of this chapter. With this brief overview of the prior art, we now discuss our contributions next.

2.1.2 Contributions

New HetNet model

In this chapter, we develop a new and more practical HetNet model for accurately capturing the non-uniform user distribution as well as correlation between the locations of the users and BSs. In particular, the user locations have been modeled as superposition of PCPs. Correlation between the users and BSs under user-centric capacity-driven deployment has been captured by assuming the BS locations as the parent point processes of the cluster processes of users. This model is flexible enough to include any kind of user distribution around any arbitrary number of BS tiers as well as user distribution that is homogeneous and independent of the BS locations. This approach builds on our recent work on modeling device-to-device networks using PCPs [53].

Downlink analysis

We derive exact expression for the coverage probability of a typical user chosen randomly from one of the clusters in this setup. The key step of our approach is the treatment of the cluster center as an individual singleton tier. This enables the characterization of key distance distributions, which ultimately lead to easy-to-use expressions for the Laplace transform of interference distribution in all cases of interest. Using these components, we derive the coverage probability of a randomly chosen user from one of the user clusters. After characterizing the coverage probability under a general distribution of users, we specialize our results for two popular PCPs, viz. Thomas and Matérn cluster processes. Next, we provide upper and lower bounds on coverage probability which are computationally more efficient than the exact expressions and reduce to closed form expressions for no shadowing when the user distribution is modeled as Thomas or Matérn cluster process. Although our analysis primarily focuses on users clustered around BS locations, we also consider users that are independently and homogeneously located over the network modeled as a PPP and use previously derived results for coverage [22] in conjunction to evaluate the overall coverage probability for any randomly chosen user in our HetNet setup with mixed user distribution.

System design insights

Our analysis leads to several system-level design insights. First, it can be observed that the coverage probability under the assumption of BS-user correlation is significantly greater than that derived under the assumption of independence. While the assumption of independence of BS and user locations does simplify analyses, the resulting coverage probability predictions may be significantly pessimistic. That being said, our results concretely

Table 2.1: Summary of Notations

Notation	Description
$\Phi_k^{(BS;o)}$, λ_k	PPP of BSs of k^{th} open access tier, density of $\Phi_k^{(BS;o)}$
$\Phi_k^{(BS;c)}$, λ_k^0	PPP of BSs of k^{th} closed access tier, density of $\Phi_k^{(BS;c)}$
B	Set of BS tiers that have users clustered around them
Φ_i^u	Point process modeling users clustered around BSs of $\Phi_i^{(BS)}$
$u^{(PPP)}$	Locations of uniformly distributed users modeled as a homogeneous PPP
$\mathbf{y}_0; Y_0$	Location of cluster center in Euclidean space, $Y_0 = \|\mathbf{y}_0\|$
$\Phi_0^{(BS;o)}$	Tier 0 containing only the cluster center
$\lambda_k; \bar{\lambda}_k$	Equivalent PPP of $\Phi_k^{(BS;o)}$ to incorporate shadowing, density of λ_k
$\lambda_k^0; \bar{\lambda}_k^0$	Equivalent PPP of $\Phi_k^{(BS;c)}$ to incorporate shadowing, density of λ_k^0
$P_k; h_k; V_k$	Transmit power, small scale fading gain, shadowing gain for all links with BSs in $\Phi_k^{(BS)}$
$\mathbf{y}_k$, $\mathbf{x}_k$	Actual location of a BS in $\Phi_k^{(BS)}$ and location in transformed space ($\mathbf{x_k} = V_k^{\frac{1}{\alpha}}\mathbf{y}_k$)
N_i	Average number of users per cluster of Φ_i^u
R_k	Modified distance of nearest BS $\in \Phi_k$, $R_k = \min\|\mathbf{x}_k\|$
$b(\mathbf{0}; r)$	Disc with radius r centered at origin
$I_{o(j;k)}$	Interference from all BSs $\in \Phi_k$ when user connects to a BS $\in \Phi_j$
$I_{c(k)}$	Interference from all BSs $\in \Phi_k^0$
$\mathtt{P}_c^{(i)}; \mathtt{P}_c^{(PPP)}$	Coverage probability of a typical user in Φ_i^u, $u^{(PPP)}$
$\mathtt{P}_c$	Overall coverage probability

demonstrate that the difference between the coverage probabilities corresponding to user-centric and independent BS deployment becomes less significant as the cluster sizes (of user cluster) increase. In the limit of cluster size going to infinity, the new coverage results are shown to mathematically converge to the results obtained under independent user distribution assumption. Second, as opposed to the previous works, the coverage probability of users clustered around BSs under interference-limited open access network is a function of BS transmission power. Our analysis shows that coverage probability can be improved by increasing transmission power of small cell BSs located at centers of the user clusters.

2.2 System Model

2.2.1 BS deployment

Consider a K-tier HetNet, where BSs across tiers (or classes) differ in terms of their transmit powers and deployment densities. For notational simplicity, define $K = \{1, 2, \ldots, K\}$ as the indices of the K tiers. The locations of the k^{th}-tier BSs are modeled by an independent homogeneous PPP $\Phi_k^{(BS)}$ of density $\lambda_k > 0$ ($k \in K$). The k^{th}-tier BSs are assumed to transmit at the same power P_k. As is usually the case, we assume that a fraction of k^{th}-tier BSs are in open access for the user of interest while the rest are in closed access. The k^{th}-tier open and closed access BSs are modeled by two independent PPPs $\Phi_k^{(BS;o)}$ and $\Phi_k^{(BS;c)}$ with densities λ_k and λ_k^0, respectively, where $\Phi_k^{(BS)} = \Phi_k^{(BS;o)} \cup \Phi_k^{(BS;c)}$ and $\lambda_k = \lambda_k + \lambda_k^0$.

2.2.2 User distribution

Unlike prior art that focused almost entirely on the performance analysis of users that are uniformly distributed in the network independent of the BS locations, we focus on a correlated setup where users are more likely to lie closer to the BSs. Since small cells are usually deployed in the areas of high user density, this is a much more accurate approach for modeling HetNets compared to the one where users and BSs are both modeled as independent PPPs. We model this scenario by modeling the locations of the users by a PCP with one small cell deployed at the center of each user cluster. To maintain generality, we assume that a subset B K tiers out of K tiers have clusters of users around the BSs. In particular, given the location of a BS in the i^{th} tier acting as cluster center (i 2 B), the users of the cluster are assumed to be symmetrically, independently, and identically distributed (i.i.d.) around it. Union of all such locations of users around the BSs of the i^{th} tier forms a PCP [13], denoted by $_i^u$, where the parent point process of $_i^u$ is $_i^{(BS)}$. To maintain generality, we assume that the user location $\mathbf{Z}_u^{(i)}$ 2 R^2 with respect to its cluster center follows some arbitrary distribution with probability density function (PDF) $f_{\mathbf{Z}_u^{(i)}}(\ )$, which may not necessarily be the same across tiers. This allows to capture the fact the cluster size may affect the choice of small cell to be deployed there. For instance, it may be sufficient to deploy a low power femtocell to serve a small cluster of users in a coffee shop, whereas a relatively higher power picocell may be needed to serve a cluster of users at a big shopping mall or at an airport. After deriving all the results in terms of the general distributions, we will specialize them to two cases of interest where $_i^u$ is modeled as: (i) *Thomas cluster process* in which the users are scattered according to a symmetric normal distribution of variance $_i^2$ around the BSs of $_i^{(BS)}$ [54], hence,

$$f_{\mathbf{Z}_u^{(i)}}(\mathbf{z}) = \frac{1}{2 \ _i^2} \exp \quad \frac{k\mathbf{z}k^2}{2 \ _i^2} \quad ; \quad \mathbf{z} \ 2 \ \mathsf{R}^2; \tag{2.1}$$

and (ii) *Matérn cluster process* which assumes symmetric uniform spatial distribution of users around the cluster center within a circular disc of radius R_i, thus

$$f_{\mathbf{Z}_u^{(i)}}(\mathbf{z}) = \begin{cases} \frac{1}{R_i^2} & \text{if } k\mathbf{z}k \quad R_i \\ 0 & \text{otherwise} \end{cases}; \tag{2.2}$$

where $\mathbf{z}$ is a realization of the random vector $\mathbf{Z}_u^{(i)}$. While our primary interest is in these clustered users, we also consider users that are homogeneously distributed over the network independent of the BS locations, for instance, pedestrians and users in transit. These users are better modeled by a PPP as done in literature (see [21,22,35,55,56] for a small subset). Thus, in addition to the user clusters modeling users in the hotspots, we also consider an independent point process of users $^{u(\mathsf{PPP})}$ which is a PPP of density $^{(\mathsf{PPP})}$. Fig. 2.1 shows the two-tier HetNet setup with high power macro-BSs overlaid with an independent PPP of denser but low power small cell BSs. Fig. 2.1a illustrates the popular system model used in the literature where users are modeled as $^{u(\mathsf{PPP})}$ [21,22,34,35,55]. Fig. 2.1b highlights the correlated setup where users are only clustered around small cell BSs. The general scenario

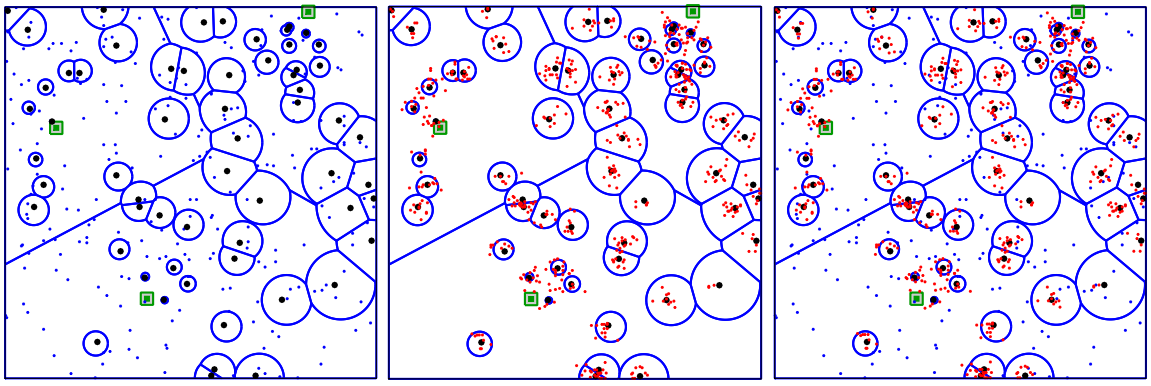

(a) Uniformly distributed users independent of the BS locations (prior art).

(b) Users clustered around small cell BSs (this chapter).

(c) *Mixed* (clustered and uniformly distributed) user distribution (this chapter).

Figure 2.1: Macro (green squares) and small cell BSs (black dots) are distributed as independent PPPs $_2 = \ ^{0}_{2} = \ _1$=10. The uniformly distributed users are represented by small blue dots and clustered users by small red dots. The average number of users per cluster (wherever applicable) is 10.

i.e. the *mixed* user distribution formed by the superposition of PPP and PCP has been depicted in Fig. 2.1c.

Since the downlink analysis at the location of a typical user of $^{u(\mathrm{PPP})}$ is well-known, in this paper we will focus exclusively on the downlink performance of a typical user of $^{u}_{i}$, which is a randomly chosen user from a randomly chosen cluster of $^{u}_{i}$, also termed as the *representative cluster*. In other words, we will primarily focus on the scenario depicted in Fig. 2.1b (and then extend our results and insights to scenario depicted in Fig. 2.1c). Since the PPPs are stationary, we can transform the origin to the location of this typical user. Quite reasonably, we assume that the BS at the center of the representative cluster is in open access mode. This assumption can be easily relaxed without much effort. Denote the location of the representative cluster center by $\mathbf{y}_0 \ 2 \ ^{(\mathrm{BS};o)}_{i}$. Now $^{(\mathrm{BS};o)}_{i}$ can be partitioned into two sets: (i) representative cluster center $\mathbf{y}_0$, and (ii) the rest of the points $^{(\mathrm{BS};o)}_{i} \ n \ \mathbf{y}_0$. By Slivnyak's theorem, it can be argued that $^{(\mathrm{BS};o)}_{i} \ n \ \mathbf{y}_0$ has the same distribution as $^{(\mathrm{BS};o)}_{i}$ [54]. For notational simplicity, we form an additional tier (call it tier 0) consisting of a single point $\mathbf{y}_0$, i.e., $^{(\mathrm{BS})}_{0} \ ^{(\mathrm{BS};o)}_{0} \ f\mathbf{y}_0 g$. Then, the set of indices of all tiers is enriched to $K_1 = f0g \ [\ K = f0; 1; 2; : : : ; K g$. The user can either connect to its own cluster center i.e. the BS in $^{(\mathrm{BS};o)}_{0}$, or to some other BS belonging to one of the tiers $^{(\mathrm{BS};o)}_{1}; : : : ; \ ^{(\mathrm{BS};o)}_{K}$.

2.2.3 Channel model and user association

The received power at the location of the typical user at origin from a BS at $\mathbf{y}_k \ 2 \ ^{(\mathrm{BS})}_{k}$ ($k \ 2 \ K_1$) is modeled as $P(\mathbf{y}_k) = P_k h_k V_k k \mathbf{y}_k k \ \ $, where, $\ > 2$ is the path loss exponent, $\mathrm{h}_y k$ is

the small-scale fading gain and V_k is the shadowing gain. Under Rayleigh fading assumption, $fh_k g$ is a sequence of i.i.d. exponential random variables (RVs) with $h_x k$ exp(1). For large scale shadowing, we assume $fV_k g$ to be sequence of i.i.d. log-normal RVs , i.e., $10 \log V_k$ $N(\ _k;\ ^2_k)$, with $_k$ and $_k$ respectively being the mean and standard deviation (in dB) of the channel power under shadowing. In this model, we assume average received power based cell selection in which a typical user connects to the BS that provides maximum received power averaged over small-scale fading. The serving BS will be one from the $K + 1$ candidate BSs from each tier. The location of such candidate serving BS from $^{(BS;o)}_k$ can be denoted as

$$\mathbf{y}_k = \arg \max_{\mathbf{y_k} 2\ ^{(BS;o)}_k} P_k V_k k\mathbf{y}_k k \quad = \arg \max_{\mathbf{y_k} 2\ ^{(BS;o)}_k} P_k \quad V_k \ ^{\frac{1}{}} k\mathbf{y}_k k \quad : \tag{2.3}$$

Since the 0^{th} tier consists of only a single BS, i.e., the cluster center, there is only one choice of the candidate serving BS from $^{(BS;o)}_0$, i.e., $\mathbf{y}_0$ $\mathbf{y}_0$. The serving BS will be one of these candidate serving BSs, denoted by

$$\mathbf{y} \ = \arg \max_{\mathbf{y} 2 f \mathbf{y_k} g} P_k V_k k\mathbf{y} k \quad : \tag{2.4}$$

Using the displacement theorem of PPPs [17, Section 1.3.3] , it was shown in [57,58] that if each point in a PPP $^{(BS;o)}_k$ ($^{(BS;c)}_k$) is independently displaced such that the transformed location becomes $\mathbf{x}_k = V_k \ ^{\frac{1}{}} \mathbf{y}_k$, then, the resultant point process remains a PPP, which we denote by $_k$ ($^{0}_k$) with density $\bar{}_k = \ _k \mathsf{E}\ V_k^{\frac{2}{}}$ ($\bar{}^{0}_k = \ ^{0}_k \mathsf{E}\ V_k^{\frac{2}{}}$). This transformation is valid for any arbitrary distribution of V_k with PDF $f_{V_k}(\ )$ as long as $\mathsf{E}(V_k^{\frac{2}{}})$ is finite, which is indeed true for log-normal distribution. Consequently, we can express instantaneous received power from a BS $2\ _k$ as $P_k h_k k\mathbf{x}_k k$. Then, the location of candidate serving BS in $_k$ can be written as

$$\mathbf{x}_k = \arg \max_{\mathbf{x_k} 2\ _k} P_k k\mathbf{x}_k k \quad : \tag{2.5}$$

For $k = 0$, we apply similar transformation to the point $\mathbf{y}_0\ 2\ ^{(BS;o)}_0$ and denote the transformed process as $_0$ where $\mathbf{x}_0$ $V_0 \ ^{\frac{1}{}} \mathbf{y}_0$. Then, the serving BS at $\mathbf{x}$ will be

$$\mathbf{x} \ = \arg \max_{\mathbf{x} 2 f \mathbf{x_k} g} P_k k\mathbf{x} k \quad : \tag{2.6}$$

It is worth noting that in the absence of shadowing, the candidate serving BS from a given tier will be the BS closest to the typical user from that tier in terms of the Euclidean distance. This is clearly not true in the presence of shadowing because of the possibility of a farther off BS providing higher average received power than the closest BS. However, by applying displacement theorem, the effect of shadowing gains has been incorporated at the modified locations $\mathbf{x}_k$ such that the strongest BS in the equivalent PPP $_k$ is also the closest in terms of the Euclidean distance. As demonstrated in the literature (e.g., see[57,58]) and the next

two Sections, this simplifies the coverage probability analysis in the presence of shadowing significantly.

We consider interference-limited network and ignore thermal noise. For notational simplicity, let us define the association event to tier j as S_j such that $\mathbf{1}_{S_j} = \mathbf{1}(\mathbf{x} = \mathbf{x}_j)$ (here $\mathbf{1}(\cdot)$ is the indicator function). The Signal-to-Interference Ratio ($\mathtt{SIR}$) experienced by a typical user at origin when $\mathbf{1}_{S_j} = 1$ can be expressed as

$$\mathtt{SIR}(\|\mathbf{x}\|) \quad \frac{P_j h_j \|\mathbf{x}\|^{-}}{\sum_{k \in K_1} \sum_{\mathbf{x}_k \in \Phi_k \setminus \{\mathbf{x}\}} P_k h_k \|\mathbf{x}_k\|^{-}}. \tag{2.7}$$

For quick reference, the notations used in this chapter are summarized in Table 4.1.

Remark 2.1. While we transform all the PPPs to equivalent PPPs to incorporate shadowing, the impact of shadowing on the link between the typical user and its cluster center, i.e., $\mathbf{x}_0 = V_0^{-1}\mathbf{y}_0$, needs to be handled separately. For this, we have two alternatives. First is to find the distribution of $\mathbf{x}_0$ as a function of the distributions of V_0 and $\mathbf{y}_0$. Second is to proceed with the analysis by conditioning on shadowing variable V_0 and decondtioning at the last step. We take the second approach since it gives simpler intermediate results which can be readily used for no-shadowing scenario by putting $V_k = 1$.

2.3 Association probability and serving distance

This is the first technical section of the chapter, where we derive the probability that a typical user is served by a given tier $j \in K_1$, which is usually termed as the *association probability*. We will then derive the distribution of $\|\mathbf{x}\|$ conditioned on S_j, i.e., the distance from the typical user to its serving BS conditioned on the the event that it belongs to the j^{th} open access tier. Recall that the candidate serving BS located at $\mathbf{x}_k$ from the equivalent PPP Φ_k is the one that is nearest to the typical user located at the origin. Let us call $R_k = \|\mathbf{x}_k\|$ as the RV denoting the distance from the typical user to the nearest point of Φ_k. Since Φ_k ($k \in K$) are independent homogeneous PPPs, the distribution of R_k, $k \in K$, is [54]

$$\text{PDF:} \qquad f_{R_k}(r_k) = 2\pi\lambda_k r_k \exp(-\pi\lambda_k r_k^2) \qquad r_k \geq 0; \tag{2.8a}$$

$$\text{CCDF:} \qquad \bar{F}_{R_k}(r_k) = \exp(-\pi\lambda_k r_k^2) \qquad r_k \geq 0. \tag{2.8b}$$

In a similar way, we can define modified distance $R_0 = \|\mathbf{x}_0\| = V_0^{-1}\|\mathbf{y}_0\|$. As noted in Remark 2.1, we will proceed with the analysis by conditioning on the shadowing gain V_0 and then deconditioning on V_0 at the very end. Since R_0 is just a scaled version of $\|\mathbf{y}_0\|$, it suffices to find the distribution of $Y_0 = \|\mathbf{y}_0\|$, which we do next.

Recall that the typical user is located at the origin, which means the relative location of the cluster center with respect to the typical user, i.e., $\mathbf{y}_0$, has the same distribution as that of $\mathbf{Z}_u^{(i)}$. Using standard transformation technique from Cartesian to polar coordinates, we

can obtain the distribution of distance Y_0 from the joint distribution of position coordinates $(t_1; t_2)$, where $\mathbf{y}_0 = (t_1; t_2)$ is in Cartesian domain. Let us denote the joint PDF of the polar coordinates $(Y_0; \ )$ as $f_{Y_0;}(\ )$. Then

$$f_{Y_0;}(y_0; \ ) = f_{\mathbf{y}_0}(t_1; t_2) \quad @ \quad \frac{t_1; t_2}{y_0; \ } \quad ; \tag{2.9}$$

where

$$@ \quad \frac{t_1; t_2}{y_0; \ } = \begin{matrix} 2 & 3 \\ 6 \frac{@t_1}{@y_0} & \frac{@t_1}{@ \ } 7 \\ 4 \frac{@t_2}{@y_0} & \frac{@t_2}{@ \ } 5 \end{matrix} :$$

From the joint distribution, the marginal distribution of distance Y_0 can now be computed by integrating over as

$$f_{Y_0}(y_0) = \int_0^{\ 2} f_{Y_0;}(y_0; \ ) \mathrm{d} \ : \tag{2.10}$$

Remark 2.2. In the special case when $\ ^u_i$ is a Thomas cluster process, user coordinates in Cartesian domain are i.i.d. normal RVs with variance $\ ^2_i$. Then, Y_0 is Rayleigh distributed with PDF and CCDF [59]:

$$\text{PDF:} \qquad f_{Y_0}(y_0) = \frac{y_0}{\ ^2_i} \exp \quad \frac{y_0^2}{2 \ ^2_i} \quad ; \qquad y_0 \quad 0; \tag{2.11a}$$

$$\text{CCDF:} \qquad \overline{F}_{Y_0}(y_0) = \exp \quad \frac{y_0^2}{2 \ ^2_i} \quad ; \qquad y_0 \quad 0: \tag{2.11b}$$

Remark 2.3. If $\ ^u_i$ is a Matérn cluster process, the PDF and CCDF of Y_0 are:

$$\text{PDF:} \qquad f_{Y_0}(y_0) = \frac{2y_0}{R_i^2}; \qquad 0 \quad y_0 \quad R_i; \tag{2.12a}$$

$$\text{CCDF:} \qquad \overline{F}_{Y_0}(y_0) = \frac{R_i^2 \quad y_0^2}{R_i^2}; \qquad 0 \quad y_0 \quad R_i: \tag{2.12b}$$

2.3.1 Association probability

To derive association probability, let us first characterize the association event $S_{\ j}$ as:

$$\mathbf{1}_{S_{\ j}} = \mathbf{1}(\arg \max_{k2K_1} P_k R_k \quad = j) = \prod_{k2K_1 \backslash} \mathbf{1} \ R_k > P_{jk} R_j \quad ; \tag{2.13}$$

where $P_{jk} = \frac{P_k}{P_j}^{1=}$ and $\mathbf{1}(\ )$ is the indicator function of the random vector $\mathbf{R} = [R_0; R_1; :::; R_k]$. Note that since the 0^{th} tier is derived from the i^{th} tier, we have $P_0 \quad P_i$. The association probability for each tier is now defined as follows.

2.3. Association probability and serving distance

Definition 2.4. Association probability, A_j for j^{th} tier, $8j \ 2 \ K_1$ is defined as the probability that the typical user will be served by the j^{th} tier. It can be mathematically expressed as

$$A_j = \mathrm{P}(S_{\ j}): \tag{2.14}$$

The following Lemma deals with the conditional association probability to $_j$.

Lemma 2.5. *Conditional association probability of the j^{th} tier given $V_0 = v_0$ is*

$$A_{jjv_0} = \begin{cases} \mathrm{E}_{Y_0}\left[\prod_{k=1} \overline{F}_{R_k}(P_{0k}v_0 \ ^{\frac{1}{}}Y_0)\right] & \text{if } j = 0; \\ \mathrm{E}_{R_j}\left[\overline{F}_{Y_0}(v_0^{\frac{1}{}}P_{j0}R_j) \prod_{\substack{k=1 \\ k\neq j}} \overline{F}_{R_k}(P_{jk}R_j)\right] & \text{otherwise:} \end{cases} \tag{2.15}$$

Proof. According to the definition of $S_{\ j}$ in (2.13), we can write from (2.14),

$$\begin{aligned} A_{jjv_0} &= \mathrm{E}_{\mathbf{R}}\left[\prod_{k2K_1 nfjg} \mathbf{1}\ R_k > P_{jk}R_j \ \ jV_0 = v_0\right] \\ &\overset{(a)}{=} \mathrm{E}_{R_j}\left[\prod_{\substack{k=0 \\ k\neq j}} \mathrm{P}\ R_k > P_{jk}R_j jv_0\right] = \mathrm{E}_{R_j}\left[\prod_{\substack{k=0 \\ k\neq j}} \overline{F}_{R_k}(P_{jk}R_j jv_0)\right]; \end{aligned} \tag{2.16}$$

where (a) comes from the fact that $_k$-s are independent, hence are R_k-s. For the rest of the proof, we need to consider the two cases of $j = 0$ and $j \neq 0$ separately. Note that only the RV R_0 among all R_j-s is the function of V_0. For **case 1:** $j = 0$

$$A_{jjv_0} = \mathrm{E}_{R_0}\left[\prod_{k=1} \overline{F}_{R_k}(P_{jk}R_0 jv_0)\right] = \mathrm{E}_{Y_0}\left[\prod_{k=1} \overline{F}_{R_k}(P_{0k}v_0 \ ^{\frac{1}{}}Y_0)\right];$$

and for **case 2:** $j \ 2 \ K$

$$\begin{aligned} A_{jjv_0} &= \mathrm{E}_{R_j}\left[\prod_{\substack{k=0 \\ k\neq j}} \mathrm{P}(R_k > P_{jk}R_j jv_0)\right] = \mathrm{E}_{R_j}\left[\mathrm{P}(v_0 \ ^{\frac{1}{}}Y_0 > P_{j0}R_j) \prod_{\substack{k=1 \\ k\neq j}} \mathrm{P}(R_k > P_{jk}R_j)\right] \\ &= \mathrm{E}_{R_j}\left[\overline{F}_{Y_0}(v_0^{\frac{1}{}}P_{j0}R_j) \prod_{\substack{k=1 \\ k\neq j}} \overline{F}_{R_k}(P_{jk}R_j)\right]: \end{aligned}$$

□

Remark 2.6. Association probabilities of the j^{th} tier can be obtained by taking expectation over A_{jjV_0} with respect to V_0, i.e.,

$$A_j = \mathrm{E}_{V_0}(A_{jjV_0}): \tag{2.17}$$

From Lemma 2.5, we can obtain the expressions for the association probabilities to different open access tiers when Φ_i^u is Thomas or Matérn cluster process. The conditional probabilities in these cases can be reduced to closed form expressions. The results are presented next.

Corollary 2.7. *When Φ_i^u is a Thomas cluster process, conditional association probability of the j^{th} tier given $V_0 = v_0$ is:*

$$A_{j|v_0} = \frac{\bar{\lambda}_j}{\sum_{k=0}^{K} P_{jk}^2 \bar{\lambda}_k}; \ \forall j \in K_1; \tag{2.18}$$

where $\bar{\lambda}_0$ is defined as $\bar{\lambda}_0 = \frac{v_0^2}{2\sigma_i^2}$:

Proof. When $j = 0$, from (2.15), we get, $A_{0|v_0} = \int_{y_0>0} \prod_{k=1}^{K} \bar{F}_{R_k}(P_{0k} v_0^{-1} y_0) \, f_{Y_0}(y_0) \, dy_0$:

Substituting $f_{Y_0}(y_0)$ from (2.11a) and $\bar{F}_{R_k}(P_{0k} v_0^{-1} y_0)$ from (2.8b), we get,

$$A_{0|v_0} = \int_0^{\infty} \exp\left(-\sum_{k=1}^{K} \bar{\lambda}_k P_{0k}^2 v_0^2 y_0^2\right) \frac{y_0}{\sigma_i^2} \exp\left(-\frac{y_0^2}{2\sigma_i^2}\right) dy_0 = \frac{\frac{v_0^2}{2\sigma_i^2}}{\frac{v_0^2}{2\sigma_i^2} + \sum_{k=1}^{K} P_{0k}^2 \bar{\lambda}_k}:$$

Putting $\bar{\lambda}_0 = \frac{v_0^2}{2\sigma_i^2}$, we get the desired result. Note that $P_{00} = 1$. For $j \neq 0$,

$$A_{j|v_0} = \int_0^{\infty} \bar{F}_{Y_0}(v_0^{-1} P_{j0} R_j) \prod_{\substack{k=1 \\ k \neq j}}^{K} \bar{F}_{R_k}(P_{jk} r_j) f_{R_j}(r_j) \, dr_j$$

$$= \int_0^{\infty} \exp\left(-\frac{(P_{j0} v_0^{-1} r_j)^2}{2\sigma_i^2}\right) \exp\left(-\sum_{\substack{k=1 \\ k \neq j}}^{K} \bar{\lambda}_k P_{jk}^2 r_j^2\right)$$

$$2\bar{\lambda}_j \exp(-\bar{\lambda}_j r_j^2) \, r_j \, dr_j = \frac{\bar{\lambda}_j}{\frac{P_{j0}^2}{2\sigma_i^2} + \sum_{k=1}^{K} P_{jk}^2 \bar{\lambda}_k} = \frac{\bar{\lambda}_j}{\sum_{k=0}^{K} P_{jk}^2 \bar{\lambda}_k}:$$

The last step was derived by putting $\bar{\lambda}_0 = \frac{v_0^2}{2\sigma_i^2}$. □

Corollary 2.8. *If Φ_i^u is a Matérn cluster process, conditional association probability of the j^{th} tier given $V_0 = v_0$ is:*

$$A_{j|v_0} = \begin{cases} \frac{v_0^2}{R_i^2 Z_0} \left(1 - \exp\left(-v_0^2 Z_0 R_i^2\right)\right) & \text{if } j = 0 \\ \frac{\pi \lambda_j}{\sum_{k=1}^{K} \pi \lambda_k P_{jk}^2 - \alpha_k} \left(\pi \lambda_j P_{j0}^2 v_0^2\right)^{1 - \exp(-\pi \lambda_j R_i^2)(Z_j R_i^2 + 1)} & \text{if } j \in \mathcal{K} \end{cases}; \tag{2.19}$$

where $Z_j = \sum_{k=1}^{K} \pi \lambda_k P_{jk}^2, \forall j \in \mathcal{K}_1$.

Proof. Similar to Corollary 2.7, for $j = 0$, plugging (2.8b) and (2.12a) in (2.15), we get,

$$A_{0|v_0} = \int_0^{R_i} \exp\left(-\sum_{k=1}^{K} \pi \lambda_k P_{0k}^2 v_0^2 y_0^2\right) \frac{2y_0}{R_i^2} \, dy_0 = \frac{v_0^2}{R_i^2 Z_0} \left(1 - \exp\left(-v_0^2 Z_0 R_i^2\right)\right);$$

where $Z_0 = \sum_{k=1}^{K} \pi \lambda_k P_{0k}^2$. Now for $j \in \mathcal{K}$, using (2.8a), (2.8b) and (2.12b) in (2.14) and proceeding according to the proof of Corollary 2.7, we get,

$$A_{j|v_0} = 2\pi\lambda_j \int_0^{R_i} \exp\left(-\sum_{k=1}^{K} \pi \lambda_k P_{jk}^2 r_j^2\right) \left(\frac{R_i^2 - (P_{j0} v_0^{-1} r_j)^2}{R_i^2}\right)^{+} r_j \, dr_j$$

$$= \frac{\pi \lambda_j}{\sum_{k=1}^{K} \pi \lambda_k P_{jk}^2 - \alpha_k} \left(\pi \lambda_j P_{j0}^2 v_0^2\right)^{1 - \exp(-\pi \lambda_j R_i^2)(Z_j R_i^2 + 1)}; \quad \text{where } Z_j = \sum_{k=1}^{K} \pi \lambda_k P_{jk}^2 \text{ for } j \in \mathcal{K}.$$

□

2.3.2 Serving distance distribution

In this section, we derive the distribution of $\|x\|$ when $\mathbf{1}_{S_j} = 1$, i.e., the serving distance from the typical user to its serving BS when it is in Φ_j. We will call this RV W_j. Conditioned on S_j, W_j is simply the distance to the nearest BS in Φ_j. Hence W_j is related to R_j as $W_j = R_j | S_j$. The conditional PDF of W_j given $V_0 = v_0$ is derived in the next Lemma.

Lemma 2.9. *Conditional distribution of serving distance W_j at $V_0 = v_0$ is obtained by*

$$f_{W_0|V_0}(w_0|v_0) = \frac{1}{A_{0|v_0}} \prod_{k=1}^{K} v_0^{-1} \overline{F}_{R_k}\left(P_{0k} w_0\right) f_{Y_0}(v_0^{-1} w_0)$$

$$f_{W_j|V_0}(w_j|v_0) = \frac{1}{A_{j|v_0}} \overline{F}_{Y_0}(v_0^{-1} P_{j0} w_j) \prod_{\substack{k=1 \\ k \neq j}}^{K} \overline{F}_{R_k}(P_{jk} w_j) f_{R_j}(w_j), \forall j \in \mathcal{K}. \tag{2.20}$$

Proof. The conditional CCDF of W_j in this case is, $\mathrm{P}[W_j > w_j | V_0] =$

$$\mathrm{P}[R_j > w_j | S_j; V_0] = \frac{\mathrm{P}(R_j > w_j | V_0; S_j | V_0)}{\mathrm{P}(S_j | V_0)} \overset{(a)}{=} \frac{1}{A_{j|v_0}} \prod_{\substack{k=1 \\ k \neq j}}^{K} \mathrm{P}(P_j R_j^{-} > P_k R_k^{-} | R_j > w_j; V_0) \ ;$$

where (a) follows from (2.16). For **case 1:** when $j = 0$, given $V_0 = v_0$, $\mathrm{P}[W_0 > w_0 | V_0 = v_0] =$

$$\frac{1}{A_{0|v_0}} \prod_{k=1}^{K} \mathrm{P}(P_0 v_0^{-} Y_0^{-} > P_k R_k^{-} | v_0^{-1} Y_0 > w_0) = \frac{1}{A_{0|v_0}} \int_{v_0^{-1} w_0}^{\infty} \prod_{k=1}^{K} \overline{F}_{R_k}(P_{0k} v_0^{-1} y_0) f_{Y_0}(y_0) \, \mathrm{d}y_0.$$

Thus, the conditional distribution of W_0 is obtained by

$$f_{W_0|V_0}(w_0 | v_0) = \frac{\mathrm{d}}{\mathrm{d}w_0} (1 - \mathrm{P}[W_0 > w_0 | V_0 = v_0]) = v_0^{-1} \frac{\prod_{k=1}^{K} \overline{F}_{R_k}(P_{0k} w_0) f_{Y_0}(v_0^{-1} w_0)}{A_{0|v_0}}.$$

For **case 2:** when $j \in K$,

$$\mathrm{P}[W_j > w_j | v_0] = \frac{1}{A_{j|v_0}} \mathrm{P}(v_0^{-1} Y_0 > P_{j0} R_j) \prod_{k=1, k \neq j}^{K} \mathrm{P}(P_j R_j^{-} > P_k R_k^{-} | R_j > w_j).$$

The rest of the proof continues in the same line of case 2 in Lemma 2.5. □

Further, we obtain closed-form expressions of $f_{W_j|V_0}(\cdot)$ for Thomas and Matérn cluster processes by putting the corresponding PDFs and CCDFs in the following Corollaries.

Corollary 2.10. *If Φ_u is Thomas cluster process, conditional PDF of serving distance given $V_0 = v_0$ can be expressed as*

$$f_{W_j|V_0}(w_j | v_0) = \frac{2 \pi \lambda_j}{A_{j|v_0}} \exp\left(-\pi \sum_{k=1}^{K} \lambda_k P_{jk}^{2/\alpha} \left(w_j^2 - w_j^2 \right) \right); \ \forall j \in K_1. \tag{2.21}$$

Proof. The serving distance distribution when the user is served by its own cluster center is

$$f_{W_0|V_0}(w_0 | v_0) = \frac{v_0^{-1}}{A_{0|v_0}} \prod_{k=1}^{K} \overline{F}_{R_k}(P_{0k} w_0) f_{Y_0}(v_0^{-1} w_0).$$

Substituting $\overline{F}_{R_k}(P_{0k} w_0)$ from (2.8b) and $f_{Y_0}(v_0^{-1} w_0)$ from (2.11a),

$$f_{W_0|V_0}(w_0 | v_0) = \frac{v_0^{-1}}{A_{0|v_0}} \prod_{k=1}^{K} \exp\left(-\lambda_k P_{0k}^{2/\alpha} w_0^2 \right) \frac{v_0^{-1} w_0}{\frac{2}{\alpha}} \exp\left(-\frac{v_0^{2/\alpha} w_0^2}{2^{\frac{2}{\alpha}}} \right). \tag{2.22}$$

Putting $\bar{}_0$ as defined before, we obtain the desired result. For other open access tiers except the 0^{th} tier we can perform similar steps to find $f_{W_j|V_0}(w_j|v_0)$. Starting from Lemma 2.9,

$$f_{W_j|V_0}(w_j|v_0) = \frac{1}{A_{j|v_0}} \bar{F}_{Y_0}(v_0^{\frac{1}{}} P_{j0} w_j) \prod_{\substack{k=1 \\ k \in j}}^{K} \bar{F}_{R_k}(P_{jk} w_j) f_{R_j}(w_j)$$

$$\overset{(a)}{=} \frac{1}{A_{j|v_0}} \exp\left(-\frac{v_0^{\frac{2}{}} P_{j0}^2 w_j^2}{2\ ^2_i}\right) \exp\left(\sum_{\substack{k=1 \\ k \in j}}^{K} -_k P_{jk}^2 w_j^2\right) 2\ ^-_j \exp\left(-^-_j w_j^2\right) w_j$$

$$= \frac{2\ ^-_j}{A_{j|v_0}} \exp\left(-\sum_{k=0}^{K} -_k P_{jk}^2 w_j^2\right) w_j;$$

where (a) follows from substitution of $f_{R_j}(\,)$, $\bar{F}_{R_k}(\,)$, $\bar{F}_{R_0}(\,)$ by (2.8a), (2.8b) and (2.11b). □

Corollary 2.11. *If ^u_i is Matérn cluster process, the conditional distribution of serving distance W_j given $V_0 = v_0$ can be expressed as*

$$f_{W_j|V_0}(w_j|v_0) = \begin{cases} \frac{1}{A_{0|v_0}} \exp\left(-\sum_{k=1}^{K} -_k P_{0k}^2 w_0^2 \ \frac{2v_0^{\frac{2}{}} w_0}{R_i^2}\right) & \text{if } j = 0 \\ \frac{1}{A_{j|v_0}} 2\ ^-_j \exp\left(-\sum_{k=1}^{K} -_k P_{jk}^2 w_j^2 \ \frac{R_i^2 \ v_0^{\frac{2}{}} w_j^2}{R_i^2}\right) w_j & \text{if } j \ 2\ K \end{cases}; \tag{2.23}$$

where $0 \quad w_j \quad R_i$. For $w_j > R_i$, $f_{W_j|V_0}(w_j|v_0) = 0$; $8j\ 2\ K_1$.

Proof. Substituting $f_{Y_0}(\,)$ for Matérn cluster process from (2.12a) and CCDF of R_k from (2.8b) in (2.20) and proceeding as before, $f_{W_0|V_0}(\,)$ can be derived. Similarly, $f_{W_j|V_0}(\,)$ is obtained by substituting $\bar{F}_{Y_0}(\,)$ from (2.12b). For $w_j > R_i$, $f_{W_j|V_0}(w_j|v_0) = 0$, $8j\ 2\ K_1$ as $f_{Y_0}(\,)$ and $\bar{F}_{Y_0}(\,)$ take zero value beyond this range. □

2.4 Coverage probability analysis

This is the second technical section of the chapter where we use the association probability and the distance distribution results obtained in the previous section to derive easy-to-use expressions for the coverage probability of a typical user of ^u_i in a *user-centric* deployment.

According to the association policy, it is easy to deduce that if the typical user is served by a BS $2\ _j$ located at a distance W_j, there exist no k^{th} tier BSs, $8k\ 2\ K_1$, within a disc of radius $P_{jk}W_j$ centered at the location of typical user (origin). We denote this *exclusion disc* by $b(\mathbf{0}; P_{jk}W_j)$. Assuming association with the j^{th} tier, the total interference experienced by the typical user originates from two independent sets of BSs: (i) $[_{k2K_1\ \ k}\, n\ b(\mathbf{0}; W_j)$, the set of open access BSs lying beyond the exclusion zone $b(\mathbf{0}; W_j)$ and (ii) $[_{k2K\ \ \emptyset_k}$,

the set of closed access BSs. As all the interferers from the k^{th} open access tier will lie outside $b(0; P_{jk}W_j)$, we define interference from the k^{th} open-access tier as $I_{o(j;k)}(W_j) = \sum_{x_k \in \Phi_k \setminus b(0;P_{jk}W_j)} P_k h_{x_k k} \|x_k\|^{-\alpha}$. We express the total contribution of interference from all open access tiers as

$$I_{o(j)}(W_j) = \sum_{k=0}^{K} I_{o(j;k)}(W_j). \tag{2.24}$$

It is clear that the interference from the open-access tiers defined above depends on the serving distance W_j. However, it is not the case with the closed access tiers. Recall that since the closed access tiers do not participate in the cell selection procedure, there is no exclusion zone in their interference field. In particular, the closed access BSs may lie closer to the typical user than its serving BS. We denote the closed access interference by $I_c = \sum_{k=1}^{K} I_{c(k)}$, where $I_{c(k)}$ is the interference from all the BSs of the k^{th} closed access tier Φ_k^0. Using the variables defined above, we can now express SIR defined in (2.7) at the typical user when it is served by the BS located at a distance W_j in a compact form as a function of the RV W_j as: $\mathrm{SIR}(W_j) = \frac{P_j h_{x_j} W_j^{-\alpha}}{I_{o(j)}(W_j) + I_c}$.

2.4.1 Coverage probability

A typical user is said to be in coverage if $\mathrm{SIR}(W_j) > \theta$, where θ denotes modulation-coding specific SIR threshold required for successful reception. The coverage probability can now be formally defined as follows.

Definition 2.12 (Coverage probability)**.** Per-tier coverage probability for Φ_j can be defined as the probability that the typical user of Φ_i^u is in coverage conditioned on the fact that it is served by a BS from Φ_j. Mathematically,

$$\mathrm{P_c}^{(i)}_j = \mathrm{E}(\mathbf{1}(\mathrm{SIR}(W_j) > \theta)). \tag{2.25}$$

The total coverage probability $\mathrm{P_c}^{(i)}$ can now be defined in terms of the per-tier coverage probability as

$$\mathrm{P_c}^{(i)} = \sum_{j=0}^{K} A_j \mathrm{P_c}^{(i)}_j, \tag{2.26}$$

where A_j is given by (2.14).

With the expressions of $A_{j|V_0}$ and $f_{W_j|V_0}(\cdot)$ at hand, we focus on the derivation of coverage probability $\mathrm{P_c}^{(i)}$. Note that using the Rayleigh fading assumption along with the fact that the open access interference terms $\{I_{o(j;k)}\}$ and the closed access interference terms $\{I_{c(k)}\}$ are all independent of each other, we can express the per-tier coverage probability in terms of the product of Laplace transforms of these interference terms. This result was presented for a special case of Thomas cluster process in the conference version of this chapter [60] (for K-tier HetNets) as well as in [61] (for single-tier cellular networks).

2.4. Coverage probability analysis

Theorem 2.13 (Coverage probability). *Conditional per-tier coverage probability of the typical user from* $\mathcal{U}_i$ *given that the serving BS being from the* j^{th} *tier and* $V_0 = v_0$ *is*

$$\mathtt{P}_{\mathtt{c}|jv_0}^{(i)} = \int_{w_j>0} \mathcal{L}_{I_{o(j;0)}|jV_0}\left(\frac{w_j}{P_j}|jv_0\right) \prod_{k=1}^{K} \mathcal{L}_{I_{o(j;k)}}\left(\frac{w_j}{P_i}\right) \mathcal{L}_{I_{c(k)}}\left(\frac{w_j}{P_j}\right) f_{W_j|jV_0}(w_j|jv_0)\,\mathrm{d}w_j; \quad (2.27)$$

and the coverage probability of a typical user from $\mathcal{U}_i$ *can be expressed as*

$$\mathtt{P}_{\mathtt{c}}^{(i)} = \mathtt{E}_{V_0}\left[\sum_{j=0}^{K} A_{j|jV_0} \mathtt{P}_{\mathtt{c}|jV_0}^{(i)}\right]; \quad (2.28)$$

where $\mathcal{L}_{I_{o(j;0)}|jV_0}(s|jv_0)$ *is the conditional Laplace transform of* $I_{o(j;0)}$*, i.e.,*

$$\mathcal{L}_{I_{o(j;0)}|jV_0}(s|jv_0) \triangleq \mathtt{E}\left[\exp(-sI_{o(j;0)})|jV_0 = v_0\right]$$

and $\mathcal{L}_{I_{o(j;k)}}(s) \triangleq \mathtt{E}\left[\exp(-sI_{o(j;k)})\right]$; $\mathcal{L}_{I_{c(k)}}(s) \triangleq \mathtt{E}\left[\exp(-sI_{c(k)})\right]$ *respectively denote the Laplace transforms of interference of the* k^{th} *open and closed access tiers (*$k \in K$*).*

Proof. Recalling the definition of $\mathtt{P}_{\mathtt{c}_j}^{(i)}$ in (2.25), we first calculate the conditional probability, $\mathtt{P}(\mathtt{SIR}(W_j) > \tau | W_j = w_j; V_0 = v_0)\ \forall j \in K_1$. The final result can be obtained by taking expectation with respect to W_j and V_0. For **case 1:** when $j \in K$,

$$\begin{aligned}
&\mathtt{P}\left(\frac{P_j h_x | w_j}{\sum_{k=0}^{K} I_{o(j;k)} + I_c} > \tau | V_0 = v_0\right) \\
&\overset{(a)}{=} \mathtt{E}\left[\exp\left(-\frac{w_j}{P_j}\tau\left(\sum_{k=0}^{K} I_{o(j;k)} + I_{c(k)}\right)\right) | jV_0 = v_0\right] \\
&\overset{(b)}{=} \mathtt{E}\left[\exp\left(-\frac{w_j}{P_j}\tau I_{o(j;0)}\right) | jV_0 = v_0\right] \mathtt{E}\left[\exp\left(-\frac{w_j}{P_j}\tau\sum_{k=1}^{K} I_{o(j;k)}\right)\right] \mathtt{E}\left[\exp\left(-\frac{w_j}{P_j}\tau\sum_{k=1}^{K} I_{c(k)}\right)\right] \\
&= \mathcal{L}_{I_{o(j;0)}}\left(\frac{w_j}{P_j}\tau|jv_0\right) \prod_{k=1}^{K} \mathcal{L}_{I_{o(j;k)}}\left(\frac{w_j}{P_j}\tau\right) \prod_{k=1}^{K} \mathcal{L}_{I_{c(k)}}\left(\frac{w_j}{P_j}\tau\right);
\end{aligned}$$

where (a) follows from $h_j \sim \exp(1)$, (b) is due to the independence of the interference from open and closed access tiers. Also note that none of the interference components except $I_{o(j;0)}$ depends on V_0.

Case 2: For $j = 0$, no contribution due to $I_{o(0;0)}$ will be accounted for. Hence,

$$\mathtt{P}(\mathtt{SIR}(W_0) > \tau | W_0 = w_0) = \prod_{k=1}^{K} \mathcal{L}_{I_{0(0;k)}}\left(\frac{w_0}{P_j}\tau\right) \prod_{k=1}^{K} \mathcal{L}_{I_{c(k)}}\left(\frac{w_0}{P_j}\tau\right);$$

□

Note that the conditioning on V_0 appears only in the first term, i.e. the Laplace transform of $I_{o(j;0)}$ since the interference from the BS at cluster center is only influenced by V_0 while the other interference terms are independent of V_0.

2.4.2 Laplace transform of interference

As evident from Theorem 2.13, the Laplace transform of interference from different tiers are the main components of the coverage probability expression. The following three Lemmas deal with the Laplace transforms of the interference from different tiers. We first focus on the interference originating from all the open access tiers except the interference from the 0^{th} tier which requires separate treatment.

Lemma 2.14. *Given a typical user of $^{u}_{i}$ is served by a BS 2 $_{j}$ $(j \ 2 \ K)$ at a distance $W_j = w_j$, Laplace transform of $I_{o(j;k)}$, $8k \ 2 \ K$, evaluated at $s = \frac{w_j}{P_j}$ is*

$$\mathcal{L}_{I_{o(j;k)}}\left(\frac{w_j}{P_j}\right) = \exp\left(-P_{jk}^{2}\,{}_{k}\mathcal{G}(\ ;\ )w_j^{2}\right); \tag{2.29}$$

$$\text{with} \quad \mathcal{G}(\ ;\ ) = \frac{2}{2}\,{}_2F_1\left[1;1-\frac{2}{};2-\frac{2}{};-\right]; \tag{2.30}$$

where ${}_2F_1[a;b;c;t] = \frac{(c)}{(b)\ (c\ \ b)}\int_0^{1}\frac{z^{b\ \ 1}(1\ \ z)^{c\ \ b\ \ 1}}{(1\ \ tz)^{a}}dz$ *is Gaussian Hypergeometric function.*

Proof. By definition, the Laplace transform of interference is $\mathcal{L}_{I_{o(j;k)}}(s) = \mathrm{E}(\exp(-sI_{o(j;k)})) =$

$$\mathrm{E}\left[\exp\left(-s\sum_{x_k\in\Phi_k\setminus b(0;P_{jk}W_j)}P_k h_x\|x_k\|^{-}\right)\right] \overset{(a)}{=} \mathrm{E}_{\Phi_k}\left[\prod_{x_k\in\Phi_k\setminus b(0;P_{jk}W_j)}\mathrm{E}_{h_k}\left[\exp\left(-sP_k h_x\|x_k\|^{-}\right)\right]\right]$$

$$\overset{(b)}{=} \mathrm{E}_{\Phi_k}\left[\prod_{x_k\in\Phi_k\setminus b(0;P_{jk}W_j)}\frac{1}{1+sP_k\|x_k\|^{-}}\right] \overset{(c)}{=} \exp\left(-2\ ^{-}_{k}\int_{P_{jk}W_j}^{\infty}\left(1-\frac{1}{1+sP_k r}\right)r\,dr\right); \tag{2.31}$$

where (a) is due to the i.i.d. assumption of h_k, (b) follows from h_k exp(1), (c) follows from the transformation to polar coordinates and probability generating functional of homogeneous PPP [54]. The final result can be obtained by using the integral in [62, Eq. 3.194.1]. □

After dealing with the interference from all open access tiers $_k$ $8k \ 2 \ K$, we now focus on the 0^{th} tier, which consists of only the cluster center.

Lemma 2.15. *Given a typical user of $\overset{u}{i}$ connects to the BS 2 $_j$ with j 2 K at a distance $W_j = w_j$, the Laplace transform of $I_{o(j;0)}$ at $s = \frac{w_j}{P_j}$ conditioned on $V_0 = v_0$ is*

$$\mathcal{L}_{I_{o(j;0)}|V_0}\left(\frac{w_j}{P_j}\,v_0\right) = \int_{y_0 > v_0^{\frac{1}{-}} P_{ji} w_j} \frac{1}{1 + \frac{y_0}{v_0^{\frac{1}{-}} P_{ji} w_j}} \frac{f_{Y_0}(y_0)}{\overline{F}_{Y_0}(v_0^{\frac{1}{-}} P_{ji} w_j)}\, dy_0. \tag{2.32}$$

Proof. Recall that since the 0^{th} tier is created from the i^{th} open-access tier, the transmit power P_0 P_i. If the serving BS 2 $_j$ (j 2 K) lies at a distance $W_j = w_j$, due to the formation of virtual exclusion zone around the typical user, the cluster center acting as an interferer will lie outside $b(\mathbf{0}; P_{ji} w_j)$. Thus, the PDF of distance from the typical user to cluster center conditioned on $Y_0 > v_0^{\frac{1}{-}} P_{ji} w_j$ is $f_{Y_0}(y_0 | Y_0 > v_0^{\frac{1}{-}} P_{ji} w_j) = \frac{f_{Y_0}(y_0)}{\overline{F}_{Y_0}\left(v_0^{\frac{1}{-}} P_{ji} w_j\right)}$, where $y_0 > v_0^{\frac{1}{-}} P_{ji} w_j$. The conditional Laplace transform $\mathcal{L}_{I_{o(j;0)}|V_0}(s|v_0)$ can be expressed as

$$\begin{aligned}
&\mathrm{E}_{Y_0}\ \mathrm{E}_{h_0}\ \exp\left(-sP_i h_0 v_0 Y_0\right) \Big| Y_0 > P_{ji} w_j \\
&\overset{(a)}{=} \mathrm{E}_{Y_0}\left[\frac{1}{1 + sP_i v_0 Y_0} \Big| Y_0 > v_0^{\frac{1}{-}} P_{ji} w_j\right] \\
&= \int_{y_0 > v_0^{\frac{1}{-}} P_{ji} w_j} \frac{1}{1 + sP_i v_0 y_0} f_{Y_0}(y_0 | Y_0 > v_0^{\frac{1}{-}} P_{ji} w_j)\, dy_0 \\
&= \int_{y_0 > v_0^{\frac{1}{-}} P_{ji} w_j} \frac{1}{1 + sP_i v_0 y_0} \frac{f_{Y_0}(y_0)}{\overline{F}_{Y_0}\left(v_0^{\frac{1}{-}} P_{ji} w_j\right)}\, dy_0;
\end{aligned} \tag{2.33}$$

where (a) follows from h_0 $\exp(1)$. This completes the proof. □

In the next Corollary, we provide closed form upper and lower bounds on the Laplace transform of interference from the BS at 0^{th} tier. The lower bound is obtained by placing the BS located at the cluster-center of the typical user on the boundary of the exclusion disc $b(\mathbf{0}; P_{ji} w_j)$. The upper bound is found by simply ignoring the interference from this BS. These bounds will be used later in this section to derive tight bounds on coverage probability.

Corollary 2.16. *Conditional Laplace transform of $I_{o(j;0)}$ given $V_0 = v_0$ at $s = \frac{w_j}{P_j}$ is bounded by*

$$\frac{1}{1 +} \quad \mathcal{L}_{I_{o(j;0)}|V_0}\left(\frac{w_j}{P_j}\,v_0\right) \quad 1. \tag{2.34}$$

Proof. Following from (2.33)

$$\mathcal{L}_{I_{o(j;0)jV_0}}(sjv_0) = \mathrm{E}_{Y_0}\left[\frac{1}{1+sP_iv_0Y_0}\,jY_0 > v_0^{\frac{1}{\cdot}}P_{ji}w_j\right]\left[\frac{1}{1+sP_iv_0y_0}\right]_{y_0=v_0^{\frac{1}{\cdot}}P_{ji}w_j}:$$

Substation of $s = \frac{w_j}{P_j}$ gives the final result. The upper bound can be obtained by

$$\mathcal{L}_{I_{o(j;0)jV_0}}(sjv_0) = \mathrm{E}_{Y_0}\left[\frac{1}{1+sP_iv_0Y_0}\,jY_0 > v_0^{\frac{1}{\cdot}}P_{ji}w_j\right]\lim_{y_0\,!\,1}\frac{1}{1+sP_iv_0y_0} = 1:$$

□

Lemma 2.17. *Given the typical user of* $\overset{u}{i}$ *connects to any BS* 2 $_j$ *at a distance* $W_j = w_j$, *8j* 2 K_1, *the Laplace transform of* $I_{c(k)}$ *at* $s = \frac{w_j}{P_j}$ *is*

$$\mathcal{L}_{I_{c(k)}}\left(\frac{w_j}{P_j}\right) = \exp\left(-\overline{\cdot}^{0}{}_kH(\ ;\ )(P_{jk}w_j)^2\right);\tag{2.35}$$

$$\textit{where}\quad H(\ ;\ ) = {}^{2=}\frac{2\csc(\frac{2}{-})}{}.\tag{2.36}$$

Proof. The proof of this fairly well-known result follows in the same lines as that of Lemma 2.14, with the only difference being the fact that $I_{c(k)}$ is independent of W_j and hence, the lower limit of the integral in (2.31) will be zero. The final form can be obtained by some algebraic manipulations and using the properties of Gamma function [62, Eq. 3.241.2]. □

The expressions of Laplace transforms of interference derived in the above three Lemmas are substituted in (2.27) to get the coverage probability. The results for no shadowing is readily obtained by putting V_k 1, which omits the final deconditioning step with respect to V_0.

Corollary 2.18 (No shadowing)**.** *Under the assumption of no shadowing, the coverage probability of a typical user belonging to* $\overset{u}{i}$ *can be expressed as*

$$\mathrm{P_c}^{(i)} = A_0\mathrm{P_{c0}}^{(i)} + \sum_{j=1}^{K} A_j\mathrm{P_{cj}}^{(i)};\quad \textit{with}\tag{2.37}$$

$$\mathrm{P_{c0}}^{(i)} = \frac{1}{A_0}\int_{w_0>0}\exp\left(-\sum_{k=1}^{K}P_{0k}^2(\ _k(G(\ ;\ )+1)+\ ^{0}_kH(\ ;\ ))w_0^2\right)f_{Y_0}(w_0)\,\mathrm{d}w_0;\tag{2.38}$$

$$\mathrm{P_{cj}}^{(i)} = \frac{2\ \ _j}{A_j}\int_{w_j>0}\exp\left(-\sum_{k=1}^{K}P_{jk}^2(\ _k(G(\ ;\ )+1)+\ ^{0}_kH(\ ;\ ))w_j^2\right)$$

$$\int_{y_0 > P_{j\,i} w_j} \frac{f_{Y_0}(y_0)}{1 + (\frac{y_0}{P_{j\,i} w_j})} \mathrm{d}y_0 \, w_j \, \mathrm{d}w_j; \tag{2.39}$$

where A_j *is the association probability to* $^{(\mathrm{BS};o)}_{j}$ *given by:* $A_j = \mathrm{E}_{Y_j}\left[\prod_{\substack{k=0 \\ k \in \mathcal{K}, k \neq j}} \overline{F}_{Y_k}(P_{jk} Y_j)\right]$; $8k \in K_1$:

Note that the PDF and CCDF of Y_k for $k \in K$ can be obtained by replacing $\bar{}_k$ ($\bar{}^{0}_{k}$) by $_k$ ($^{0}_{k}$) in (2.8).

2.4.3 Bounds on coverage probability

In this section, we derive upper and lower bounds on coverage probability $\mathrm{P_c}^{(i)}$ by using the results obtained in Corollary 2.16.

Proposition 2.19 (Bounds on Coverage)**.** *The conditional per-tier coverage probability for* $j \in K$ *can be bounded as* $\mathrm{P_c}^{(i);L}_{jjV_0} \leq \mathrm{P_c}^{(i)}_{jjV_0} \leq \mathrm{P_c}^{(i);U}_{jjV_0}$, *where*

$$\mathrm{P_c}^{(i);U}_{jjV_0} = \int_{w_j > 0} \prod_{k=1}^{K} L_{I_{o(j;k)}}\left(\frac{w_j}{P_i}\right) L_{I_{c(k)}}\left(\frac{w_j}{P_j}\right) f_{W_j|V_0}(w_j|v_0)\mathrm{d}w_j \quad \text{and} \tag{2.40}$$

$$\mathrm{P_c}^{(i);L}_{jjV_0} = \frac{1}{1 + \int_{w_j > 0} \prod_{k=1}^{K} L_{I_{o(j;k)}}\left(\frac{w_j}{P_i}\right) L_{I_{c(k)}}\left(\frac{w_j}{P_j}\right) f_{W_j|V_0}(w_j|v_0)\mathrm{d}w_j}. \tag{2.41}$$

Hence, from (2.28)*, coverage probability* $\mathrm{P_c}^{(i)}$ *can be bounded by*

$$\left[\mathrm{E}_{V_0}\left[A_{0|V_0}\mathrm{P_c}^{(i)}_{jjV_0} + \sum_{j=1}^{K} A_{j|V_0}\mathrm{P_c}^{(i);L}_{jjV_0}\right]\right] \leq \mathrm{P_c}^{(i)} \leq \left[\mathrm{E}_{V_0}\left[A_{0|V_0}\mathrm{P_c}^{(i)}_{jjV_0} + \sum_{j=1}^{K} A_{j|V_0}\mathrm{P_c}^{(i);U}_{jjV_0}\right]\right]. \tag{2.42}$$

Proof. Using Corollary 2.16, bounds on $\mathrm{P_c}^{(i)}_{jjV_0}$ can be directly obtained by substituting the bounds on $L_{I_{o(j;0)|V_0}}(\,)$ from (2.34) in (2.27). □

For no shadowing, we can write simpler expressions for the upper and lower bound of $\mathrm{P_c}^{(i)}$. This result is presented in the following Proposition.

Proposition 2.20 (Bounds on Coverage: No Shadowing)**.** $\mathrm{P_c}^{(i)}_{j}$ *can be bounded by*

$$\frac{2\,{}_j}{A_j(1 + {}_j)} \int_{w_j > 0} \exp\left(-\sum_{k=1}^{K} P_{jk}^2(\,{}_k(G(\,;\,) + 1) + {}^{0}_{k}H(\,;\,))w_j^2\right) \overline{F}_{Y_0}(P_{j0}w_j)\, w_j \, \mathrm{d}w_j \quad \mathrm{P_c}^{(i)}_{j}$$

$$\frac{2\ \ j}{A_j}\int_{w_j>0}^{\infty}\exp\left(-\sum_{k=1}^{K}P_{jk}^2(\ \ _k(G(\ \ ;\ \ )+1)+\ \ _k^{0}H(\ \ ;\ \ ))w_j^2\right)\ \overline{F}_{Y_0}(P_{j0}w_j)\ w_j\ \mathrm{d}w_j: \tag{2.43}$$

The upper and lower bounds on $\mathrm{P_c}^{(i)}$ *can be obtained by substituting* $\mathrm{P_{c_j}}^{(i)}$ *with its upper and lower bounds in* (2.37).

It can be readily observed from Proposition 2.19 and 2.20 that the bounds on per-tier coverage probability (for $j\ \ 2\ \ K$) are simplified expressions due to the elimination of one integration by bounding $L_{I_{o(j;0)}}(\ \ )$. In the following Propositions, we present closed form bounds on coverage probability under no shadowing for Thomas and Matérn cluster processes. The tightness of the proposed bounds will be investigated in Section 2.5.2.

Proposition 2.21 (Bounds on Coverage: Thomas cluster process)**.** *When* $\ \ _i^{u}$ *is Thomas cluster process,* $\mathrm{P_c}^{(i)}$ *can be bounded by*

$$\frac{\ \ _0}{M_0}+\frac{1}{1+\ \ }\sum_{j=1}^{K}\frac{\ \ _j}{M_j}\quad \mathrm{P_c}^{(i)}\quad \sum_{j=0}^{K}\frac{\ \ _j}{M_j}; \tag{2.44}$$

where $M_j\ =\ \ _0+\sum_{k=1}^{K}P_{jk}^2(\ \ _k(G(\ \ ;\ \ )+1)+\ \ _k^{0}H(\ \ ;\ \ ))$.

Proposition 2.22 (Bounds on Coverage: Matérn cluster process)**.** *When* $\ \ _i^{u}$ *is Matérn cluster process,* $\mathrm{P_c}^{(i)}$ *can be bounded by*

$$P_0+\frac{1}{1+\ \ }\sum_{k=1}^{K}P_j\quad \mathrm{P_c}^{(i)}\quad P_0+\sum_{k=1}^{K}P_j; \tag{2.45}$$

where $P_j\ =\ A_j\mathrm{P_{c_j}}^{(i)}$ *which can be obtained by replacing* Z_j *by* $\sum_{k=1}^{K}P_{jk}^2(\ \ _k(G(\ \ ;\ \ )+1)+\ \ _k^{0}H(\ \ ;\ \ ))$, $\overline{\ \ }_k$ $(\overline{\ \ }_k)$ *by* $\ \ _k$ $(\ \ _k^{0})$ *and putting* $V_0\quad 1$ *in the expression of conditional association probability when* $\ \ _i^{u}$ *is a Matérn cluster process (*(2.19)*).*

2.4.4 Asymptotic analysis of coverage

In this section, we examine the limiting behavior of the coverage probability expressions with respect to the cluster size. As the cluster size increases, the typical user is pushed away from the cluster center, which reduces its association probability with the BS located at its cluster center. Also the interference and coverage provided by the BS at the cluster center will be diminished due to reduced received signal power from this BS.

As the cluster size increases, let us assume that the distance of the typical user from the cluster center Y_0 is scaled to $Z\ =\ \ Y_0$, where $\ \ >1$ is the scaling factor. Then, the

PDF of Z is $f_Z(z) = \frac{1}{}f_{Y_0}(z=\ )$. The scaling of the distance from the cluster center and increasing the cluster size are equivalent, for instance, when $\ _i^u$ is a Matérn cluster process, $0 < Y_0 < R_i$ implies that $0 < Z < \ R_i$. When $\ _i^u$ is Thomas cluster process, since the users have a Gaussian distribution around cluster center, 99.7% of the total users in cluster will lie within a disc of radius $3\ _i$. Thus $\ _i$ can be treated as the metric of cluster size and $\ _i$ scales with $\ $.

In the following Lemma, we formally claim that, irrespective of the distribution of Y_0, if the size of the cluster is expanded, the total coverage probability $\mathsf{P}_\mathsf{c}^{(i)}$ converges to $\mathsf{P}_\mathsf{c}^{(\mathrm{PPP})}$, i.e., the coverage probability obtained for a typical user under the assumption of PPP distribution of users independent of the BS point processes, which is derived in [22].

Lemma 2.23 (Convergence). *If distance of the a typical user and cluster center Y_0 is scaled by $\ (\ > 1)$, then the following limit can be established:*

$$\lim_{!\ 1} \mathsf{P}_\mathsf{c}^{(i)} = \mathsf{P}_\mathsf{c}^{(\mathrm{PPP})} = \sum_{j=1}^{\aleph} \frac{\bar{\ }_j}{\sum_{k=1}^{} P_{jk}\ \bar{\ }_k(G(\ ;\ )+1) + \bar{\ }_k^{0} H(\ ;\ )}. \tag{2.46}$$

Proof. As will be evident from the proof, the limiting arguments as well as the final limit remain the same irrespective of the value of random variable V_0. Therefore, for notational simplicity, we provide this proof for the no shadowing scenario, which is without loss of generality. The Euclidean distance from the typical user to its cluster center is now $Z = \ Y_0$. In the expression of $\mathsf{P}_{\mathsf{c}j}^{(i)}$ in (2.39), we are particularly interested in inner integral which comes from the Laplace transform of interference from the BS at 0^{th} tier derived in Lemma 2.15. From (2.32) with the substitution $P_{ji}w_j = x$ and $v_0 = 1$, we can write:

$$\int_x^{\infty} \frac{1}{1+\ (\frac{z}{x})} \frac{f_Z(z)}{\bar{F}_Z(x)} dz = \mathrm{E}_Z\left[\frac{1}{1+\ \frac{Z}{x}} \middle| Z > x\right] = \mathrm{E}_{Y_0}\left[\frac{1}{1+\ \frac{Y_0}{x}} \middle| Y_0 > \frac{x}{}\right].$$

Hence,

$$\lim_{!\ 1} \int_{\underline{x}}^{\infty} \frac{1}{1+\ \frac{Y_0}{x}} \frac{f_{Y_0}(y_0)}{\bar{F}_{Y_0}(\frac{x}{})} dy_0 = \int_0^{\infty} f_{Y_0}(y_0) dy_0 = 1.$$

Thus, as $\ !\ 1$, the inner integral tends to 1. So,

$$\lim_{!\ 1} \mathsf{P}_{\mathsf{c}j}^{(i)} = \frac{\bar{\ }_j}{\sum_{k=1}^{} P_{jk}^2\ \bar{\ }_k(G(\ ;\ )+1) + \bar{\ }_k^{0} H(\ ;\ )}.$$

Now we are left with the limit of the first term $A_0\mathsf{P}_{\mathsf{c}0}^{(i)}$ i.e., the contribution of the 0^{th} tier in $\mathsf{P}_\mathsf{c}^{(i)}$ which will obviously go to zero as $\ !\ 1$.

□

2.4.5 Overall coverage probability

The results so far are concerned with the users belonging to Φ_i^u. Recall that in our system model we considered that the users form a mixed point process consisting of Φ_i^u ($i \in B$) and $\Phi^{u(\mathrm{PPP})}$. So the overall coverage probability will be a combination of all these individual coverage probabilities $\mathrm{P_c}^{(i)}$ ($i \in B$) and also $\mathrm{P_c}^{(\mathrm{PPP})}$ corresponding to the users in $\Phi^{u(\mathrm{PPP})}$, which are distributed independently of the BS locations. The overall user point process can be expressed as $\Phi^u = \Phi^{u(\mathrm{PPP})} \cup \bigcup_{i \in B} \Phi_i^u$. The average number of points of Φ^u in any given set $A \subset \mathbb{R}^2$ is given by

$$\mathrm{E}(\Phi^u(A)) = \mathrm{E}(\Phi^{u(\mathrm{PPP})}(A)) + \sum_{i \in B} \mathrm{E}(\Phi_i^u(A)),$$

where $\mathrm{E}(\Phi^{u(\mathrm{PPP})}(A)) = \Lambda^{(\mathrm{PPP})}A$; $\mathrm{E}(\Phi_i^u(A)) = N_i \lambda_i A$. To avoid notational complication, we use the symbol Φ to denote a point process as well as the associated counting measure. Since each point has an equal chance to be selected as location of the typical user, the probability that a randomly chosen user from Φ^u belongs to $\Phi^{u(\mathrm{PPP})}$ (Φ_i^u), denoted by p_0 (p_i) respectively, is

$$p_0 = \frac{\Lambda^{(\mathrm{PPP})}}{\Lambda^{(\mathrm{PPP})} + \sum_{j \in B} N_j \lambda_j} \quad \text{and} \quad p_i = \frac{N_i \lambda_i}{\Lambda^{(\mathrm{PPP})} + \sum_{j \in B} N_j \lambda_j}; \tag{2.47}$$

where N_i is the average number of users per cluster of Φ_i^u ($i \in B$). Now, using these probabilities p_0 and p_i, the overall coverage probability is formally stated in the next Theorem.

Theorem 2.24 (Overall Coverage Probability)**.** *Overall coverage probability with respect to any randomly chosen user in a K-tier HetNet with mixed user distribution is:*

$$\mathrm{P_c} = p_0 \mathrm{P_c}^{(\mathrm{PPP})} + \sum_{i \in B} p_i \mathrm{P_c}^{(i)}; \tag{2.48}$$

where $\mathrm{P_c}^{(\mathrm{PPP})}$ and $\mathrm{P_c}^{(i)}$ are given by (2.46) and (2.28), respectively.

2.5 Numerical results and discussions

2.5.1 Validation of results

In this section, the analytical results derived so far are validated and key insights for the new HetNet system model with users clustered around BSs are provided. For the sake of concreteness, we restrict our simulation to two tiers: one macrocell tier ($\Phi_1^{(\mathrm{BS};o)}$) with density λ_1 with all open access BSs, and one small cell tier ($\Phi_2^{(\mathrm{BS})}$) with a mix of open and closed access BSs. For $\Phi_2^{(\mathrm{BS})}$, the open and closed access BS densities are λ_2 and $\lambda_2^{\emptyset}$, respectively. We choose $\lambda_2 = \lambda_2^{\emptyset} = 100\,\lambda_1 = 100$ BSs per $(500)^2$ m^2. We assume the

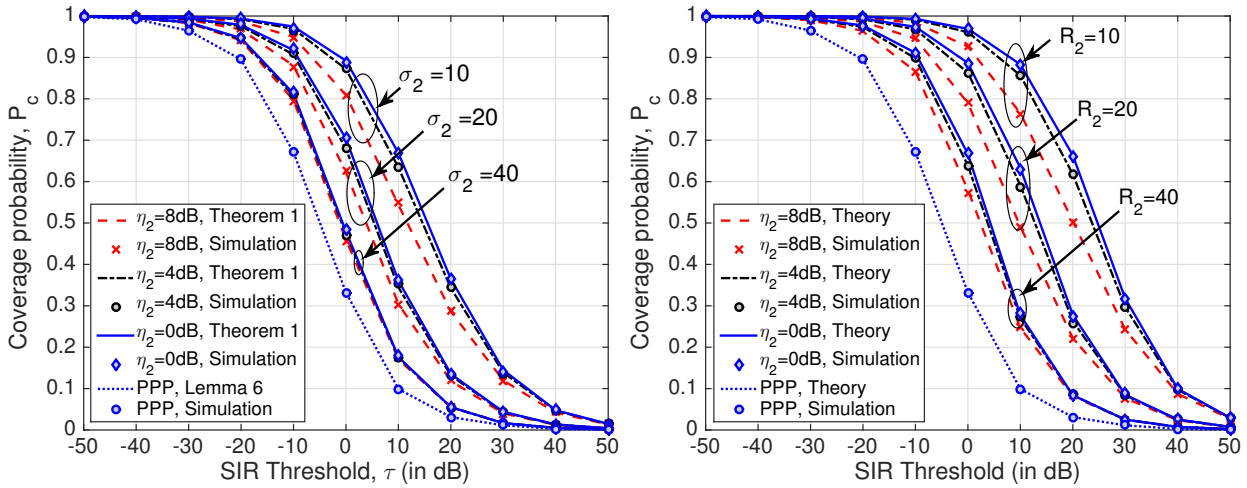

(a) Users in Thomas cluster process (b) Users in Matérn cluster process

Figure 2.2: Comparison of coverage probabilities with cluster size for various shadowing environments. The baseline case when the user distribution is a PPP is also included. The lines and markers correspond to the analytical and simulation results, respectively.

transmit powers are related by $P_1 = 10^3 P_2$. The user process is considered to be Φ_2^u only, i.e., a PCP around $\Phi_2^{(BS)}$. For every realization, a BS in the i^{th} tier is randomly selected and location of a typical user is generated according to the density function of (i) Thomas cluster process ((2.11)), and (ii) Matérn cluster process ((2.12)). For shadowing, we have chosen log-normal distribution parameters as $\mu_k = 0$, $\sigma_k = 8$ dB, 4 dB and 0 dB (no shadowing) for all $k = 0; 1; 2$. In Fig. 2.2, the coverage probability ($\mathtt{P_c}$, equivalently $\mathtt{P_c}^{(2)}$) is plotted for different values of SIR threshold τ and cluster size (i.e. different σ_2-s for Thomas and R_2-s for Matérn cluster processes). It can be observed that the analytically obtained results exactly match the simulation results. For comparison, $\mathtt{P_c}^{(PPP)}$, i.e., the coverage probability assuming homogeneity of users (i.e., independent PPP assumption) is also plotted. The plots clearly indicate that under clustering, $\mathtt{P_c}$ is significantly higher than $\mathtt{P_c}^{(PPP)}$ and increases for denser clusters. Also the convergence towards $\mathtt{P_c}^{(PPP)}$ is evident as cluster size increases. In Fig. 8.2, the association probabilities are plotted for different cluster size with $\mu_k = 4$ dB. The figure clearly illustrates that a user is more likely to be served by its cluster center if the distribution is more "dense" around the cluster center. As the cluster expands, association probability to the BS at cluster center (equivalently the 0^{th} tier) decreases whereas the association probabilities to the other open access tiers increase.

2.5.2 Tightness of the bounds

In Proposition 2.19, we derived upper and lower bounds on $\mathtt{P_c}^{(i)}$. We found that for no shadowing, these bounds reduce to closed form expression when Φ_i^u is Thomas or Matérn cluster process (Propositions 2.21 and 2.22). In Fig. 2.4, we plot these upper and lower

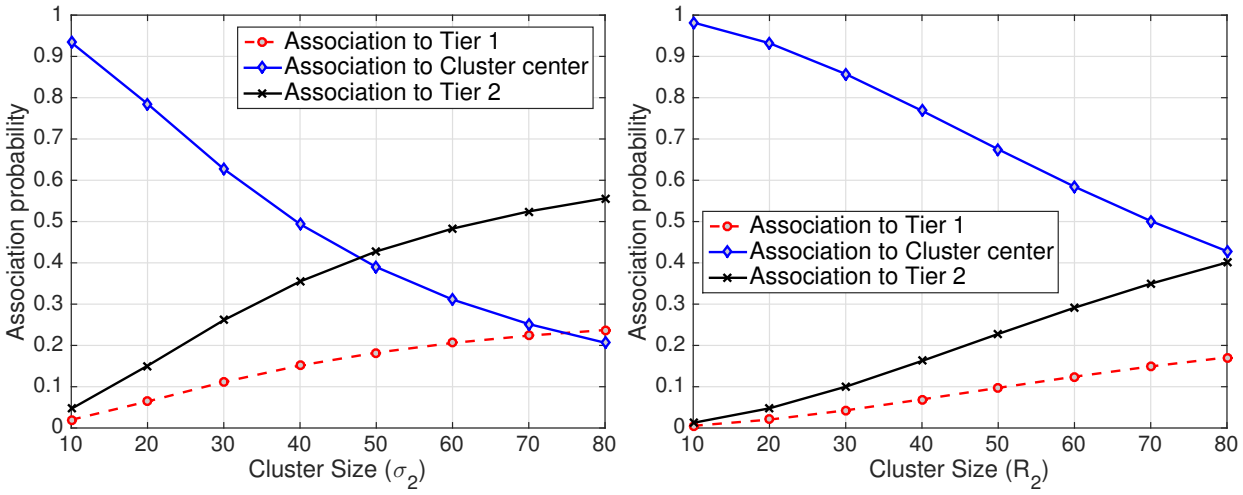

(a) Users in Thomas cluster process (b) Users in Matérn cluster process

Figure 2.3: Comparison of the association probabilities to the two tiers and the cluster center.

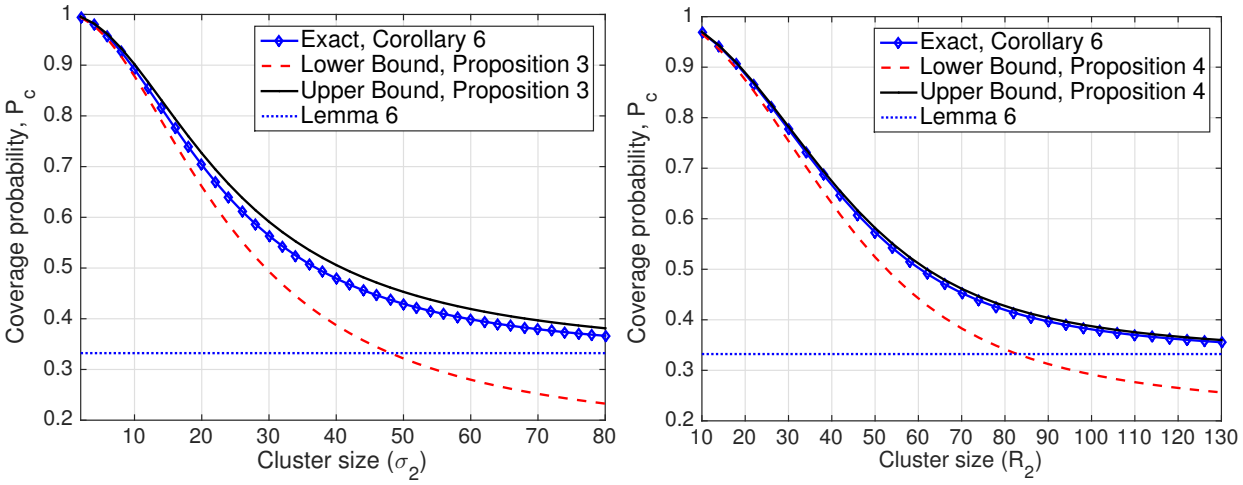

(a) Users in Thomas cluster process (b) Users in Matérn cluster process

Figure 2.4: Inspection of the proposed closed form bound with variation of cluster size for constant SIR threshold, = 0 dB.

bounds on $\mathtt{P_c}$. Recall that the lower bound was obtained by placing the BS of the cluster-center (in the representative cluster) on the boundary of the exclusion disc when the typical user connects to other BSs and the upper bound was found by simply ignoring the interference from this BS (see Corollary 2.16 for details). We observe that the lower bound becomes loose as the cluster size increases and for large user clusters, $\mathtt{P_c}^{(\mathtt{PPP})}$ becomes tighter lower bound. This is because the interference from the cluster center is significantly overestimated by placing the BS of the cluster center at the boundary of the exclusion zone. The upper bound remains tight for the entire range of cluster sizes. This can be explained by looking at the cases of small and large clusters separately. For small clusters, the typical user will likely connect to the BS at its cluster center most of the time and hence the interference term in question (Laplace transform of interference from the cluster center; see Corollary 2.16) will not even appear in the coverage probability expression. On the other hand, for large clusters, the interference from the BS at the cluster center of the representative cluster will be negligible compared to the other interference terms due to large distance between the typical user and this BS.

2.5.3 Power control of small cell BSs

If ^{u} is a PPP independent to BS locations, then $\mathtt{P_c}^{(\mathtt{PPP})}$ is independent of the BS trasmission power and it predicts that no further gain in coverage can be achieved by increasing P_2=P_1 (for interference-limited scenario under the assumption that the target SIR is the same for all the tiers, as is the case in this chapter) [21]. However, referring to Figs. 2.5a and 2.5b, it is evident that $\mathtt{P_c}$ improves significantly with P_2=P_1. In the figures, we can identify three regions of $\mathtt{P_c}$: (i) For lower value of P_2=P_1, P_c is close to $\mathtt{P_c}^{(\mathtt{PPP})}$, (ii) $\mathtt{P_c}$ is enhanced as P_2=P_1 increases since the user is likely to be served by the cluster center, (iii) if P_2=P_1 is further increased, $\mathtt{P_c}$ is saturated since association probability to other BSs will diminish. Again, the gain of $\mathtt{P_c}$ is stronger for denser clusters. Thus, coverage gain can be harnessed by increasing the transmit powers of small cell BSs in a certain range.

2.6 Summary

While random spatial models have been used successfully to study various aspects of HetNets in the past few years, quite remarkably all these works assume the BS and user distributions to be independent. In particular, the analysis is usually performed for a typical user whose location is sampled independently of the BS locations. This is clearly not the case in current capacity-driven user-centric deployments where the BSs are deployed in the areas of high user density. This chapter presented a comprehensive analysis of such user-centric HetNet deployments in which the user and BS locations are naturally correlated. In particular, modeling the user locations as a general Poisson cluster process, with BSs being the cluster centers, we have developed new tools leading to tractable results for the downlink coverage probability of a typical user. We have specialized the results for the case of Thomas cluster process in which the users are Gaussian distributed around BSs, and Matérn

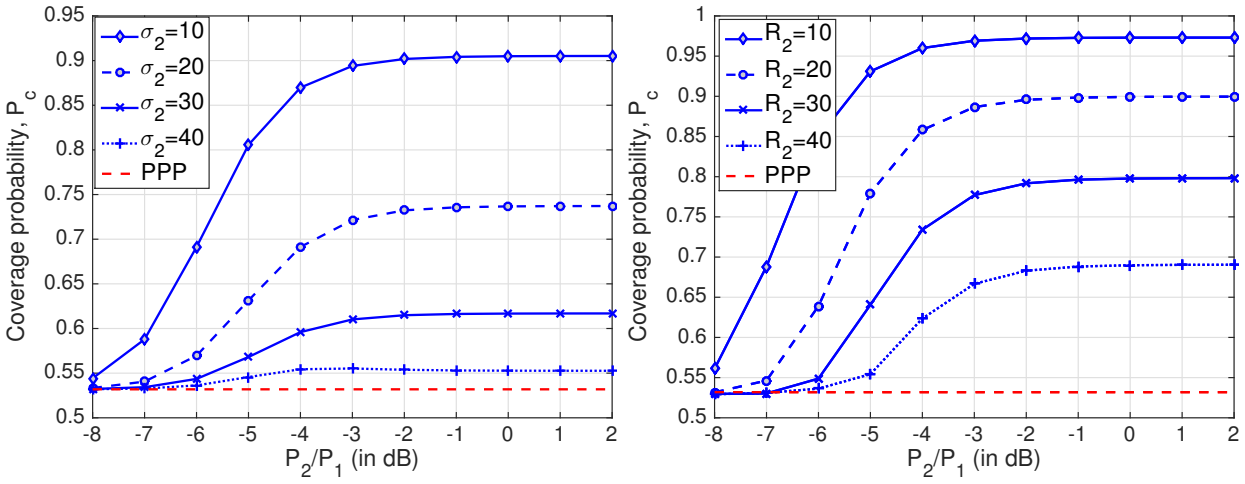

(a) Users in Thomas cluster process

(b) Users in Matérn cluster process

Figure 2.5: Effect of increasing small cell power on coverage.

cluster process where the users are uniformly distributed inside a disc centered at the BS. We have also examined the bounds and the limiting nature of the coverage probability as cluster size goes to infinity. We have derived the overall coverage probability for a mixed user distribution containing users uniformly distributed and clustered around small cell BSs. Overall, this work opens up a new dimension in the HetNet analysis by providing tools for the analysis of non-uniform user distributions correlated to the BS locations.

3

General HetNet Model: Part-I

3.1 Introduction

In order to handle the exponential growth of mobile data traffic, macrocellular networks of yesteryears have gradually evolved into more denser heterogeneous cellular networks in which several types of low power BSs (called small cells) coexist with macrocells. While macro BSs (MBSs) were deployed fairly uniformly to provide a ubiquitous coverage blanket, the small cell BSs (SBSs) are deployed somewhat organically to complement capacity of the cellular networks (primarily at user hotspots) or to patch their coverage dead-zones. This naturally couples the locations of the SBSs with those of the users, as a result of which we now need to consider plethora of deployment scenarios in the system design phase as opposed to only a few in the macro-only networks of the past. While the simulation models considered by 3GPP are cognizant of this evolution and consider several different configurations of user and SBS locations [2, 3], the stochastic geometry-based analyses of HetNets still rely on the classical PPP-based K-tier HetNet model [21, 34], which is not rich enough to capture aforementioned coupling. In this chapter, we show that this ever-increasing gap between the PPP-based HetNet model and the real-word deployments can be reduced by modeling a fraction of users and an arbitrary number of BS tiers using PCPs. The 3GPP-based spatial models of HetNets were already discussed in Chapter 1. We discuss the stochastic geometry-based HetNet models next.

3.1.1 Stochastic geometry-based approaches

In parallel to the realistic simulation models used by 3GPP, *analytical* HetNet models with foundations in stochastic geometry have gained prominence in the last few years [23, 31–33]. The main idea here is to endow the locations of the BSs and users with distributions and then use tools from stochastic geometry to derive easy-to-compute expressions for key performance metrics, such as coverage and rate[1]. In order to maintain tractability, the locations of the users and different types of BSs are usually modeled by independent homogeneous PPPs. We will henceforth refer to homogeneous PPP as a PPP unless stated otherwise. This model, usually referred to as a K-tier HetNet model, was first introduced in [20,21] and generalized in several important ways in [22,26,35,36]. Reviewing the rich and diverse collection of the followup works is outside the scope of this paper. Interested readers

[1] A careful reader will note that 3GPP models also endow the locations of users and SBSs with distributions, which technically makes them stochastic models as well.

are advised to refer to extensive surveys in [23, 31–33]. Since the fundamental assumption in this PPP-based K-tier HetNet model is the mutual independence of all the BS and user locations, it is not rich enough to capture spatial coupling that exists in HetNets. As a result, there have been many attempts in the recent past to use more sophisticated point processes to model different elements of HetNets. However, as will be evident from the discussion below, most of the efforts have been focused at modeling intra- and inter-tier *repulsion* that exists in the BS locations due to cell planning. There is relatively less attention given to modeling user-BS attraction, which is the main focus of this paper.

1) *Intra-tier coupling.* One of the conspicuous shortcomings of the PPP model is its inability to model minimum inter-site distance that exists in cellular networks due to cell site planning. This motivated several works in which the BS locations were modeled by *repulsive* point processes, such as Matérn hard-core process [63], Gauss-Poisson process [64], Ginibre point process [65], and determinantal point process [66]. For completeness, it should be noted that in high shadowing regime, the network topology does *appear* Poissonian to the receiver even if it follows a repulsive process [9]. This justifies the use of a PPP for modeling BS locations if the propagation channels exhibit sufficiently strong shadowing that is independent across links [9, 67].

2) *Inter-tier coupling.* Another conspicuous shortcoming of the K-tier HetNet model is the assumption of independence in the locations of the BSs across tiers. While this independence can be justified to some extent between MBSs and user-deployed SBSs (because users do not usually know the MBS topology), it is a bit more questionable for the SBSs deployed by the operators who will tend to concentrate them towards the cell edge away from the MBSs. This has motivated the use of Poisson hole process (PHP) [68] for modeling HetNets [68–70]. In this model, the MBSs are first modeled by a PPP. Inhibition zone of a fixed radius is then created around each MBS. The SBS locations are then modeled by a PPP *outside* these inhibition zones. This introduces repulsion between the locations of the MBSs and SBSs.

3) *User-SBS coupling.* As discussed already, coupling in the locations of the users and SBSs originate from the deployment of SBSs in the user hotspots. This coupling is at the core of several important user and SBS configurations considered in the 3GPP simulation models for HetNets [1–3]. Some relevant configurations motivated by this coupling are summarized in Table 3.1. Note that while the inter- and intra-tier couplings discussed above were modeled using repulsive point processes, accurate modeling of user-SBS coupling requires the use of point processes that exhibit inter-point attraction. Despite the obvious relevance of this coupling in HetNets, until recently this was almost completely ignored in stochastic geometry-based HetNet models. One exception is [50], which proposed a conditional thinning-based method of biasing the location of the typical user towards the BSs, thus inducing coupling in the BS and user locations. While this provided a good enough first order solution, it lacks generality and is not easily extendible to HetNets. The first work to properly incorporate this user-SBS coupling in a K-tier HetNet model is [60, 71], in which the users were modeled as a PCP (around SBS locations) instead of an independent PPP

Table 3.1: Relevant user and SBS configurations used in 3GPP HetNet models (synthesized from the configurations discussed in [1, Table A.2.1.1.2-4], [2, 3]).

Configuration	User distribution within a macrocell	SBS distribution within a macrocell	Comments
1	Uniform	Uncorrelated	Captured by Model 1
2	Clustered	Correlated, hotspot center	Capacity centric deployment Captured by Model 2
3	Clustered	Correlated, small cell cluster	Deployed at user hotspots Cluster size may vary from small to large, Captured by Model 3
4	Uniform	Clustered	Applies for pedestrians Captured by Model 4

as was the case in the classical K-tier model. There are some other recent works that use PCPs to model SBS and/or user locations. Instead of simply listing them here, we discuss them next in the context of four 3GPP-inspired generative models, which collectively model several key user and SBS configurations of interest in HetNets.

3.1.2 3GPP-inspired generative models using PPP and PCP

As discussed above already in Section 1.3, we need to incorporate inter-point interaction in the HetNet models to capture user-SBS coupling accurately. A simple way of achieving that, which is also quite consistent with the 3GPP configurations listed in Table 3.1, is to use PCPs. By combining PCP with a PPP, we can create generative models that are rich enough to model different HetNet configurations of Table 3.1. We discuss these generative models next.

- *Model 1: SBS PPP, user PPP.* This is the PPP-based K-tier *baseline* model most commonly used in HetNet literature and is in direct agreement with the 3GPP models with *uniform* user and *uncorrelated* SBS distribution (configuration 1 in Table 3.1).

- *Model 2: SBS PPP, user PCP.* Proposed in our recent work [60, 71], this model can accurately characterize *clustered* users and *uncorrelated* SBSs. In particular, we model the clustered user and SBS locations jointly by defining PCP of users around PPP distributed SBSs. This captures the coupling between user and SBS locations. More precisely, this model closely resemblances the 3GPP configuration of single SBS per user hotspot in a HetNet, which is listed as configuration 2 in Table 3.1.

- *Model 3: SBS PCP, user PCP.* The SBS locations exhibit inter-point attraction (and coupling with user locations) when multiple SBSs are deployed in each user hotspot. For modeling such scenarios, two PCPs with the same parent PPP but independent and identically distributed (i.i.d.) offspring point processes can be used to model the

user and SBS locations. Coupling is modeled by having the same parent PPP for both the PCPs. We proposed and analyzed this model for HetNets in [72] (models configuration 3 listed in Table 3.1).

- *Model 4: SBS PCP, user PPP.* This scenario can occur in conjunction with the previous one since some of the users may not be a part of the user clusters but are still served by the clustered SBSs. PPP is a good choice for modeling user locations in this case [44,45]. This corresponds to configuration 4 in Table 3.1.

These generative models are illustrated in Fig. 3.1. Clearly, they collectively encompass a rich set of 3GPP HetNet configurations. In this chapter, we unify these four models and develop a general analytical approach for the derivation of downlink coverage probability. Unlike prior works on PCP-based HetNet models that focused exclusively on *max-power based association* policy, we will consider *max-*SIR *cell association*, which will require a completely new formalism compared to these existing works. It is worth noting that this work is the first to consider max-SIR based association in PCP enhanced HetNets. More details about the contributions are provided next.

3.1.3 Contributions

A unified framework with PCP and PPP modeled BSs and users

Inspired by the user and SBS configurations considered in the 3GPP simulation models for HetNets (summarized in Table 3.1), we propose a unified K-tier HetNet model in which an arbitrary number of BS tiers and a fraction of users is modeled by PCPs. The PCP assumption for the BS tier incorporates spatial coupling among the BS locations. On the other hand, the coupling between user and BS locations is captured when the users are also modeled as a PCP with each cluster having either (1) a BS at its cluster center, or (2) a BS cluster with same cluster center as that of the user cluster. As will be evident soon, the four generative models discussed above (and the four user and SBS configurations listed in Table 3.1) can all be treated as special cases of this general setup.

Sum-product functional and coverage probability analysis

We derive coverage probability (or equivalently SIR distribution) of a typical user for the proposed unified HetNet model under the max-SIR cell association. We demonstrate that the coverage probability for this setup can be expressed as a summation of a functional over the BS point processes which we define as *sum-product functional*. As a part of the analysis, we characterize this functional for PPP, PCP and its associated offspring point process, thus leading to new results from stochastic geometry perspective that may find broader applications in the field. After deriving all results in terms of *general* PCP, we specialize them to two cases: when all the clustered BS tiers and users are modeled as (i) Matérn cluster process (MCP), and (ii) Thomas cluster process (TCP).

Limiting behavior

We also study the limiting behavior of PCP in the context of this model. In particular, we show that when the cluster size tends to infinity: (i) the PCP *weakly* converges to a PPP, (ii) the limiting PPP and the parent PPP become independent point processes. Although, to the best of our knowledge, these limiting results have not been reported in the communications literature (due to limited application of PCPs to communication network modeling), it would not be prudent to claim that they are not known/available in some form in the broader stochastic geometry literature. Regardless, as a consequence of this limiting result, we are able to formally demonstrate that the coverage probability obtained under this general framework converges to the well-known closed-form coverage probability result of [21] obtained for the baseline PPP-based HetNet model where all the BS tiers and users are modeled as independent PPPs.

One of the key take-aways of this study is the fact that the performance trends in HetNets strongly depend on the network topology and are highly impacted by the spatial coupling between the user and BS locations. While the PPP-based baseline HetNet model provided useful initial design guidelines, it is perhaps time to focus on more realistic models that are in better agreement with the models used in practice, such as the ones in the 3GPP simulation models. Our numerical studies demonstrate several fundamental differences in the coverage probability trends in Models 1-4 when the parameters of the BS and user point processes are changed.

3.2 System model

Before we introduce the proposed PCP-based system model for K-tier HetNet, we provide a formal introduction to PCP next.

Definition 3.1 (PCP)**.** A PCP $(\ _{\mathrm{p}}; f; p_n)$ can be uniquely defined as:

$$= \bigcup_{\mathbf{z} \in\ _{\mathrm{p}}} \mathbf{z} + B^{\mathbf{z}}; \tag{3.1}$$

where $_{\mathrm{p}}$ is the parent PPP of intensity $_{\mathrm{p}}$ and $B^{\mathbf{z}}$ denotes the offspring point process corresponding to a cluster center $\mathbf{z} \in\ _{\mathrm{p}}$ where $\{\mathbf{s} \in B^{\mathbf{z}}\}$ is an i.i.d. sequence of random vectors with arbitrary probability density function (PDF) $f(\mathbf{s})$. The number of points in $B^{\mathbf{z}}$ is denoted by N, where $N \quad p_n$ $(n \in \mathbb{N})$.

PCP can be viewed as a collection of offspring process $B^{\mathbf{z}}$ translated by $\mathbf{z}$ for each $\mathbf{z} \in\ _{\mathrm{p}}$. Then the sequence of points $\{\mathbf{t}\}$ $\mathbf{z} + B^{\mathbf{z}}$ is conditionally i.i.d. with PDF $f(\mathbf{t}|\mathbf{z}) = f(\mathbf{t} \quad \mathbf{z})$. A special class of PCP is known as Neyman-Scott process in which N $\mathtt{Poisson}(m)$. Throughout this chapter, we will denote the Neyman-Scott process by $(\ _{\mathrm{p}}; f; m)$ and will refer to it as a PCP unless stated otherwise.

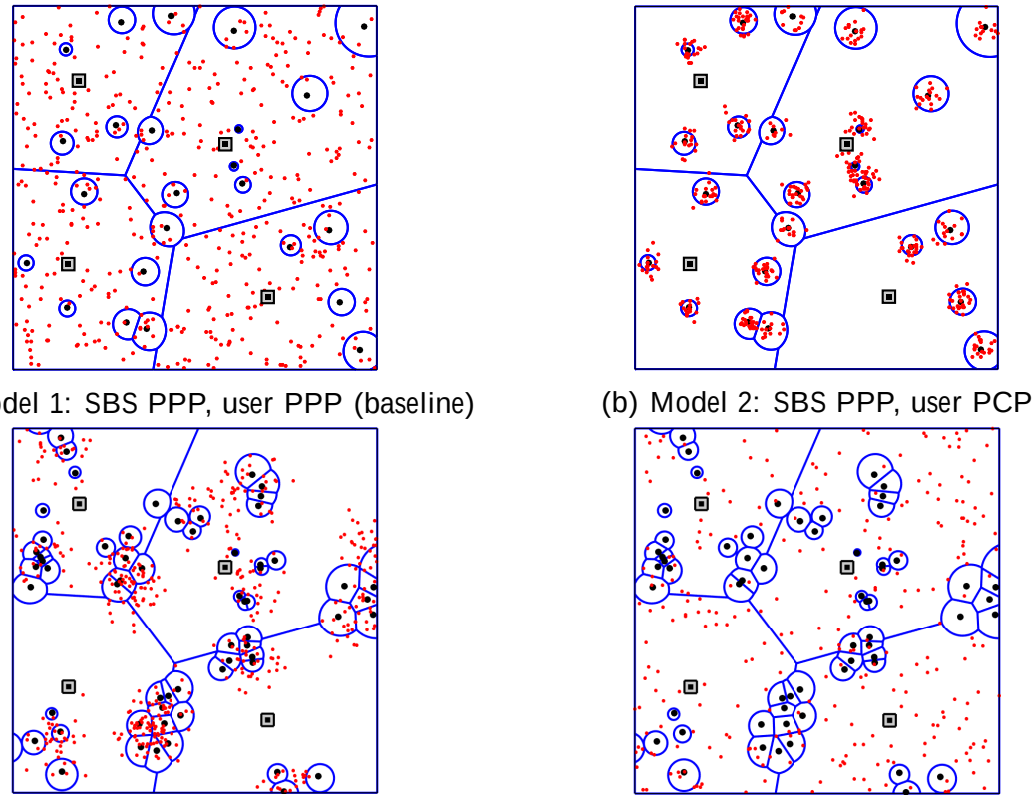

(a) Model 1: SBS PPP, user PPP (baseline)

(b) Model 2: SBS PPP, user PCP

(c) Model 3: SBS PCP, user PCP

(d) Model 4: SBS PCP, user PPP

Figure 3.1: Illustration of the four generative HetNet models developed by combining PPP and PCP. The black square, black dot and red dot refer to the MBS, SBS, and users, respectively.

3.2.1 K-tier HetNet model

We assume a K-tier HetNet consisting of K different types of BSs distributed as PPP or PCP. Let K_1 and K_2 denote the index sets of the BS tiers being modeled as PPP and PCP, respectively, with $jK_1 \,[\, K_2 j = K$ $(K_1 \setminus K_2 = \emptyset)$. We denote the point process of the k^{th} BS tier as Φ_k, where Φ_k is either a PPP with intensity λ_k $(\forall k \in K_1)$ or a PCP i.e. $\Phi_k(\Phi_{p_k}; f_k; m_k)$ $(\forall k \in K_2)$. We assume that each BS of Φ_k transmits at constant power P_k. Define Φ_u as the user point process. Contrary to the common practice in the literature, Φ_u is not necessarily a PPP independent of the BS locations, rather this scenario will appear as a special case in our analysis. In particular, we consider three different configurations for users:

- Case 1 (*uniform users*): Φ_u is a PPP. This corresponds to Models 1 and 4 from the previous Section.
- Case 2 (*clustered users*): $\Phi_u(\Phi_q; f_q; m_q)$ is a PCP with parent PPP Φ_q $(q \in K_1)$, which corresponds to Model 2 (single SBS deployed in a user hotspot).
- Case 3 (*clustered users*): $\Phi_u(\Phi_{p_q}; f_q; m_q)$ is a PCP having same parent PPP as that of Φ_q $(q \in K_2)$, which corresponds to Model 3 (multiple SBSs deployed at a user hotspot).

We perform our analysis for a *typical* user which corresponds to a point selected uniformly at random from Φ_u. Since both PPP and PCP are stationary, the typical user is assumed to be located at the origin without loss of generality. In case 2 and case 3, the locations of the users and BSs are coupled. Hence, when we select a typical user, we also implicitly select the cluster to which it belongs. For case 2, let $\mathbf{z}_0 \in \Phi_q$ $(q \in K_1)$ be the location of the BS at the cluster center of the typical user. For case 3, let us define the *representative* BS cluster $B_q^{\mathbf{z}_0} \in \Phi_q$ $(q \in K_2)$ having the cluster center at $\mathbf{z}_0$ which is also the cluster center of the typical user located at origin. Having defined all three possible configurations/cases of Φ_u, we define a set

$$\Phi_0 = \begin{cases} \emptyset; & \text{case 1,} \\ \{\mathbf{z}_0\}; & \text{case 2,} \\ \mathbf{z}_0 + B_q^{\mathbf{z}_0}; & \text{case 3.} \end{cases} \tag{3.2}$$

This set can be interpreted as the locations of the BSs whose locations are coupled with that of the typical user (alternatively the BSs that lie in the same cluster as the typical user). For the sake of analysis, we remove Φ_0 from Φ_q and treat it as a separate BS tier (call it the 0^{th} tier). Thus, for case 2, we remove singleton $\{\mathbf{z}_0\}$ from $\Phi_q(q \in K_1)$. In case 3, we remove finite process $\mathbf{z}_0 + B_q^{\mathbf{z}_0}$, which is a representative cluster of BSs with properties $(f_q; m_q)$ being inherited from Φ_q $(q \in K_2)$. According to Slivnyak's theorem [13], this removal of a point (case 2) or a representative cluster (case 3) does not change the distribution of Φ_q, i.e., $\Phi_q \overset{d}{=} \Phi_q \setminus \Phi_0$, where '$\overset{d}{=}$' denotes equality in distribution. Note that

since Φ_0 is constructed from Φ_q ($q \in K_1 \cup K_2$), the transmit power of the BS(s) in Φ_0 is $P_0 \quad P_q$. Hence, the BS point process is a superposition of independent point processes defined as: $\quad = \cup_{k_1 \in K_1} \Phi_{k_1} \cup_{k_2 \in K_2} \Phi_{k_2} \cup \Phi_0$; and the corresponding index set is enriched as: $K = K_1 \cup K_2 \cup \{0\}$. For the simplicity of exposition, the thermal noise is assumed to be negligible compared to the interference power. Assuming the serving BS is located at $\mathbf{x} \in \Phi_k$, $\mathtt{SIR}(\mathbf{x})$ is defined as:

$$\mathtt{SIR}(\mathbf{x}) = \frac{P_k h_{\mathbf{x}} \|\mathbf{x}\|^{-}}{I(\Phi_k \setminus \{\mathbf{x}\}) + \sum_{j \in K \setminus \{k\}} I(\Phi_j)}; \tag{3.3}$$

where $I(\Phi_i) = \sum_{\mathbf{y} \in \Phi_i} P_i h_{\mathbf{y}} \|\mathbf{y}\|^{-}$ is the aggregate interference from Φ_i ($i \in K$). For the channel model, we assume that the signal from a BS at $\mathbf{y} \in \mathbb{R}^2$ undergoes independent Rayleigh fading, more precisely $\{h_{\mathbf{y}}\}$ is an i.i.d. sequence of random variables, with $h_{\mathbf{y}}$ $\mathtt{exp}(1)$, and > 2 is the path-loss exponent. Assuming β_k is the $\mathtt{SIR}$-threshold defined for Φ_k for successful connection and the user connects to the BS that provides maximum $\mathtt{SIR}$, coverage probability is defined as:

$$\mathtt{P_c} = \mathbb{P}\Big[\bigcup_{k \in K} \bigcup_{\mathbf{x} \in \Phi_k} \{\mathtt{SIR}(\mathbf{x}) > \beta_k\}\Big]. \tag{3.4}$$

Note that $\Phi_0 \quad \Phi_q$ for $\mathtt{case}$ 2 and $\mathtt{case}$ 3, as discussed above already. The main goal of this chapter is to provide exact characterization of $\mathtt{P_c}$ for this general model under $\mathtt{max\text{-}SIR}$ connectivity. Note that there is another popular user association policy known as the $\mathtt{max}$-power connectivity, where the user connects to the BS which provides the maximum received power averaged over fading. However, the characterization of coverage probability under $\mathtt{max}$-power connectivity requires completely different formalism [32] and the necessary analytical tools for the analyses of the four Models have been developed in [22, 71–74].

3.3 Point Process functionals

This is the first main technical section of this chapter, where we characterize the sum-product functional and probability generating functional (PGFL) of a point process with respect to both its original and reduced Palm distributions, where can be either a PPP, PCP or its associated offspring process. While PGFLs of point processes are widely-known functionals in stochastic geometry [13], sum-product functionals are not as well-studied. Perhaps the most relevant prior work on sum-product functionals is [75] but it was limited to PPPs. These point process functionals will be used in the analysis of coverage probability under max-$\mathtt{SIR}$ connectivity in the next Section. We begin by providing their formal definitions.

Definition 3.2 (Sum-product functional)**.** Sum-product functional of a point process is

defined in this chapter as:

$$\mathrm{E}\left[\sum_{\mathbf{x}\in\Phi} g(\mathbf{x}) \prod_{\mathbf{y}\in\Phi\setminus\{\mathbf{x}\}} v(\mathbf{x},\mathbf{y})\right], \tag{3.5}$$

where $g(\mathbf{x}) : \mathbb{R}^2 \to [0,1]$ and $v(\mathbf{x},\mathbf{y}) : [\mathbb{R}^2 \times \mathbb{R}^2] \to [0,1]$ are measurable.

Note that our definition of the sum-product functional is slightly different from the way it was defined (for PPPs) in [75]. In (3.5), while taking product over Φ, we exclude the point $\mathbf{x}$ appearing in the outer summation. It will be evident later that this invokes reduced Palm measures of Φ. Also note that the above functional form can be treated as a special case of the functional that appears in the definition of Campbell-Mecke theorem [13]. Next we define the PGFLs of a point process with respect to its original and reduced Palm distribution.

Definition 3.3 (PGFL)**.** The PGFL of a point process Φ evaluated at $v(\mathbf{x},\mathbf{y})$ is defined as:

$$G(v(\mathbf{x},\mathbf{y})) = \mathrm{E}\left[\prod_{\mathbf{y}\in\Phi} v(\mathbf{x},\mathbf{y})\right], \tag{3.6}$$

where $v(\mathbf{x},\mathbf{y}) : [\mathbb{R}^2 \times \mathbb{R}^2] \to [0,1]$ is measurable. The PGFL of Φ under the condition of removing a point of Φ at $\mathbf{x}$ or alternatively the PGFL of Φ under its reduced Palm distribution is defined as:

$$\breve{G}(v(\mathbf{x},\mathbf{y})) = \mathrm{E}^!_{\mathbf{x}}\left[\prod_{\mathbf{y}\in\Phi} v(\mathbf{x},\mathbf{y})\right] = \mathrm{E}\left[\prod_{\mathbf{y}\in\Phi\setminus\{\mathbf{x}\}} v(\mathbf{x},\mathbf{y})\right]. \tag{3.7}$$

Although it is natural to define PGFL of a point process at some $v'(\mathbf{y})$ where $v' : \mathbb{R}^2 \to [0,1]$ is measurable, we define PGFL at $v(\mathbf{x},\mathbf{y})$, where '$\mathbf{x}$' appears as a dummy variable, to be consistent with the notation used throughout this chapter.

3.3.1 Sum-product functionals

In this Subsection, we characterize the sum-product functionals of different point processes that appear in the expression for coverage probability of a typical user in the next Section. The sum-product functional when Φ is a PPP is presented in the next Lemma.

Lemma 3.4. *The sum-product functional of Φ when Φ is a PPP of intensity λ is:*

$$\mathrm{E}\left[\sum_{\mathbf{x}\in\Phi} g(\mathbf{x}) \prod_{\mathbf{y}\in\Phi\setminus\{\mathbf{x}\}} v(\mathbf{x},\mathbf{y})\right] = \int_{\mathbb{R}^2} g(\mathbf{x})\breve{G}(v(\mathbf{x},\mathbf{y}))\mathrm{d}\mathbf{x}, \tag{3.8}$$

where $\breve{G}(v(\mathbf{x},\mathbf{y}))$ is the PGFL of Φ with respect to its reduced Palm distribution and $\breve{G}(v(\mathbf{x},\mathbf{y})) = G(v(\mathbf{x},\mathbf{y}))$.

Proof. We can directly apply Campbell-Mecke Theorem [13] to evaluate (3.5) as:

$$\mathrm{E}\Big[\sum_{x\in\Phi} g(x)\prod_{y\in\Phi\setminus\{x\}} v(x,y)\Big] = \int_{\mathbb{R}^2} g(x)\mathrm{E}_x^{!}\Big[\prod_{y\in\Phi} v(x,y)\Big]\,\Lambda(dx) = \int_{\mathbb{R}^2} g(x)\mathcal{G}(v(x,y))\,\Lambda(dx),$$

where $\Lambda(\cdot)$ is the intensity measure of Φ and $\mathcal{G}(\cdot)$ denotes the PGFL of Φ under its reduced Palm distribution. When Φ is homogeneous PPP, $\Lambda(dx) = \lambda\,dx$ and $\mathcal{G}(v(x,y)) = G(v(x,y)) = \mathrm{E}\big[\prod_{y\in\Phi} v(x,y)\big]$, by Slivnyak's theorem [13]. □

Sum-product functional of Φ when Φ is a PCP requires more careful treatment since selecting a point from $\mathbf{x}\in\Phi$ implies selecting a tuple $(\mathbf{x},\mathbf{z})$, where $\mathbf{z}$ is the cluster center of $\mathbf{x}$. Alternatively, we can assign a two-dimensional mark $\mathbf{z}$ to each point $\mathbf{x}\in\Phi$ such that $\mathbf{z}$ is the cluster center of $\mathbf{x}$. Then $(\mathbf{x},\mathbf{z})$ is a point from the marked point process $\hat{\Phi}$ $\mathbb{R}^2$ $\mathbb{R}^2$. It should be noted that $\hat{\Phi}$ is simply an alternate representation of Φ, which will be useful in some proofs in this Section. Taking A, B $\mathbb{R}^2$, its intensity measure can be expressed as:

$$\begin{aligned}\Lambda(A,B) = \mathrm{E}\Big[\sum_{(\mathbf{x},\mathbf{z})\in\hat{\Phi}} \mathbf{1}(\mathbf{x}\in A,\mathbf{z}\in B)\Big] &\overset{(a)}{=} \mathrm{E}\Big[\sum_{\mathbf{z}\in\Phi_p\cap B}\ \sum_{\mathbf{x}\in A} m f(\mathbf{x}|\mathbf{z})\,d\mathbf{x}\Big]\\ &= m_p \int_{\mathbf{z}\in B}\int_{\mathbf{x}\in A} f(\mathbf{x}|\mathbf{z})\,d\mathbf{x}\,d\mathbf{z}, \qquad (3.9)\end{aligned}$$

where in step (a), the expression under summation is the intensity of $\mathbf{z}+B^{\mathbf{z}}$, i.e., the offspring process with cluster center at $\mathbf{z}$. The last step follows from Campbell's theorem [13]. Hence,

$$\Lambda(d\mathbf{x},d\mathbf{z}) = {}_p m f(\mathbf{x}|\mathbf{z})\,d\mathbf{z}\,d\mathbf{x}. \qquad (3.10)$$

We now evaluate the sum-product functional of PCP in the next Lemma.

Lemma 3.5. *The sum-product functional of Φ when Φ is a PCP can be expressed as follows:*

$$\mathrm{E}\Big[\sum_{x\in\Phi} g(x)\prod_{y\in\Phi\setminus\{x\}} v(x,y)\Big] = \int_{\mathbb{R}^2}\int_{\mathbb{R}^2} g(x)\mathcal{G}(v(x,y)|z)\,\Lambda(dx,dz), \qquad (3.11)$$

where

$$\mathcal{G}(v(x,y)|z) = G(v(x,y))\mathcal{G}_c(v(x,y)|z) \qquad (3.12)$$

denotes the PGFL of Φ when a point $\mathbf{x}\in\Phi$ with cluster center at $\mathbf{z}$ is removed from Φ. $G(\cdot)$ is the PGFL of Φ and $\mathcal{G}_c(\cdot|\mathbf{z})$ is the PGFL of $\mathbf{z}+B^{\mathbf{z}}$, which is a cluster of Φ centered at $\mathbf{z}$ under its reduced Palm distribution.

Proof. Starting from (3.5), we apply Campbell-Mecke theorem on $\hat{}$ as follows:

$$\mathsf{E}\Big[\sum_{(\mathbf{x};\mathbf{z})\in\hat{}} g(\mathbf{x}) \prod_{(\mathbf{y};\mathbf{z}')\in\hat{}\setminus n(\mathbf{x};\mathbf{z})} v(\mathbf{x};\mathbf{y})\Big] = \int_{\mathbb{R}^2}\int_{\mathbb{R}^2} \mathsf{E}^{!}_{(\mathbf{x};\mathbf{z})}\Big[g(\mathbf{x}) \prod_{(\mathbf{y};\mathbf{z}')\in\hat{}} v(\mathbf{x};\mathbf{y})\Big]\,(d\mathbf{x};d\mathbf{z}).$$

The Palm expectation in the last step can be simplified as:

$$\begin{aligned}
&\mathsf{E}^{!}_{(\mathbf{x};\mathbf{z})}\Big[g(\mathbf{x}) \prod_{(\mathbf{y};\mathbf{z}')\in\hat{}} v(\mathbf{x};\mathbf{y})\Big] \\
&= g(\mathbf{x})\mathsf{E}\Big[\prod_{\mathbf{y}\in n(\mathbf{z}+B^{\mathbf{z}}_k)} v(\mathbf{x};\mathbf{y}) \prod_{\mathbf{y}\in(\mathbf{z}+B^{\mathbf{z}}_k)\cap n\setminus\{\mathbf{x}\}} v(\mathbf{x};\mathbf{y})\Big] \\
&\overset{(a)}{=} g(\mathbf{x})\mathsf{E}\Big[\prod_{\mathbf{y}\in n(\mathbf{z}+B^{\mathbf{z}})} v(\mathbf{x};\mathbf{y})\Big]\,\mathsf{E}\Big[\prod_{\mathbf{y}\in(\mathbf{z}+B^{\mathbf{z}})\cap n\setminus\{\mathbf{x}\}} v(\mathbf{x};\mathbf{y})\Big] \\
&\overset{(b)}{=} g(\mathbf{x})\mathsf{E}\Big[\prod_{\mathbf{y}\in n} v(\mathbf{x};\mathbf{y})\Big]\,\mathsf{E}^{!}_{\mathbf{x}}\Big[\prod_{\mathbf{y}\in(\mathbf{z}+B^{\mathbf{z}})} v(\mathbf{x};\mathbf{y})\Big];
\end{aligned}$$

where (a) follows from the independence of the processes $\mathbf{z}+B^{\mathbf{z}}$ and $n(\mathbf{z}+B^{\mathbf{z}})$ and (b) follows from Slivnyak's theorem for PCP, i.e. $n(\mathbf{z}+B^{\mathbf{z}}) \overset{d}{=} n$ [76]. Substituting the PGFLs as $\mathsf{E}\big[\prod_{\mathbf{y}\in n} v(\mathbf{x};\mathbf{y})\big] = G(v(\mathbf{x};\mathbf{y}))$, and $\mathsf{E}^{!}_{\mathbf{x}}\big[\prod_{\mathbf{y}\in\mathbf{z}+B^{\mathbf{z}}} v(\mathbf{x};\mathbf{y})\big] = \mathfrak{C}_c(v(\mathbf{x};\mathbf{y})|\mathbf{z})$, we get the final result. □

The similar steps for the evaluation of the sum-product functional can not be followed when $$ is a finite point process, specifically, $ = \mathbf{z} + B^{\mathbf{z}}$, the cluster of a randomly chosen point $\mathbf{x} \in$ centered at $\mathbf{z}$.

Lemma 3.6. *The sum-product functional of $$ when $ = \mathbf{z} + B^{\mathbf{z}}$, i.e., the offspring point process of a PCP centered at $\mathbf{z}$ can be expressed as follows:*

$$\begin{aligned}
\mathsf{E}\Big[\sum_{\mathbf{x}\in} g(\mathbf{x}) \prod_{\mathbf{y}\in\setminus\{\mathbf{x}\}} v(\mathbf{x};\mathbf{y})\Big] = {}& \int_{\mathbb{R}^2} g(\mathbf{x}) \exp\Big(-m\int_{\mathbb{R}^2}(1-v(\mathbf{x};\mathbf{y}))f(\mathbf{y}|\mathbf{z})d\mathbf{y}\Big) \\
& \Big(m\int_{\mathbb{R}^2} v(\mathbf{x};\mathbf{y})f(\mathbf{y}|\mathbf{z})d\mathbf{y} + 1\Big) f(\mathbf{x}|\mathbf{z})d\mathbf{x}. \quad (3.13)
\end{aligned}$$

Proof. Note that $$ is conditioned to have at least one point (the one located at $\mathbf{x}$) and the number of points in $$ follows a weighted distribution, $\mathbb{N} \ni \frac{np_n}{m}$ $(n \in \mathbb{Z}^+)$ [13]. Now, starting

from (3.5),

$$\begin{aligned}
&\int_{N} g(\mathbf{x}) \sum_{\mathbf{x}\in\mathbf{y}} \prod_{\mathbf{y}\in\mathbf{y}\setminus\{\mathbf{x}\}} v(\mathbf{x};\mathbf{y}) P(\mathrm{d}\mathbf{y}) \\
&\overset{(a)}{=} \sum_{n=1}^{\infty} \int_{N_n} g(\mathbf{x}) \sum_{\mathbf{x}\in\mathbf{y}} \prod_{\mathbf{y}\in\mathbf{y}\setminus\{\mathbf{x}\}} v(\mathbf{x};\mathbf{y}) P(\mathrm{d}\mathbf{y}) \\
&= \sum_{n=1}^{\infty} \int_{[\mathbf{x}_1,\ldots,\mathbf{x}_n]\in\mathbb{R}^{2n}} \sum_{i=1}^{n} g(\mathbf{x}_i) \prod_{\substack{j=1;\\ j\neq i}} v(\mathbf{x}_i;\mathbf{x}_j) h_{(}\mathbf{x}_j|\mathbf{z}) \mathrm{d}\mathbf{x}_j \\
&f(\mathbf{x}_i|\mathbf{z})\mathrm{d}\mathbf{x}_i \frac{np_n}{m} = \sum_{n=1}^{\infty} n \int_{\mathbb{R}^2} g(\mathbf{x}) \Bigg(\int_{\mathbb{R}^2} v(\mathbf{x};\mathbf{y}) f(\mathbf{y}|\mathbf{z}) \mathrm{d}\mathbf{y} \Bigg)^{n-1} f(\mathbf{x}|\mathbf{z}) \mathrm{d}\mathbf{x}\, \frac{p_n}{m};
\end{aligned} \tag{3.14}$$

where N denotes the space of locally finite and simple point sequences in $\mathbb{R}^2$. In (a), N is partitioned into $\{N_n : n \geq 1\}$ where N_n is the collection of point sequences having n points and denotes a realization of $(\mathbf{z} + B^{\mathbf{z}})$. Under the condition of removing a point $\mathbf{x}$ from $(\mathbf{z} + B^{\mathbf{z}})$, this point process will have at least one point. Hence, the number of points in $(\mathbf{z} + B^{\mathbf{z}})$ will follow the weighted distribution: $\tilde{N} \sim \frac{np_n}{m}$ $(n \geq 1, n \in \mathbb{Z}^+)$. The final expression is obtained by substituting $p_n (\forall\, n \geq 1, n \in \mathbb{N})$ by the probability mass function (PMF) of Poisson distribution followed by basic algebraic manipulations. □

3.3.2 Probability generating functional

In this Section, we evaluate the PGFLs of different point processes that appeared in the expressions of the sum-product functionals in the previous Section. While the PGFLs of the PPP and PCP are known [54], we list them in the next Lemma for completeness.

Lemma 3.7. *The PGFL of when is a PPP of intensity is given by:*

$$G(v(\mathbf{x};\mathbf{y})) = \exp\left(\int_{\mathbb{R}^2} (1 - v(\mathbf{x};\mathbf{y})) \mathrm{d}\mathbf{y} \right); \tag{3.15}$$

When is a PCP, the PGFL of $(\ _{\mathrm{p}}; f; m)$ is given by:

$$G(v(\mathbf{x};\mathbf{y})) = \exp\left(\int_{\mathbb{R}^2} \left(1 - \exp\left(m \int_{\mathbb{R}^2} (1 - v(\mathbf{x};\mathbf{y}) f(\mathbf{y}|\mathbf{z}) \mathrm{d}\mathbf{y} \right) \right) \mathrm{d}\mathbf{z} \right); \tag{3.16}$$

Proof. Please refer to [54, Theorem 4.9, Corollary 4.13]. □

We have pointed out in Lemma 3.4 that the PGFLs with respect to the original and reduced Palm distributions are the same when is a PPP. However, this is not true for

PCP. It was shown in Lemma 3.5 that when is a PCP, the PGFL of ($_p; f; m$) with respect to its reduced Palm distribution is given by the product of its PGFL $G(v(\mathbf{x}; \mathbf{y}))$ and $\tilde{G}_c(v(\mathbf{x}; \mathbf{y})|z)$, where $\tilde{G}_c(v(\mathbf{x}; \mathbf{y})|z)$ is the PGFL of $\mathbf{z} + B^z$ with respect to its reduced Palm distribution. We characterize $G_c(v(\mathbf{x}; \mathbf{y})|z)$ and $\tilde{G}_c(v(\mathbf{x}; \mathbf{y})|z)$ in the next Lemma.

Lemma 3.8. *The PGFL of when $= \mathbf{z} + B^z$ conditioned on the removal of a point at $\mathbf{x}$ is:*

$$\tilde{G}_c(v(\mathbf{x}; \mathbf{y})|z) = G_c(v(\mathbf{x}; \mathbf{y})|z); \tag{3.17}$$

where $G_c(v(\mathbf{x}; \mathbf{y}))$ is the PGFL of $\mathbf{z} + B^z$ which is given by:

$$G_c(v(\mathbf{x}; \mathbf{y})|z) = \exp\left(m \int_{R^2} v(\mathbf{x}; \mathbf{y}) f(\mathbf{y}|z) d\mathbf{y} \right); \tag{3.18}$$

Proof. The PGFL of with respect to its reduced Palm distribution can be expressed as:

$$\begin{aligned}
\tilde{G}_c(v(\mathbf{x}; \mathbf{y})|z) &= \int_{N} \prod_{\mathbf{y} \in } v(\mathbf{x}; \mathbf{y}) P^!_{\mathbf{x}}(d) \\
&\overset{(a)}{=} \sum_{n=1}^{\infty} \int_{N_n} \prod_{\mathbf{y} \in \setminus \{\mathbf{x}\}} v(\mathbf{x}; \mathbf{y}) P(d) \\
&= \sum_{n=1}^{\infty} \int_{[\mathbf{y}_1, \ldots, \mathbf{y}_{n-1}] \in R^{2n-2}} \prod_{i=1}^{m-1} v(\mathbf{x}; \mathbf{y}_i) f(\mathbf{y}_i|z) d\mathbf{y}_i \frac{np_n}{m} \\
&= \sum_{n=1}^{\infty} \left(\int_{R^2} v(\mathbf{x}; \mathbf{y}) f(\mathbf{y}|z) d\mathbf{y} \right)^{n-1} \frac{np_n}{m};
\end{aligned} \tag{3.19}$$

where (a) follows on similar lines of step (a) in the proof of Lemma 3.6. This means we have partitioned N in the same way as we did in the proof of Lemma 3.6. Since we condition on a point $\mathbf{x}$ of to be removed, it implies that will have at least one point. Hence, the number of points in will follow the weighted distribution: $N \frac{np_n}{m}$ (as was the case in Lemma 3.6). Similarly, the PGFL of $= \mathbf{z} + B^z$ with respect to its original distribution can be obtained by

$$G_c(v(\mathbf{x}; \mathbf{y})|z) = \sum_{n=0}^{\infty} \left(\int_{R^2} v(\mathbf{x}; \mathbf{y}) f(\mathbf{y}|z) d\mathbf{y} \right)^{n} p_n. \tag{3.20}$$

Substituting p_n by the PMF of Poisson distribution, we get the desired expression. □

Remark 3.9. We observe that the PGFLs of the offspring point process associated with the PCP are the same under the original and the reduced Palm distribution. From the proof of Lemma 3.8, it is evident that this result is a consequence of the fact that the number of points in the offspring point process is Poisson [13, Section 5.3].

Note that if the number of offspring points are not Poisson distributed, $\bar{\mathcal{G}}_c(v(\mathbf{x}))$ and $G_c(v(\mathbf{x}))$ can be explicitly computed using (3.19) and (3.20), respectively.

3.4 Coverage probability analysis

This is the second main technical section of this chapter, where we evaluate the coverage probability of a typical user in the unified HetNet model which was defined in (3.4). Using the results for the point process functionals derived in the previous Section, we first characterize the coverage probability when clustered nodes (users and/or BSs) are modeled as Neyman-Scott cluster process, and then specialize our result to the case when clustered users and/or BSs are distributed according to MCPs and TCPs.

3.4.1 Neyman-Scott cluster process

We now provide our main result of downlink coverage probability of a typical user for the general K-tier HetNet setup defined in Section 3.2.1 in the following Theorem.

Theorem 3.10. *Assuming that the typical user connects to the BS providing maximum* SIR *and* $_k > 1;\ 8\ k\ 2\ K$*, coverage probability can be expressed as follows:*

$$\mathsf{P}_c = \sum_{k2K} \mathsf{P}_{ck} = \sum_{k2K} \mathsf{E} \sum_{x2\ _k} \prod_{j2Knfkg} G_j(v_{k;j}(\mathbf{x};\mathbf{y})) \prod_{y2\ _knfxg} v_{k;k}(\mathbf{x};\mathbf{y}) \tag{3.21}$$

with

$$v_{i;j}(\mathbf{x};\mathbf{y}) = \frac{1}{1 + \ _i \frac{P_j}{P_i} \ \frac{kxk}{kyk}};\tag{3.22}$$

where P_{ck} *denotes per-tier coverage probability, more precisely, the joint probability of the event that the serving BS belongs to* $_k$ *and the typical user is under coverage, and* $G_j(\ );8j\ 2\ K_1\ [\ K_2$ *is given by Lemma 3.7.*

Proof. Under the assumption that $_k > 1;\ 8\ k\ 2\ K$, there will be at most one BS in satisfying the condition for coverage [21]. Continuing from (3.4),

$$\mathsf{P}_c = \sum_{k2K} \mathsf{E} \sum_{x2\ _k} 1\ \frac{P_k h_x k x k}{I(\ _k n\ fxg) + \sum_{j2Knfkg} I(\ _j)} > \ _k$$

$$= \sum_{k\in K} \mathbb{E}\Big[\sum_{x\in\Phi_k} \mathbb{P}\Big(h_x > \frac{\tau_k}{P_k} I(\Phi_k \cap f x g) + \sum_{j\in K\setminus f k g} I(\Phi_j)\, \|x\|^{\alpha}\Big) \overset{(a)}{=} \sum_{k\in K} \mathbb{E}\Big[\sum_{x\in\Phi_k} \exp\Big(-\frac{\tau_k}{P_k} I(\Phi_k \cap f x g) + \sum_{j\in K\setminus f k g} I(\Phi_j)\, \|x\|^{\alpha}\Big)$$

$$= \sum_{k\in K} \mathbb{E}\Big[\sum_{x\in\Phi_k} \exp\Big(-\frac{\tau_k}{P_k}\|x\|^{\alpha}\Big)\, \mathcal{I}_k(x)\Big]: \tag{3.23}$$

Here, step (a) follows from $h_x \sim \exp(1)$. The final step follows from the independence of Φ_k, $\forall\, k \in K$, where,

$$\mathcal{I}_k(x) = \prod_{j\in K\setminus f k g} \mathbb{E}\Big[\exp\Big(-\frac{\tau_k}{P_k}\|x\|^{\alpha} I(\Phi_j)\Big)\Big]$$

$$= \prod_{j\in K\setminus f k g} \mathbb{E}\Big[\exp\Big(-\frac{\tau_k \|x\|^{\alpha}}{P_k} \sum_{y\in\Phi_j} P_j h_y \|y\|^{\alpha}\Big)\Big]$$

$$= \prod_{j\in K\setminus f k g} \mathbb{E}\Big[\prod_{y\in\Phi_j} \mathbb{E}_{h_y}\Big[\exp\Big(-\frac{\tau_k \|x\|^{\alpha}}{P_k} P_j h_y \|y\|^{\alpha}\Big)\Big]\Big]$$

$$\overset{(a)}{=} \prod_{j\in K\setminus f k g} \mathbb{E}\Big[\prod_{y\in\Phi_j} \frac{1}{1+\tau_k \frac{P_j}{P_k}\frac{\|x\|^{\alpha}}{\|y\|^{\alpha}}}\Big]$$

$$= \prod_{j\in K\setminus f k g} \mathcal{G}_j(v_{k;j}(x;y)):$$

Step (a) follows from the fact that $f h_y g$ is an i.i.d. sequence of exponential random variables. Following from (3.23), we get,

$$\mathbb{P}_c = \sum_{k\in K} \mathbb{E}\Big[\sum_{x\in\Phi_k} \mathcal{I}_k(x) \exp\Big(-\frac{\tau_k}{P_k}\|x\|^{\alpha} I(\Phi_k \cap f x g)\Big)\Big]:$$

The exponential term can be simplified following on similar lines as that of $\mathcal{I}_k(x)$ and hence we obtain the final expression. □

Remark 3.11 (Coverage probability is the summation of $K+1$ sum-product functionals)**.** In (3.21), $\mathbb{P}_c$ is the summation of $(K+1)$ per-tier coverage probabilities, due to the contribution of $(K+1)$ tiers in $\Phi = \bigcup_{k\in K} \Phi_k$. Recalling Definition 4.10, $\mathbb{P}_{ck}$ is in the form of sum-product functional over Φ_k, with $g(x) \equiv \prod_{j\in K\setminus f k g} \mathcal{G}_j(v_{k;j}(x;y))$ and $v(x;y) \equiv v_{k;k}(x;y)$ in (3.5).

In the previous Section, we have computed the sum-product functional over PPP, PCP and the offspring point process in terms of arbitrary measurable functions $g(x)$ and $v(x;y)$. We directly apply these results to compute $\mathbb{P}_{ck}$. We first provide the expression of PGFL of Φ_0 evaluated at $v_{k;0}(x;y)$. Depending on the construction of Φ_0 based on three different configurations of Φ_u (refer to (3.2)), we will have different expressions of $\mathcal{G}_0(\,)$.

Lemma 3.12. *The PGFL of* Φ_0 *is given by:*

- case *1:* $G_0(v_{k;0}(\mathbf{x};\mathbf{y})) = 1$;
- case *2:*
$$G_0(v_{k;0}(\mathbf{x};\mathbf{y})) = \int_{\mathbb{R}^2} \frac{1}{1+\frac{P_{0\ k}}{P_k}\|\mathbf{x}\|\ \|\mathbf{y}\|^{\alpha}} f_0(\mathbf{y})d\mathbf{y};$$
- case *3:*
$$G_0(v_{k;0}(\mathbf{x};\mathbf{y})) = \int_{\mathbb{R}^2} G_{c_0}(v_{k;0}(\mathbf{x};\mathbf{y})|\mathbf{z}')f_0(\mathbf{z}')d\mathbf{z}';$$

where $G_c(\cdot|\mathbf{z})$ *is given by Lemma 3.8.*

Proof. In case 1, Φ_0 is a null set if users are distributed according to a PPP, and hence $G_0(v_{k;0}(\mathbf{x};\mathbf{y})) = 1$. In case 2, where users are distributed as a PCP with parent PPP Φ_j $(j \in \mathcal{K}_1)$,
$$G_0(v_{k;0}(\mathbf{x};\mathbf{y})) = \int_{\mathbb{R}^2} v_{k;0}(\mathbf{x};\mathbf{y})f_0(\mathbf{y})d\mathbf{y}. \tag{3.24}$$
In case 3, $\Phi_0 = B_j^{\mathbf{z}_0}$ is a cluster of Φ_j $(j \in \mathcal{K}_2)$ centered at $\mathbf{z}_0$. Its PGFL is provided by Lemma 3.8, and the final result is obtained by taking expectation over $\mathbf{z}_0 \sim f_0(\mathbf{z}_0)$. □

Having characterized the PGFLs of Φ_k $\forall k \in \mathcal{K}$, we evaluate $\mathtt{P}_{ck}$ in the following Lemmas.

Lemma 3.13. *When the BS tier* Φ_k *is a PCP, i.e.,* $k \in \mathcal{K}_2$*, per-tier coverage can be expressed as:*
$$\mathtt{P}_{ck} = \int_{\mathbb{R}^2}\int_{\mathbb{R}^2} G_k(v_{k;k}(\mathbf{x};\mathbf{y}))\bar{G}_{c_k}(v_{k;k}(\mathbf{x};\mathbf{y})|\mathbf{z}) \prod_{j\in\mathcal{K}\setminus\{k\}} G_j(v_{k;j}(\mathbf{x};\mathbf{y}))\ \Lambda_k(d\mathbf{x};d\mathbf{z}),\ k \in \mathcal{K}_2; \tag{3.25}$$
where $\Lambda_k(\mathbf{x};\mathbf{z})$ *is given by* (3.10)*,* $\bar{G}_{c_k}(\cdot)$ *is obtained by Lemmas 3.8.* $G_j(\cdot)$ *and* $G_k(\cdot)$ *are given by Lemma 3.7.*

Proof. The result is obtained by the direct application of Lemma 3.5. □

Remark 3.14. When Φ_j is a PPP, i.e., $j \in \mathcal{K}_1$, $G_j(v_{k;j}(\mathbf{x};\mathbf{y}))$ presented in Lemma 3.7 can be further simplified as:
$$G_j(v_{k;j}(\mathbf{x};\mathbf{y})) = \exp\left(-\pi\lambda_j\left(\frac{P_{j\ k}}{P_k}\right)^{\frac{2}{\alpha}}\|\mathbf{x}\|^2 C(\alpha)\right), \forall j \in \mathcal{K}_1; \tag{3.26}$$
with $C(\alpha) = \frac{2}{\alpha}\sin(\frac{2}{\alpha})$. See [21, Theorem 1] for an elaborate proof.

3.4. Coverage probability analysis

In the next Lemma, we present per-tier coverage probability $\mathtt{P}_{ck}$ ($k \in K_1$).

Lemma 3.15. *When the BS tier is a PPP, per-tier coverage can be expressed as:*

$$\mathtt{P}_{ck} = \int_{\mathbb{R}^2} \prod_{j \in K} G_j(v_{k;j}(\mathbf{x};\mathbf{y}))\mathrm{d}\mathbf{x}; \qquad k \in K_1; \tag{3.27}$$

where $G_j(\cdot)$ is obtained by (3.26) for $j \in K_1$. When $j \in K_2$, $G_j(\cdot)$ is given by Lemma 3.7.

Proof. The result is obtained by the direct application of Lemma 3.4. □

Having characterized per-tier coverage $\mathtt{P}_{ck}$ for $k \in K_1 \cup K_2$, we are left with the evaluation of $\mathtt{P}_{c0}$ which we do next. Similar to Lemma 3.12, we will have three different cases for $\mathtt{P}_{c0}$ owing to different user configurations.

Lemma 3.16. $\mathtt{P}_{c0}$ *can be expressed as follows.*

$$\mathtt{P}_{c_0} = \begin{cases} 0; \text{when } \mathcal{Z}_0 = \emptyset \text{ (case 1)}, \\ \int_{\mathbb{R}^2} \prod_{j \in K \cup \{0\}} G_j(v_{0;j}(\mathbf{z}_0;\mathbf{y})) f_0(\mathbf{z}_0)\mathrm{d}\mathbf{z}_0; \\ \text{when } \mathcal{Z}_0 = \{\mathbf{z}_0\} \text{ (case 2)}, \\ \int_{\mathbb{R}^2}\int_{\mathbb{R}^2} \exp\left(-m_0 \int_{\mathbb{R}^2} 1 - v_{0;0}(\mathbf{x};\mathbf{y}) f_0(\mathbf{y}|\mathbf{z}_0)\mathrm{d}\mathbf{y} - m_0 \int_{\mathbb{R}^2} v_{0;0}(\mathbf{x};\mathbf{y}) f_0(\mathbf{y}|\mathbf{z}_0)\mathrm{d}\mathbf{y} + 1\right) \\ \prod_{j \in K \cup \{0\}} G_j(v_{0;j}(\mathbf{x};\mathbf{y})) f_0(\mathbf{x}|\mathbf{z}_0) f_0(\mathbf{z}_0)\,\mathrm{d}\mathbf{x}\,\mathrm{d}\mathbf{z}_0; \\ \text{when } \mathcal{Z}_0 = B_q^{\mathbf{z}_0} \text{ (case 3)}, \end{cases}$$

where $G_j(\cdot)$ is given by Lemma 3.12 and $f_0(\mathbf{z}_0)$ is the PDF of $\mathbf{z}_0$ which is defined in (3.2).

Proof. Case 1 is trivial. For case 2, $\mathcal{Z}_0$ has only one point with PDF $f_0(\mathbf{z}_0)$. For case 3, we use Lemma 3.6 with $g(\mathbf{x}) = \prod_{j \in K \cup \{0\}} G_j(v_{0;j}(\mathbf{x};\mathbf{y}))$ and $v(\mathbf{x};\mathbf{y}) = v_{0;0}(\mathbf{x};\mathbf{y})$ and take expectation with respect to $\mathbf{z}_0 \sim f_0(\mathbf{z}_0)$. □

Note that although we have derived $\mathtt{P}_c$ for cases 1-3 separately, in real networks the user distribution is a mixture of these cases. We can easily extend this analysis for such mixed user distribution following the arguments presented in [71, Section IV-E].

3.4.2 Convergence

In this Section, we prove that as cluster size of all the PCPs (i.e. $_k$, $8\ k\ 2\ K_2$ and $_u$ for case 2 and case 3) tends to infinity, our general model converges to the PPP-based baseline model where all BS and users are modeled as independent PPPs. First, we focus on the limiting nature of the BS point process $^0 = [_{k2K_1[K_2} \ _k$. As the cluster size of $_k$ $8\ k\ 2\ K_2$ increases, the limiting baseline model in this case consists of BS tiers all modeled as PPPs, i.e., $= [_{k2K_1[K_2} \ _k$, where $f \ _k = \ _k : k\ 2\ K_1 g$ is the collection of the PPP BS tiers in the original model and $f \ _k : k\ 2\ K_2 g$ is the collection of BS tiers which are also PPP with intensity $m_k \ _{p_k}$. We will show that as the cluster size of $_k$ $(k\ 2\ K_2)$ goes to infinity, $_k$ converges to $_k$ which is independent of the parent PPP $_{p_k}$.

We first formally introduce the notion of increasing the *cluster size* of a PCP $_k$ $(k\ 2\ K_2)$ which means that the points in offspring process (i.e., $\mathbf{z} + B_k^{\mathbf{z}}$) will lie farther away from the cluster center $(\mathbf{z}\ 2\ _{p_k})$ with high probability. One way of modeling this notion is to scale the positions of the offspring points with respect to the cluster center by , i.e., $\mathbf{z} + B_k^{\mathbf{z}} = fyg = f\mathbf{z} + \ sg$. Then the density function defined in R^2 becomes

$$f_{k;}(\mathbf{y}jz) \quad f_{k;}(\mathbf{y} \quad \mathbf{z}) = \frac{1}{2} f_k \ \frac{\mathbf{y} \quad \mathbf{z}}{\quad}\ ; \qquad 8\ \mathbf{y}\ 2\ \mathbf{z} + B_k^{\mathbf{z}}: \tag{3.28}$$

The limiting nature of PCP to PPP is formally proved in the following Proposition.

Proposition 3.17 (Weak Convergence of PCP to PPP). *For a PCP* $_k$ $(\ _{p_k}; f_{k;}\ ; m_k)$,

$$_k \ ! \quad _k \ (\textit{weakly})\ \textit{as} \quad ! \ \ 1\ ; \tag{3.29}$$

where $_k$ *is a PPP of intensity* $m_k \ _{p_k}$ *if* $\sup(f_k) < \ 1$.

Proof. A simple point process $_k$ $(k\ 2\ K_2)$ converges weekly to $_k$ if [77, Theorem 9.1.2]

$$\mathsf{E}[\ _k(A)] \ ! \ \mathsf{E}[\ _k(A)]; \tag{3.30a}$$

$$\mathsf{P}(\ _k(A) = 0) \ ! \ \mathsf{P}(\ _k(A) = 0); \tag{3.30b}$$

for any closed $A \quad \mathsf{R}^2$. Here the same notation has been used to designate a point process and its associated counting measure. Since $\mathsf{E}[\ _k(A)] = \mathsf{E}[\ _k(A)] = m_k \ _{p_k}$, (3.30a) is satisfied. Next, we observe from (3.28) that as long as $f_k(\ )$ is bounded, $f_{k;}(\mathbf{s}) \ ! \ 0$ as $! \ \ 1$. Now, the void probability of $_k$ i.e. the probability that no points of $_k$ will lie in A along with the limit $! \ \ 1$ can be written as:

$$\lim_{! \ 1} \mathsf{P}(\ _k(A) = 0) = \lim_{! \ 1} \mathsf{E} \left[\prod_{\mathbf{z}2 \ _{p_k}} \prod_{\mathbf{y}2\mathbf{z}+B_k^{\mathbf{z}}} \mathbf{1}(\mathbf{y} \not{2} A) \right]$$

$$= \lim_{! \ 1} \exp\left(\ _{p_k} \int_{\mathsf{R}^2} \left[1 \quad \exp\left(m_k \int_{\mathsf{R}^2 n A} f_{k;}(\mathbf{y} \quad \mathbf{z}) d\mathbf{y} \right) \right] d\mathbf{z} \right)$$

$$
\begin{aligned}
&= \lim_{\lambda \to 1} \exp\left(-\int_{\mathbb{R}^2} \left(1 - \exp\left(-\int_A f_{k,\lambda}(\mathbf{y}-\mathbf{z})\,d\mathbf{y} \right) \right) d\mathbf{z} \right) \\
&\overset{(a)}{=} \lim_{\lambda \to 1} \exp\left(-\int_{\mathbb{R}^2} \int_A f_{k,\lambda}(\mathbf{y}-\mathbf{z})\,d\mathbf{y}\,d\mathbf{z} \right) \\
&\overset{(b)}{=} \exp\left(-\mu_k |A| \right) = \mathbb{P}(\Phi_k(A) = 0),
\end{aligned}
$$

where (a) follows from Taylor series expansion of the exponential function under integration and neglecting the higher order terms as $\lambda \to 1$ and (b) follows from interchanging the order of integrals and the fact that $|A|$ is finite. □

We now argue that as $\lambda \to 1$, Φ_k becomes independent of its parent PPP Φ_{p_k}.

Proposition 3.18. *The limiting PPP Φ_k and the parent PPP Φ_{p_k} of Φ_k $(k = 1, \ldots, K_2)$ are independent, i.e.,*

$$
\lim_{\lambda \to 1} \mathbb{P}(\Phi_k(A_1) = 0, \Phi_{p_k}(A_2) = 0) = \mathbb{P}(\Phi_k(A_1) = 0)\mathbb{P}(\Phi_{p_k}(A_2) = 0), \tag{3.31}
$$

where $A_1, A_2 \subset \mathbb{R}^2$ are arbitrary closed compact sets.

Proof. Following Choquet theorem for random closed sets [13, Theorem 6.1], (3.31) is a sufficient condition to claim independence of Φ_k and Φ_{p_k}. Under the limit $\lambda \to 1$:

$$
\begin{aligned}
&\lim_{\lambda \to 1} \mathbb{P}(\Phi_k(A_1) = 0, \Phi_{p_k}(A_2) = 0) \\
&= \lim_{\lambda \to 1} \mathbb{P}(\Phi_k(A_1) = 0 \mid \Phi_{p_k}(A_2) = 0)\mathbb{P}(\Phi_{p_k}(A_2) = 0) \\
&= \lim_{\lambda \to 1} \mathbb{E}\left[\prod_{\mathbf{z} \in \Phi_{p_k} \setminus A_2^c} \prod_{\mathbf{y} \in 2\mathbf{z} + B_k^{\mathbf{z}}} \mathbf{1}(\mathbf{y} \notin A_1) \right] \mathbb{P}(\Phi_{p_k}(A_2) = 0) \\
&= \lim_{\lambda \to 1} \exp\left(-\int_{\mathbb{R}^2 \setminus A_2} p_k \left(1 - \exp\left(-\int_{A_1} f_{k,\lambda}(\mathbf{y}-\mathbf{z})\,d\mathbf{y} \right) \right) d\mathbf{z} \right) \mathbb{P}(\Phi_{p_k}(A_2) = 0) \\
&\overset{(a)}{=} \lim_{\lambda \to 1} \exp\left(-\mu_k \int_{\mathbb{R}^2 \setminus A_2} \int_{A_1} f_{k,\lambda}(\mathbf{y}-\mathbf{z})\,d\mathbf{y}\,d\mathbf{z} \right) \\
&\qquad \mathbb{P}(\Phi_{p_k}(A_2) = 0) \\
&= \lim_{\lambda \to 1} \exp\left(-\mu_k \int_{\mathbb{R}^2} \int_{A_1} f_{k,\lambda}(\mathbf{y}-\mathbf{z})\,d\mathbf{y}\,d\mathbf{z} \right) \\
&\qquad \exp\left(-\mu_k \int_{A_2} \int_{A_1} f_{k,\lambda}(\mathbf{y}-\mathbf{z})\,d\mathbf{y}\,d\mathbf{z} \right) \mathbb{P}(\Phi_{p_k}(A_2) = 0)
\end{aligned}
$$

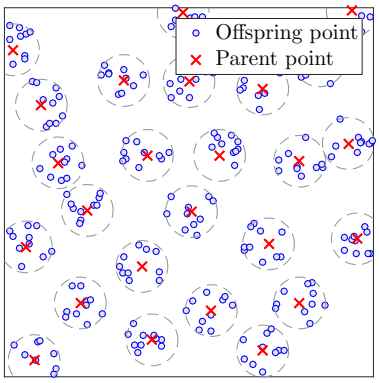

Figure 3.2: A realization of a Matérn cluster process.

$$\overset{(b)}{=} \exp\left(-\lambda_k m_k \pi A_1 - \mathrm{P}(\Phi_k(A_2) = 0)\right)$$

$$= \lim_{\lambda \to 1} \mathrm{P}(\Phi_k(A_1) = 0)\mathrm{P}(\Phi_k(A_2) = 0);$$

where (a) follows on the similar lines of step (a) in the proof of Proposition 3.17. In (b), we apply the limit $\lambda \to 1$. The first term in the product follows from Proposition 3.17 and the second term goes to 1 as the double integral over a finite region $(A_1 \times A_2)$ tends to zero as $\lim_{\lambda \to 0} f_{k,\lambda}(s) = 0$. □

Remark 3.19. Using Propositions 3.17 and 3.18, we can claim that the K-tier HetNet model under case 2 (Φ_u is a PCP around Φ_q $(q \in K_1)$) converges to that of case 1 (i.e., users form a PPP independent of BS locations) as the cluster size of Φ_u increases to infinity. Further, for case 3, where Φ_u and Φ_q are coupled by the same parent PPP Φ_{p_q}, as the cluster size of Φ_u as well as Φ_q $(q \in K_2)$ increase to infinity, Φ_u and Φ_q become independent PPPs.

From this Proposition, we can directly conclude the following.

Corollary 3.20. *When cluster size of Φ_k, $\forall k \in K_2$ tends to infinity, coverage probability can be written as [21, Corollary 1]:*

$$\mathrm{P_c} = \frac{\sum_{k \in K_1} \frac{\lambda_k P_k^{\frac{2}{\alpha}}}{\mathrm{C}(\delta,\alpha)} + \sum_{k \in K_2} \frac{m_k \lambda_k P_k^{\frac{2}{\alpha}}}{\mathrm{C}(\delta,\alpha)}}{\sum_{j \in K_1} \lambda_j P_j^{\frac{2}{\alpha}} + \sum_{j \in K_2} m_j \lambda_j P_j^{\frac{2}{\alpha}}}; \tag{3.32}$$

where $\mathrm{C}(\delta,\alpha) = \frac{2\pi}{\alpha}\csc(\frac{2\pi}{\alpha})$.

Having derived the expression for coverage probability under the general framework, we now focus on two special cases as follows.

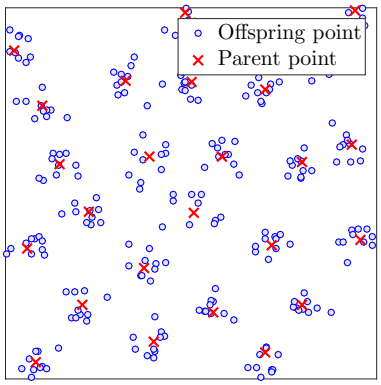

Figure 3.3: A realization of a Thomas cluster process.

3.4.3 Matérn cluster process

We assume that all BS tiers $_k$, $8\,k\;2\;K_2$ and user tier $_u$ (for case 2 and case 3) are modeled as MCP. We choose MCP for $_k$ ($8\,k\;2\;K_2$) since it closely resembles 3GPP model for SBS and user clusters. We first formally define MCP $_k$ ($k\;2\;K_2$) as follows.

Definition 3.21 (MCP)**.** A PCP $_k$ ($_{p_k}; f_k; m_k$) is called a MCP if the distribution of the offspring points in B_k^z is uniform within a disc of radius r_{d_k} around the origin denoted by $b(0; r_{d_k})$, i.e., if $\mathbf{s} = (ksk; \arg(\mathbf{s}))$ $(s; \ _s)\;2\;B_k^z$ denotes a point of the offspring point process B_k^z with cluster center at origin, then the joint PDF of the polar coordinates of $\mathbf{s}$ is denoted by:

$$f_k(\mathbf{s}) = f_k(s; \ _s) = \frac{2s}{r_{d_k}^2}\ \frac{1}{2}; \qquad 0 < s \quad r_{d_k}; 0 < \ _s \quad 2\ : \tag{3.33}$$

Note that we will use $(s; \ _s)$ and $(ksk; \arg(\mathbf{s}))$ as the representation of $\mathbf{s}\;2\;\mathsf{R}^2$ in Polar coordinates interchangeably. A realization of an MCP is illustrated in Fig. 3.2. First, we observe that the functions associated with the sum-product functional in the coverage probability expression in Theorem 3.10 are isotropic, i.e., referring to (3.5), $v(\mathbf{x}; \mathbf{y}) = v(x; y)$ $v_{k;k}(x; y)$ and $g(\mathbf{x}) = g(x)$ $\prod_{j2Knfkg} G_j(v_{k;j}(x; y))$, $8\,k; j\;2\;K$. Thus, the sum-product functional for $_k$ appearing in P_{ck} in (3.21) is in the form: $\mathsf{E}\left[\sum_{\mathbf{x}2\ _k} g(x) \prod_{\mathbf{y}2\ _{k^nfxg}} v(x; y)\right]$. Following Lemmas 3.4, 3.5 and 3.8, it is sufficient to evaluate the PGFLs $G_j(v_{k;j}(x; y))$ and $G_{c_j}(v_{k;j}(x; y))$ for P_{ck}, which we do next. We will use these results to derive the final expression of coverage probability.

Remark 3.22. We observe that the integrals appearing in (3.16) and (3.21) are in the form:

$$\int_0^{\ _1}\int_0^{\ _2} (x; z) f_k(\mathbf{x}jz)\mathrm{d}x\,\mathrm{d}\ _x = \int_0^{\ _1} (x; z) \int_0^{\ _2} f_k(x; \ _xjz)\mathrm{d}\ _x\,\mathrm{d}x: \tag{3.34}$$

Here $\int_0^{R_2} f_k(x; \ _xjz)\mathrm{d}\ _x$ is the marginal distribution of the magnitude of $\mathbf{x}\;2\;\ _k$ ($k\;2\;K_2$) conditioned on $\mathbf{z}\;2\;\ _{p_k}$.

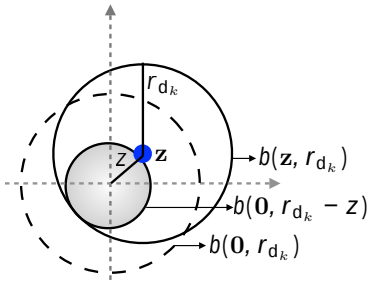

(a) $\mathbf{z} \in b(\mathbf{0}; r_{d_k})$; $\mathbf{x} \in b(\mathbf{0}; r_{d_k} - z)$, or $\mathbf{z} \in b(\mathbf{0}; r_{d_k})$; $\mathbf{x} \in b(\mathbf{z}; r_{d_k}) \cap b(\mathbf{0}; r_{d_k} - z)$.

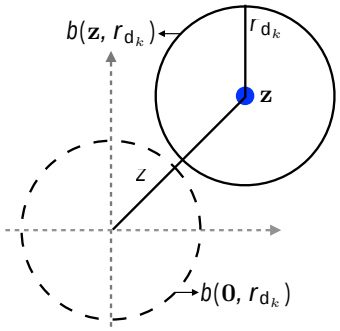

(b) $\mathbf{z} \notin b(\mathbf{0}; r_{d_k})$; $\mathbf{x} \in b(\mathbf{z}; r_{d_k})$.

Figure 3.4: Possible positions of a cluster center at $\mathbf{z}$ for the evaluation of the distribution of distance of a randomly chosen point $\mathbf{x} \in \mathbf{z} + B_k^{\mathbf{z}}$ of an MCP from origin.

In order to characterize the conditional magnitude distribution of $\mathbf{x}$ given $\mathbf{z} \in$ $_{p_k}$, we define three regions $R_k^{(1)}; R_k^{(2)}; R_k^{(3)}$ $\mathbb{R}^2$ $\mathbb{R}^2$ as:

$$R_k^{(1)} \quad \mathbf{z} \in b(\mathbf{0}; r_{d_k}); \ \mathbf{x} \in b(\mathbf{0}; r_{d_k} - z); \tag{3.35a}$$

$$R_k^{(2)} \quad \mathbf{z} \in b(\mathbf{0}; r_{d_k}); \ \mathbf{x} \in b(\mathbf{z}; r_{d_k}) \cap b(\mathbf{0}; r_{d_k} - z); \tag{3.35b}$$

$$R_k^{(3)} \quad \mathbf{z} \notin b(\mathbf{0}; r_{d_k}); \ \mathbf{x} \in b(\mathbf{z}; r_{d_k}): \tag{3.35c}$$

Illustrations of these regions are provided in Fig. 3.4. For each region, the marginal distribution of x conditioned on $\mathbf{z}$ is given by [78]: $\int_0^{R_2} f_k(x; \ _x|z)\mathrm{d}\ _x = \ _k^{(\ell)}(x; z)$ when $(\mathbf{z}; \mathbf{x}) \in R_k^{(\ell)}$ $(\ell = 1; 2; 3)$, where

$$_k^{(1)}(x; z) = \frac{2x}{r_{d_k}^2}; 0 < x < r_{d_k} \quad z; 0 < z \quad r_{d_k}; \tag{3.36a}$$

$$_k^{(2)}(x; z) = \frac{2x}{r_{d_k}^2} \cos^{-1} \quad \frac{x^2 + z^2 \quad r_{d_k}^2}{2xz} \quad ;$$

$$r_{d_k} \quad z < x < r_{d_k} + z; 0 < z \quad r_{d_k}; \tag{3.36b}$$

$$_k^{(3)}(x; z) = \frac{2x}{r_{d_k}^2} \cos^{-1} \quad \frac{x^2 + z^2 \quad r_{d_k}^2}{2xz} \quad ;$$

$$z \quad r_{d_k} < x < z + r_{d_k}; z > r_{d_k}: \tag{3.36c}$$

We now present the expressions of PGFLs of $_k$ $(k \in K_2)$.

Corollary 3.23 (PGFL of MCP)**.** *The PGFL of MCP* $_j$ *(*$j \in K_2$*) evaluated at* $v_{k;j}(x; y)$ *is:*

$$G_j(v_{k;j}(x; y)) = \exp \quad 2 \quad _{p_j} \int_0^{r_{d_j}} 1 \quad \exp \quad m_j$$

$$\int_0^{r_{\mathrm{d}_j}} z \left(1 - v_{k;j}(x;y)\right) {}^{(1)}_{j}(y;z)\mathrm{d}y + \int_{r_{\mathrm{d}_j}}^{z} \left(1 - v_{k;j}(x;y)\right) {}^{(2)}_{j}(y;z)\mathrm{d}y \, z\mathrm{d}z \Big)^{2\pi\mathrm{p}_j} \int_{r_{\mathrm{d}_j}}^{1} 1 - \exp\left(-m_j \int_{z-r_{\mathrm{d}_j}}^{z+r_{\mathrm{d}_j}} \left(1 - v_{k;j}(x;y)\right) {}^{(3)}_{j}(y;z)\mathrm{d}y \, z\mathrm{d}z\right); \quad (3.37)$$

where ${}^{(\ell)}_{j}(x;z)$ *(*$\ell = 1;2;3$*) are given by* (6.3).

Proof. The expression can be derived from (3.16) using Remark 3.22. □

Corollary 3.24 (PGFL of Offspring Point Process of MCP)**.** *The PGFL of* $B_j^{\mathbf{z}}$*, which is the offspring process of* $_j$ *(*$j \in K_2$*) centered at* $\mathbf{z}$*, evaluated at* $v_{k;j}(x;y)$ *is given by*

$$G_{c_j}(v_{k;j}(x;y)|\mathbf{z}) = \begin{cases} G^{(1)}_{c_j}(v_{k;j}(x;y)|\mathbf{z}) & z \le r_{\mathrm{d}_j} \\ G^{(2)}_{c_j}(v_{k;j}(x;y)|\mathbf{z}) & z > r_{\mathrm{d}_j}; \end{cases} \quad (3.38)$$

where $G^{(1)}_{c_j}(v_{k;j}(x;y)|\mathbf{z}) = \exp\left(-m_j \int_0^{r_{\mathrm{d}_j}} \int_{z-r_{\mathrm{d}_j}}^{z} \left(1 - v_{k;j}(x;y)\right) {}^{(1)}_{j}(y;z)\mathrm{d}y + \int_{r_{\mathrm{d}_j}}^{z+r_{\mathrm{d}_j}} v_{k;j}(x;y) \, {}^{(2)}_{j}(y;z)\mathrm{d}y\right)$

and $G^{(2)}_{c_j}(v_{k;j}(x;y)|\mathbf{z}) = \exp\left(-m_j \int_{z-r_{\mathrm{d}_j}}^{z+r_{\mathrm{d}_j}} \left(1 - v_{k;j}(x;y)\right) {}^{(3)}_{j}(y;z)\mathrm{d}y\right)$.

Proof. The expression can be derived from (3.18) using Remark 3.22. □

We can now obtain the PGFL of an MCP under its reduced Palm distribution at $v_{k;k}(x;y)$ by rewriting (3.12) and using (3.17) as: $\breve{G}_k(v_{k;k}(x;y)|\mathbf{z}) =$

$$\begin{cases} \breve{G}^{(1)}_k(v_{k;k}(x;y)|\mathbf{z}) = G_k(v_{k;k}(x;y)) G^{(1)}_{c_k}(v_{k;k}(x;y)|\mathbf{z}); \\ \qquad z \le r_{\mathrm{d}_k}; \\ \breve{G}^{(2)}_k(v_{k;k}(x;y)|\mathbf{z}) = G_k(v_{k;k}(x;y)) G^{(2)}_{c_k}(v_{k;k}(x;y)|\mathbf{z}); \\ \qquad z > r_{\mathrm{d}_k}; \end{cases} \quad (3.39)$$

where $G_k(v_{k;k}(x;y))$ and $\breve{G}_{c_k}(v_{k;k}(x;y)|\mathbf{z})$ are given by Corollaries 3.23 and 3.24, respectively. We are left with the PGFL of $_0$, i.e., $G_0(v_{0;k}(x;y))$ can be obtained by substitution of $f_0(\,)$ in Lemma 3.12 with (4.23). For case 2, this can be given as:

$$G_0(v_{k;0}(x;y)) = \int_0^{r_{\mathrm{d}_0}} \frac{1}{1 + \frac{P_{0\ k}}{P_k} \frac{x}{y}} \frac{2y}{r_{\mathrm{d}_0}^2}\mathrm{d}y.$$

For case 3,

$$G_0(v_{k;0}(x;y)) = \int_0^{r_{d_0}} G_{c_0}(v_{k;0}(x;y)|z_0)\frac{2z_0}{r_{d_0}^2}\mathrm{d}z_0.$$

We now present the expression of per-tier coverage P_{ck} for $k \in \mathcal{K}_2$.

Corollary 3.25. *Per-tier coverage probability for $k \in \mathcal{K}_2$ when all BS tiers in $\mathcal{K}_2$ are modeled as MCPs can be expressed as:*

$$\begin{aligned}\mathsf{P}_{ck} = 2\pi\lambda_k \int_0^{r_{d_k}}\int_0^{r_{d_k}-z} g(x)G_k(v_{k;k}(x;y))G_{c_k}^{(1)}(v_{k;k}(x;y)|z)\,\mathcal{A}_k^{(1)}(x;z)\mathrm{d}x\,z\mathrm{d}z \\ + 2\pi\lambda_k \int_0^{r_{d_k}}\int_{r_{d_k}-z}^{r_{d_k}+z} g(x)G_k(v_{k;k}(x;y))G_{c_k}^{(1)}(v_{k;k}(x;y)|\mathbf{z})\,\mathcal{A}_k^{(2)}(x;z)\mathrm{d}x\,z\mathrm{d}z \\ + 2\pi\lambda_k \int_{r_{d_k}}^{1}\int_{z-r_{d_k}}^{r_{d_k}} g(x)G_k(v_{k;k}(x;y))G_{c_k}^{(2)}(v_{k;k}(x;y)|\mathbf{z})\,\mathcal{A}_k^{(3)}(x;z)\mathrm{d}x\,z\mathrm{d}z;\ k \in \mathcal{K}_2;\end{aligned}$$

where $g(x) = \prod_{j\in\mathcal{K}_1} G_j(v_{k;j}(x;y)) \prod_{j\in\mathcal{K}_2\setminus\{k\}} G_j(v_{k;j}(x;y))$. Here $G_j(v_{k;j}(x;y))$ is given by (3.26) and (3.37) for $j \in \mathcal{K}_1$ and $j \in \mathcal{K}_2$, respectively, and $G_{c_k}^{(1)}(\,)$, $G_{c_k}^{(2)}(\,)$ are given by Corollary 3.24.

Proof. The expression is obtained from Lemma 3.13 by using the Polar domain representation of the vectors and the distance distribution introduced in (6.3). □

As noted earlier, P_{c0} can be obtained by computing sum-product functional over Φ_0 which has three different forms depending on the user configuration. While case 1 and case 2 are simple, for case 3, we need to evaluate sum-product functional of $\mathbf{z} + B_k^{\mathbf{z}}$.

Corollary 3.26. *Per-tier coverage probability for $k = 0$ when all BS tiers in $\mathcal{K}_2$ are modeled as MCPs can be expressed as:* P_{c0}

$$= \begin{cases} 0; & \text{case 1;} \\ \int_0^{r_{d_0}} \prod_{j\in\mathcal{K}\setminus\{0\}} G_j(v_{0;j}(z_0;y))\, f_0(z_0)\mathrm{d}z_0; & \text{case 2;} \\ \int_0^{r_{d_0}}\int_0^{r_{d_0}-z_0} H(x;z_0)\,\mathcal{A}_0^{(1)}(x;z_0)\mathrm{d}x \\ \quad + \int_{r_{d_0}-z_0}^{r_{d_0}+z_0} H(x;z_0)\,\mathcal{A}_0^{(2)}(x;z_0)\mathrm{d}x\; 2z_0/r_{d_0}^2\mathrm{d}z_0; & \text{case 3;} \end{cases}$$

and

$$H(x;z) = \prod_{j \in Knf0g} G_j(v_{0;j}(x;y)) \exp\Big(m_0 \int_0^{r_{d_0} - z} (1 - v_{0;0}(x;y))\, {}_0^{(1)}(y;z)dy + \int_{r_{d_0} - z}^{r_{d_0}+z} (1 - v_{0;0}(x;y))\, {}_0^{(2)}(y;z)dy \int_{r_{d_0} - z}^{r_{d_0} - z} m_0 \int_0^{r_{d_0} - z} v_{0;0}(x;y)\, {}_0^{(1)}(y;z)dy + \int_0^{r_{d_0} - z} v_{0;0}(x;y)\, {}_0^{(2)}(y;z)dy + 1 \Big) \quad : \quad (3.40)$$

Proof. For case 1 and case 2, the result follows directly from Lemma 3.16. For case 3, we need the sum-product functional of $_0 = \mathbf{z}_0 + B_q^{z_0} \quad \mathbf{z}_0 + B_0^{z_0}$. Now, by construction, $z_0 < r_{d_q} \quad r_{d_0}$. Since the representative BS cluster $B_0^{z_0}$ has the same cluster center $\mathbf{z}_0$ of the typical user located at origin. We first evaluate the sum-product functional of $\mathbf{z} + B_0^z$ following Lemma 3.6, which can be written as: $\mathsf{E}\Big[\prod_{x \in (\mathbf{z}+B_0^z)} g(x) \prod_{y \in (\mathbf{z}+B_0^z) nf x g} v(x;y) \Big] =$

$$g(x) \exp\Big(m_0 \int_0^{r_{d_0} - z} (1 - v(x;y))\, {}_0^{(1)}(y;z)dy + \int_{r_{d_0} - z}^{0} {}^{r_{d_0}+z} (1 - v(x;y))\, {}_0^{(2)}(y;z)dy \int_{r_{d_0} - z}^{r_{d_0} - z} m_0 \int_0^{r_{d_0} - z} v(x;y)\, {}_0^{(1)}(y;z)dy + \int_{r_{d_0} - z}^{r_{d_0}+z} v(x;y)\, {}_0^{(2)}(y;z)dy + 1 \Big) \; ; \quad z \quad r_{d_0}.$$

Now substituting $g(x)$ by $\prod_{j \in Knf0g} G_j(v_{0;j}(x;y))$ and $v(x;y)$ by $v_{0;0}(x;y)$ (given by (3.21) and (3.22), respectively) and deconditioning over z_0, we get the final form. □

3.4.4 Thomas cluster process

We further provide the results of coverage probability when all BS tiers $_k$, $8\, k \in K_2$ are modeled as TCP. We first formally define TCP as follows.

Definition 3.27 (TCP)**.** A PCP $_k$ ($_{p_k}; f_k; m_k$) is called a TCP if the distribution of the offspring points in B_k^z is Gaussian around the cluster center at origin, i.e. for all $\mathbf{s} \in B_k^z$,

$$f_k(\mathbf{s}) = f_k(s; \ _s) = \frac{s}{\frac{2}{k}} \exp\Big(\frac{s^2}{2 \ \frac{2}{k}} \Big) \frac{1}{2}; s > 0; 0 < \ _s \quad 2 \quad : \quad (3.41)$$

A realization of a TCP is illustrated in Fig. 3.3. It will be evident at the end of this Section that compared to MCP, TCP yields simpler expression of coverage probability (due to infinite support of $f_k(\mathbf{s})$). Note that while TPC does not directly analogous to the notion of *cluster* adopted in 3GPP HetNet, we include it here to demonstrate the generality of the proposed framework that surpasses that of the cluster-based simulation models adopted by 3GPP. Given that $\mathbf{z}$ is the cluster center of $\mathbf{x}$, i.e., $\mathbf{x} \in \mathbf{z} + B_k^z$, we write the conditional PDF of x as [59]:

$$\int_0^{2} f_k(x; \ _x|z)\mathrm{d}\ _x = \ _k(x;z) \tag{3.42}$$

$$= \frac{x}{\frac{2}{k}} \exp\left(\frac{x^2+z^2}{2\ \frac{2}{k}}\right) I_0\left(\frac{xz}{\frac{2}{k}}\right); \qquad x;z>0; \tag{3.43}$$

where $I_0(\ )$ is the modified Bessel function of the first kind with order zero. As we have done for MCP, we first provide the expressions of $G_j(v_{k;j}(x;y))$ and $G_{c_j}(v_{k;j}(x;y))$ for $j \in K_2$.

Corollary 3.28 (PGFL of TCP)**.** *The PGFL of TCP* $_j$ *evaluated at* $v_{k;j}(x;y)$ *is given by:*

$$G_j(v_{k;j}(x;y)) = \exp\left(-2\ p_j \int_0^{\infty} \left(1 - \exp\left(-\left(1 - m_j \int_0^{\infty} (1 - v_{k;j}(x;y))\ _j(y;z)\mathrm{d}y\right)z\right)\mathrm{d}z\right)\right).$$

Proof. Similar to Corollary 3.23, the expression can be derived from (3.16) using Remark 3.22. □

Corollary 3.29 (PGFL of Offspring Point Process of TCP)**.** *When* $\mathbf{z} + B_j^z$ *is the offspring process of a TCP* $_j$*, its PGFL evaluated at* $v_{k;j}(x;y)$ *is given by:* $G_{c_j}(v_{k;j}(x;y)|\mathbf{z}) =$

$$\exp\left(-m_j \int_0^{\infty} (1 - v_{k;j}(x;y))\ _j(y;z)\mathrm{d}y\right). \tag{3.44}$$

Proof. Similar to Corollary 3.24, the expression can be derived from Lemma 3.8 using Remark 3.22. □

For PGFL of $_0$, i.e., $G_0(v_{0;k}(x;y))$, we can substitute $f_0(\ )$ in Lemma 3.12 with (4.22). For case 2,

$$G_0(v_{k;0}(x;y)) = \int_0^{\infty} \frac{1}{1 + \frac{P_0\ _k}{P_k}\ \frac{x}{y}} \frac{y}{\frac{2}{0}} \exp\left(-\frac{y^2}{2\ \frac{2}{0}}\right)\mathrm{d}y.$$

For case 3,

$$G_0(v_{k;0}(x;y)) = \int_0^{\infty} G_{c_0}(v_{k;0}(x;y)|z_0) \frac{z_0}{\frac{2}{0}} \exp\left(-\frac{z_0^2}{2\ \frac{2}{0}}\right)\mathrm{d}z_0.$$

We finally provide the expression of per-tier coverage probability for $k \in K \cap \{0\}$.

Corollary 3.30. *Per-tier coverage probability for $k \in K_2$ when all BS tiers in K_2 are modeled as TCPs can be expressed as:*

$$\mathtt{P}_{ck} = 2\pi p_k m_k \int_0^{\infty}\int_0^{\infty} \prod_{j\in K} G_j(v_{k;j}(x;y)) G_k(v_{k;k}(x;y)) \, G_{c_k}(v_{k;k}(x;y)\mid z) \, f_k(x;z)\,\mathrm{d}x\, z\,\mathrm{d}z. \tag{3.45}$$

Proof. Similar to Corollary 3.25, the expression can be derived from Lemma 3.5 using Remark 3.22. □

We can obtain $\mathtt{P}_{c0}$ following the same arguments provided in the previous Section.

Corollary 3.31. *Per-tier coverage probability for $k = 0$ when all BS tiers in K_2 are modeled as TCPs can be expressed as:* $\mathtt{P}_{c0} =$

$$\begin{cases} 0; & \text{case 1,} \\ \int_0^{\infty} \prod_{j\in K\cap\{0\}} G_j(v_{0;j}(z_0;y)) f_0(z_0)\mathrm{d}z_0; & \text{case 2;} \\ \int_0^{\infty}\int_0^{\infty} \prod_{j\in K\cap\{0\}} G_j(v_{0;j}(x;y)) \\ \exp\left(-m_k \int_0^{\infty} (1 - v_{0;0}(x;y)) f_0(y;z_0)\mathrm{d}y\right) \\ \left(m_0 \int_0^{1} v_{0;0}(x;y) f_0(y;z_0)\mathrm{d}y + 1 - \int_0^{\infty} f_0(x;z_0)\mathrm{d}x\right) \frac{z_0}{\sigma_0^2} \exp\left(-\frac{z_0^2}{2\sigma_0^2}\right) \mathrm{d}z_0; & \text{case 3:} \end{cases}$$

Proof. Similar to Corollary 3.26, the expression can be derived from Lemma 3.6 using Remark 3.22. □

3.5 Results and discussions

In this Section, we compare the performance of Models 1-4 introduced in Section 3.1.2 in terms of the coverage probability, $\mathtt{P}_c$. We first verify the analytical results with simulation of the K-tier HetNet. For all numerical results, we fix $\alpha_1 = \alpha_2 = \alpha$, and $\alpha = 4$. All the BSs in the same tier transmit at fixed powers with P_1=P_2 = 30 dB. For Models 1 and 2, we choose $K = 2$, $K_1 = \{1;2\}$, $K_2 = ?$. Users in Model 2 are distributed as a PCP, Φ_u with Φ_2 being the parent PPP. For Models 3 and 4, we choose $K = 2$, $K_1 = \{1\}$, $K_2 = \{2\}$. We have also computed $\mathtt{P}_c$ by Monte Carlo simulation with 10^5 iterations, where the user and BS point processes were generated in a circular shaped simulation window of area 30 Km^2.

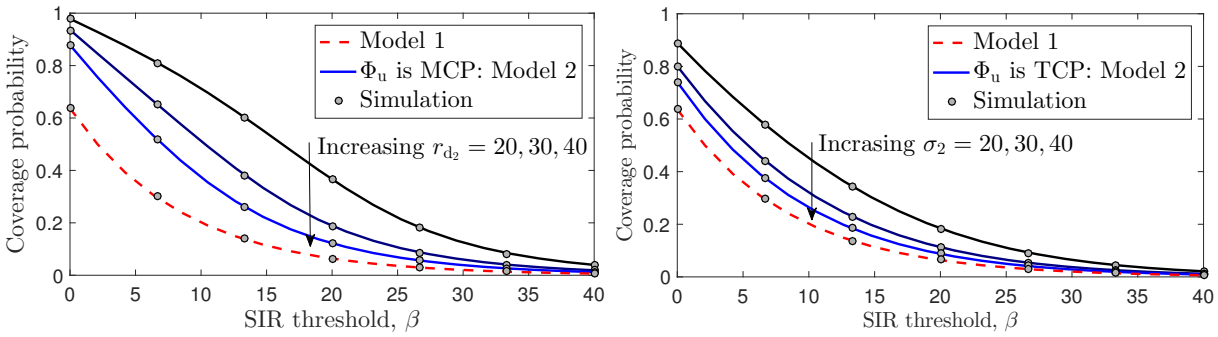

(a) $_u$ is MCP (b) $_u$ is TCP

Figure 3.5: Coverage probability as a function of SIR threshold (= 4, $_1$ = 1Km ^{2}, $P_1 = 1000P_2$, and $_2$ = $_{p_2}$ = 100 $_1$).

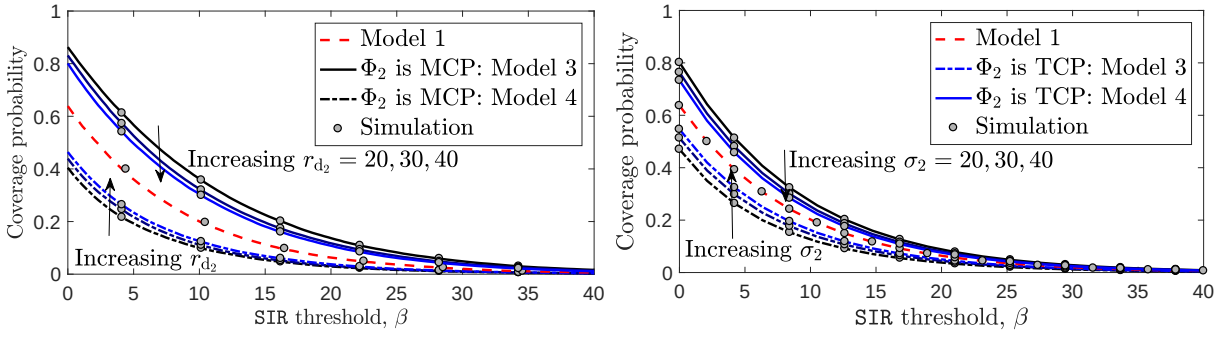

(a) $_2$ is MCP. (b) $_2$ is TCP.

Figure 3.6: Coverage probability as a function of SIR threshold (= 4, $_1$ = 1Km ^{2}, $P_1 = 1000P_2$, $_{p_2}$ = 25 $_1$, and $m_2 = 4$).

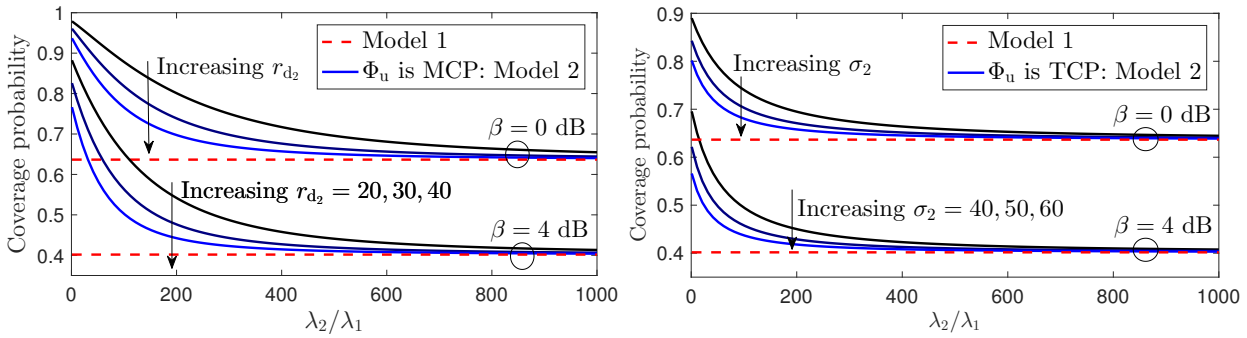

(a) $_u$ is a MCP. (b) $_u$ is a TCP.

Figure 3.7: Coverage probability as a function of $_2$= $_1$ (= 4, $_1$ = 1Km ^{2}, P_1 = 1000P_2, and $_2$ = $_{p_2}$ = 100 $_1$).

The perfect match between the simulation and analytical results verifies the accuracy of our analysis. From Figs. 3.5-3.6, we conclude that $\mathtt{P_c}$ strongly depends on the choice of HetNet models. For instance, a typical user experiences enhanced coverage in Model 2 than Model 1. From Fig. 3.6, we observe that $\mathtt{P_c}$ of Model 1 is a lower bound on $\mathtt{P_c}$ of Model 4 and is an upper bound on $\mathtt{P_c}$ of Model 3. These observations bolster the importance of choosing appropriate models for different BS and user configurations that are cognizant of the coupling in the locations of the BSs and users.

3.5.1 Effect of variation of cluster size

We vary the cluster size of the PCP and observe the trend in $\mathtt{P_c}$ for Models 2-4. For Model 2, we find in Fig. 3.5 that $\mathtt{P_c}$ decreases as cluster size (i.e. r_{d_2} for MCP, $_2$ for TCP) increases and converges towards that of Model 1. The reason of the coverage boost for denser cluster is that the SBS at cluster center lies closer to the typical user with high probability, hence improving the signal quality of the serving link. Moving to Models 3 and 4 in Fig. 3.6, we again observe that $\mathtt{P_c}$ of the two models converges to that of Model 1 as the cluster size (i.e. r_{d_2} for MCP, $_2$ for TCP) tends to infinity. We proved this convergence in Section 3.4.2. We further observe from Fig. 3.6 that increasing cluster size has a conflicting effect on $\mathtt{P_c}$ for Models 3 and 4: $\mathtt{P_c}$ of Model 4 increases whereas that of Model 3 decreases. This can be explained as follows. For Model 3, as cluster size increases, the collocated user and SBS clusters become sparser and the candidate serving SBS lies farther to the typical user with high probability. On the contrary, for Model 4 where the user locations form an independent PPP, the distance between the candidate serving SBS and the typical user decreases more likely with the increment of cluster size.

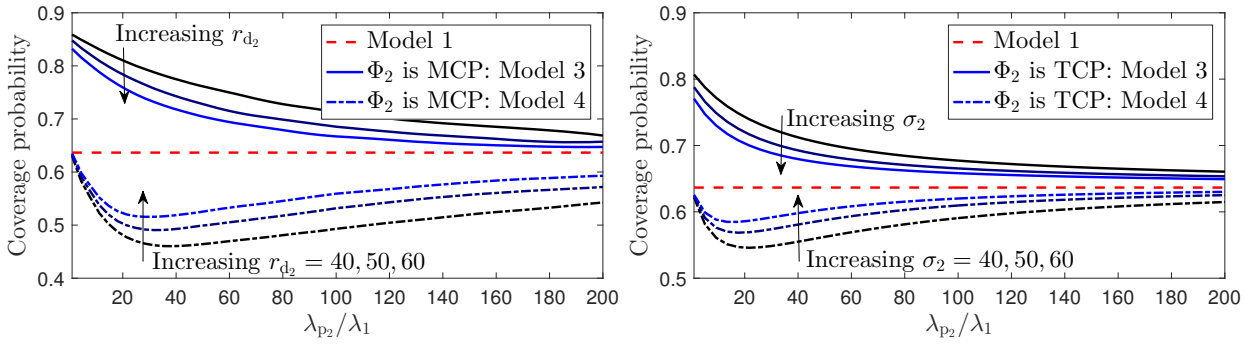

(a) $_u$ is a MCP. (b) $_u$ is a TCP.

Figure 3.8: Coverage probability as a function of $_{p_2} = _1$ ($= 4$, $_1 = 1\text{Km}^2$, $P_1 = 1000P_2$, $_{p_2} = 25\ _1$, and $m_2 = 4$).

3.5.2 Effect of variation of intensity of parent PPP

We study the effect of the variation of the intensity of the parent PPP on $\mathtt{P_c}$ for Models 2-4 ($_2$ for Model 2 and $_{p_2}$ for Models 3 and 4) in Figs. 3.7 and 3.8. For Model 1, it is well-known that $\mathtt{P_c}$ is independent of the intensities of BS PPPs [21]. The intuition behind the observation is the fact that changing intensity of a PPP is equivalent to scaling the locations of all the points by same factor. Hence the scaling factor cancels out from the serving and interfering powers in the SIR expression. However, changing the intensity of the parent PPP of a PCP is not equivalent to the location scaling of all the points by same factor. Thus, $\mathtt{P_c}$ for Models 2-4 varies as a function of the intensity of the parent PPP. We also observe that as intensity of parent PPP increases, $\mathtt{P_c}$ for Models 2-4 approaches to that of Model 1.

3.6 Summary

In this chapter, we developed a unified HetNet model by combining PPP and PCP that accurately models variety of spatial configurations for SBSs and users considered in practical design of HetNets, such as in the 3GPP simulation models. This is a significant generalization of the PPP-based K-tier HetNet model of [21,50], which was not rich enough to model non-uniformity and coupling across the locations of users and SBSs. For this model, we characterized the downlink coverage probability under max-SIR cell association. As a part of our analysis, we evaluated the sum-product functional for PCP and the associated offspring point process. We also formally proved that a PCP weakly converges to a PPP when cluster size tends to infinity. Finally we specialized our coverage probability results assuming that the PCPs in the model are either TCPs or MCPs.

4

General HetNet Model: Part II

4.1 Introduction

Network heterogeneity is at the heart of current 4G and upcoming 5G networks. A key consequence of the heterogeneous deployments is the emergence of different types of spatial couplings across the locations of BSs and users. Perhaps the most prominent one is the *user-BS coupling*, where the users tend to form spatial clusters or *hotspots* [44, 48, 79] and small cell BSs (SBSs) are deployed within these hotspots to provide additional capacity. Further, depending on the deployment objectives, the point patterns of BSs of a particular tier may exhibit some *intra-tier coupling*, such as clustering patterns for small cells [2,3] and repulsive patterns for macrocells deployed under a minimum inter-site distance constraint. Further, *inter-tier coupling* may exist between the locations of BSs of different tiers, for instance, macrocells and small cells when the latter are deployed at the macrocell edge to boost cell edge coverage [1].

Not surprisingly, the HetNet simulation models used by the standardization bodies, such as the third generation partnership project (3GPP), are cognizant of the existence of this spatial coupling [1]. Unfortunately, this is not true for the stochastic geometry based analytical HetNet models, e.g., see [20,21], which mostly still rely on the assumption that all network elements (BSs and users) are modeled as independent PPPs. That said, it has been recently shown that PCP-based models are well-suited to capture the aforementioned spatial coupling in a similar way as it is incorporated in 3GPP simulation models [61,71,72,79]. Since PCPs are defined in terms of PPPs, they are also very amenable to mathematical analysis. A key prior work in this area is [79], which completely characterized the downlink coverage probability for a PCP-based HetNet model under max-SINR based association scheme in which the typical user connects to the BS offering maximum *instantaneous* received SINR [79]. However, the downlink analysis for the more practical association scheme in which the typical user in the HetNet connects to the BS offering the strongest received power requires a very different mathematical treatment and has not been done yet. In this chapter, we plug this knowledge gap by providing a complete characterization of coverage probability under this association model.

4.1.1 Background and related works

Since the use of PPPs for modeling HetNets is by now fairly well-known, we advise interested readers to refer to books, surveys and tutorials, such as [23,31–33,80] to learn more about this direction of research. Although sparse, there have been some works on modeling spatial coupling between BSs and users in random spatial models for cellular networks. In [50], user-BS coupling was introduced in a PPP-based single tier cellular network model by conditionally thinning the user PPP and biasing user locations towards the BS locations. Owing to the natural connection of the formation of hotspots to the clustering patterns of PCPs, PCP was used to model the user distributions in [60, 61, 71, 81], where coupling between the users and BS locations was introduced by placing the SBSs at the cluster centers (parent points) of the user PCP. Further, since intra-tier coupling can be either attractive or repulsive, no single point process is the *best* choice for capturing it. For modeling repulsions, Matérn hard-core process [70, 82], Gauss-Poisson process [64], Strauss hardcore process [83], Ginibre point process [84, 85], and more general determinantal point processes [66] have been used for BS distributions. On the other hand, for modeling attraction, PCP [72] and Geyer saturation process [83] have been proposed. For modeling inter-tier coupling, Poisson hole process (PHP) has been a preferred choice [68, 69], where the macro BSs (MBSs) are modeled as PPP and the SBSs are modeled as another PPP outside the exclusion discs (holes) centered at the MBS locations. Among these "beyond-PPP" spatial models of HetNets, the PCP has attracted significant interest because of its generality in modeling variety of user and BS configurations and its mathematical tractability [79, 86]. We now provide an overview of the existing work on PCP-based models for HetNets.

In [69, 87], the authors assumed that the SBSs in a two-tier HetNet are distributed as a PCP and derived downlink coverage probability assuming that the serving BS is located at a fixed distance from the receiver, which circumvented the need to consider explicit cell association. While this setting provides useful initial insights, the analysis cannot be directly extended to incorporate realistic cell association rules, such as max-power based association [22]. The primary challenge in handling cell association in a stochastic geometry setting is to jointly characterize the serving BS distance and the interference field. This challenge does not appear when BS is assumed to lie at a fixed distance from the receiver, such as in [69, 87]. It is worth noting that the distance of the serving BS from the receiver under max-power based association can be evaluated using contact distance distributions of PCPs, which have recently been characterized in [73, 74]. However, these alone do not suffice because we need to jointly characterize the serving BS distance and the interference field, which is much more challenging. This is the main reason why this problem has remained open for several years. In [88], the authors characterized handoff rates for a typical user following an arbitrary trajectory in a HetNet with PPP and PCP-distributed BSs. Although the setup is very similar to this chapter, the metric considered in [88] did not require the characterization of coverage probability. In [89], the authors developed analytical tools to handle this correlation and derived coverage probability when the BSs are modeled as a Matérn cluster process (MCP). However, the analysis is dependent on the geometrical constructions which is very

specific to an MCP and is hence not directly applicable to a general PCP. The coverage analysis for a general PCP was provided in [72] where analytical tractability was preserved by assuming that the SBSs to be operating in a *closed access* mode, i.e, a user can only connect to a SBS of the same cluster. In [79], we have provided a comprehensive coverage analysis for the unified HetNet model under max SINR-based association strategy with SINR threshold greater than unity. However, the analysis cannot be directly extended to the max power-based association setup because of the fundamental difference in the two settings from the analytical perspective (please refer to [32] for a more detailed discussion of the differences in analytical approaches for the characterization of coverage probability for the two association strategies). Recently, in [90], the open problem of the coverage analysis for a single tier cellular network under max-power connectivity with PCP-distributed BSs and independent user locations was solved by expressing coverage probability as a sum-product functional over the parent PPP of the BS PCP. Motivated by this novel analytical approach, in this chapter we provide the complete coverage analysis for max-power based association strategy for the unified HetNet model introduced in [79].

4.1.2 Contributions

We derive the coverage probability of a typical user of a unified K-tier HetNet in which the spatial distributions of K_1 BS tiers are modeled as PCPs and K_2 BS tiers are modeled as PPPs ($K_1 + K_2 = K$). The PCP assumption for the BS tier introduces spatial coupling among the BS locations. We consider two types of users in this network, Type 1: users having no spatial coupling with the BSs, and Type 2: users whose locations are coupled with the BS locations. For Type 1, the user locations are modeled as a stationary point process independent of the BS point processes. For Type 2, the coupling between user and BS locations is incorporated by modeling the user locations as a PCP with each user cluster sharing the same cluster center with a BS cluster. The key contributions are highlighted next.

Exact coverage probability analysis. Assuming that a user connects to the BS offering the maximum average received power, we provide an exact analysis of coverage probability for a typical user which is an arbitrarily selected point from the user point process. The key enabler of the coverage probability analysis is a fundamental property of PCP that conditioned on the parent PPP, the PCP can be viewed as an inhomogeneous PPP, which is a relatively more tractable point process compared to PCP. Using this property, we condition on the parent PPPs of all the BS PCPs and derive the conditional coverage probability. Finally, while deconditioning over the parent PPPs, we observe that the coverage probability can be expressed as the product of PGFLs and sum-product functionals of the parent PPPs. This analytical formulation of coverage probability in terms of known point process functionals over the parent PPPs is the key contribution of the chapter and yields an easy-to-compute expression of coverage probability under max-power based association. We then specialize the coverage probability for two instances when the PCPs associated with the BSs are either (i) Thomas cluster process (TCP), where the offspring points are normally distributed around

the cluster center, or (ii) MCP, where the offspring points are distributed uniformly at random within a disc centered at the cluster center.

System-level insights. Using the analytical results, we study the impact of spatial parameters such as cluster size, average number of points per cluster and BS density on the coverage probability. Our numerical results demonstrate that the variation of coverage probability with cluster size has conflicting trends for Cases 1 and 2: for Type 1, coverage decreases as cluster size increases, and for Type 2, coverage increases as cluster size decreases. As cluster size increases, the coverage probabilities under Type 1 and Type 2 approach the same limit which is the well-known coverage probability of the PPP-based K-tier HetNet [22], but from two opposite directions. Our numerical results demonstrate that the impact of the variation of cluster size on coverage probability is not as prominent in Type 2 as in Type 1.

4.2 System Model

4.2.1 PCP preliminaries

Before we introduce the proposed PCP-based system model for K-tier HetNet, we provide a formal introduction to PCP.

Definition 4.1 (Poisson Cluster Process)**.** A PCP $\Phi(\Phi_p; g; m)$ in $\mathbb{R}^2$ can be defined as:

$$\Phi(\Phi_p; g; m) = \bigcup_{\mathbf{z} \in \Phi_p} \mathbf{z} + B^{\mathbf{z}}; \tag{4.1}$$

where $\Phi_p = \Phi(\Phi_p)$ is the parent PPP with intensity Φ_p and $B^{\mathbf{z}}$ denotes the offspring point process corresponding to a cluster center at $\mathbf{z} \in \Phi_p$ where $\{\mathbf{s} \in B^{\mathbf{z}}\}$ is an independently and identically distributed (i.i.d.) sequence of random vectors with probability density function (PDF) $g(\mathbf{s})$. The number of points in $B^{\mathbf{z}}$ is denoted by M, where $M \sim \text{Poisson}(m)$.

Notation. While we reserve the symbol Φ to denote any point process, to indicate whether it is a PCP or PPP we specify the parameters in parentheses accordingly, i.e., $\Phi(\Phi_p; g; m)$ denotes a PCP according to Definition 5.1 and $\Phi(\lambda)$ denotes a PPP with intensity λ.

A PCP can be viewed as a collection of offspring process $B^{\mathbf{z}}$ translated by $\mathbf{z}$ for each $\mathbf{z} \in \Phi_p$. Then the sequence of points $\{\mathbf{t}\} \sim \mathbf{z} + B^{\mathbf{z}}$ is conditionally i.i.d. with PDF $f(\mathbf{t}|\mathbf{z}) = g(\mathbf{t} - \mathbf{z})$. Note that the conditional distribution of the point coordinates given its cluster center at $\mathbf{z}$ is equivalent to translating a cluster centered at the origin to $\mathbf{z}$. For a PCP, the following result can be established.

Proposition 4.2. *Conditioned on the parent point process Φ_p, $\Phi(\Phi_p; g; m)$ is an inhomogeneous PPP with intensity*

$$\lambda(\mathbf{x}) = m \sum_{\mathbf{z} \in \Phi_p} f(\mathbf{x}|\mathbf{z}). \tag{4.2}$$

4.2. System Model

Table 4.1: List of Notations.

K	Index set of all BS tiers ($jKj = K$)
$K_1; K_2$	Index set of all BS tiers modeled as PCP and PPP
$_k = (\ _{p_k}; g_k; m_k)$	The point process of the k^{th} BS tier, $k\ 2\ K_1$, which is a PCP.
$_k = (\ _k)$	The point process of the k^{th} BS tier, $k\ 2\ K_2$, which is a PPP.
P_k	Transmit power of a BS in $_k$
	Path-loss exponent (> 2)
$_k$	Coverage threshold of $_k$
$P_{j;k}$	$(P_j=P_k)^{1=}$
$f_{d_k}(jz)$	Conditional PDF of distance of a point of $_k$ ($k\ 2\ K_1$) from origin given its cluster center is located at $\mathbf{z}$ ($z = k\mathbf{z}k$)
$f_{c_k}( ); F_{c_k}( )$	PDF and CDF of contact distance of $_k$
$C_{j;k}(r; z)$	$\exp \quad m_k \ 1 \quad \int_{P_{j;k}}^{1} (1 + \frac{_k P_k r}{P_k} y\ )^{\ 1} f_{d_j}(yjz)dy$
$(\ _i;\ \ )$	$1 + \ _i^{2=} \int_{\ _i^{2=}}^{} \frac{1}{1+t^{\ =2}} dt = 1 + \frac{2\ _i}{2} {}_2F_1\ \ 1; 1\ \ \frac{2}{}; 2\ \ \frac{2}{}; \quad _i$

Proof. While one can prove this result for a more general setting of Cox processes (see [13]), we prove this result for PCP for completeness as follows. Let N be the random counting measure associated with the point process . Then, for a Borel set $A\ 2\ B(\mathbb{R}^2)$, where $B(\mathbb{R}^2)$ is the Borel -algebra on $\mathbb{R}^2$, $N\ (A)$ is a random variable denoting the number of points of falling in A. First it is observed that for $B^{\mathbf{z}}$, $N_{B^{\mathbf{z}}}(A)\quad \text{Poisson}(m \int_A f(\mathbf{y}jz)\mathbf{dy})$ since the probability generating function (PGF) of $N_{B^{\mathbf{z}}}(A)$ is

$$\begin{aligned}
&E\ \ ^{N_{B^{\mathbf{z}}}(A)} = E\ \ ^{\left[\ \sum_{i=1}^{M} 1(\mathbf{s}_i 2A)\right]} = E\ \ ^{\left[\ \prod_{i=1}^{M} 1(\mathbf{s}_i 2A)\right]} \overset{(a)}{=} E\ \ ^{\left[\ \prod_{i=1}^{M} E\ \ ^{1(\mathbf{s}_i 2A)}\right]} \\
&\overset{(b)}{=} E\ \ ^{\left[\ \prod_{i=1}^{M} 1 \quad (1 \quad) \int_A f(\mathbf{y}jz)\mathbf{dy}\right]} = E\ \ ^{\left[\ 1 \quad (1 \quad) \int_A f(\mathbf{y}jz)\mathbf{dy}\right]^M} \\
&\overset{(c)}{=} \exp \quad m \int_A f(\mathbf{y}jz)\mathbf{dy}\,(1 \quad) \quad ;
\end{aligned}$$

where $\mathbf{s}_i$ denotes the i^{th} point of $B^{\mathbf{z}}$. Here (a) follows from the fact that the offspring points are i.i.d. around the cluster center at $\mathbf{z}$, (b) and (c) are obtained by using the PGF of Bernoulli and Poisson distributions, respectively. Hence $N_{B^{\mathbf{z}}}(A)\quad \text{Poisson}(m \int_A f(\mathbf{y}jz)\mathbf{dy})$. Now, conditioned on $_p$ the PGF of $N\ (A)$ is expressed as:

$$E[\ ^{N\ (A)}j\ _p] = E\ \ ^{\left[\ \sum_{z2\ _p} N_{B^{\mathbf{z}}}(A)\right]}\ _p\ = E\left[\ \prod_{z2\ _p} \ ^{N_{B^{\mathbf{z}}}(A)}j\ _p\right] \overset{(a)}{=} \prod_{z2\ _p} E\ \ ^{N_{B^{\mathbf{z}}}(A)}j\ _p$$

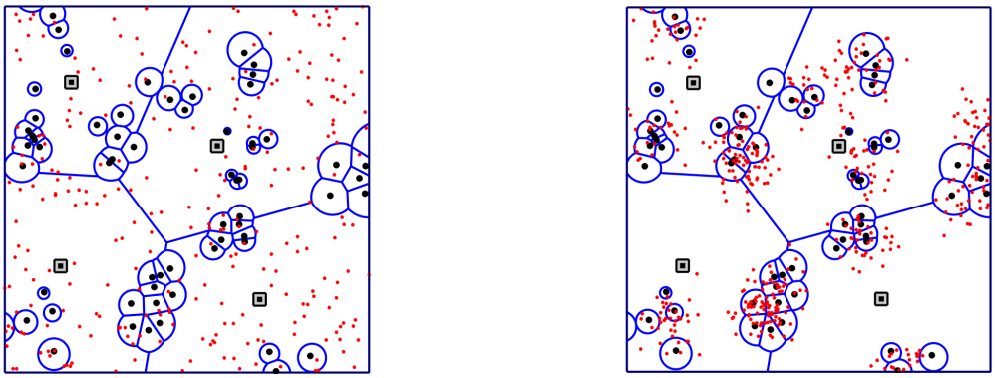

(a) Type 1 (b) Type 2

Figure 4.1: An illustration of the a two-tier HetNet, where Φ_1 is a PCP of SBSs (illustrated as black dots) and Φ_2 is a PPP of MBSs (illustrated as squares). The users (points of Φ_u) are illustrated as red dots. In (a), Φ_u is a PPP, and in (b), Φ_u is a PCP with the same parent PPP as that of Φ_1.

$$\overset{(b)}{=} \prod_{z \in \Phi_p} \exp\left(m \int_A f(y|z)dy(1-\quad)\right) = \exp\left(@\, m \sum_{z \in \Phi_p} \int_A f(y|z)dy(1-\quad)\right)A\,;$$

where (a) follows from the fact that conditioned on Φ_p, $\{B^z\}$ is sequence of i.i.d. offspring point processes, (b) is obtained by substituting the PGF of $N_{B^z}(A)$. Hence it is observed that $N(A)|\Phi_p \sim \text{Poisson}\left(m \sum_{z \in \Phi_p} \int_A f(y|z)dy\right)$. Thus $|\Phi_p$ is an inhomogeneous PPP with intensity measure $(A) = m \sum_{z \in \Phi_p} \int_A f(y|z)dy$. □

4.2.2 K-tier HetNet model

We assume a K-tier HetNet where BSs of each tier are distributed as a PPP or PCP. Let K_1 and K_2 denote the index sets of the BS tiers which are modeled as PCP and PPP, respectively, with $|K_1 \cup K_2| = K$ and $K_1 \cap K_2 = \emptyset$. We denote the point process of the k^{th} BS tier as Φ_k, where Φ_k is either a PCP i.e. $(\Phi_{p_k}; g_k; m_k)$ $(\forall k \in K_1)$ where $\Phi_{p_k} = (\Phi_{p_k})$ is the parent PPP or a PPP (Φ_k) $(\forall k \in K_2)$. Also define $f_k(x|z) = g_k(x - z); \forall k \in K_1$. Each BS of Φ_k transmits at constant power P_k. We assume that the users are distributed according to a stationary point process Φ_u. We now consider two types of users in the network.

case 1: *No user-BS coupling.* The first type of users are uniformly distributed over the network, such as, the pedestrians and users in transit, and their locations are independent of the BS locations. There is no restriction on the distribution of these users as long as the distribution is stationary. For instance, one way of modeling the locations of these users is to assume that they are distributed as a homogeneous PPP.

case 2: *User-BS coupling.* The second type of users are assumed to form spatial clusters (also called *user hotspots*) and their locations can be modeled as a PCP $\Phi_u = (\Phi_{p_u}; g_u; m_u)$ [71, 79]. When the users are clustered, we also assume that one BS tier (say, the q^{th} tier, $q \in K_1$) is deployed to serve the user hotspots, thus introducing coupling between Φ_u and Φ_q. In other words, Φ_u and Φ_q are two PCPs having same parent PPP $\Phi_{p_q} = \Phi_{p_u}$. Hence conditioned on Φ_{p_q}, Φ_u and Φ_q are (conditionally) independent but not identically distributed. This assumption is motivated by the way SBSs are placed at higher densities in the locations of user hotspots in 3GPP simulation models of HetNets [2, 3].

Remark 4.3. For case 1, Φ_u can be any general stationary point process including PPP and for case 2, we do not specify m_u of Φ_u, since m_u does not appear explicitly in the coverage analysis. However, these specifications of Φ_u are required when one has to characterize other metrics like BS load and rate coverage probability [24, 37]. Further, the coverage probability analysis that follows can be extended for a general user distribution which is the superposition of PPP and PCPs along similar lines to [71].

In Fig. 7.1, we provide an illustration of the system model. For both types of user distributions, we perform our analysis for a *typical* user which corresponds to a point selected uniformly at random from Φ_u. Since Φ_u is stationary, the typical user is assumed to be located at the origin without loss of generality. For case 1, since Φ_u and Φ_k, $8\, k \in K$ are independent, the selection of the typical user does not bias the distribution of Φ_k. However, for case 2, the selection of the typical user affects the BS point process Φ_q due to the existence of user-BS coupling. We assume that the typical user belongs to a cluster centered at $\mathbf{z}_0$. By construction, Φ_q is always conditioned to have a cluster centered at $\mathbf{z}_0$. Hence, the typical user will *see* the palm version of Φ_q which, by Slivnyak's theorem, is equivalent to the superposition of Φ_q and $\mathbf{z}_0 + B^{z_0}$ where Φ_q and $\mathbf{z}_0 + B^{z_0}$ are independent. For case 2, we modify Φ_q as $\Phi_q = (\Phi_{p_q}; g_q; m_q) \cup \mathbf{z}_0 + B^{z_0}$. Consequently, the underlying parent point process is modified as $\Phi_{p_q} = (\Phi_{p_q}) \cup \{\mathbf{z}_0\}$. The BS cluster B^{z_0} is termed as the *representative cluster*.

Considering the typical user at origin, the downlink power received from a BS at $\mathbf{x} \in \Phi_k$ is expressed as $P_k h_{\mathbf{x}} \|\mathbf{x}\|^{-\alpha}$, where $h_{\mathbf{x}}$ and α denote the small scale fading and path-loss exponent, respectively. We assume that each link undergoes Rayleigh fading, hence $\{h_{\mathbf{x}}\}$ is a sequence of i.i.d. random variables with $h_{\mathbf{x}} \sim \exp(1)$. The user connects to the BS providing the maximum received power averaged over fading. Thus, if $\mathbf{x}$ is the location of the serving BS, then, $\mathbf{x} = \arg\max_{\{\mathbf{x}_k; k \in K\}} P_k \|\mathbf{x}_k\|^{-\alpha}$, where $\mathbf{x}_k = \arg\max_{\mathbf{x} \in \Phi_k} P_k \|\mathbf{x}_k\|^{-\alpha} = \arg\min_{\mathbf{x} \in \Phi_k} \|\mathbf{x}\|$ is the location of candidate serving BS in Φ_k. Note that the candidate serving BS in Φ_k is the BS in Φ_k which is geometrically closest to the user. We first define the *association event* corresponding to the i^{th} tier as the event that the serving BS belongs to Φ_i, denoted as $S_i = \{\mathbf{x} = \mathbf{x}_i\}$. Conditioned on S_i, the SINR experienced by the typical user is

$$\mathrm{SINR}(\mathbf{x}) = \frac{P_i h_{\mathbf{x}} \|\mathbf{x}\|^{-\alpha}}{N_0 + \sum_{j \in K} \sum_{\mathbf{x} \in \Phi_j \setminus \{\mathbf{x}\}} P_j h_{\mathbf{x}} \|\mathbf{x}\|^{-\alpha}}; \tag{4.3}$$

where N_0 is the thermal noise power. We define the coverage probability as the probability of the union of K mutually exclusive coverage events

$$P_c = P\left(\bigcup_{i \in K} \{SINR(x) > \beta_i; S_i\}\right) = \sum_{i \in K} P(SINR(x) > \beta_i; S_i); \quad (4.4)$$

where we call the i^{th} term under the summation as the i^{th} *tier coverage probability* which is the joint probability of the events S_i and $\{SINR(x) > \beta_i\}$. Here β_i is the SINR threshold for the i^{th} tier required for successful demodulation and decoding of the received signal.

4.3 Coverage probability analysis

We begin our coverage analysis by first conditioning on every parent PPP, i.e., Φ_k; $\forall k \in K_1$. Following Proposition 4.2, $\Phi_k | \Phi_k$ will be inhomogeneous PPP with intensity $\lambda_k(x) = m_k \sum_{z \in \Phi_k} f_k(x|z)$. A slightly different situation occurs for Φ_q in case 2. However, once Φ_q is modified by adding a point at z_0 to the original parent PPP, $\Phi_q | \Phi_q$ again becomes an inhomogeneous PPP with intensity $m_q \sum_{z \in \Phi_q \cup \{z_0\}} f_q(x|z)$.

Notation. To denote the distance of a point $y \in \mathbb{R}^2$, we use y and $\|y\|$ interchangeably.

4.3.1 Contact distance distribution

First we will derive the distribution of $\|x_k\|$, $k \in K$, or the distance distribution of the candidate serving BS of tier k. Since $\|x_k\|$ is the nearest BS to the typical user which is at origin, the distribution of $\|x_k\|$ is the same as the contact distance distribution of Φ_k, denoted as $f_{c_k}(r|\Phi_k)$. Let $f_{d_k}(r|z)$ and $F_{d_k}(r|z)$ denote the PDF and CDF of the distance of a randomly selected point of Φ_k ($k \in K_1$) given its cluster center is located at z. Before presenting the contact distance distributions, we observe the following property of the conditional distance distribution.

Lemma 4.4. *If the offspring points are isotropically distributed around the cluster center i.e., the radial coordinates of the offspring points with respect to the cluster center have the joint PDF $g_k(s, \theta_s) = g_{k(1)}(s)\frac{1}{2\pi}$, where $g_{k(1)}(\cdot)$ is the marginal PDF of the radial coordinate, then, $f_{d_k}(r|z) = f_{d_k}(r|z)$ and $F_{d_k}(r|z) = F_{d_k}(r|z)$. That is, the conditional distance distribution depends only on the magnitude of z.*

Proof. Let $x \in \Phi_k$ is the location of the point whose cluster center is located at z. Then,

$$F_{d_k}(r|z) = P(\|x_k\| < r|z) = \int_{b(0;r)} g_k(x - z)dx$$

$$= \int_0^{2\pi} \frac{1}{2\pi} \int_0^r g_{k(1)}\left(\sqrt{x^2 + z^2 - 2xz\cos(\theta_x - \theta_z)}\right)x\,dx\,d\theta_x$$

$$= \int_{z}^{2Z+z} \frac{1}{2} \int_{0}^{Z^r} g_{k(1)}(\sqrt{x^2+z^2-2xz\cos\ }) x \mathrm{d}x \mathrm{d}\ :$$

Here $b(\mathbf{0};r)$ denotes a disc of radius r centered at the origin. Differentiating with respect to r,

$$f_{d_k}(rjz) = \int_{z}^{2Z+z} \frac{1}{2} g_{k(1)}(\sqrt{r^2+z^2-2rz\cos\ }) r \mathrm{d}\ : \tag{4.5}$$

Since the region of the integral over is the perimeter of the disc $b(\mathbf{0};z)$, it is independent of the choice of $_z$. □

We now characterize the PDF of $k\mathbf{x}_k k$.

Lemma 4.5. *For $k \in K_1$, conditioned on $_{p_k}$, the PDF and CDF of $k\mathbf{x}_k k$ are given as:*

$$f_{c_k}(rj\ _{p_k}) = m_k \sum_{\mathbf{z}2\ _{p_k}} f_{d_k}(rjz) \prod_{\mathbf{z}2\ _{p_k}} \exp(-m_k F_{d_k}(rjz)); \qquad r \geq 0; \tag{4.6}$$

and

$$F_{c_k}(rj\ _{p_k}) = 1 - \exp\left(-m_k \sum_{\mathbf{z}2\ _{p_k}} \int_0^{Z^r} f_{d_k}(yjz)\mathrm{d}y\right); \qquad r \geq 0. \tag{4.7}$$

Proof. For $k \in K_1$, the CDF of $k\mathbf{x}_k k$ is

$$\begin{aligned} F_{c_k}(rj\ _{p_k}) &= 1 - P(\ (b(\mathbf{0};r)) = 0j\ _{p_k}) \\ &= 1 - \exp\left(-\int_{b(\mathbf{0};r)} {}_k(\mathbf{x})\mathrm{d}\mathbf{x}\right) \\ &= 1 - \exp\left(-m_k \sum_{\mathbf{z}2\ _{p_k b(\mathbf{0};r)}} \int_Z f_k(\mathbf{y}jz)\mathrm{d}\mathbf{y}\right) \\ &= 1 - \exp\left(-m_k \sum_{\mathbf{z}2\ _{p_k}} \int_0^{Z^r} f_{d_k}(yjz)\mathrm{d}y\right) : \end{aligned}$$

The last step is due the fact that integrating a joint PDF of polar coordinates over $b(\mathbf{0};r)$ is equivalent to integrating the marginal PDF of radial coordinate over $(0;r]$. The final result in (4.6) can be obtained by differentiating the CDF with respect to r. □

Note that one can obtain the PDF of the contact distance of PCP by deconditioning $f_{c_k}(rj\ _{p_k})$ over $_{p_k}$ [90]. This is an alternative approach to the one presented in [73, 74] for the derivation of contact distance distribution of PCP.

When Φ_k is a PPP, i.e., $k \in \mathcal{K}_2$, the distribution of $\|X_k\|$ is the well-known Rayleigh distribution, given by:

$$f_{c_k}(r) = 2\pi\lambda_k r \exp(-\pi\lambda_k r^2),\ F_{c_k}(r) = 1 - \exp(-\pi\lambda_k r^2),\ r \geq 0. \tag{4.8}$$

4.3.2 Association probability and serving distance distribution

We define association probability to the i^{th} tier as $\mathbb{P}(\mathcal{S}_i)$. The association probability is derived as follows.

Lemma 4.6. *Conditioned on $\Phi_k, \forall k \in \mathcal{K}_1$, the association probability to the i^{th} tier is given by:* $\mathbb{P}(\mathcal{S}_i | \Phi_k, \forall k \in \mathcal{K}_1) =$

$$\pi\lambda_i \int_0^\infty \sum_{z \in \Phi_i} f_{\mathrm{d}_i}(rjz) \prod_{j_1 \in \mathcal{K}_1} \prod_{z \in \Phi_{j_1}} \exp\left(-\pi\lambda_{j_1} F_{\mathrm{d}_{j_1}}\left(P_{j_1;i} rjz\right)\right) \prod_{j_2 \in \mathcal{K}_2} \exp\left(-\pi\lambda_{j_2} P_{j_2;i}^2 r^2\right) \mathrm{d}r, \quad \text{if } i \in \mathcal{K}_1, \tag{4.9a}$$

$$2\pi\lambda_i \int_0^\infty \prod_{j_1 \in \mathcal{K}_1} \prod_{z \in \Phi_{j_1}} \exp\left(-\pi\lambda_{j_1} F_{\mathrm{d}_{j_1}}\left(P_{j_1;i} rjz\right)\right) \prod_{j_2 \in \mathcal{K}_2} \exp\left(-\pi\lambda_{j_2} P_{j_2;i}^2 r^2\right) r \mathrm{d}r; \text{if } i \in \mathcal{K}_2; \tag{4.9b}$$

where $P_{j;i} = (P_j/P_i)^{1/\alpha}$.

Proof. When $i \in \mathcal{K}_1$,

$$\begin{aligned}
\mathbb{P}(\mathcal{S}_i | \Phi_k, \forall k \in \mathcal{K}_1) &= \mathbb{P}\left(\bigcap_{j \in \mathcal{K}\setminus i} P_i \|X_i\|^{-\alpha} > P_j \|X_j\|^{-\alpha} \,\middle|\, \Phi_k, \forall k \in \mathcal{K}_1\right) \\
&= \prod_{j_1 \in \mathcal{K}_1\setminus i} \mathbb{P}\left(\|X_{j_1}\| > \left(\frac{P_{j_1}}{P_i}\right)^{1/\alpha} \|X_i\| \,\middle|\, \Phi_i\right) \prod_{j_2 \in \mathcal{K}_2} \mathbb{P}\left(\|X_{j_2}\| > \left(\frac{P_{j_2}}{P_i}\right)^{1/\alpha} \|X_i\| \,\middle|\, \Phi_i\right) \\
&\overset{(a)}{=} \int_0^\infty \prod_{j_1 \in \mathcal{K}_1\setminus i} F_{c_{j_1}}\left(\left(\frac{P_{j_1}}{P_i}\right)^{1/\alpha} r \,\middle|\, \Phi_{j_1}\right) \prod_{j_2 \in \mathcal{K}_2} F_{c_{j_2}}\left(\left(\frac{P_{j_2}}{P_i}\right)^{1/\alpha} r\right) f_{c_i}(r|\Phi_i)\mathrm{d}r \\
&\overset{(b)}{=} \int_0^\infty \prod_{j_1 \in \mathcal{K}_1\setminus i} \prod_{z \in \Phi_{j_1}} \exp\left(-\pi\lambda_{j_1} F_{\mathrm{d}_{j_1}}\left(\left(\frac{P_{j_1}}{P_i}\right)^{1/\alpha} r z\right)\right) \prod_{j_2 \in \mathcal{K}_2} \exp\left(-\pi\lambda_{j_2}\left(\frac{P_{j_2}}{P_i}\right)^{2/\alpha} r^2\right) \\
&\quad \sum_{z \in \Phi_i} f_{\mathrm{d}_i}(rjz) \prod_{z \in \Phi_j} \exp\left(-\pi\lambda_j F_{\mathrm{d}_j}(rjz)\right) \mathrm{d}r \\
&= \pi\lambda_i \int_0^\infty \sum_{z \in \Phi_i} f_{\mathrm{d}_i}(rjz) \prod_{j_1 \in \mathcal{K}_1} \prod_{z \in \Phi_{j_1}} \exp\left(-\pi\lambda_{j_1} F_{\mathrm{d}_{j_1}}\left(\left(\frac{P_{j_1}}{P_i}\right)^{1/\alpha} r z\right)\right)
\end{aligned}$$

$$\exp\left(-\sum_{j_2 \in K_2} \lambda_{j_2} \left(\frac{P_{j_2}}{P_i}\right)^{2/\alpha} r^2\right) \mathrm{d}r.$$

Here (a) follows from the fact that Φ_i-s are independent, (b) follows from Lemma 4.5, and $F_{\bar{C}_j}(\cdot)$ denotes the complementary CDF (CCDF) of $\|x_j\|$. When $i \in K_2$,

$$\begin{aligned}
&\mathrm{P}(S_i > \theta_k, \Phi; \forall k \in K_1) \\
&= \prod_{j_1 \in K_1} \mathrm{P}\left(\|x_{j_1}\| > \left(\frac{P_{j_1}}{P_i}\right)^{1/\alpha} \|x_i\|\right) \Phi_{j_1}\left(\prod_{j_2 \in K_2 \setminus i} \mathrm{P}\left(\|x_{j_2}\| > \left(\frac{P_{j_2}}{P_i}\right)^{1/\alpha} \|x_i\|\right)\right) \\
&= \int_0^\infty \prod_{j_1 \in K_1} F_{C_{j_1}}\left(\left(\frac{P_{j_1}}{P_i}\right)^{1/\alpha} r\right) \Phi_{j_1}\left(\prod_{j_2 \in K_2 \setminus i} F_{C_{j_2}}\left(\left(\frac{P_{j_1}}{P_i}\right)^{1/\alpha} r\right)\right) f_{c_i}(r)\mathrm{d}r \\
&= 2\pi\lambda_i \int_0^\infty \prod_{j_1 \in K_1 \cap \mathbb{Z}^2} \exp\left(-\Phi_{j_1}\left(m_{j_1} F_{\mathrm{d}_{j_1}}\left(\left(\frac{P_{j_1}}{P_i}\right)^{1/\alpha} r z\right)\right)\right) \\
&\quad \exp\left(-\sum_{j_2 \in K_2} \lambda_{j_2} \left(\frac{P_{j_2}}{P_i}\right)^{2/\alpha} r^2\right) r \mathrm{d}r;
\end{aligned}$$

where the last step follows from Lemma 4.5. □

We now derive the PDF of the conditional serving distance i.e. $\|x_i\|$ given S_i and $\Phi_k; \forall k \in K_1$.

Lemma 4.7. *The PDF of $\|x_i\|$ conditioned on association to the i^{th} tier and $\Phi_k; \forall k \in K_1$ is given as: $f_{S_i}(r|S_i; \Phi_k; \forall k \in K_1) =$*

$$\frac{m_i}{\mathrm{P}(S_i > \theta_k, \Phi; \forall k \in K_1)} \sum_{z \in \Phi_i} f_{\mathrm{d}_i}(r|z) \prod_{j_1 \in K_1 \cap \mathbb{Z}^2} \prod_{\Phi_{j_1}} \exp\left(-m_{j_1} F_{\mathrm{d}_{j_1}}\left(P_{j_1,i} r|z\right)\right)$$
$$\prod_{j_2 \in K_2} \exp\left(-\lambda_{j_2} P_{j_2,i}^{2/\alpha} r^2\right); \quad r \geq 0; \text{if } i \in K_1; \tag{4.10a}$$

$$\frac{2\pi\lambda_i}{\mathrm{P}(S_i > \theta_k, \Phi; \forall k \in K_1)} \prod_{j_1 \in K_1 \cap \mathbb{Z}^2} \prod_{\Phi_{j_1}} \exp\left(-m_{j_1} F_{\mathrm{d}_{j_1}}\left(P_{j_1,i} r|z\right)\right) \prod_{j_2 \in K_2} \exp\left(-\lambda_{j_2} P_{j_2,i}^{2/\alpha} r^2\right) r;$$
$$r \geq 0; \text{if } i \in K_2: \tag{4.10b}$$

Proof. The conditional CCDF of $\|x_i\|$ given S_i and $\Phi_k; \forall k \in K_1$: is given by:

$$F_{S_i}(r|S_i; \Phi_k; \forall k \in K_1) = \mathrm{P}(\|x_i\| > r|S_i; \Phi_k; \forall k \in K_1) = \mathrm{P}(\|x_i\| > r|S_i; \Phi_k; \forall k \in K_1)$$

$$= \frac{\mathrm{P}(k\text{-}\mathrm{th}_i k > r; S_i j \ \ \mathrm{p}_k; 8\ k\ 2\ K_1)}{\mathrm{P}(S_i j \ \ \mathrm{p}_k; 8\ k\ 2\ K_1)}.$$

Now

$$\mathrm{P}(k\text{-}\mathrm{th}_i k > r; S_i j \ \ \mathrm{p}_k; 8\ k\ 2\ K_1) = \mathrm{P}\Big(\prod_{j2Knfig} P_i k\text{-}\mathrm{th}_i k \quad > P_j k\text{-}\mathrm{th}_j k \quad ; k\text{-}\mathrm{th}_i k > r j \ \ \mathrm{p}_k; 8\ k\ 2\ K_1\Big).$$

This expression is similar to the expression appearing in the computation of association probability with the additional event that $k\text{-}\mathrm{th}_i k > r$ which can be handled by changing the lower limit of the integral in (4.9). The final step is to differentiate the CCDF with respect to r. □

4.3.3 Coverage probability

Before deriving the main results on coverage probability, we first introduce PGFL and sum-product functional of a point process which will be appearing repeatedly into the coverage analysis.

Definition 4.8 (PGFL)**.** PGFL of a point process is defined as: $\mathrm{E}\Big[\prod_{x2} (\mathbf{x})\Big]$, where $(\mathbf{x}) : \mathrm{R}^2 \ ! \ [0; 1]$ is measurable.

Lemma 4.9. *When* $((\mathbf{x}))$ *is a PPP, the PGFL is given as [13]:*

$$\mathrm{E}\Big[\prod_{x2} (\mathbf{x})\Big] = \exp\Big(-\int_{\mathrm{R}^2} (\mathbf{x})(1 \quad (\mathbf{x}))\mathrm{d}\mathbf{x}\Big). \tag{4.11}$$

When $(\mathbf{x}) = (x)$ and $( )$ is homogeneous, then (4.11) becomes:

$$\mathrm{E}\Big[\prod_{y2} (y)\Big] = \exp\Big(-2\int_0^1 (1 \quad (y))y\mathrm{d}y\Big). \tag{4.12}$$

Definition 4.10 (Sum-product functional)**.** Sum-product functional of a point process is defined in this chapter as $\mathrm{E}\Big[\prod_{x2} (\mathbf{x}) \sum_{y2} (\mathbf{y})\Big]$, where $(\mathbf{x}) : \mathrm{R}^2 \ ! \ \mathrm{R}^+$ and $(\mathbf{y}) : \mathrm{R}^2 \ ! \ [0; 1]$ are measurable.

For a PPP, the sum-product functional is given by the following Lemma.

Lemma 4.11. *When* $((\mathbf{x}))$ *is a PPP, the sum-product functional is given as [75, 79]*

$$\mathrm{E}\Big[\sum_{x2} (\mathbf{x}) \prod_{y2} (\mathbf{y})\Big] = \int_{\mathrm{R}^2} (\mathbf{x}) \ (\mathbf{x}) \ (\mathbf{x})\mathrm{d}\mathbf{x} \exp\Big(-\int_{\mathrm{R}^2} (\mathbf{y})(1 \quad (\mathbf{y}))\mathrm{d}\mathbf{y}\Big). \tag{4.13}$$

When $(\mathbf{x}) \quad (x)$, $(\mathbf{x}) \quad (x)$, and $(\ )$ is homogeneous, then (4.13) becomes:

$$\mathrm{E}\left[\sum_{x2} (x) \sum_{y2} (y)\right] = 2 \int_0^{Z1} (x)\ (x)x\mathrm{d}x \exp\left(-2 \int_0^{Z1} (1 \quad (y))y\mathrm{d}y\right): \tag{4.14}$$

Before providing the final expression of coverage probability, we provide an important intermediate expression of the conditional i^{th} tier coverage probability given all parent point processes. In fact, a key contribution of this chapter, as will be evident in sequel, is to show that this conditional coverage probability can be factored as a product of standard functionals (such as PGFL and sum-product functional) of the parent PPPs.

Lemma 4.12. *The i^{th} tier coverage probability given $_{\mathrm{p}_k}; 8\ k\ 2\ K_1$ is given by* $\mathrm{P}(\mathtt{SINR}(\mathrm{x}) > {}_i; S_i j\ {}_{\mathrm{p}_k}; 8\ k\ 2\ K_1) =$

$$m_i \int_0^{Z1} \exp\left(-\frac{{}_i \mathrm{N}_0 r}{P_i}\right) \prod_{j_1 2 K_1 n f i g} \prod_{\mathtt{z}2\ {}_{\mathrm{p}_{j_1}}} C_{j_1;i}(r;z) \prod_{j_2 2 K_2} \exp\left(-r^2\ {}_{j_2} P_{j_2;i}^2\ (\ {}_i;\ \ )\right)$$
$$\left(\sum_{\mathtt{z}2\ {}_{\mathrm{p}_i}} f_{\mathrm{d}_i}(r j z) \prod_{\mathtt{z}2\ {}_{\mathrm{p}_i}} C_{i;i}(r;z)\right) \mathrm{d}r; \textit{when } i\ 2\ K_1; \tag{4.15a}$$

$$2\ {}_i \int_0^{Z1} \exp\left(-\frac{{}_i \mathrm{N}_0 r}{P_i}\right) \prod_{j_1 2 K_1} \prod_{\mathtt{z}2\ {}_{\mathrm{p}_{j_1}}} C_{j_1;i}(r;z)$$
$$\prod_{j_2 2 K_2} \exp\left(-r^2\ {}_{j_2} P_{j_2;i}^2\ (\ {}_i;\ \ )\right) r\mathrm{d}r; \textit{when } i\ 2\ K_2; \tag{4.15b}$$

where

$$C_{j;k}(r;z) = \exp\left(-\ m_j \left(1 \int_{P_{j;k} r}^{Z1} \frac{f_{\mathrm{d}_j}(y j z)}{1 + {}_k \frac{(P_{j;k} r)}{y}} \mathrm{d}y\right)\right); \tag{4.16}$$

and, $(\ {}_i;\ \ ) = 1 + {}_i^{2=} \int_{{}_i^{2=}}^{R1} \frac{1}{1+t^{\ =2}} \mathrm{d}t = 1 + \frac{2\ {}_i}{2} {}_2F_1\ 1; 1\ \ \frac{2}{}; 2\ \ \frac{2}{}; \ \ {}_i$, *where* ${}_2F_1$ *is the Gauss hypergeometric function [22].*

Proof. We first compute the probability of the i^{th} coverage event given $_{\mathrm{p}_k}; 8\ k\ 2\ K_1$ as follows.

$$\mathrm{P}(\mathtt{SINR}(\mathrm{x}) > {}_i; S_i j\ {}_{\mathrm{p}_k}; 8\ k\ 2\ K_1) = \mathrm{P}(S_i j\ {}_{\mathrm{p}_k}; 8\ k\ 2\ K_1)\mathrm{P}(\mathtt{SINR}(\mathrm{x}) > {}_i j S_i;\ {}_{\mathrm{p}_k}; 8\ k\ 2\ K_1);$$

where $\mathsf{P}(\mathrm{SINR}(\mathbf{x}) > \beta_i \mid S_i, \{p_k; k \in K_1\}) =$

$$
\begin{aligned}
&\mathsf{P}\left(\frac{P_i h_{\mathbf{x}} \|\mathbf{x}\|^{-\alpha}}{N_0 + \sum_{j \in K_2} \sum_{\mathbf{y} \in \Phi_j \setminus \{\mathbf{x}\}} P_j h_{\mathbf{y}} \|\mathbf{y}\|^{-\alpha}} > \beta_i \mid S_i, \{p_k; k \in K_1\}\right) \\
&= \mathsf{P}\left(h_{\mathbf{x}} > \frac{\beta_i \|\mathbf{x}\|^{\alpha}}{P_i}\left(N_0 + \sum_{j \in K_2} \sum_{\mathbf{y} \in \Phi_j \setminus \{\mathbf{x}\}} P_j h_{\mathbf{y}} \|\mathbf{y}\|^{-\alpha}\right) \mid S_i, \{p_k; k \in K_1\}\right) \\
&\overset{(a)}{=} \mathsf{E}\left[\exp\left(-\frac{\beta_i \|\mathbf{x}\|^{\alpha}}{P_i}\left(N_0 + \sum_{j \in K_2} \sum_{\mathbf{y} \in \Phi_j \setminus \{\mathbf{x}\}} P_j h_{\mathbf{y}} \|\mathbf{y}\|^{-\alpha}\right)\right) \mid S_i, \{p_k; k \in K_1\}\right] \\
&= \mathsf{E}\left[\exp\left(-\frac{\beta_i N_0 \|\mathbf{x}\|^{\alpha}}{P_i}\right) \prod_{j \in K_2} \prod_{\mathbf{y} \in \Phi_j \setminus \{\mathbf{x}\}} \exp\left(-\frac{\beta_i P_j h_{\mathbf{y}}}{P_i} \frac{\|\mathbf{x}\|^{\alpha}}{\|\mathbf{y}\|^{\alpha}}\right) \mid S_i, \{p_k; k \in K_1\}\right] \\
&\overset{(b)}{=} \mathsf{E}\left[\exp\left(-\frac{\beta_i N_0 \|\mathbf{x}\|^{\alpha}}{P_i}\right) \prod_{j \in K_2} \prod_{\mathbf{y} \in \Phi_j \setminus \{\mathbf{x}\}} \mathsf{E}_{h_{\mathbf{y}}}\left[\exp\left(-\frac{\beta_i P_j h_{\mathbf{y}}}{P_i} \frac{\|\mathbf{x}\|^{\alpha}}{\|\mathbf{y}\|^{\alpha}}\right)\right] \mid S_i, \{p_k; k \in K_1\}\right] \\
&\overset{(c)}{=} \mathsf{E}\left[\exp\left(-\frac{\beta_i N_0 \|\mathbf{x}\|^{\alpha}}{P_i}\right) \prod_{j \in K_2} \prod_{\mathbf{y} \in \Phi_j \setminus b\left(\mathbf{0}; P_{j,i} \|\mathbf{x}\|^{\alpha}\right)^c} \frac{1}{1 + \frac{\beta_i P_j}{P_i} \frac{\|\mathbf{x}\|^{\alpha}}{\|\mathbf{y}\|^{\alpha}}} \mid S_i, \{p_k; k \in K_1\}\right] \\
&= \int_0^{\infty} \exp\left(-\frac{\beta_i N_0 r}{P_i}\right) \prod_{j_1 \in K_1} \mathsf{E}\left[\prod_{\mathbf{y} \in \Phi_{j_1} \setminus b\left(\mathbf{0}; P_{j_1,i} r\right)^c} \frac{1}{1 + \frac{\beta_i P_{j_1}}{P_i} \frac{r}{\|\mathbf{y}\|^{\alpha}}}\right] p_{j_1} \\
&\qquad \prod_{j_2 \in K_2} \mathsf{E}\left[\prod_{\mathbf{y} \in \Phi_{j_2} \setminus b\left(\mathbf{0}; P_{j_2,i} r\right)^c} \frac{1}{1 + \frac{\beta_i P_{j_2}}{P_i} \frac{r}{\|\mathbf{y}\|^{\alpha}}}\right] f_{s_i}(r \mid S_i, \{p_k; k \in K_1\}) \, \mathrm{d}r \\
&= \int_0^{\infty} \exp\left(-\frac{\beta_i N_0 r}{P_i}\right) \prod_{j_1 \in K_1} \exp\left(-\int_{z \in \mathbb{R}^2 \setminus b\left(\mathbf{0}; P_{j_1,i} r\right)} m_{j_1} f_{d_{j_1}}(y \mid z) \left(1 - \frac{1}{1 + \frac{\beta_i P_{j_1}}{P_i} \frac{r}{y}}\right) \mathrm{d}y\right) \\
&\qquad \prod_{j_2 \in K_2} \exp\left(-2\pi \int_{P_{j_2,i} r}^{\infty} \left(1 - \frac{1}{1 + \frac{\beta_i P_{j_2}}{P_i} \frac{r}{y}}\right) y \mathrm{d}y\right) f_{s_i}(r \mid S_i, \{p_k; k \in K_1\}) \, \mathrm{d}r.
\end{aligned}
\tag{4.16}
$$

Here (a) follows from the fact that $h_{\mathbf{x}} \sim \exp(1)$, (b) follows from the assumption that all links undergo i.i.d. fading, and (c) is justified since in $\Phi_j \setminus \{\mathbf{x}\}$, there exists no points inside the disc $b(\mathbf{0}; P_{j,i} \|\mathbf{x}\|^{\alpha})$, which is known as the *exclusion disc*. In the last step, we use the

PGFL of PPP from Lemma 4.9. When $i \in K_1$, substituting $f_{s_i}(rjS_i;\ \Phi_k; \forall k \in K_1)$ from (4.10a), $\mathtt{P}(\mathtt{SINR}(x) > \ _i; S_i | \ \Phi_k; \forall k \in K_1) =$

$$m_i \int_0^\infty \exp\left(\frac{-\ _i N_0 r}{P_i}\right) \prod_{j_1 \in K_1} \prod_{z \in \Phi_{j_1}} \exp\left(-m_{j_1} F_{d_{j_1}}(P_{j_1;i} rjz) - m_{j_1} \int_{P_{j_1;i} r}^\infty f_{d_{j_1}}(yjz)\left(1 - \frac{1}{1 + \frac{\ _i P_{j_1}}{P_i}\frac{r}{y}}\right) dy\right)$$
$$\exp\left(-\sum_{j_2 \in K_2} \int_{P_{j_2;i} r}^\infty \left(1 - \frac{1}{1 + \frac{\ _i P_{j_2}}{P_i}\frac{r}{y}}\right) y dy \sum_{j_2 \in K_2} j_2 P_{j_2;i}^2 r^2 \sum_{z \in \Phi_i} f_{d_i}(rjz) dr\right)$$
$$= m_i \int_0^\infty \exp\left(\frac{-\ _i N_0 r}{P_i}\right) \prod_{j_1 \in K_1} \prod_{z \in \Phi_{j_1}} \exp\left(-m_{j_1}\left(1 - \int_{P_{j_1;i} r}^\infty \frac{f_{d_{j_1}}(yjz)}{1 + \frac{\ _i P_{j_1}}{P_i}\frac{r}{y}} dy\right)\right)$$
$$\exp\left(-r^2 \sum_{j_2 \in K_2} j_2 P_{j_2;i}^2 \ _i^{2=} \int_{\ _i^{-2=}}^\infty \frac{1}{1 + t^{=2}} dt \sum_{j_2 \in K_2} j_2 P_{j_2;i}^2 r^2 \sum_{z \in \Phi_i} f_{d_i}(rjz) dr\right).$$

In the last step, we substitute $\frac{\ _i P_{j_2} r}{P_i y} = t^{-=2}$. The final expression is obtained by some algebraic simplification. When $i \in K_2$, substituting $f_{s_i}(rj\ \Phi_k; k \in K_1)$ in (4.16) by (4.10b), we get $\mathtt{P}(\mathtt{SINR}(x) > \ _i; S_i | \ \Phi_k; \forall k \in K_1) =$

$$2\ _i \int_0^\infty \exp\left(\frac{-\ _i N_0 r}{P_i}\right) \prod_{j_1 \in K_1} \prod_{z \in \Phi_{j_1}} \exp\left(-m_{j_1} F_{d_{j_1}}(P_{j_1;i} rjz) - m_{j_1} \int_{P_{j_1;i} r}^\infty f_{d_{j_1}}(yjz)\left(1 - \frac{1}{1 + \frac{\ _i P_{j_1}}{P_i}\frac{r}{y}}\right) dy\right)$$
$$\exp\left(-\sum_{j_2 \in K_2} 2 \int_{P_{j_2;i} r}^\infty \left(1 - \frac{1}{1 + \frac{\ _i P_{j_2}}{P_i}\frac{r}{y}}\right) y dy \sum_{j_2 \in K_2} j_2 r^2 \left(\frac{P_{j_2}}{P_i}\right)^{2=}\right) r dr.$$

The final expression is obtained by some algebraic simplification. □

Looking closely at the expressions of the i^{th} tier coverage probability given $\Phi_k; \forall k \in K_1$, we find two terms: (i) $\prod_{z \in \Phi_{j_1}} C_{j_1;i}(r; z)$ in (4.15a) and (4.15b), and (ii) $\sum_{z \in \Phi_i} f_{d_i}(rjz) \prod_{z \in \Phi_i} C_{i;i}(r; z)$

in (4.15a). These two terms are respectively product and sum-product over all points of Φ_k which will be substituted by the PGFL and sum-product functional of Φ_k while decond-tioning over Φ_k.

Remark 4.13. In order to apply PGFL and sum-product functional expressions of PPP given by (4.12) and (4.14), respectively, we require the condition: $\int_0^\infty \log(|C_{j_1;i}(r,z)|)z\,dz < \infty;\ \forall\ j_1 \in K_1$. In [90, Appendix B], it was shown that this condition always holds for the form of $C_{j_1;i}(r,z)$ given by (4.16).

Until this point, all results were conditioned on $\Phi_k; \forall\ k \in K_1$. Remember that in Section 4.2.2, we introduced two types of spatial interaction between the users and BSs. Since, by construction, these two types differ only in Φ_q for some $q \in K_1$, we were able to treat case 1 and case 2 within the same analytical framework. We now present the final expression of $\mathtt{P_c}$ for the two types explicitly by deconditioning the conditional coverage probability over $\Phi_k; \forall\ k \in K_1$ in the following Theorems.

Theorem 4.14 (case 1)**.** *The coverage probability is given as:*

$$\mathtt{P_c} = \sum_{i=1}^{K} \mathtt{P}(\mathtt{SINR} > \beta_i; S_i), \tag{4.17}$$

where, the i^{th} tier coverage probability, $\mathtt{P}(\mathtt{SINR} > \beta_i; S_i) =$

$$2\pi\lambda_i m_i \int_0^\infty \exp\left(-\frac{\beta_i N_0 r}{P_i}\right) \prod_{j_1 \in K_1} \exp\left(-2\pi\lambda_{j_1}\int_0^\infty (1 - C_{j_1;i}(r,z))\,z\,dz\right) \exp\left(-r^2 \sum_{j_2 \in K_2} \lambda_{j_2} P_{j_2;i}^2\, \beta_i^{\delta}\right) \int_0^\infty f_{d_i}(r|z)\, C_{i;i}(r,z)\,z\,dz\,dr;\ \text{for } i \in K_1; \tag{4.18a}$$

$$2\pi\lambda_i \int_0^\infty \exp\left(-\frac{\beta_i N_0 r}{P_i}\right) \prod_{j_1 \in K_1} \exp\left(-2\pi\lambda_{j_1}\int_0^\infty (1 - C_{j_1;i}(r,z))\,z\,dz\right) \exp\left(-r^2 \sum_{j_2 \in K_2} \lambda_{j_2} P_{j_2;i}^2\, \beta_i^{\delta}\right) r\,dr;\ \text{for } i \in K_2. \tag{4.18b}$$

Proof. When $i \in K_1$, we get from (4.15a),

$$\mathtt{P}(\mathtt{SINR} > \beta_i; S_i) = \mathtt{E}\left[\mathtt{P}(\mathtt{SINR} > \beta_i; S_i \mid \Phi_k; \forall\ k \in K_1)\right] =$$

$$m_i \int_0^{\infty} \exp\left(-\frac{\beta_i N_0 r}{P_i}\right) \prod_{j_1 \in \{K_1 \setminus \{i\}\}} \mathbb{E}_{\Phi_{j_1}}\left[\prod_{z \in \Phi_{j_1}} C_{j_1,i}(r,z)\right] \exp\left(-r^2 \sum_{j_2 \in K_2} \beta_{j_2} P_{j_2,i}^{2/\alpha_{j_2}} \Gamma(1+\alpha_{j_2}/2)\right) \mathbb{E}_{\Phi_i}\left[\sum_{z \in \Phi_i} f_{d_i}(r|z) \prod_{z \in \Phi_i} C_{i,i}(r,z)\right] dr.$$

This step is enabled by the assumption that β_j-s are independent $\forall\, j \in K$. The final expression is obtained by substituting the PGFL of Φ_k for $k \in K_1 \setminus \{i\}$ from (4.12) and the sum-product functional of Φ_i from (4.14). The final expression follows from some algebraic simplifications. Now, for $i \in K_2$, from (4.15b), we get

$$\mathtt{P}(\mathtt{SINR} > \beta_i, S_i) = 2\pi_i \int_0^{\infty} \exp\left(-\frac{\beta_i N_0 r}{P_i}\right) \prod_{j_1 \in K_1} \mathbb{E}_{\Phi_{j_1}}\left[\prod_{z \in \Phi_{j_1}} C_{j_1,i}(r,z)\right] \exp\left(-r^2 \sum_{j_2 \in K_2} \beta_{j_2} P_{j_2,i}^{2/\alpha_{j_2}} \Gamma(1+\alpha_{j_2}/2)\right) r\, dr.$$

We then use the PGFL of Φ_{j_1} from (4.12) to obtain the final expression. □

Theorem 4.15 (case 2). *The coverage probability* $\mathtt{P_c}$ *can be written as* (4.17)*, where the* i^{th} *tier coverage probability is:* $\mathtt{P}(\mathtt{SINR} > \beta_i, S_i) =$

$$2\pi_i m_i \int_0^{\infty} \exp\left(-\frac{\beta_i N_0 r}{P_i}\right) \prod_{j_1 \in K_1} \exp\left(-2\pi\lambda_{j_1} \int_0^{\infty} (1 - C_{j_1,i}(r,z))\, z\, dz\right) \int_0^{\infty} C_{q,i}(r,z_0) f_{d_u}(z_0|0) dz_0 \exp\left(-r^2 \sum_{j_2 \in K_2} \beta_{j_2} P_{j_2,i}^{2/\alpha_{j_2}} \Gamma(1+\alpha_{j_2}/2)\right) \int_0^{\infty} f_{d_i}(r|z) C_{i,i}(r,z) z\, dz\, dr; \text{ for } i \in K_1 \setminus \{q\}; \quad (4.19a)$$

$$m_q \int_0^{\infty} \exp\left(-\frac{\beta_q N_0 r}{P_q}\right) \prod_{j_1 \in K_1} \exp\left(-2\pi\lambda_{j_1} \int_0^{\infty} (1 - C_{j_1,q}(r,z))\, z\, dz\right) \exp\left(-r^2 \sum_{j_2 \in K_2} \beta_{j_2} P_{j_2,q}^{2/\alpha_{j_2}} \Gamma(1+\alpha_{j_2}/2)\right) \int_0^{\infty} f_{d_q}(r|z_0) C_{q,q}(r,z_0) f_{d_u}(z_0|0) dz_0$$
$$+ 2\pi_q \int_0^{\infty} f_{d_q}(r|z) C_{q,q}(r,z) z\, dz \int_0^{\infty} C_{q,q}(r,z_0) f_{d_u}(z_0|0) dz_0\, dr; \text{ for } i = q; \quad (4.19b)$$

$$2\int_0^{\infty} \exp\left(-\frac{\beta_i N_0 r}{P_i}\right) \prod_{j_1 \in K_1} \exp\left(-2\int_0^{\infty} \left(1 - C_{j_1,i}(r,z)\right) z\,dz\right) \int_0^{\infty} C_{q,i}(r,z_0) f_{d_u}(z_0|0)\,dz_0 \exp\left(-r^2 \sum_{j_2 \in K_2} \pi_{j_2} P_{j_2,i}^{2/\alpha_{j_2}} \Gamma\left(1+\frac{\alpha_{j_2}}{2}\right)\right) r\,dr, \text{ for } i \in K_2. \quad (4.19c)$$

Here $f_{d_u}(z_0|0)$ denotes the distance distribution of a point of Φ_u from its cluster center which resides at origin.

Proof. When $i \in K_1 \setminus \{q\}$, $\mathrm{P}(\mathtt{SINR} > \beta_i, S_i) =$

$$m_i \int_0^{\infty} \exp\left(-\frac{\beta_i N_0 r}{P_i}\right) \prod_{j_1 \in K_1 \setminus \{i,q\}} \mathrm{E}_{\Phi_{j_1}}\left[\prod_{z \in \Phi_{j_1}} C_{j_1,i}(r,z)\right] \mathrm{E}_{\Phi_q}\left[\prod_{z \in \Phi_q} C_{q,i}(r,z)\right] \exp\left(-r^2 \sum_{j_2 \in K_2} \pi_{j_2} P_{j_2,i}^{2/\alpha_{j_2}} \Gamma\left(1+\frac{\alpha_{j_2}}{2}\right)\right) \mathrm{E}_{\Phi_i}\left[\sum_{z \in \Phi_i} f_{d_i}(r|z) \prod_{z \in \Phi_i} C_{i,i}(r,z)\right] dr.$$

As opposed to case 1, the product over all points of Φ_q has to be handled explicitly. The PGFL of Φ_q for case 2 evaluated at $C_{q,i}(r,z)$ is given by

$$\mathrm{E}\left[\prod_{z \in \Phi_q} C_{q,i}(r,z)\right] = \mathrm{E}\left[C_{q,i}(r,z_0)\right] \mathrm{E}\left[\prod_{z \in \Phi_q \setminus \{z_0\}} C_{q,i}(r,z)\right] = \mathrm{E}\left[C_{q,i}(r,z_0)\right] \exp\left(-2\int_0^{\infty} \left(1 - C_{q,i}(r,z)\right) z\,dz\right).$$

This step is enabled by the fact that $\mathbf{z}_0$ and $\Phi_q \setminus \{\mathbf{z}_0\}$ are independent. Substituting $\mathcal{C}(\mathbf{z}) = C_{q,i}(z,r)$ and proceeding on similar lines of the proof of Theorem 4.14, we obtain the final expression. Also note that since the function of $\mathbf{z}_0$ under consideration is only dependent on $\|\mathbf{z}_0\| = z_0$, while taking expectation over $\mathbf{z}_0$, it is sufficient to consider the magnitude distribution of $\mathbf{z}_0$ which is denoted as $f_{d_u}(z_0|0)$. Now when $i = q$,

$$\mathrm{P}(\mathtt{SINR} > \beta_i, S_i) = m_q \int_0^{\infty} \exp\left(-\frac{\beta_q N_0 r}{P_q}\right) \prod_{j_1 \in K_1 \setminus \{q\}} \mathrm{E}_{\Phi_{j_1}}\left[\prod_{z \in \Phi_{j_1}} C_{j_1,q}(r,z)\right] \exp\left(-r^2 \sum_{j_2 \in K_2} \pi_{j_2} P_{j_2,q}^{2/\alpha_{j_2}} \Gamma\left(1+\frac{\alpha_{j_2}}{2}\right)\right) \mathrm{E}_{\Phi_q}\left[\sum_{z \in \Phi_q} f_{d_q}(r|z) \prod_{z \in \Phi_q} C_{q,q}(r,z)\right] dr,$$

where the last term in the expression under integral is the sum-product functional over Φ_q which is computed as:

$$\mathrm{E}_{\Phi_q}\Big[\sum_{z\in\Phi_q} f_{d_q}(rjz)\prod_{z\in\Phi_q} C_{q;q}(r;z)\Big] = \mathrm{E}\big[f_{d_q}(rjz_0)C_{q;q}(r;z_0)\big]\,\mathrm{E}_{(\Phi_q)}\Big[\prod_{z\in(\Phi_q)} C_{q;q}(r;z)\Big]$$
$$+\,\mathrm{E}_{(\Phi_q)}\Big[\sum_{z\in\Phi_q} f_{d_q}(rjz)\prod_{z\in\Phi_q} C_{q;q}(r;z)\Big]\mathrm{E}[C_{q;q}(r;z_0)]$$
$$= \int_0^{\infty} f_{d_q}(rjz_0)C_{q;q}(r;z_0)f_{d_u}(z_0j0)dz_0 \exp\Big(-2\pi_q\int_0^{\infty}(1-C_{q;q}(r;z))zdz\Big)$$
$$+\,2\pi_q\int_0^{\infty} f_{d_q}(rjz)C_{q;q}(r;z)zdz\exp\Big(-2\pi_q\int_0^{\infty}(1-C_{q;q}(r;z))zdz\Big)\int_0^{\infty} C_{q;q}(r;z_0)f_{d_u}(z_0j0)dz_0$$
$$= \exp\Big(-2\pi_q\int_0^{\infty}(1-C_{q;q}(r;z))zdz\Big)\int_0^{\infty} f_{d_q}(rjz_0)C_{q;q}(r;z_0)f_{d_u}(z_0j0)dz_0$$
$$+\,2\pi_q\int_0^{\infty} f_{d_q}(rjz)C_{q;q}(r;z)zdz\int_0^{\infty} C_{q;q}(r;z_0)f_{d_u}(z_0j0)dz_0\ :$$

The final expression can be obtained by proceeding on similar lines of the proof of Theorem 4.14. Now, for $i \in K_2$, $\mathrm{P}(\mathrm{SINR} > \beta_i; S_i) =$

$$2\pi_i\int_0^{\infty}\exp\Big(-\frac{\beta_i N_0 r}{P_i}\Big)\prod_{j_1\in K_1\setminus\{q\}}\mathrm{E}_{\Phi_{j_1}}\Big[\prod_{z\in\Phi_{j_1}} C_{j_1;i}(r;z)\Big]$$
$$\mathrm{E}_{\Phi_q}\Big[\prod_{z\in\Phi_q} C_{q;i}(r;z)\Big]\exp\Big(-r^2\sum_{j_2\in K_2}\beta_{j_2}P_{j_2;i}^{2}\,\Big(\tfrac{2}{\alpha_i};\beta_i\Big)\Big)\,rdr:$$

Since expression is very similar to the expression of $\mathrm{P}(\mathrm{SINR} > \beta_i; S_i)$ obtained for $i \in K_1 \setminus \{q\}$, we omit the next steps leading to the final expression. □

We conclude this discussion with the following remark.

Remark 4.16. The analytical framework developed in this Section provisions to model the k^{th} BS tier, where $k \in K_1$ as any arbitrary PCP $(\Phi_k; g_k; m_k)$. By looking into the expressions of $\mathrm{P_c}$ in Theorems 4.14 and 4.15, it is apparent that given K_1 PCPs with arbitrary distributions, i.e., $f_k = (\Phi_k; g_k; m_k); k \in K_1\}$, the only non-trivial step is to find the conditional distance distributions $\{f_{d_k}(xjz)\}$ which need to be simply plugged into the expressions of $\mathrm{P}(\mathrm{SINR} > \beta_i; S_i)$ in (4.18)-(4.19).

The unified model discussed in this chapter reduces to the conventional PPP-based HetNet model with no spatial coupling between users and BS locations by setting $K_1 = ?$. For this scenario, Type 2 becomes irrelevant and the coverage probability is given by the following Corollary.

Corollary 4.17. *Setting $K_1 = ?$, coverage probability for* Type *1 is given by:*

$$P_c = \sum_{i2K_2} 2 \int_0^{Z^1} \exp\left(-\frac{{}_i N_0 r}{P_i}\right) \exp\left(-r^2 \sum_{j2K_2} {}_{j2} P_{j;i}^2 \, (\,{}_i;\,)\right) r\,dr; \tag{4.20}$$

and, for interference-limited networks ($N_0 = 0$),

$$P_c = \sum_{i2K_2} \frac{{}_i P_i^{\frac{2}{}}}{\sum_{j2K_2} {}_j P_j^{\frac{2}{}} \, (\,{}_i;\,)}: \tag{4.21}$$

Proof. This result can be obtained directly from (4.18b) by setting $K_1 = ?$. See [22, 32] for the intermediate steps between (4.20) and (4.21). □

4.3.4 Special cases: TCP and MCP

For the purpose of numerical evaluation of coverage probability, we assume that ${}_k$ is either a TCP or an MCP which are defined as follows.

Definition 4.18 (Thomas Cluster Process)**.** A PCP ${}_k\,(\,{}_{p_k}; g_k; m_k)$ is called a TCP if the distribution of the offspring points in B_k^z is Gaussian around the cluster center at the origin, i.e. for all $\mathbf{s} \; 2 \; B_k^z$, if $\mathbf{s} = (ksk; \arg(\mathbf{s}))$ $(s;\,{}_s) \; 2 \; B_k^z$ denotes a point of the offspring point process B_k^z with cluster center at origin,

$$g_k(\mathbf{s}) = g_k(s;\,{}_s) = \frac{s}{{}_k^2} \exp\left(-\frac{s^2}{2\,{}_k^2}\right) \frac{1}{2}; \; s \quad 0; 0 < {}_s \quad 2 \; : \tag{4.22}$$

Definition 4.19 (Matérn Cluster Process)**.** A PCP ${}_k\,(\,{}_{p_k}; g_k; m_k)$ is called an MCP if the distribution of the offspring points in B_k^z is uniform within a disc of radius r_{d_k} around the origin denoted by $b(\mathbf{0}; r_{d_k})$. Hence,

$$g_k(\mathbf{s}) = g_k(s;\,{}_s) = \frac{2s}{r_{d_k}^2} \frac{1}{2}; \quad 0 \quad s \quad r_{d_k}; 0 < {}_s \quad 2 \; : \tag{4.23}$$

We now provide the conditional distance distributions of TCP and MCP. When ${}_k$ is a TCP, given that $\mathbf{z}$ is the cluster center of $\mathbf{x}$, i.e., $\mathbf{x} \; 2 \; \mathbf{z} + B_k^z$, we can write the conditional PDF of x as [59]:

$$f_{d_k}(xjz) = \frac{x}{{}_k^2} \exp\left(-\frac{x^2 + z^2}{2\,{}_k^2}\right) I_0\left(\frac{xz}{{}_k^2}\right); \quad x; z \quad 0; \tag{4.24}$$

where $I_0(\cdot)$ is the modified Bessel function of the first kind with order zero, and,

$$f_{d_k}(x|0) = \frac{x}{\sigma_k^2} \exp\left(\frac{x^2}{2\sigma_k^2}\right); \quad x \geq 0. \tag{4.25}$$

When Φ_k is an MCP, $f_{d_k}(x|z) = \mathcal{A}_k^{(\ell)}(x;z)$; $(\ell = 1,2)$, where

$$\mathcal{A}_k^{(1)}(x;z) = \frac{2x}{r_{d_k}^2}; \quad 0 \leq x \leq r_{d_k}, z>0 \text{ or } z \geq r_{d_k}; \tag{4.26a}$$

$$\mathcal{A}_k^{(2)}(x;z) = \frac{2x}{r_{d_k}^2} \cos^{-1}\left(\frac{x^2+z^2-r_{d_k}^2}{2xz}\right); \quad |z-r_{d_k}| < x < r_{d_k}+z. \tag{4.26b}$$

4.4 Results and discussions

We now numerically evaluate the expressions of $\mathtt{P_c}$ derived in Theorems 4.14 and 4.15. For the numerical evaluation, we choose a two tier network ($K = 2$) with one tier of sparsely deployed MBSs and another tier of densely deployed SBSs. The SBSs are distributed as a PCP and the MBSs are distributed as a PPP, i.e., $K_1 = \{1\}$ and $K_2 = \{2\}$. We assume that the network is interference limited ($\mathtt{N_0} = 0$) and the downlink transmit powers of each BS in Φ_1 and Φ_2 are set such that $P_2/P_1 = 10^3$. Also, Φ_1 is assumed to be denser than Φ_2, i.e., $m_1 p_1 > \lambda_2$. We also assume $\alpha = 4$ and $\beta_1 = \beta_2 = \beta$. We first verify the analytical results presented in Theorems 4.14 and 4.15 with Monte Carlo simulations of the network, for which we set $m_1 = 4$; $p_1 = 25$ km^{-2} and $\lambda_2 = 1$ km^{-2}. The values of $\mathtt{P_c}$ for different values of β from simulation and analysis are plotted in Fig. 4.2, where Fig. 4.2a and 4.2b corresponds to Φ_1 being TCP and MCP, respectively. The perfect match between simulation and analytical results, indicated by small circles and curves, respectively, verifies the accuracy of our analysis. The Matlab scripts of the analytical expressions presented in Theorems 4.14 and 4.15 as well as the Monte Carlo simulation of the two-tier HetNet are provided in [91].

Also note that $\mathtt{P_c}$ for Type 2 users is always greater than $\mathtt{P_c}$ for Type 1 users. This ordering can be interpreted as follows. Due to the ergodicity of the network, coverage probability can be alternatively defined as the fraction of users in the whole network that can achieve SINR greater than a threshold (β). Thus, the outage probability or $(1 - \mathtt{P_c})$ is a measure of the fraction of users on average who fail to meet the SINR threshold β. These users are more likely to be the ones who lie farther away from the serving BS. Thus, the higher outage for Type 1 users compared to Type 2 users implies more number of users receive SINR less than β in Type 1 compared to Type 2 on average. The reason is that for Type 1 users, since there is no spatial coupling between the user and BS locations, more users lie farther away from their serving BSs on average. On the other hand, Type 2 users will lie closer to their serving BSs on average because of the spatial coupling.

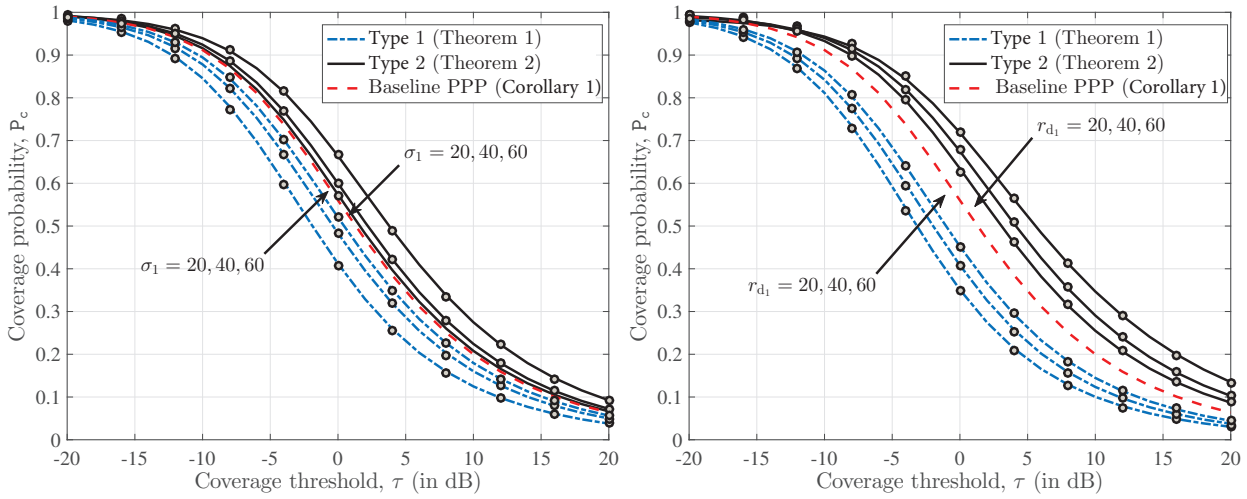

(a) $_1$ is a TCP. (b) $_1$ is an MCP.

Figure 4.2: Coverage probability as a function of SIR threshold (= 4, $P_2 = 10^3 P_1$, $_2$ = 1 km ^{2}, $_{p_1}$ = 25 km ^{2}, and $m_1 = 4$).

4.4.1 Variation of cluster size

In Fig. 4.2, P_c is plotted for different cluster sizes of $_1$. The cluster size precisely refers to $_1$ when $_1$ is a TCP (in Fig. 4.2a) and r_{d_1} when $_1$ is an MCP (in Fig. 4.2b). We observe that the cluster size has a conflicting effect on P_c: for Type 1, P_c increases with cluster size and for Type 2, P_c decreases with cluster size. This can be explained as follows. In Type 2, due to the spatial coupling between $_1$ and $_u$, the candidate serving BS of $_1$ is more likely to belong to the representative cluster (i.e., the BS cluster with the cluster center of the typical user) and as cluster size increases, this candidate serving BS moves farther away from the user on average. On the other hand, for Type 1, as cluster size increases, the BSs of $_1$ on average lie closer to the typical user. This phenomenon is the consequence of the spatial coupling between BSs and users and is also observed for the max-SINR based association strategy in the similar setup [79]. For both types, as cluster size increases, P_c converges to the coverage probability for a two tier network with both BS tiers being modeled as PPP, more precisely, $K_1 = ?$, $K_2 = f1; 2g$, with intensities $_1 = m_1$ $_{p_1}$ and $_2$, respectively. The reason for this convergence is the fact that as cluster size tends to infinity, the limiting distribution of a PCP is a PPP [13]. Since the trends of P_c are very similar for $_1$ being TCP and MCP, we set $_1$ as TCP for the rest of the discussion.

Another interesting observation from Fig. 4.2 is that the variation of P_c with cluster size is not as prominent for Type 2 as it is for Type 1. For further investigation, we focus on the scenario where $_1$ is a TCP, fix = 0 dB and plot the variation of P_c with $_1$ in Fig. 4.3. We observe that the P_c versus $_1$ curves for Type 2 are almost flat. The reason can be explained as follows. For Type 2, as cluster size is increased, the nearest BS of $_1$ belonging to the representative cluster lies farther away while the nearest BS of $_1$ which

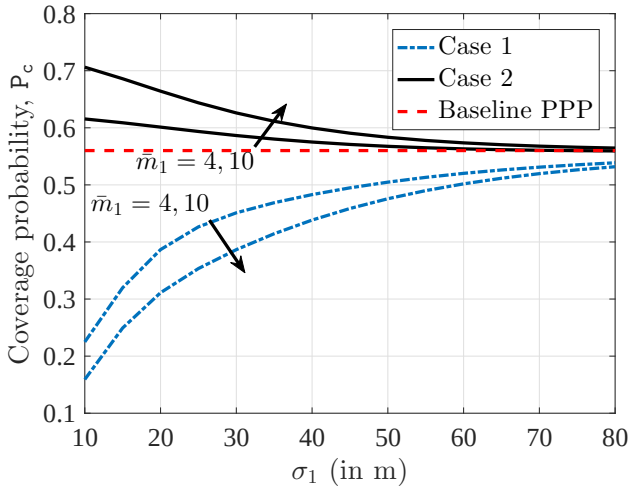

Figure 4.3: Coverage probability as a function of $_1$ ($= 4$, $P_2 = 10^3 P_1$, $_{p_1} = 25$ km ^{2}, $_2 = 1$ km ^{2}, and $= 0$ dB).

does not belong to the representative cluster comes closer. Also, as cluster size increases, the intra-cluster interference, i.e., the aggregate interference from the BSs of the representative cluster decreases while the inter-cluster interference, i.e., the aggregate interference from the BSs of $_1$ except the representative cluster increases. Due to these conflicting effects, the cluster size variation do not impact $\mathtt{P_c}$ strongly for Type 2. On the other hand, for Type 1 these conflicts are not present because $_u$ and $_1$ are not coupled and hence there is no representative BS cluster.

4.4.2 Variation of BS intensity

We now vary the intensity of the parent PPP ($_{p_1}$) keeping $_2$ constant and plot the coverage probability in Fig. 4.4. For an interference-limited HetNet with the same SIR threshold for all tiers, it is a well-known result that if the BSs are modeled as PPPs, $\mathtt{P_c}$ is independent of the BS intensity. This can be readily verified by putting $_i = \ \delta\ i$ in (4.21) which yields $\mathtt{P_c} = 1/(\ ;\ )$. However, once the spatial distribution of BSs is changed to PCP, we see that $\mathtt{P_c}$ is rather strongly dependent on the BS intensity under similar set of assumptions. From Fig. 4.4, we also observe that for large values of $_{p_1}$, $\mathtt{P_c}$ converges to $1/(\ ;\ )$, i.e., the coverage when the BSs are modeled as PPPs.

Remark 4.20. Although it is difficult to visualize the variation of $\mathtt{P_c}$ in the parameter space, which for the two tier network under consideration is $_{p_1}$ $_2$ m_1 $_1$, using the results in [92], it is possible to find the trajectories (known as equi-coverage contours) in the parameter space along which $\mathtt{P_c}$ remains constant. The family of equicoverage contours are generated by $(\ _{p_1}/l^2;\ _2/l^2;\ _1 l)$ where $l > 0$ is a scalar. When $_1$ is an MCP, a similar result can be obtained by replacing $_1$ by r_{d_1}.

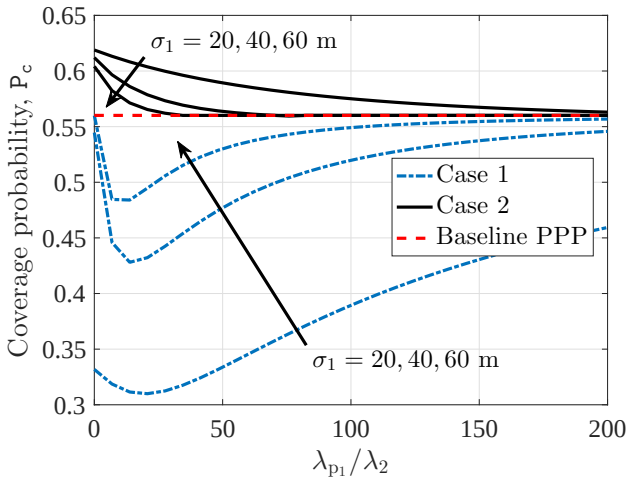

Figure 4.4: Coverage probability as a function of $_{p_1}= _2$ ($= 4$, $P_2 = 10^3 P_1$, $= 0$ dB, and $m_1 = 10$).

4.4.3 Variation of transmission power

We vary the transmission powers of the BSs of two tiers to observe its effect on coverage. Since we assumed that the network is interference-limited, the transmission powers contribute to $\mathtt{P_c}$ through ratios. Hence, for the two-tier setup it is sufficient to vary P_2=P_1 instead of their absolute values. In Fig. 4.5, we have plotted $\mathtt{P_c}$ versus P_2=P_1 for the two types of users. We first discuss the network behavior in two extremes of P_2=P_1 for which the two-tier network is equivalent to a single tier network in terms of coverage. For instance, the network $_1$ [$_2$ is equivalent to $_1$ when P_2=P_1 ! 0. Similarly, $_1$ [$_2$ is equivalent to $_2$ when P_2=P_1 ! 1 . Thus, for the two extreme cases of P_2=P_1, $\mathtt{P_c}$ of the two-tier network converges to the $\mathtt{P_c}$ obtained by considering only $_1$ and $_2$. Since $_2$ is a PPP, it is obvious that $\lim_{P_2=P_1 \,!\, 1} \mathtt{P_c} = 1/(1 + (\ ;\ ))$; which is the expression of $\mathtt{P_c}$ under the assumtion that the BSs are distributed as a homogeneous PPP [22]. For the other side of the limit, i.e., when P_2=P_1 ! 0, we observe that $\mathtt{P_c}$ for Type 1 and Type 2 users deviate from each other: $\mathtt{P_c}$ increases for Type 1 users and decreases for Type 2 users as P_2=P_1 ! 0. Observing the limiting values of $\mathtt{P_c}$ for Type 1 and Type 2 users, we conclude that the clustering of BS locations improves the coverage for the users as long as the BS locations are coupled with the user locations (as is the case for Type 2 users). However, if the users has no coupling with the BS distributions (as is the case for Type 1 users), the clustering pattern in the BS locations is detrimental for coverage.

4.4.4 Effect of adding BS tiers

In this Section, we investigate the effect of adding more BS tiers on the coverage probability of the network. Note that, if all tiers are modeled as PPPs (thus no spatial coupling

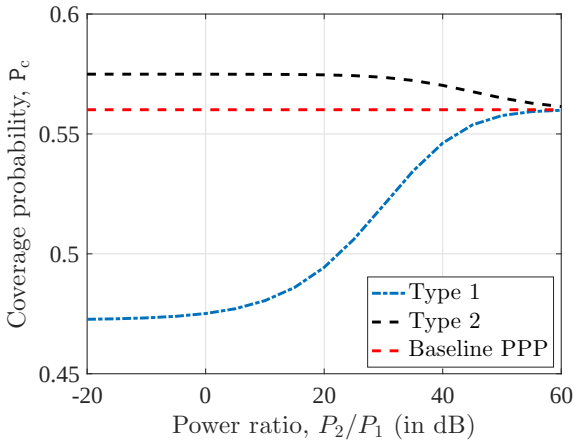

Figure 4.5: Effect of transmission powers on coverage (= 4, $_{p_1}$ = 25 km ^{2}, $_2$ = 1 km ^{2}, = 0 dB, $_1$ = 20 m, and m_1 = 4).

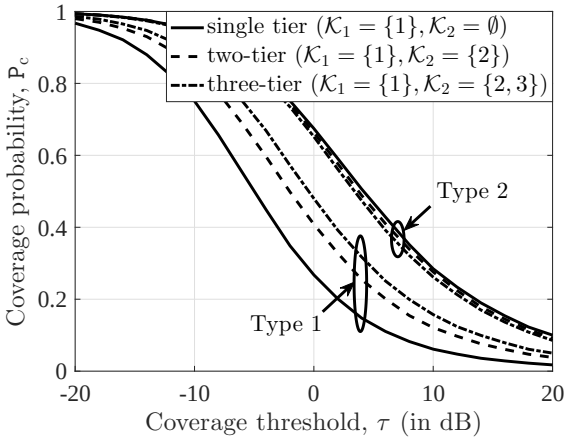

Figure 4.6: Effect of adding BS tiers on coverage (details of the network parameters are mentioned in Section 4.4.4.

in the network), adding a new tier does not change $\mathtt{P_c}$ as long as the network is interference limited [22]. However, this is not the case if at least one BS tier is modeled as a PCP. We consider three network configurations, (i) a single tier network with $K_1 = \{1\}$ and $K_2 = ?$, (ii) a two-tier network with $K_1 = \{1\}$ and $K_2 = \{2\}$, and (iii) a three-tier network with $K_1 = \{1\}$ and $K_2 = \{2, 3\}$, where $\ _1 = 20$ m. While $\ _1$ and $\ _2$ have the same configurations as mentioned in Section 4.4.1, $\ _3$ is a homogeneous PPP with $\ _3 = 5$ km ^{2} and $P_3 = 100P_1$. As observed in Fig. 4.6, coverage changes with the addition of BS tiers: $\mathtt{P_c}$ increases for Type 1 users and decreases for Type 2 users. For Type 1 users, the trend can be simply explained as follows. More number of BS tier implies more number of candidate serving BSs. Thus the power on the serving link increases more than the increase of the interference power, on average. On the contrary, the Type 2 users will most likely connect to the BSs of the same cluster because of the spatial coupling with $\ _1$. In that case, the addition of more BSs will only contribute towards increasing the interference power. Even if they connect to the BS of the other tier, the strong interference from the BSs of the representative cluster of $\ _1$ will decrease the SINR.

4.4.5 Effect of clustering on the second BS tier

We consider another two-tier network configuration where both BS tiers are modeled as PCPs, i.e., $K_1 = \{1, 2\}$, $K_2 = ?$ and the Type 2 users share the same cluster centers with $\ _1$. We plot $\mathtt{P_c}$ for different $\ $ in Fig. 4.7a. We observe that $\mathtt{P_c}$ decreases as cluster size ($\ _2$) decreases for both the scenarios. To concretely demonstrate the effect of clustering of $\ _2$ on $\mathtt{P_c}$, we plot $\mathtt{P_c}$ for a fixed coverage threshold ($\ = 0$ dB) versus $\ _2$ in Fig. 4.7b. Note that neither Type 1 nor Type 2 users have any spatial coupling with the BS locations of $\ _2$. Thus, from Fig 4.7, we can conclude that the BS clustering has a detrimental effect on coverage if the user distribution has no spatial coupling with the BS distribution.

4.5 Summary

In this chapter, we developed an analytical framework for evaluating the coverage probability of a typical user in a K-tier HetNet where the locations of a fraction of BS tiers are modeled as PCPs and the rest are modeled as PPPs. This work, along with our previous work [79] (focused on max-SINR based association), provides a complete characterization of downlink coverage probability in the unified HetNet model, which is an important generalization of the well-known baseline PPP-based model. To be consistent with 3GPP HetNet models, we considered two types of user distribution: users that are placed independently of the BS locations (Type 1 users), and users whose locations are spatially coupled with the BS locations (Type 2 users). We captured this spatial coupling between the locations of Type 2 users and BSs by modeling BS and user locations as two PCPs sharing the same cluster centers. Our numerical results concretely reveal the implication of spatial coupling of users and BS locations on coverage, such as Type 2 users experience better coverage than the Type 1 users. We also found that denser BS clusters improve the coverage for Type 2

4.5. Summary

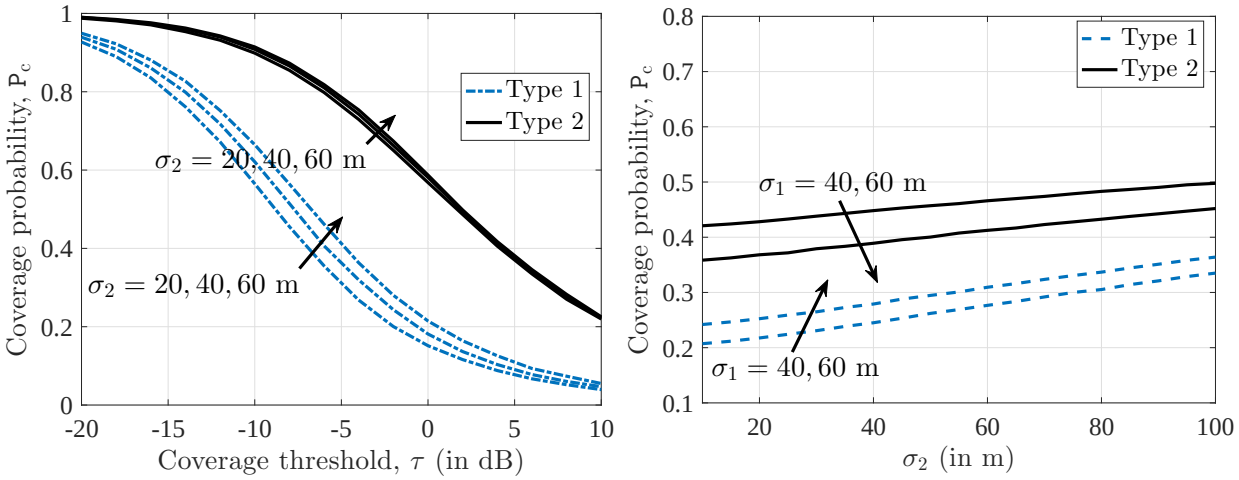

(a) $\mathrm{P_c}$ for different σ_2 for fixed σ_1 ($\sigma_1 = 20$) (b) $\mathrm{P_c}$ for different σ_2 for fixed σ_1 ($\sigma_1 = 0$ dB)

Figure 4.7: Effect of clutering of the BSs in σ_2 on coverage ($\alpha = 4$, $P_2 = 10^3 P_1$, $\lambda_{p_1} = 25$ km^{-2}, $\lambda_{p_2} = 1$ km^{-2}, $m_1 = 4$, $m_2 = 10$).

users, but diminishes the coverage for Type 1 users. While BS densification is mostly assumed to improve coverage, our results uncover a few special cases where addition of BS tiers may not necessarily improve coverage. For instance, for Type 2 users who are already spatially coupled with one BS tier, addition of BSs whose locations are not coupled with the locations of this BS tier will actually diminish their coverage.

5

SIR Meta Distribution in the General HetNet Model

5.1 Introduction

The last few years have seen two major enhancements in the baseline approach to the modeling and analysis of cellular networks using stochastic geometry. (i) *Enhancements in the model:* While the baseline network models relied on homogeneous point processPs to model the spatial distribution of the BSs and users [32], the recent efforts have focused on using more sophisticated point processes to capture the spatial couplings between the locations of the BSs and users. A key set of works in this direction is based on the PCPs which along with PPPs result in a more general HetNet model [93] with the PPP-based baseline network model being its special case. (ii) *Enhancements in the metrics:* The conventional analyses of HetNets using stochastic geometry have focused on the coverage probability which is the complementary cumulative distribution function (CCDF) of the signal-to-interference-and-noise-ratio (SINR). While coverage is a useful *first-order* metric, it does not provide any information on the variation of SINR over the network. To obtain a more fine-gained information on the SINR performance of the network, it is important to characterize the meta distribution of SINR from which the SINR-coverage can be obtained as a special case [94]. While the meta distribution of SINR has been extensively studied for the *baseline PPP-based HetNet models*, this characterization for the PCP-driven general HetNet model, proposed in Chapter 4, is not known, which is the main objective of this chapter.

Prior Art. The coverage analysis of the PPP-based cellular models is fairly mature by now (see [31,32] and the references therein). The meta distribution of SIR was first studied in [94] for the Poisson bipolar and cellular networks. It was subsequently extended to the K-tier PPP-based HetNet model in [95,96]. On the modeling side, a more general HetNet model based on the combination of PPPs and PCPs was recently proposed in [79,93]. While this model yields several spatial configurations of cellular network that are of practical interest (including the baseline PPP-based model as its special case), its analytical treatment thus far has been limited to the coverage probability. In this chapter, we derive the meta distribution of the downlink SIR for this model.

Contributions. In this chapter, we consider a general K-tier HetNet model where the BSs and the user locations are modeled as either a PCP or a homogeneous PPP. For this model, we characterize the meta distribution of downlink SIR of the typical user assuming that the network is operating in an interference-limited regime and the typical user connects to the BS providing maximum received power averaged over fading. To enable the analysis, we construct an equivalent single tier cellular network by projecting the BS PPs in $\mathbb{R}^2$ on the positive half line $\mathbb{R}^+$ that will have the same distribution of SIR as the original 2-D K-tier network. Although the equivalence of the analyses using this single tier network in $\mathbb{R}^+$ and the K-tier HetNet in $\mathbb{R}^2$ is quite well-known for the PPP-based model (see [36]), this letter makes the first attempt to develop this approach for the new PCP-based HetNet models. While this alternate analytical framework for the general HetNet model is novel in its own right, we use this framework to derive the exact analytical expressions of the b-th moment of the conditional success probability for the typical user under Rayleigh fading. The exact expression of the meta distribution being computationally infeasible, we use the b-th moments to provide an accurate beta approximation of the CCDF of the meta distribution.

5.2 System model

We model a HetNet as a K-tier cellular network in which BSs in the i-tier are distributed as a point process $\{x_g$ $_i$ $\mathbb{R}^2$ and transmit with power P_i, which is assumed to be fixed for all the BSs in $_i$. The point process $_i$ is either a homogenous PPP with intensity $_i$ or a PCP. We denote the index sets of the BS tiers being modeled as PPP and PCP by K_1 and K_2, respectively with $jK_1j + jK_2j = K$. While PPP, used as a baseline spatial model for cellular networks [32] needs no introduction, we define PCP for completeness as follows.

Definition 5.1. A PCP $_i(\ _{p_i}; m_i; f_i)$ for $i \ 2 \ K_2$ is defined as:

$$_i(\ _{p_i}; m_i; f_i) = \bigcup_{z2 \ _{p_i}} z + B_i^z;$$

where $_{p_i}$ is the parent PPP with intensity $_{p_i}$ and B_i^z is the offspring point process. The offspring point process is a sequence of independently and identically distributed (i.i.d.) random variables with probability density function (PDF) $f_i(s)$. The number of points in B_i^z is Poisson distributed with mean m_i.

We further assume that the offspring points are isotropically distributed around the cluster center. Thus the joint PDF of the radial coordinates of the offspring points with respect to the cluster center is denoted as: $f_i(s; \ _s) = f_{i(1)}(s)\frac{1}{2}$. That said, the PDF of the distance of a point of $_i$ from the origin given its cluster center at $z \ 2 \ _{p_i}$ is given by: $f_{d_i}(rjz) = f_{d_i}(rjz)$, where $kzk = z$. For the numerical results, we choose a special case of PCP, known as Thomas cluster process (TCP) where the offspring points in B^z are distributed normally around the origin, i.e., $f_i(s) = \frac{1}{\ _i^2} \exp \ \frac{ksk^2}{2 \ _i^2}$: Here $_i^2$ is the cluster

variance. When $_i$ is a TCP, the conditional distance distribution given $kzk = z$ is Rician with PDF:

$$f_{d_i}(xjz) = \frac{x}{\frac{2}{i}} e^{\frac{x^2+z^2}{2\frac{2}{i}}} I_0\left(\frac{xz}{\frac{2}{i}}\right) \quad ; x; z \quad 0; i \; 2 \; K_2; \tag{5.1}$$

where $I_0(\,)$ is the modified Bessel function of the first kind with order zero. We now focus on the user point process which is denoted as $_u$. We consider two types of users in the network:

- Type 1 (independent user and BS PPs): $_u$ follows a stationary distribution independent of the BS PPs.
- Type 2 (coupled user and BS PPs): $_u$ is a PCP with the same parent point process as that of $_q$ for some $q \; 2 \; K_2$ with cluster variance $\frac{2}{q}$.

We now focus on the typical user in this network. Since the network is stationary, we can assume that the typical user is located at the origin. It should be noted that the selection of the typical user in Type 2 implies the selection of a cluster of $_q$ as well. We denote the center of this BS cluster by $\mathbf{z}_0$. As a consequence, $_q$ is always conditioned on having a cluster $\mathbf{z}_0 + B_q^{\mathbf{z}_0}$. Thus the typical user perceives the palm version of $_q$, which, by Slivnyak's theorem [13] is equivalent to $_q \; [\; \mathbf{z}_0 + B_q^{\mathbf{z}_0}$ where $_q$ and $\mathbf{z}_0 + B_q^{\mathbf{z}_0}$ are independent. For Type 1 users, this construction does not arise since the selection of the typical user does not impose any restriction on the BS distributions. In order to unify the analyses of Type 1 and Type 2 users, we define $_0$ as a set of BSs whose locations are coupled with that of the typical user as follows:

$$_0 = \begin{cases} ?; & \text{Type } 1; \\ \mathbf{z}_0 + B_q^{\mathbf{z}_0}; & \text{Type } 2: \end{cases} \tag{5.2}$$

The BS point process perceived by the typical user can be defined as the superposition of $K + 1$ BS PPs: $= [_{i2K} \; _i$, where $K = K_1 \; [\; K_2 \; [\; f0g$. The downlink SIR of the typical user is denoted as:

$$\text{SIR} = \frac{P_{i2K} \; P_k h_{\mathbf{x}} \; k\mathbf{x} \; k}{P_{\mathbf{x}2 \; _i nf\mathbf{x} \; g} P_i h_{\mathbf{x}} k\mathbf{x}k}; \tag{5.3}$$

where $fh_{\mathbf{x}}g$ is an i.i.d. sequence of random variables where $h_{\mathbf{x}}$ is the fading coefficient associated with the link between the typical user and the BS at $\mathbf{x}$. We assume Rayleigh fading i.e. $h_{\mathbf{x}} \quad \exp(1)$ and > 2 is the path loss exponent. Here $k\mathbf{x} \; k$ is the location of the serving BS which is the BS that provides the maximum received power averaged over fading. Thus

$$\mathbf{x} \; = \arg \max_{\mathbf{x}2f\mathbf{x}_k g} P_k k\mathbf{x}k \quad ; \tag{5.4}$$

where $\mathbf{x}_k = \arg\max_{x \in \Phi_k} P_k \|x\|^{-\alpha}$ is the location of the candidate serving BS in Φ_k. In this letter, we are interested in a fine-grained analysis of SIR in terms of its meta distribution which is defined as follows.

Definition 5.2. The meta distribution of SIR is the CCDF of the conditional success probability $P_s(\tau) \triangleq \mathrm{P}(\mathrm{SIR} > \tau \mid \Phi)$, i.e.,

$$F(\tau, \lambda) = \mathrm{P}[P_s(\tau) > \lambda], \quad \tau \in \mathbb{R}^+, \quad \lambda \in (0, 1]. \tag{5.5}$$

Due to the ergodicity of Φ, $F(\tau, \lambda)$ can be interpreted as the fraction of links in each realization of Φ that have an SIR greater than τ with probability at least λ. By this definition, the standard coverage probability [93] is the mean of $P_s(\tau)$ obtained by integrating (5.5) over $\lambda \in [0, 1]$.

5.3 Meta distribution of SIR

In this section, we will construct the equivalent single tier representation of the $K+1$ tier network defined in Section 9.4.1 by projecting $\mathbb{R}^2$ on $\mathbb{R}^+$. For a PPP-based model, the equivalent network in $\mathbb{R}^+$ remains analytically tractable [36] because of the application of the mapping theorem [13], which is stated as follows.

Theorem 5.3. *If Φ is a PPP in $\mathbb{R}^d$ with intensity $\Lambda(x)$ and $f : \mathbb{R}^d \mapsto \mathbb{R}^s$ is a measurable map with $\Lambda_{\mathrm{R}}(f^{-1}\{y\}) = 0, \forall y \in \mathbb{R}^s$, then $f(\Phi) = \bigcup_{x \in \Phi} f(x)$ is a PPP with intensity measure $\tilde{\Lambda}(B') = \int_{f^{-1}(B')} \Lambda(x)\mathrm{d}x$, for all compact $B' \in \mathbb{R}^s$.*

Following this Theorem, since $f\{z\} = \|z\|^{\alpha}$ $\mathbb{R}^2$ $(\forall i \in K_2)$ is a homogeneous PPP with intensity $\pi\lambda_i$, then $\tilde{\Lambda}_{\mathrm{p}_i}(\cdot)$, $\{\|x\|^{\alpha}\}$ is an inhomogeneous PPP in $\mathbb{R}^+$ with intensity and density:

$$\tilde{\Lambda}_{\mathrm{p}_i}(z) = 2\pi\lambda_i z; \quad \tilde{\lambda}_{\mathrm{p}_i}(z) = \pi\lambda_i z^2; z > 0; \tag{5.6}$$

respectively. Since Theorem 5.3 does not hold when Φ_i $(i \in K_2)$ is PCP, the projection of Φ_i on $\mathbb{R}^+$ cannot be handled on similar lines of [36]. The key enabler of our analysis is the following property of PCP which allows the application of Theorem 5.3 to Φ_i for $i \in K_2$.

Lemma 5.4. *If $\Phi_i \triangleq \{x\} \subset \mathbb{R}^2$ is a PCP, then the sequence Φ_i, $\{\|x\|\} \subset \mathbb{R}^+$ conditioned on $\tilde{\Lambda}_{\mathrm{p}_i}$ is an inhomogeneous PPP with density and intensity:*

$$\Lambda_i(x|\tilde{\Lambda}_{\mathrm{p}_i}) = m_i \sum_{z \in \tilde{\Lambda}_{\mathrm{p}_i}} F_{\mathrm{d}_i}(x|z); x > 0; \quad \forall i \in K_2;$$
$$\lambda_i(x|\tilde{\Lambda}_{\mathrm{p}_i}) = m_i \sum_{z \in \tilde{\Lambda}_{\mathrm{p}_i}} f_{\mathrm{d}_i}(x|z). \tag{5.7}$$

Proof. See [93, Proposition 1]. □

Following the same argument, for Type 2 users, $\tilde{\Phi}_0 = \{x \in \Phi_0 : x \notin b(z_0, \|z_0\|)\}$ is also a PPP conditioned on z_0 with intensity $\lambda_0 f_{d_0}(x|z_0) \, \mathbb{A}(b(z_0,\|z_0\|)) + \lambda_q f_{d_q}(x|z_0)$. Hence, we begin our analysis by first conditioning on the locations of the points in every parent PPP, i.e., $\tilde{\Phi}_{p_i}$, $\forall i \in \mathcal{K}_2^0 \setminus \mathcal{K}_1, \mathcal{K}_2 \subset \{0\}$. Following Lemma 5.4, we have a sequence of BS PPPs $\{\tilde{\Phi}_i; i \in \mathcal{K}_2^0\}$ in $\mathbb{R}^+$ conditioned on $\bigcup_{i \in \mathcal{K}_2^0} \tilde{\Phi}_{p_i}$.

Let us define $\tilde{\Phi}_i = \{P_i^{-1} x^{\alpha} : \forall x \in \Phi_i\}$ as the projection of Φ_i $(\forall i \in \mathcal{K}_1 \cup \mathcal{K}_2^0)$ on $\mathbb{R}^+$. For $i \in \mathcal{K}_1$, using Theorem 5.3, the density of this 1-D inhomogeneous PPP $\tilde{\Phi}_i$ is

$$\tilde{\lambda}_i(x) = \int_0^{2} \int_0^{(xP_i)^{1/\alpha}} \lambda_i x'^{\alpha} dx' d\theta = \pi \lambda_i (xP_i)^{\frac{2}{\alpha}}.$$

For $\Phi_i (i \in \mathcal{K}_2^0)$ conditioned on $\tilde{\Phi}_{p_i}$, the density of $\tilde{\Phi}_i = \{P_i^{-1} x^{\alpha} : \forall x \in \Phi_i\}$ is: $\tilde{\lambda}_i(x|\tilde{\Phi}_{p_i}) =$

$$\int_0^{(xP_i)^{\frac{1}{\alpha}}} m_i \sum_{z \in \tilde{\Phi}_{p_i}} f_{d_i}(x'|z) dx' = m_i \sum_{z \in \tilde{\Phi}_{p_i}} F_{d_i}\left((xP_i)^{\frac{1}{\alpha}}|z\right).$$

Using the superposition theorem for PPP [13], the density function of the 1-D PPP $\tilde{\Phi} = \bigcup_{i \in \mathcal{K}} \tilde{\Phi}_i$, which is the projection of the $K+1$ tier HetNet Φ, can be obtained as follows: $\tilde{\lambda}(x|\bigcup_{i \in \mathcal{K}_2^0} \tilde{\Phi}_{p_i}) =$

$$\begin{aligned} &= \sum_{i \in \mathcal{K}_1} \lambda_i(x) + \sum_{i \in \mathcal{K}_2^0} \lambda_i(x|\tilde{\Phi}_{p_i}) \\ &= \sum_{i \in \mathcal{K}_1} \pi \lambda_i (xP_i)^{\frac{2}{\alpha}} + \sum_{i \in \mathcal{K}_2^0} m_i \sum_{z \in \tilde{\Phi}_{p_i}} F_{d_i}\left((xP_i)^{\frac{1}{\alpha}}|z\right); \end{aligned} \tag{5.8}$$

and intensity: $\tilde{\lambda}(x|\bigcup_{i \in \mathcal{K}_2^0} \tilde{\Phi}_{p_i}) = \frac{d}{dx} \tilde{\lambda}(x|\bigcup_{i \in \mathcal{K}_2^0} \Phi_{p_i}) =$

$$\sum_{i \in \mathcal{K}_1} 2\pi \lambda_i P_i^{\frac{2}{\alpha}} x^{\frac{2}{\alpha}-1} + \sum_{i \in \mathcal{K}_2^0} m_i \sum_{z \in \tilde{\Phi}_{p_i}} P_i^{\frac{1}{\alpha}} \frac{1}{\alpha} x^{\frac{1}{\alpha}-1} f_{d_i}\left((xP_i)^{\frac{1}{\alpha}}|z\right). \tag{5.9}$$

We are now in a position to define SIR of the typical user as:

$$\mathrm{SIR} = \frac{h_{x^*} \|x^*\|^{-\alpha}}{\sum_{x \in \tilde{\Phi}; x > x^*} h_x \|x\|^{-\alpha}}, \tag{5.10}$$

where $x^* = \arg\min_{x \in \tilde{\Phi}} \|x\|$ is the point in $\tilde{\Phi}$ closest to the origin. The equivalence of the SIR-s expressed in terms of Φ and $\tilde{\Phi}$ is formally stated in the following proposition.

Proposition 5.5. *The* SIR *of a typical user in the $K+1$-tier HetNet $\Phi \subset \mathbb{R}^2$ with the BSs of the i-th tier transmitting at power P_i and* max-power based user association *(defined in*

(5.3)) *has the same distribution as that of a single tier 1-D network* $\tilde{\Phi} \subset \mathbb{R}^+$ *with nearest BS association, where* $\tilde{\Phi}$ *is an inhomogeneous PPP with intensity* $\tilde{\Phi}(x) = \sum_{i \in K_2 \setminus \{0\}} \tilde{p}_i$*), or equivalently, density* $\tilde{\Phi}(x) = \sum_{i \in K_2 \setminus \{0\}} \tilde{p}_i$ *with all BSs transmitting at unit power. Here* $\tilde{p}_0 = ?$ *for* Type *1 users and* $\tilde{p}_0 = z_0 \quad f_{d_q}(z_0|0)$ *for* Type *2 users.*

The distribution of $\tilde{\Phi}$ being unknown, the main contribution of the paper is to use the fact that conditional version of $\tilde{\Phi}$ given $\sum_{i \in K_2^0} \tilde{p}_i$ is a PPP. We will then leverage the tractability of the PPP under the conditioning of the parent PPs and decondition with respect to $\sum_{i \in K_2^0} \tilde{p}_i$ at the last step of the analysis. Since $\tilde{\Phi} \setminus \sum_{i \in K_2^0} \tilde{p}_i$ is a PPP, the PDF of x is given by [13]:

$$f_x(x) = \quad (x) \exp \qquad (x) \; ; x > 0. \tag{5.11}$$

The direct calculation of the meta distributions being infeasible even for the baseline PPP-based models [95], we first derive the expressions of the b-th order moments of $P_s(\ )$: $M_b(\ ) \ , \ \mathsf{E}[P_s(\ )^b]$. Note that the coverage probability of the typical user in this setting, which was studied in our previous work [93], is a special case of this result and can be obtained directly by setting $b = 1$.

Theorem 5.6. *The* b*-th moment of* $P_s(\ )$*,* $b \in \mathbb{C}$ *can be expressed as:* $M_b(\ ) =$

$$\sum_{i \in K_1} \frac{2}{} P_i^{\frac{2}{}} \int_0^{\infty} Q(r) \prod_{j \in K_2^0} PG_{\tilde{\Phi}_{p_j}}(r) r^{\frac{2}{} - 1} dr + \sum_{i \in K_2^0 \setminus 0} \int_0^{\infty} Q(r) \prod_{j \in K_2^0 \setminus \{i\}} PG_{\tilde{\Phi}_{p_j}}(r) SP_{\tilde{\Phi}_{p_i}}(r) dr; \tag{5.12}$$

where $Q(r) =$

$$\exp \qquad r^{\frac{2}{}} \sum_{j \in K_1} {}_j P_j^{\frac{2}{}} \, {}_2F_1 \quad b; \quad \frac{2}{}; \frac{2+}{}; \qquad ; \tag{5.13}$$

where ${}_2F_1$ *is the hypergeometric function and*

$$PG_{\tilde{\Phi}_{p_j}}(r) := \mathsf{E} \prod_{z \in \tilde{\Phi}_{p_j}} g_j(r; z) \; ; \tag{5.14a}$$

$$\text{and } SP_{\tilde{\Phi}_{p_i}}(r) := \mathsf{E} \sum_{z \in \tilde{\Phi}_{p_i}} {}_i(r; z) \prod_{z^0 \in \tilde{\Phi}_{p_i}} g_i(r; z^0) \tag{5.14b}$$

are the probability generating functional (PGFL) and sum-product functional (SPFL) of $\tilde{\Phi}_{p_j}$ *and* $\tilde{\Phi}_{p_i}$*, respectively* $(i; j \in K_2^0)$ *with*

$$g_j(r; z) = \exp \qquad m_j P_j^{\frac{1}{}} \frac{1}{} - r^{\frac{1}{}} \int_r^{\infty} u(r; x) f_{d_j}(xP_j)^{\frac{1}{}} jz \; dx$$

$$m_j F_{\mathrm{d}_j}\left(rP_j\right)^{\frac{1}{}} jz \quad ; \tag{5.15a}$$

$$_i(r;z) = m_i P_i^{\frac{1}{}} \frac{1}{-} r^{\frac{1}{}} {}^{1} f_{\mathrm{d}_i}\left(rP_i\right)^{\frac{1}{}} jz \ ; \tag{5.15b}$$

where $u(r;x) = (1 \quad (1 + \quad r=x)^{\ b})$*:*

Proof. From (5.10), $P_s(\ ) = \mathrm{P}\ h_{\ast} > \ \ast^{\ \mathrm{P}_{x2\tilde{};x>\ast}\ h_x x^{\ 1}} \overset{(a)}{=}$

$$\mathrm{E}\ \exp\left(\ \ast \sum_{\substack{x2\tilde{};\\ x>\ast}} h_x x^{\ 1}\right) = \mathrm{E} \prod_{x2\tilde{};x>\ast} \frac{1}{1 + \ \ast x^{\ 1}} \ :$$

Here (a) follows from the CCDF of exponential distribution and the last step follows from the fact that $fh_x g$ is a sequence of i.i.d. exponential random variables. Now, $P_s(\ )^b j\left[_{i2K_2\left[f0g\right.}\right.\tilde{}_{\mathrm{p}_i} = \mathrm{E}\left(\prod_{x2\tilde{};x>\ast} \frac{1}{1+\frac{\ast}{x}^{\ b}} \prod_{i2K_2^{\emptyset}} \tilde{}_{\mathrm{p}_i}\right) \overset{(a)}{=}$

$$\exp\left(\ast \underbrace{\int_{r}^{1} \left(1 - \left(1 + \frac{\ast}{x}\right)^{\ b}\right) \tilde{}(xj\left[_{i2K_2^{\emptyset}}\right.\tilde{}_{\mathrm{p}_i})\mathrm{d}x}_{u(\ast\ ;x)}\right)$$

$$\overset{(b)}{=} \exp\left(\int_{0}^{r} u(r;x)\tilde{}(xj\left[_{i2K_2^{\emptyset}}\right.\tilde{}_{\mathrm{p}_i})\mathrm{d}x\right) \exp\left(\int_{r}^{1} \tilde{}(rj\left[_{i2K_2^{\emptyset}}\right.\tilde{}_{\mathrm{p}_i}) \ \tilde{}(rj\left[_{i2K_2^{\emptyset}}\right.\tilde{}_{\mathrm{p}_i})\mathrm{d}r\right.$$

$$= \exp\left(\int_{0}^{r} u(r;x)\tilde{}(xj\left[_{i2K_2^{\emptyset}}\right.\tilde{}_{\mathrm{p}_i})\mathrm{d}x\right) \quad \tilde{}(rj\left[_{i2K_2^{\emptyset}}\right.\tilde{}_{\mathrm{p}_i})$$

$$\sum_{i2K_1} {}_{i}\frac{2}{-} P_i^{\frac{2}{}} r^{\frac{2}{}\ 1} + \sum_{i2K_2^{\emptyset}} m_i \int_{z2\tilde{}_{\mathrm{p}_i}} P_i^{\frac{1}{}} \frac{1}{-} r^{\frac{1}{}\ 1} f_{\mathrm{d}_i}\left(rP_i\right)^{\frac{1}{}} jz \quad \mathrm{d}r$$

$$T_1\left[_{i2K_2^{\emptyset}}\right.\tilde{}_{\mathrm{p}_i} + T_2\left[_{i2K_2^{\emptyset}}\right.\tilde{}_{\mathrm{p}_i} \ ;$$

where

$$T_1\left[_{i2K_2^{\emptyset}}\right.\tilde{}_{\mathrm{p}_i} = \sum_{i2K_1} {}_{i}\frac{2}{-} P_i^{\frac{2}{}} \int_{0}^{r} \exp\left(\int_{r}^{1} u(r;x)\tilde{}(xj\left[_{i2K_2^{\emptyset}}\right.\tilde{}_{\mathrm{p}_i})\mathrm{d}x\right) \tilde{}(rj\left[_{i2K_2^{\emptyset}}\right.\tilde{}_{\mathrm{p}_i})$$

$$r^{\frac{2}{}\ 1}\mathrm{d}r;$$

$$T_2\left[_{i2K_2^{\emptyset}}\right.\tilde{}_{\mathrm{p}_i} = \sum_{i2K_2^{\emptyset}} m_i \int_{0}^{r} \sum_{z2\tilde{}_{\mathrm{p}_i}} P_i^{\frac{1}{}} \frac{1}{-} r^{\frac{1}{}\ 1} f_{\mathrm{d}_i}\left(rP_i\right)^{\frac{1}{}} jz$$

$$\exp\left(-\int_r^{\infty} u(r,x)\tilde{}(x\,|\,[_{i\in K_2^0}\tilde{}\,\mathrm{p}_i)\mathrm{d}x \;\; \tilde{}(r\,|\,[_{i\in K_2^0}\tilde{}\,\mathrm{p}_i)\,\mathrm{d}r\right).$$

Here (a) follows from the PGFL of PPP (see Lemma 5.7), (b) is obtained by deconditioning over x whose PDF is given by (5.11). We are left with deconditioning T_1 and T_2 w.r.t. the distributions of the parent PPs for $i \in K_2$ and z_0 for Type 2 users. We now derive the expressions of $\mathrm{E}[T_1 \;\; [_{i\in K_2^0}\tilde{}\,\mathrm{p}_i}\,]$ and $\mathrm{E}[T_2 \;\; [_{i\in K_2^0}\tilde{}\,\mathrm{p}_i}\,]$ as follows: $\mathrm{E}[T_1 \;\; [_{i\in K_2^0}\tilde{}\,\mathrm{p}_i}\,] =$

$$\sum_{i\in K_1} \frac{2}{\lambda_i}P_i^{\frac{2}{\alpha}} \int_0^{\infty} \mathrm{E}\left[\exp\left(-\int_r^{\infty} u(r,x)\tilde{}(x\,|\,[_{i\in K_2^0}\tilde{}\,\mathrm{p}_i)\mathrm{d}x\right) \tilde{}(r\,|\,[_{i\in K_2^0}\tilde{}\,\mathrm{p}_i)\right] r^{\frac{2}{\alpha}-1}\mathrm{d}r = \sum_{i\in K_1} \frac{2}{\lambda_i}P_i^{\frac{2}{\alpha}} r^{\frac{2}{\alpha}-1}$$

$$\int_0^{\infty} \prod_{j\in K_1} \exp\left(-\underbrace{\int_r^{\infty} u(r,x)\,\frac{2}{\lambda_j}P_j^{\frac{2}{\alpha}} x^{\frac{2}{\alpha}-1}\mathrm{d}x}_{Q(r)}\right) \lambda_j (rP_j)^{\frac{2}{\alpha}}$$

$$\prod_{j\in K_2^0} \mathrm{E}_{z\in[_{\mathrm{p}_j}} \left[\exp\left(-\underbrace{\int_r^{\infty} m_j P_j^{\frac{1}{\alpha}}\tfrac{1}{\alpha} r^{\frac{1}{\alpha}-1} u(r,x) f_{\mathrm{d}_j}\left(xP_j\right)^{\frac{1}{\alpha}} jz\,\mathrm{d}x}_{g_j(r;z)}\right) m_j F_{\mathrm{d}_j}\left(rP_j\right)^{\frac{1}{\alpha}} jz\right] \mathrm{d}r,$$

where the last step is obtained by substituting $\tilde{}$ and $\tilde{}$ with (5.8) and (5.9), respectively. Applying the same substitution, we can simplify $\mathrm{E}\left[T_2 \;\; [_{i\in K_2^0}\tilde{}\,\mathrm{p}_i}\right]$ as

$$\sum_{i\in K_2^0} \int_0^{\infty} m_i \mathrm{E}\left[\sum_{z\in[_{\mathrm{p}_i}} P_i^{\frac{1}{\alpha}}\tfrac{1}{\alpha} r^{\frac{1}{\alpha}-1} f_{\mathrm{d}_i}\left(rP_i\right)^{\frac{1}{\alpha}} jz \right.$$

$$\left. \exp\left(-\int_r^{\infty} u(r,x)\tilde{}(x\,|\,[_{i\in K_2^0}\tilde{}\,\mathrm{p}_i)\mathrm{d}x \;\; \tilde{}(r\,|\,[_{i\in K_2^0}\tilde{}\,\mathrm{p}_i)\right)\right] \mathrm{d}r$$

$$= \sum_{i\in K_2^0} \int_0^{\infty} \mathrm{E}\left[\sum_{z\in[_{\mathrm{p}_i}} m_i P_i^{\frac{1}{\alpha}}\tfrac{1}{\alpha} r^{\frac{1}{\alpha}-1} f_{\mathrm{d}_i}\left(rP_i\right)^{\frac{1}{\alpha}} jz\right]$$

$$\exp\left(-\int_r^{\infty} u(r,x)\left(\sum_{j\in K_1} \frac{2}{\lambda_j}P_j^{\frac{2}{\alpha}} x^{\frac{2}{\alpha}-1} + \sum_{j\in K_2^0}\sum_{z\in[_{\mathrm{p}_j}} m_j P_j^{\frac{1}{\alpha}}\tfrac{1}{\alpha} x^{\frac{1}{\alpha}-1} f_{\mathrm{d}_j}\left(xP_j\right)^{\frac{1}{\alpha}} jz\right)\mathrm{d}x\right)$$

$$\left. \sum_{j\in K_1} \lambda_j (rP_j)^{\frac{2}{\alpha}} + \sum_{j\in K_2^0}\sum_{z\in[_{\mathrm{p}_j}} m_j F_{\mathrm{d}_j}\left(rP_j\right)^{\frac{1}{\alpha}} jz \right) \mathrm{d}r$$

$$= \sum_{i\in K_2^0} \sum_{0} \prod_{j\in K_1} \exp\left(-\int_r^\infty u(r;x)\left(\lambda_j - P_j^{\frac{2}{\alpha}} x^{\frac{2}{\alpha}-1}\right)\mathrm{d}x - \lambda_j (rP_j)^{\frac{2}{\alpha}}\right)$$
$$\mathrm{E}\left[\sum_{z\in\tilde{\Phi}_{p_i}} m_i P_i^{\frac{1}{\alpha}} \frac{1}{r^{\frac{1}{\alpha}-1}} f_{\mathrm{d}_i}\left((rP_i)^{\frac{1}{\alpha}}, z\right)\right]$$
$$\prod_{j\in K_2^0} \prod_{z\in\tilde{\Phi}_{p_j}} \exp\left(-\int_r^\infty u(r;x) m_j P_j \frac{1}{x^{\frac{1}{\alpha}-1}} f_{\mathrm{d}_j}\left((xP_j)^{\frac{1}{\alpha}}, z\right)\mathrm{d}x - m_j F_{\mathrm{d}_j}\left((rP_j)^{\frac{1}{\alpha}}, z\right)\mathrm{d}r\right)$$
$$= \sum_{i\in K_2^0} \sum_{0} Q(r) \prod_{j\in K_2^0 \setminus \{i\}} PG_{\tilde{\Phi}_{p_j}}(r) \mathrm{E}\left[\sum_{z\in\tilde{\Phi}_{p_i}} \underbrace{P_i^{\frac{1}{\alpha}} \frac{1}{r^{\frac{1}{\alpha}-1}} m_i f_{\mathrm{d}_i}\left((rP_i)^{\frac{1}{\alpha}}, z\right)}_{\mathcal{I}_i(r;z)}\right]$$
$$\prod_{z\in\tilde{\Phi}_{p_i}} \exp\left(-\int_r^\infty u(r;x) m_i P_i \frac{1}{x^{\frac{1}{\alpha}-1}} f_{\mathrm{d}_i}\left((xP_i)^{\frac{1}{\alpha}}, z\right)\mathrm{d}x - m_i F_{\mathrm{d}_i}\left((rP_i)^{\frac{1}{\alpha}}, z\right)\mathrm{d}r\right).$$
$$\underbrace{\qquad\qquad\qquad\qquad\qquad\qquad\qquad\qquad\qquad\qquad}_{g_i(r;z)}$$

The expression spanning over the last two lines can be identified as $SP_{\tilde{\Phi}_{p_i}}(r)$ (see (5.14b)). In the above expressions, $Q(r)$ can be further simplified to (5.13). □

We note that $P_s(\ )$ in (5.12) is expressed in terms of the PGFL and SPFL of $\tilde{\Phi}_{p_i}$. Hence we are left with the expressions of PGFL and SPFL of $\tilde{\Phi}_{p_i}$ for $i \in K_2^0$. When $i \in K_2$, the PGFL and SPFL of $\tilde{\Phi}_{p_i}$ are known since it is a PPP [93, Lemmas 5,6]. For Type 2 users, the PGFL and SPFL of $\tilde{\Phi}_{p_0}$ can be obtained by deconditioning over z_0, i.e. $PG_{\tilde{\Phi}_{p_0}}(r) = E_{z_0}[g_0(r;z_0)]$ and $SP_{\tilde{\Phi}_{p_0}}(r) = \mathrm{E}_{z_0}[\ _0(r;z_0) g_0(r;z_0)]$. We summerize the expressions of PGFL and SPFL in the following lemmas.

Lemma 5.7. *The PGFL of $\tilde{\Phi}_{p_i}$ is given as: $PG_{\tilde{\Phi}_{p_i}}(r) =$*

$$\begin{cases} \exp\left(-\int_0^\infty 2\pi\lambda_{p_i} z (1 - g_i(r;z))\mathrm{d}z\right); & i \in K_2; \\ \int_0^\infty g_q(r;z) f_{\mathrm{d}_q}(z|0)\mathrm{d}z; & i = 0, \text{Type 2}. \end{cases} \tag{5.16}$$

Lemma 5.8. *The SPFL of $\tilde{\Phi}_{p_i}$ is given as: $SP_{\tilde{\Phi}_{p_i}}(r) =$*

$$\begin{cases} \int_0^1 2\pi\lambda_{p_i} z\ _i(r;z) g_i(r;z)\mathrm{d}z \exp\left(-\int_0^1 2\pi\lambda_{p_i} z' (1 - g_i(r;z'))\mathrm{d}z'\right); & i \in K_2; \\ \int_0^\infty {}_q(r;z) g_q(r;z) f_{\mathrm{d}_q}(z|0)\mathrm{d}z; & i = 0, \text{Type 2}. \end{cases} \tag{5.17}$$

The final expression of $M_b(\ )$ is obtained by substituting $PG_{\tilde{\ }_{p_i}}(r)$ and $SP_{\tilde{\ }_{p_i}}(r)$ given by (9.21) and (5.17) to (5.12). The accuracy of these expressions is verified with the Monte Carlo simulations in Fig. 5.1a. Note that we can also derive $M_b(\ )$ on similar lines of [93] by conditioning on the association to the BSs of the i-th tier (i 2 K). However, the single tier projection presented in this letter offers an alternate and more compact derivation of $M_b(\ )$. Further note that $M_1(\ )$ and $M_2(\ )$ for Type 1 and 2 users converge to $M_1(\ )$ and $M_2(\ )$ for the baseline PPP model (i.e. where $_i$ (for all i 2 K) and $_u$ are homogeneous PPPs) as $_2$ increases. This is because of the fact that the PCP weakly converge to PPP as the cluster size tends to infinity [79, Sec. IV-B].

5.3.1 Approximation of meta distributions

From the b-th moment of the conditional success probability, the meta distribution of SIR can be obtained by using the Gil-Pelaez theorem [97] as:

$$F(\ ;\ ) = \frac{1}{2} + \frac{1}{\ } \int_0^{Z^1} \frac{\mathrm{Im}(e^{\ jt\log\ } M_{jt}(\ ))}{t} \mathrm{d}t;$$

where $\mathrm{Im}(z)$ denotes the imaginary part of z 2 C. As it can be readily observed, the expression of the exact meta distribution is not computationally efficient since it requires integration over the imaginary moments. Hence, following the approach of [94, 98], we approximate $F(\ ;\ )$ with a beta-kernel:

$$F(\ ;\ ) \quad 1 \quad \frac{1}{B(\ _1;\ _2)} \int_0^{Z} t^{\ 1\ 1}(1 \quad t)^{\ 2\ 1}\mathrm{d}t; \tag{5.18}$$

where $B(\ ;\ )$ is the beta function and $(\ _1;\ _2)$ is given by solving the following system of equations:

$$M_1 = \frac{1}{\ _1 + \ _2} \text{ and } M_2 = \frac{\frac{2}{1}}{(\ _1 + \ _2)^2} \quad \frac{2}{\ _1(\ _1 + \ _2 + 1)} + 1 \ :$$

In Fig. 5.1b, we plot $F(\ ;\ )$ for a specific network configuration for Type 1 and Type 2 users. Clearly, (5.18) provides a reasonably tight approximation for the meta distribution of SIR for a wide range of . Further, we observe that the meta distribution of Type 2 users is greater than the baseline PPP-based model and the meta distribution of Type 1 users is less than the baseline PPP-based model. This ordering is same as the ordering observed for coverage probability (see Fig. 5.1a and [93, Sec. IV]). However, it is a stronger result than the ordering of coverage. This implies that for a given and same user density, there exists more number of Type 2 users satisfying SIR > than Type 1 users in the network.

5.4 Summary

In this chapter, we characterized the meta distribution of the downlink SIR for the typical user in the general K-tier HetNet model where the BSs are distributed as a PPP or a

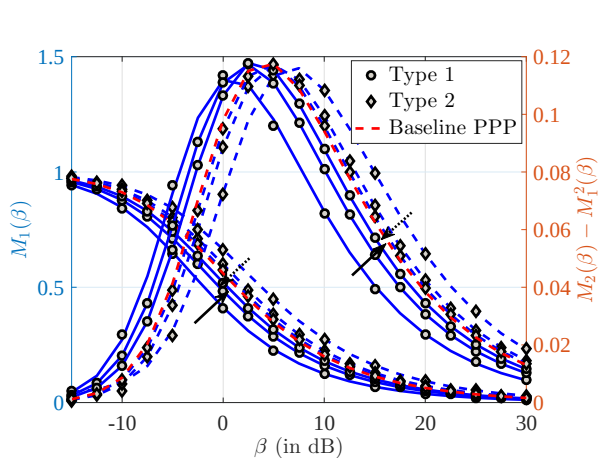

(a) Mean and variance of meta distribution.

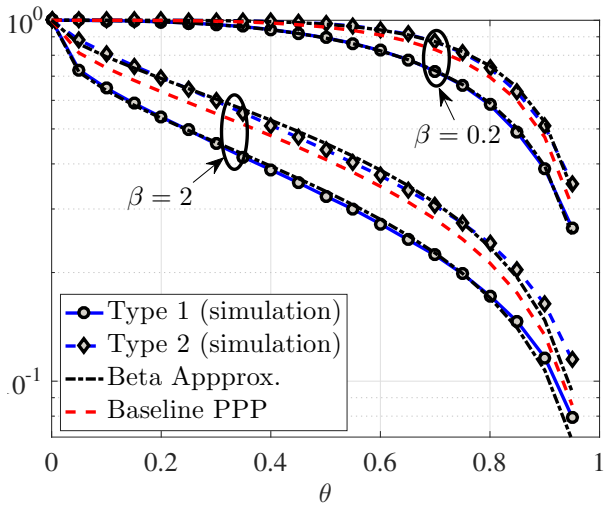

(b) Meta distribution.

Figure 5.1: Meta distribution of SIR for Type 1 and Type 2 users in a two tier network. Details of the network configuration: $K = 2$, $K_1 = \{1\}$, $K_2 = \{2\}$, $q = 2$ for Type 2, $= 4$, $P_2 = 10^2 P_1$, $_{p_2} = 2.5$ km ^{2}, $_{p_1} = 1$ km ^{2}, and $m_2 = 4$. Markers indicate the values obtained from Monte Carlo simulations. The solid and dotted arrows in Fig. 5.1a indicate the shift of the quantities with the increase in cluster size ($_2 = \{20, 40, 60\}$ m). For Fig. 5.1b, $_2 = 40$ m.

5.4. Summary

PCP. The main technical contribution is the accurate derivation of the b-th order moments of the conditional success probability. The key enabling step of the analysis is to condition on the parent point process of the BS PCPs which allows us to treat the PCPs as inhomogeneous PPPs. Under this conditioning, we obtain a sequence of BS PPPs in R^2 which are projected on R^+ to construct a single tier equivalence of the multi-tier HetNet. Using this single tier network, we present a compact derivation of the b-th order moments of the conditional success probability by applying the PGFL and SPFL of the parent PPPs. We finally use the moments of the conditional success probability to compute a beta approximation of the meta distribution of SIR.

6

Load on the Typical Poisson Voronoi Cell with Clustered User Distribution

6.1 Introduction

A vast majority of the existing literature on the analysis of cellular networks using stochastic geometry focuses on the distribution of downlink signal-to-interference-and-noise-ratio (SINR) under a variety of settings [32]. While this is important for evaluating the downlink coverage of the network, the SINR distribution by itself is not sufficient to compute the distribution of the effective downlink rate perceived by the users, which is an equally important metric. In order to derive the rate distribution of the typical user, we additionally need information about the fraction of resources allocated to that user, which in turn depends upon the load (number of users served) on its serving BS [24]. Naturally, load characterization further depends upon the user distribution. While this problem is well-studied for the canonical PPP-based models (where both user and BS locations are modeled as independent PPPs), the same is not true for the recently developed PCP-based models for cellular networks [79]. As a step towards this direction, we characterize load on the typical cell of a PCP-based cellular network model in which the BSs follow a PPP while the users are distributed as an independent PCP.

Prior Art. The distributions of the load on the typical cell and the zero cell (i.e. the cell containing the origin) for the cannonical PPP-based models are well-known in the literature [24, 57]. However, the analysis becomes intractable for the *non-PPP* models, i.e. when the PPP assumption on either of the distributions of BSs or users is relaxed. In [99], the authors characterize the load distributions for any general distribution for BSs which is asymptotically exact under strong shadowing. In [100], the authors derive the load distributions assuming that the BSs are distributed as PPP and the users are distributed as a Cox process driven by a Poisson line process. While these works evince the tractability of load distributions for the non-PPP models in general, the analyses do not simply extend to the PCP-based models developed in [79]. The current paper presents the first work towards the characterization of load distributions for the PCP-based models.

Contributions. We consider a cellular network where the BSs are distributed as a homogeneous PPP and the users are distributed as an independent PCP. For this network, we derive the first two moments (or equivalently the mean and variance) of the typical *cell load*, which is defined as the number of points of PCP falling in the typical cell of the Poisson Voronoi (PV) tessellation generated by the BS PPP. The key enabling step is the derivation of the n^{th} moment of typical cell load for a general user point process (PP), whose exact expression is derived in Theorem 6.7. As a special case, we evaluate the first and second moments of cell load when the user PP is a PCP (Corollary 6.8). To the best of our knowledge, this is the first result on the variance of the cell load for a PCP-based cellular model. While these exact results for the moments are key contributions by themselves, it is unfortunately not very computationally efficient to evaluate these expressions for $n > 2$. For this reason, we provide an alternate formulation of the load PGF by approximating the typical cell as a circle with the same area. We then obtain an easy-to-use expression for the PMF of the typical cell load by inverting the PGF. After verifying the accuracy of the analysis with Monte Carlo simulations, we consider the downlink of the cellular network as a case study and apply this PMF to compute the rate coverage of a randomly chosen user in the typical cell.

Notations. (i) We denote a PP and its associated counting measure by the same notation, i.e., if denotes a PP, then (A) denotes the number of points of falling in $A \in \mathcal{B}(\mathbb{R}^2)$, where $\mathcal{B}(\mathbb{R}^2)$ denotes the Borel- algebra in $\mathbb{R}^2$, (ii) $j \ j$ denotes the Lebesgue measure in $\mathbb{R}^2$ (i.e., for a set B $\mathbb{R}^2$, jBj denotes the area of B), (iii) $b(\mathbf{x}; R)$ denotes a disc of radius R centered at $\mathbf{x} \in \mathbb{R}^2$, (iv) the position vector of a point in $\mathbb{R}^2$ is denoted as boldface (such as $\mathbf{x}$) with magnitude $k\mathbf{x}k$ x, (v) $\mathbf{1}(\ )$ denotes the indicator function, and (vi) $A_u(R_1; R_2; r)$ and $A_i(R_1; R_2; r)$ denote the areas of union and intersection of two discs of radii R_1 and R_2, whose centers are separated by a distance r.

6.2 System model

We consider a cellular network where the BSs are distributed as a homogeneous PPP $_b$ $\mathbb{R}^2$ with density $_b$. The users are assumed to be distributed as another independent PP $_u$. If each user associates with the BS which provides maximum average power, the association cells of the network form the PV tessellation generated by $_b$ [32]. Therefore, the association cell of a BS in $_b$ is defined as: $C(\mathbf{x}) =$

$$f\mathbf{y} \in \mathbb{R}^2 : k\mathbf{y} \quad \mathbf{x}k \quad k\mathbf{y} \quad \mathbf{t}k; \forall \mathbf{t} \in \quad gj\mathbf{x} \in \quad _b: \tag{6.1}$$

Thus $_u(C(\mathbf{x}))$ is the number of users associated with the BS at $\mathbf{x}$, equivalently the load on the BS at $\mathbf{x}$ [24]. We are interested in characterizing the distribution of the load on the typical BS (termed typical cell load). Following Slivnyak's theorem, the typical BS can be placed at the origin [13]. Thus, the typical cell load can be denoted as $_u(C(\mathbf{0}))$ $_{u_0}$. When $_u$ is a homogeneous PPP, the PMF of $_{u_0}$ is well-known in the literature [24]. However, not much is known if the user distribution is not a PPP. In this chapter, we derive the distribution of

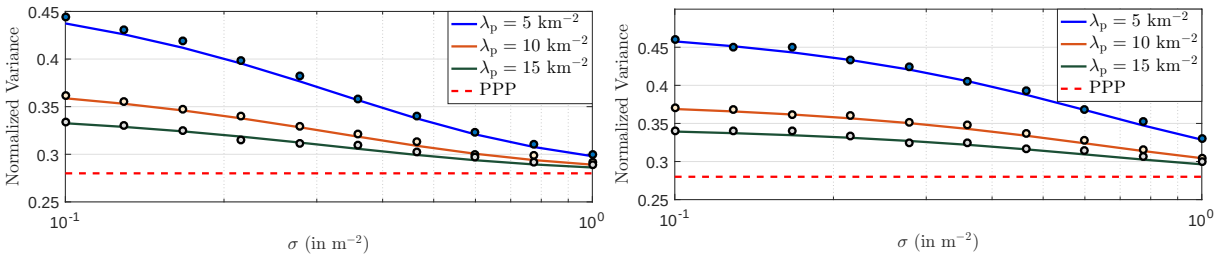

(a) $_u$ is TCP. (b) $_u$ is MCP.

Figure 6.1: Normalized variance of $_{u_0}$ ($_b = 1$ km ^{2}). The markers denote the values obtained by Monte Carlo simulation.

$_{u_0}$ when $_u$ is distributed as a PCP independent of $_b$. In the rest of this Section, we will introduce the fundamentals of PCP.

Definition 6.1 (PCP)**.** A PCP $_u(_p; m; f)$ is defined as $_u = \bigcup_{z2 _p} \mathbf{z} + B^z;$ where $_p$ is the parent PPP with intensity $_p$ and B^z denotes the offspring PP centered at $\mathbf{z}\ 2\ _p$. The offspring point process is defined as an independently and identically distributed (i.i.d.) sequence of random vectors $f\mathbf{s}\ 2\ B^z g$ where $\mathbf{s}$ follows a probability density function (PDF) $f(\mathbf{s})$ and $B^z(\mathbb{R}^2)$ is a Poisson random variable with mean m.

In this chapter, we focus on two well-known special cases of PCP known as the Thomas cluster process (TCP) and Matérn cluster process (MCP) which are defined as follows.

Definition 6.2 (TCP)**.** A PCP $_u (_p; m; f)$ is called a TCP if the offspring points in B^z are distributed normally around $\mathbf{z}$, i.e., $f(\mathbf{s}) = \frac{1}{2 \ _2} e^{\frac{ksk^2}{2\ 2}}$. Here ^{2} is the cluster variance.

Definition 6.3 (MCP)**.** A PCP $_u (_p; m; f)$ is called an MCP if the distribution of the offspring points in B^z is uniform within $b(\mathbf{0}; r_d)$. Hence, $f(\mathbf{s}) = f(s; \ _s) = \frac{2s}{R^2}\ \frac{1}{2}; 0\ \ s\ R; 0 < \ _s\ \ 2\ :$

If the offspring points are isotropically distributed around the cluster center i.e., the radial coordinates of the offspring points with respect to the cluster center have the joint PDF $f(s; \ _s) = f_{(1)}(s)\frac{1}{2}$, where $f_{(1)}( )$ is the marginal PDF of the radial coordinate, then the PDF of the distance of a point of from the origin given its cluster center at $\mathbf{z}\ 2\ _p$ is given by: $f_d(rjz) = f_d(rjz)$, i.e. the conditional distance distribution depends only on the magnitude of $\mathbf{z}$. We now provide the conditional distance distributions of TCP and MCP. When is a TCP, the conditional distance distribution is Rician with PDF:

$$f_d(xjz) = \frac{x}{\ _2} \exp\ \ \frac{x^2 + z^2}{2\ ^2}\ \ I_0\ \ \frac{xz}{\ _2}\ ; x; z\ \ 0; \tag{6.2}$$

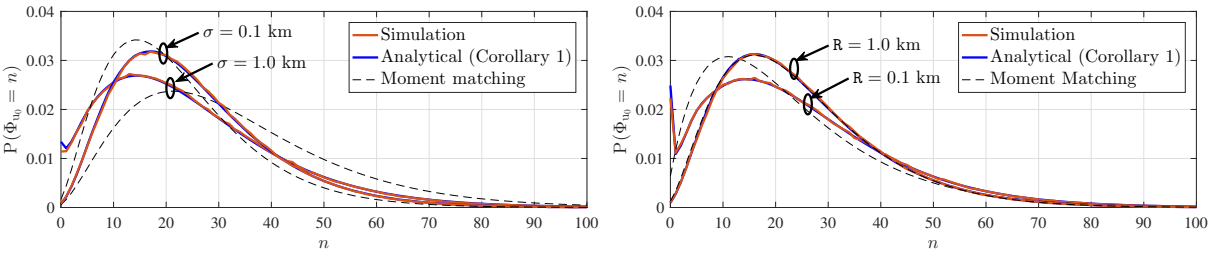

(a) $_u$ is TCP. (b) $_u$ is MCP.

Figure 6.2: Load on the typical cell: comparison of the proposed PMF and the actual PMF when $_u$ is a TCP ($_b$ = 1 km ^{2}, $_p$ = 5 km ^{2}, m = 5).

where $I_0(\,)$ is the modified Bessel function of the first kind with order zero. When $_k$ is an MCP, $f_d(xjz)$ =

$$^{(1)}(x;z) = \frac{2x}{R^2};0 \quad x \quad R \quad z;0 \quad z \quad R; \tag{6.3}$$

$$^{(2)}(x;z) = \frac{2x}{R^2}\cos^{\ 1}\frac{x^2+z^2 \quad R^2}{2xz} \;;jR \quad zj < x \quad R+z:$$

6.3 Moments of the typical cell load

In this Section, we derive the n^{th} moments of $_{u_0}$. The key enabler of the analysis is the Campbell's theorem [13], which is stated as follows.

Theorem 6.4. *For a measurable $g : \mathrm{R}^{2n} \not\to [0;1]$,*

$$\mathrm{E}\Big[\sum_{fx_ig \ u} g(fx_ig)\Big] = \int_{R^2} \cdots \int_{R^2} g(fx_ig)\%^{(n)}(fx_ig)\mathrm{d}(x_i);$$

where fx_ig is a sequence of n distinct points of $_u$ and $\%^{(n)} : \mathrm{R}^{2n} \not\to \mathrm{R}^+$ is the reduced n^{th} moment density of $_u$.

Informally, $\%^{(n)}(fx_ig)$ is the joint probability that there are n points specified at the locations $x_1;\cdots;x_n$ in the infinitesimal volumes $dx_1;\cdots;dx_n$. In the following Lemma, we provide $\%^{(n)}(\,)$ of PCP for $n = 1;2$.

Lemma 6.5. *For a PCP, $\%^{(1)}(x) = m_{R\ p}$ and $\%^{(2)}(x_1;x_2) \quad \%^{(2)}(kx_1 \quad x_2k) = {}^2_p m^2(1 + {}_p{}^1 g \quad g(kx_1 \quad x_2k))$, where $g \quad g(x) = \int_{R^2} g(z)g(z+x)dz$.*

Lemma 6.5 allows further simplications of $\%^{(2)}(r)$ for PCP as follows.

Corollary 6.6. *The second moment density of a PCP is expressed as:* $\%^{(2)}(k\mathbf{x}_1 \quad \mathbf{x}_2 k)$ $\%^{(2)}(r) =$

$$\begin{cases} {}_{\mathrm{p}}^{2} m^2 + \frac{{}_{\mathrm{p}} m^2}{4 \ {}^{2}} \exp \quad \frac{r^2}{4 \ {}^{2}} & \text{when } {}_{\mathrm{u}} \text{ is TCP} \\ {}_{\mathrm{p}}^{2} m^2 + 1(r \quad 2\mathrm{R}) \frac{{}_{\mathrm{p}} m^2 A_{\mathrm{i}}(\mathrm{R};\mathrm{R};r)}{{}^{2}\mathrm{R}^4} & \text{when } {}_{\mathrm{u}} \text{ is MCP} \end{cases}; \tag{6.4}$$

where $A_{\mathrm{i}}(\mathrm{R}_1;\mathrm{R}_2;r) = \mathrm{R}_1^2 \arctan \ \frac{r^2+\mathrm{R}_1^2 \quad \mathrm{R}_2^2}{t} \ + \mathrm{R}_2^2 \arctan \ \frac{r^2 \quad \mathrm{R}_1^2+\mathrm{R}_2^2}{t} \quad \frac{t}{2}$; *with* $t = \ (\mathrm{R}_1 + \mathrm{R}_2 + r)(\mathrm{R}_1 + \mathrm{R}_2 \quad r)(\mathrm{R}_1 \quad \mathrm{R}_2 + t)(\ \mathrm{R}_1 + \mathrm{R}_2 + t)^{\frac{1}{2}}$ *and* $0 \quad r \quad \mathrm{R}_1 + \mathrm{R}_2$.

Please see [13] for more details on the derivation of these expressions. The following Theorem demonstrates that the n^{th} moment of ${}_{\mathrm{u}_0}$ for any general distribution of ${}_{\mathrm{u}}$ can be expressed in terms of its $\%^{(n)}(\ )$.

Theorem 6.7. *The* n^{th} *moment of* ${}_{\mathrm{u}_0}$ *for any general distribution of* ${}_{\mathrm{u}}$ *independent of* ${}_{\mathrm{b}}$ *can be written as:*

$$\mathrm{E}[(\ {}_{\mathrm{u}_0})^n] = \int_{\mathrm{R}^2} \int_{\mathrm{R}^2} \exp \quad {}_{\mathrm{b}} \left[\prod_{i=1} b(\mathbf{x}_i; x_i) \quad \%^{(n)}(f\mathbf{x}_i g) \mathrm{d}(f\mathbf{x}_i g): \right. \tag{6.5}$$

Proof. We can write $\mathrm{E}[(\ {}_{\mathrm{u}_0})^n]$ as:

$$\begin{aligned} & \mathrm{E} \left[\sum_{f\mathbf{x}_i g 2 \ {}_{\mathrm{u}}} \prod_{i=1} \mathbf{1}(\mathbf{x}_i \ 2 \ C(\mathbf{0})) \right] \\ & = \mathrm{E} \left[\sum_{f\mathbf{x}_i g 2 \ {}_{\mathrm{u}}} \mathrm{P} \left[\bigcap_{y 2 \ {}_{\mathrm{b}}} \prod_{i=1} \mathbf{1}(x_i < k\mathbf{x}_i \quad \mathbf{y} k) \right] \right] \\ & = \mathrm{E} \left[\sum_{f\mathbf{x}_i g 2 \ {}_{\mathrm{u}}} \mathrm{P} \left[{}_{\mathrm{b}} \left[\prod_{i=1} b(\mathbf{x}_i; x_i) \quad = 0 \right] \right] \right] \\ & = \mathrm{E} \left[\sum_{f\mathbf{x}_i g 2 \ {}_{\mathrm{u}}} \mathrm{P} \left[{}_{\mathrm{b}} \left[\prod_{i=1} b(\mathbf{x}_i; x_i) \quad = 0 \right] \right] \right] \\ & \overset{(a)}{=} \mathrm{E} \left[\sum_{f\mathbf{x}_i g 2 \ {}_{\mathrm{u}}} \exp \quad {}_{\mathrm{b}} \left[\prod_{i=1} b(\mathbf{x}_i; x_i) \quad ; \right. \right. \end{aligned}$$

where step (a) is given by the void probability of PPP [13]. The final expression is obtained by using Theorem 6.4. □

Given $\%^{(n)}(r)$ for $n = 1; 2$ in (6.4), we can simplify (6.5) to obtain the first two moments of ${}_{\mathrm{u}_0}$ as follows.

6.3. Moments of the typical cell load

Corollary 6.8. *When* Φ_u *is a PCP, the first two moments of* Φ_{u_0} *are given by:* $\mathbb{E}[\Phi_{u_0}] = \frac{m_p}{b}$; *and*

$$\mathbb{E}[\Phi_{u_0}^2] = \int_0^{\mathcal{Z}} \int_0^{\mathcal{Z}} \int_0^{\mathcal{Z}} \exp\left(-\lambda_b A_u(x_1, x_2, d(x_1, x_2, \theta))\right) \aleph^{(2)}(d(x_1, x_2, \theta)) x_1 x_2 \, dx_1 dx_2 d\theta ;$$

where $d(x_1, x_2, \theta) := (x_1^2 + x_2^2 - 2x_1 x_2 \cos\theta)^{\frac{1}{2}}$.

Corollary 6.9. *The variance of* Φ_{u_0} *is given by* $\mathbb{V}\mathrm{ar}[\Phi_{u_0}] =$

$$\frac{m_p^2}{b^2} 0.28 + \frac{2}{\theta_p^2} \int_0^{\theta} \int_0^{\mathcal{Z}} \int_0^{x_1} \exp\left(-\lambda A_u(x_1, x_2, d(x_1, x_2, \theta)) - \frac{d(x_1, x_2, \theta)^2}{4\lambda_b^2}\right) x_1 x_2 \, dx_2 \, dx_1 d\theta ;$$

when Φ_u *is TCP,* (6.6)

$$\frac{m_p^2}{b^2} 0.28 + \frac{4}{\theta_p R^2} \int_0^{\mathcal{Z}} \int_0^{\theta} \int_0^{\mathcal{Z}} \exp\left(-\lambda_b A_u(x, (x^2 + r^2 + 2xr\cos\theta), r) - A_i(R, R, r)\right) x \, r \, dr \, d\theta \, dx ;$$

when Φ_u *is MCP.* (6.7)

Proof. The proof follows from Corollary 6.8 by substituting $\aleph^{(2)}(r)$ for TCP and MCP provided in Corollary 6.6 and some algebraic manipulation, which is skipped due to the space constraint. □

Note that the first term in (6.6) denotes the variance of Φ_{u_0} if Φ_u is a PPP. Also, $\mathbb{E}[\Phi_{u_0}]$ is independent of the cluster size (which is θ for TCP and R for MCP) and is hence the same as the mean cell load under the assumption that Φ_u is a PPP of density m_p. However, the variance of Φ_{u_0} is higher if Φ_u is a PCP. The accuracy of (6.6) is verified in Fig. 6.1, where we notice that the normalized variance $\mathbb{V}\mathrm{ar}[\Phi_{u_0}]/\mathbb{E}[\Phi_{u_0}]^2$ for TCP and MCP computed using Corollary 6.6 matches with the Monte Carlo simulations.

Remark 6.10. Although Theorem 6.7 gives the exact expressions of the moments of Φ_{u_0}, we can not go beyond the first two moments since the computation of (6.5) will be limited by the unavailability of the reduced moment measures of PCP for $n \geq 2$ in closed form. This motivates us to formulate a useful approximation to characterize the distribution of Φ_{u_0}, which will be presented in the next Section.

Before proceeding further, using moment matching, we demonstrate that it is not quite possible to accurately construct the PMF of Φ_{u_0} using only its mean and variance. To this end, we assume that Φ_{u_0} follows a negative binomial (NB) distribution, i.e., $\Phi_{u_0} \sim NB(r, t) \Rightarrow \mathbb{P}(\Phi_{u_0} = n) = \binom{r+n-1}{n} (1-t)^r t^n$ (for some $r \in \mathbb{Z}^+, t \in (0, 1]$). The intuition behind choosing $NB(r, t)$ is that given any closed subset $B \subseteq \mathbb{R}^2$, $\Phi_u(B)$ is known to follow a super-Poissonian distribution (i.e. the variance is greater than the mean) [13], and NB

is a standard distribution for such random variables. By moment matching, we obtained: $\hat{r} = 1 \quad E[\ _{u_0}]/\mathrm{Var}(\ _{u_0})$ and $\hat{r} = b(1 \quad t)E[\ _{u_0}]/tc$. In Fig. 6.2, we plot the resulting PMF obtained by moment matching. We observe that for small cluster size (i.e. small $\quad$ and R for TCP and MCP, respectively), the NB PMF deviates significantly from the empirical PMF of $\ _{u_0}$ obtained from simulation. In particular, the NB distribution significantly underestimates the void probability $P(\ _{u_0} = 0)$. Hence the first two moments are not clearly enough to characterize the distribution of $\ _{u_0}$. Since obtaining the exact expressions of higher order moments is not possible using this route, we provide an alternate formulation for the PMF of $\ _{u_0}$ in the next Section.

6.4 Derivation of the load PMF

This is the second contribution of the chapter, where we start from an approximation of the typical PV cell which eventually leads us to a reasonably accurate characterization of the load PMF. In order to enable the analysis, we approximate the typical cell as a circle with the same area. We formally state this approximation as follows.

Assumption 1. We assume that $\ _u(C(\mathbf{0})) \quad \ _u(b(\mathbf{0}; R_c))$, where $R_c^2 = jC(\mathbf{0})j$.

While this approximation is inspired by the fact that the large cells in a PV tessellation are circular [101], we will demonstrate that this approximation for any typical cell provides reasonably accurate values of the PMF of $\ _{u_0}$. We first characterize the PGF of $\ _{u_0}$ in the following Theorem.

Theorem 6.11. *The PGF of* $\ _{u_0}$ *is given as:* $G_{\ _{u_0}}(\ ) =$

$$E\left[\ ^{u_0}\right] = \int_0^{\infty} \exp\left(\quad 2\ \sqrt{\ }\int_0^{\infty}\left(1 \quad \exp\left(\quad m\ (1 \quad)f_d(ujv)du \quad vdv\right)\right) f_{R_c}(r)dr; \right. \tag{6.8}$$

where $f_{R_c}(r) = \frac{2\ 3{:}5^{3{:}5}}{(3{:}5)} r^6 \exp(\ 3{:}5r^2)$.

Proof. Following [102], the random variable $\ _b jC(\mathbf{0})j$ follows a Gamma distribution with PDF: $f(x; \ ; \ ) = \frac{}{(\ )} x^{\ 1} e^{\ \frac{x}{}}; \ x > 0;$ where $\quad = 3{:}5$ and $\quad = 3{:}5^{\ 1}$. Since $R_c^2 = jC(\mathbf{0})j$, $\sqrt{\ _b R_c}$ follows a Nakagami distribution with PDF $f_{R_c}(x; m; \ ) = \frac{2m^m}{(m)\ ^m} x^{2m\ 1} \exp\left(\quad \frac{m}{}x^2\right); \ x > 0;$ where $m = 3{:}5$ and $\quad = 1$. We now focus on the conditional PGF of $\ _u(b(\mathbf{0}; R_c))$ given R_c:

$$G_{\ _u(b(\mathbf{0};R_c))}(\ ) = E\left[\ ^{\sum_{x \in \ _u(b(\mathbf{0};R_c))} \mathbf{1}(kxk<R_c)}\right]$$

$$= \mathrm{E}\left[\prod_{x \in \Phi_u} \mathbf{1}(\|x\| < R_c)\right].$$

The final step follows from the PGFL of PCP ([79, Lemma 4]) and deconditioning over R_c. □

We now evaluate $G_{\Phi_u(C(0))}(\cdot)$ when Φ_u is a TCP (MCP) in the following Corollary.

Corollary 6.12. *When Φ_u is a TCP,*

$$G_{\Phi_u(C(0))}(\cdot) = \int_0^{\infty} \exp\left(-2\pi p \int_0^{\infty} \left(1 - \exp\left(-m(1-\cdot)\right)\right) \right.$$
$$\left. \left(1 - Q_1(v^{-1}; r^{-1})\right) v\,dv\right) f_{R_c}(r)\,dr, \quad (6.9)$$

where $Q_1(\cdot\,;\cdot) = \int_1^{\cdot} y e^{-\frac{y^2+\cdot^2}{2}} I_0(\cdot\, y)\,dy$ is the Marcum Q-function. Here $I_0(\cdot)$ is the modified Bessel function of order zero. When Φ_u is an MCP, $G_{\Phi_u(C(0))}(\cdot)$ is given by:

$$\int_0^{\infty} \exp\left(-2\pi p \int_0^{\infty} \left(1 - \exp\left(-m(1-\cdot)\right)\right) \Delta(r,v)\, v\,dv\right) f_{R_c}(r)\,dr, \quad (6.10)$$

where

$$\Delta(r,v) = \frac{1}{R^2}\left(\min(r, \max(R - v, 0))\right)^2 + \frac{2}{\pi} \int_{\min(r, |R-v|)}^{\min(r, R+v)} u \arccos\left(\frac{u^2 + v^2 - R^2}{2uv}\right) du \quad (6.11)$$

Finally the PMF of Φ_{u_0}, denoted as $\{p_n; n \geq 0\}$, can be obtained by performing the inverse z-transform of the PGF which is given by:

$$p_n = \frac{R^n}{2} \int_{-\pi}^{\pi} G_{\Phi_{u_0}}(Re^{j\theta}) e^{-j\theta n}\, d\theta, \quad (6.12)$$

where R is chosen such that $G_{\Phi_{u_0}}(Re^{j\theta})$ is finite for all $-\pi < \theta < \pi$. For numerical computation, this integral can approximated as a summation at N distinct points:

$$\hat{p}_n = \frac{R^n}{N} \sum_{m=0}^{N-1} G_{\Phi_{u_0}}(Re^{j2\pi m/N}) e^{-j2\pi nm/N}. \quad (6.13)$$

Note that this step is nothing but the inverse discrete Fourier transform (DFT) of $\{G_{\Phi_{u_0}}(Re^{j2\pi m/N}); m = 0, 1, \ldots, N-1\}$, scaled by R^n [103]. In Fig. 6.2, we observe that $\{\hat{p}_n\}$ are very close to $\mathrm{P}(\Phi_{u_0} = n)$, empirically computed from the Monte Carlo simulations of the network.

6.5 Application to rate analysis

In this Section, we will apply the PMF of $_{u_0}$ to characterize the downlink rate in the cellular network under the system model defined in Section 9.4.1. In particular, we evaluate the complementary cumulative density function (CCDF) of rate for a representative user, which is selected uniformly at random from $_{u_0}$ conditioned on the fact that the typical cell has at least one user, i.e., $_{u_0} > 0$. Assuming that this user is located at $\mathbf{u}$, the signal-to-interference-ratio (SIR) is defined as:

$$\text{SIR} = \frac{h_0 u}{\sum_{x \in \Phi \setminus \{0\}} h_x k\mathbf{x} \quad \mathbf{u}k}. \tag{6.14}$$

Here $h_{\mathbf{x}}$ denotes fading on the link between the representative user and the BS at $\mathbf{x} \in$ $_b$, and > 2 is the pathloss exponent. We assume Rayleigh fading, i.e., $\{h_{\mathbf{x}}\}$ is a sequence of i.i.d. random variables with $h_{\mathbf{x}}$ exp(1). Assuming interference-limited network and the system bandwidth (BW) (W) is equally partitioned between the users associated with a BS, the rate of the representative user conditioned on $_u(C_0) > 0$ is defined as:

$$\text{Rate} = \min\left\{\frac{W}{u_0}\log(1+\text{SIR}), \frac{R_b}{u_0}\right\}; \tag{6.15}$$

where R_b is the backhaul constraint on the BS imposed by the fiber connecting the BS to the network core which can support a maximum rate of R_b bps. Hence the rate of each user cannot exceed $R_b/ _{u_0}$. We define the rate coverage probability as the CCDF of Rate: $P_r( ) = P(\text{Rate} > \ j \ _{u_0} > 0)$, where is the target rate threshold. We now provide the expression for the rate coverage in the following Theorem.

Theorem 6.13. *The rate coverage probability for the representative user is expressed as:*

$$P_r( ) = \sum_{n=1}^{\lfloor \frac{R_b}{c} \rfloor} P_c\left(2^{\frac{n}{W}} \quad 1\right) \frac{\hat{p}_n}{1 \quad \hat{p}_0}; \tag{6.16}$$

where $\hat{p}_n$ is obtained from (6.13) and $P_c( ) = P(\text{SIR} > \ )$ is the CCDF of SIR that can be expressed as:

$$P_c( ) = \ ^2 \quad ^{\frac{2}{}} \int_0^{\frac{2}{}} \frac{(t)^{\ 2}}{1+t^{\frac{2}{}}} dt; \tag{6.17}$$

where $(t) = t^{\ 1} \int_t^{\infty} \frac{1}{1+u^{\frac{2}{}}} du$, *with* $= \frac{9}{7}$.

Proof. Given the backhaul constraint, the maximum users that can be supported with a rate is given by $\lfloor bR_b/c \rfloor$. First we note that Rate is a function of SIR and $_{u_0}$, which

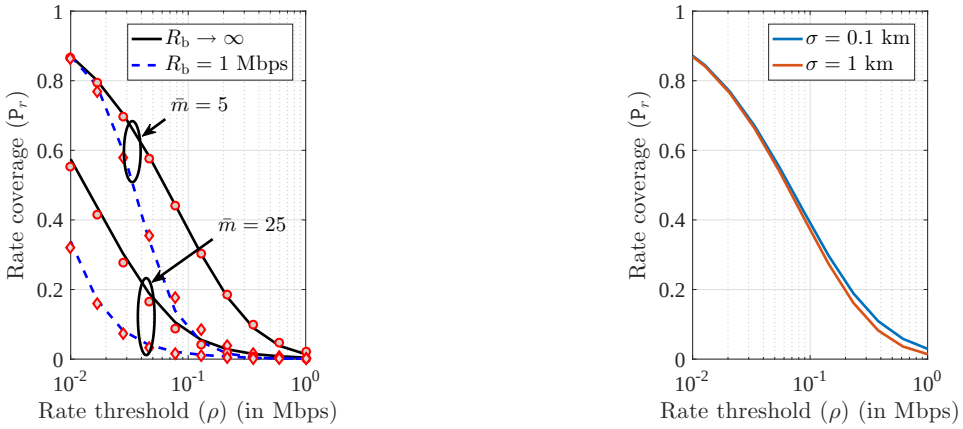

Figure 6.3: Rate coverage probability: (a) for different m (markers indicate the values obtained from Monte Carlo simulation) and (b) for different with R_b ! 1 ((b; p) = (1; 5)km 2).

are in general correlated. However, the joint distribution of SIR and u0 is intractable. For tractability, we assume that these two random variables are independent. This is a well-accepted assumption in the literature that preserves the accuracy of the analysis [57]. Under this assumption, the rate coverage can be expressed as: $P_r(\ ) = P\left[\frac{W}{u(C_0)}\log(1+\text{SIR}) > \right.$

$$\left. j\ u(C_0) > 0\right] = P\left[\text{SIR} > 2^{\frac{u(C_0)}{W}} \quad 1 \quad u(C_0) > 0\right] =$$

$$= \sum_{n=1}^{\lfloor \frac{R_b}{c} \rfloor} \underbrace{P_c(2n \ =W \quad 1)}_{\text{SIR distribution}} \underbrace{P(C_0(\ u) = n j C_0(\ u) > 0)}_{\text{load distribution}};$$

The load distribution can be simplified as: $\frac{P(C_0(\ u)=n;C_0(\ u)>0)}{P(C_0(\ u)>0)}$. Hence we are left with the characterization of P_c, or the CCDF of SIR. Since u and b are independent and u is a stationary distribution (i.e. the distribution of u is invariant under translation of its points), the representative user is equivalent to a randomly selected point in C_0. The SIR distribution of this point has been recently characterized in [104]. The expression of $P_c(\ )$ in (6.17) is obtained from [104, Theorem 2]. □

We verify the accuracy of Theorem 6.13 in Fig. 6.3a where we observe a close match between the analytical and empirical results. Because of the space constraint, we only present the results when u is a TCP. We observe that P_r decreases as (i) m increases as more number of users share the resources and (ii) R_b decreases as it imposes an upper bound on the per user rate. In Fig. 6.3b, we plot P_r for different which is a measure of the cluster size. We observe that P_r is almost invariant to . The reason is that the rate coverage is mostly

dominated by the first moment of load (see [24, Corollary 1]) which is independent of the cluster size (Corollary 6.8).

6.6 Summary

Due to the limitation of PPP in modeling spatial coupling in the network, there has been an increasing interests in developing non-PPP models of cellular networks, such as the PCP-based models which capture coupling between the users (such as in hotspots) and between users and BSs [79]. While the SINR distribution for the PCP-based models is by now well-understood, the load distribution in these networks has not received much attention. In this chapter, we made the first attempt towards this direction by characterizing the distribution of the typical cell load where the BSs are distributed as a homogeneous PPP and the users are distributed as an independent PCP. We also demonstrated the utility of this result by using it to characterize the user rate for a representative user in the typical cell.

7

Modeling and Analysis of Integrated Access and Backhaul

7.1 Introduction

With the exponential rise in data-demand far exceeding the capacity of the traditional macro-only cellular network operating in sub-6 GHz bands, network densification using mm-wave base stations (BSs) is becoming a major driving technology for the 5G wireless evolution [105]. While heterogeneous cellular networks (HetNets) with low power SBSs overlaid with traditional macro BSs improve the spectral efficiency of the access link (the link between a user and its serving BS), mm-wave communication can further boost the data rate by offering high bandwidth. That said, one of the main hindrances in the way of large-scale deployment of small cells is that the existing high-speed optical fiber backhaul network that connects the BSs to the network core is not scalabale to the extent of ultra-densification envisioned for small cells [106–108]. However, with recent advancement in mm-wave communication with highly directional beamforming [109,110], it is possible to replace the so-called *last-mile fibers* for SBSs by establishing fixed mm-wave backhaul links between the SBS and the MBS equipped with fiber backhaul, also known as the anchored BS (ABS), thereby achieving Gigabits per second (Gbps) range data rate over backhaul links [27]. While mm-wave fixed wireless backhaul is targetted to be a part of the first phase of the commercial roll-out of 5G [111], 3GPP is exploring a more ambitious solution of IAB where the ABSs will use the same spectral resources and infrastructure of mm-wave transmission to serve cellular users in access as well as the SBSs in backhaul [112]. In this chapter, we develop a tractable analytical framework for IAB-enabled mm-wave cellular networks using tools from stochastic geometry and obtain some design insights that will be useful for the ongoing pre-deployment studies on IAB.

7.1.1 Background and related works

Over recent years, stochastic geometry has emerged as a powerful tool for modeling and analysis of cellular networks operating in sub-6 GHz [54]. The locations of the BSs and users are commonly modeled as independent Poisson point processes (PPPs) over an infinite plane. This model, initially developed for the analysis of traditional macro-only cellular networks [20], was further extended for the analysis of HetNets in [21, 22, 35]. In the followup works, this PPP-based HetNet model was used to study many different aspects

of cellular networks such as load balancing, BS cooperation, multiple-input multiple-output (MIMO), energy harvesting, and many more. Given the activity this area has seen over the past few areas, any attempt towards summarizing all key relevant prior works here would be futile. Instead, it would be far more beneficial for the interested readers to refer to dedicated surveys and tutorials [23, 31–33] that already exist on this topic. While these initial works were implicitly done for cellular networks operating in the sub-6 GHz spectrum, tools from stochastic geometry have also been leveraged further to characterize their performance in the mm-wave spectrum [29, 113–115]. These mm-wave cellular network models specifically focus on the mm-wave propagation characteristics which signifantly differ from those of the sub-6 GHz [109], such as the severity of blocking of mm-wave signals by physical obstacles like walls and trees, directional beamforming using antenna arrays, and inteference being dominated by noise [116]. These initial modeling approaches were later extended to study different problems specific to mm-wave cellular networks, such as, cell search [117], antenna beam alignment [118], and cell association in the mm-wave spectrum [119]. With this brief introduction, we now shift our attention to the main focus of this chapter which is IAB in mm-wave cellular networks. In what follows, we provide the rationale behind mm-wave IAB and how stochastic geometry can be used for its performance evaluation.

For traditional cellular networks, it is reasonable to assume that the capacity achieved by the access links is not limited by the backhaul constraint on the serving BS since all BSs have access to the high capacity wired backhaul. As expected, backhaul constraint was ignored in almost all prior works on stochastic geometry-based modeling and analysis of cellular networks. However, with the increasing network densification with small cells, it may not be feasible to connect every SBS to the wired backhaul network which is limited by cost, infrastructure, maintenance, and scalability. These limitations motivated a significant body of research works on the expansion of the cellular networks by deploying relay nodes connected to the ABS by wireless backhaul links, e.g. see [120]. Among different techniques of wireless backhaul, 3GPP included layer 3 relaying as a part of the long term evolution advanced (LTE-A) standard in Release 10 [121,122] for coverage extension of the cellular network. Layer 3 relaying follows the principle of IAB architecture, which is often synonymously referred to as *self-backhauling*, where the relay nodes have the functionality of SBS and the ABS multiplexes its time-frequency resources to establish access links with the users and wireless backhaul links with SBSs that may not have access to wired backhaul [123]. However, despite being the part of the standard, layer 3 relays have never really been deployed on a massive scale in 4G mostly due to the spectrum shortage in sub-6 GHz. For instance, in urban regions with high capacity demands, the operators are not willing to relinquish any part of the cellular bandwidth (costly and scarce resource) for wireless backhaul. However, with recent advancement in mm-wave communication, IAB has gained substantial interest since spectral bottleneck will not be a primary concern once high bandwidth in mm-wave spectrum (at least 10x the cellular BW in sub-6 GHz) is exploited. Some of the notable industry initiatives driving mm-wave IAB are mm-wave small cell access and backhauling (MiWaveS) [124] and 5G-Crosshaul [125]. In 2017, 3GPP also started working on a new study item to investigate the performance of IAB-enabled mm-wave cellular network [112].

Although backhaul is becoming a primary bottleneck of cellular networks, there is very little existing work on the stochastic geometry-based analyses considering the backhaul constraint [126–128]. While these works are focused on the traditional networks in sub-6 GHz, contributions on IAB-enabled mm-wave HetNet are even sparser, except an extension of the PPP-based model [129], where the authors modeled wired and wirelessly backhauled BSs and users as three independent PPPs. In [130, 131], similar modeling approach was used to study IAB in sub-6 GHz using full duplex BSs. The fundamental shortcoming of these PPP-based models is the assumption of independent locations of the BSs and users which are spatially coupled in actual networks. For instance, in reality, the users form spatial clusters, commonly known as *user hotspots* and the centers of the user hotspots are targetted as the potential cell-cites of the short-range mm-wave SBSs [71]. Not surprisingly, such spatial configurations of users and BSs are at the heart of the 3GPP simulation models [79]. To address this shortcoming of the analytical models, in this chapter, we propose the *first 3GPP-inspired stochastic geometry-based* finite network model for the performance analysis of HetNets with IAB. The key contributions are summarized next.

7.1.2 Contributions

New tractable model for IAB-enabled mm-wave HetNet. We develop a realistic and tractable analytical framework to study the performance of IAB-enabled mm-wave HetNets. Similar to the models used in 3GPP-compliant simulations [112], we consider a two-tier HetNet where a circular macrocell with ABS at the center is overlaid by numerous low-power small cells. The users are assumed to be non-uniformly distributed over the macrocell forming hotspots and the SBSs are located at the geographical centers of these user hotspots. The non-uniform distribution of the users and the spatial coupling of their locations with those of the SBSs means that the analysis of this setup is drastically different from the state-of-the-art PPP-based models. Further, the consideration of a single macrocell (justified by the noise-limited nature of mm-wave communications), allows us to glean crisp insights into the coverage zones, which further facilitate a novel analysis of load on ABS and SBSs[1]. Assuming that the total system BW is partitioned into two splits for access and backhaul communication, we use this model to study the performance of three backhaul BW partition strategies, namely, (i) *equal partition*, where each SBS gets equal share of BW irrespective of its load, (ii) *instantaneous load-based partition*, where the ABS frequently collects information from the SBSs on their instantaneous loads and partitions the backhaul BW proportional to the instantaneous load on each SBS, and (iii) *average load-based partition*, where the ABS collects information from the SBSs on their average loads and partitions the backhaul BW proportional to the average load on each SBS.

New load modeling and downlink rate analysis. For the purpose of performance evaluation and comparisons between the aforementioned strategies, we evaluate the downlink

[1] In our discussion, BS load refers to the number of users connected to the BS.

rate coverage probability i.e. probability that the downlink data rate experienced by a randomly selected user will exceed a target data rate. As key intermediate steps of our analysis we characterize the two essential components of rate coverage, which are (i) signal-to-noise-ratio (SNR)-coverage probability, and (ii) the distribution of ABS and SBS load, which directly impacts the amount of resources allocated by the serving BS to the user of interest. We compute the probability mass functions (PMFs) of the ABS and the SBS loads assuming the number of users per hotspot is fixed. We then relax this fixed user assumption by considering independent Poisson distribution on the number of users in each hotspot. Due to a significantly different spatial model, our approach of load modeling is quite different from the load-modeling in PPP-based networks [128].

System design insights. Using the proposed analytical framework, we obtain the following system design insights.

- We compare the three backhaul BW partition strategies in terms of three metrics, (i) rate coverage probability, (ii) median rate, and (iii) 5^{th} percentile rate. Our numerical results indicate that for a given combination of the backhaul BW partition strategy and the performance metric of interest, there exists an optimal access-backhaul BW split for which the metric is maximized.
- Our results demonstrate that the optimal access-backhaul partition fractions for median and 5^{th} percentile rates are not very sensitive to the choice of backhaul BW partition strategies. Further, the median and 5^{th} percentile rates are invariant to system BW.
- For given infrastructure and spectral resources, the IAB-enabled network outperforms the macro-only network with no SBSs up to a critical volume of total cell-load, beyond which the performance gains disappear and its performance converges to that of the macro-only network. Our numerical results also indicate that this critical total cell-load increases almost linearly with the system BW.

7.2 System model

7.2.1 mm-wave cellular system model

BS and user locations

Inspired by the spatial configurations used in 3GPP simulations [79, 112] for a typical outdoor deployment scenario of a two-tier HetNet, we assume that n SBSs are deployed inside a circular macrocell of radius R (denoted by $b(\mathbf{0}; R)$) with the macro BS at its center. We assume that this BS is connected to the core network with high speed optical fiber and is hence an ABS. Note that, in contrast to the infinite network models (e.g. the PPP-based

7.2. System model

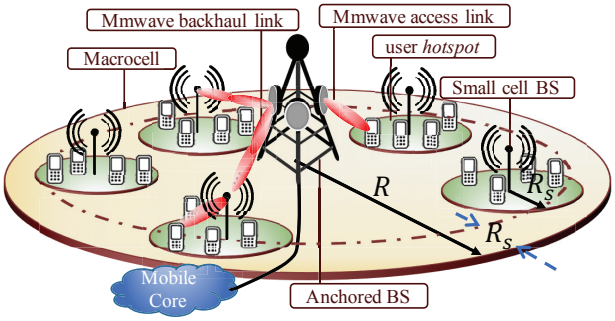

(a) User and BS locations

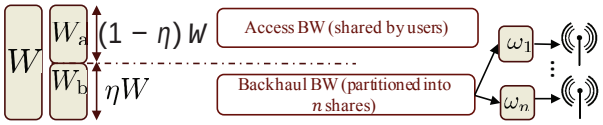

(b) Resource Allocation

Figure 7.1: Illustration of the system model.

networks defined over R^2) which are suitable for interference-dominated networks (such as conventional cellular networks in sub-6 GHz), we are limiting the complexity of the system model by considering single macrocell. This assumption is justified by the noise-limited nature of mm-wave communications [116]. Moreover, as will be evident in the sequel, this setup will allow us to glean crisp insights into the properties of this network despite a more general user distribution model (discussed next) compared to the PPP-based model.

We model a user hotspot at $\mathbf{x}$ as $b(\mathbf{x}; R_s)$, i.e., a circle of radius R_s centered at $\mathbf{x}$. We assume that the macrocell contains n user hotspots, located at $f\mathbf{x}_i \quad (x_i; '_i); i = 1; : : : ; ng$, which are distributed uniformly at random in $b(\mathbf{0}; R \quad R_s)$.[2] Thus, $f\mathbf{x}_i g$ is a sequence of independently and identically distributed (i.i.d.) random vectors with the distribution of $\mathbf{x}_i$ being:

$$f_{\mathbf{X}}(\mathbf{x}_i) = \begin{cases} \frac{x_i}{(R \quad R_s)^2}; & \text{when } 0 < x_i \quad R \quad R_s; 0 < '_i \quad 2 \ ; \\ 0; & \text{otherwise.} \end{cases} \tag{7.1}$$

The marginal probability density function (PDF) of x_i is obtained as: $f_X(x_i) = 2x_i=(R \quad R_s)^2$ for $0 < x_i \quad R \quad R_s$ and $'_i$ is a uniform random variable in $(0; 2 \ ]$. Note that this construction ensures that all hotspots lie entirely inside the macrocell, i.e., $b(\mathbf{x}_i; R_s) \setminus b(\mathbf{0}; R)^c = ?; \ 8 \ i$. We assume that the number of users in the hotspot centered at $\mathbf{x}_i$ is $N_{\mathbf{x}_i}$, where Type 1: $N_{\mathbf{x}_i} = m$ is fixed and equal for all $i = 1; : : : ; n$ and Type 2: $fN_{\mathbf{x}_i} g$ is a sequence of i.i.d. Poisson random variables with mean m. These $N_{\mathbf{x}_i}$ users are assumed to be located *uniformly at random* independently of each other in each hotspot. Thus, the location of a user belonging to the hotspot at $\mathbf{x}_i$ is denoted by $\mathbf{x}_i + \mathbf{u}$, where $\mathbf{u} \quad (u; \ )$ is a random vector in R^2 with

[2] For notational simplicity, we use $x \quad kxk; \ 8 \ \mathbf{x} \ 2 \ \mathsf{R}^2$.

PDF:

$$f_{\mathrm{U}}(\mathbf{u}) = \begin{cases} \frac{u}{R_{\mathrm{s}}^2}; & \text{when } 0 < u \quad R_{\mathrm{s}}; 0 < \quad 2 \\ 0; & \text{otherwise.} \end{cases} \tag{7.2}$$

The marginal PDF of u is: $f_U(u) = 2u/R_{\mathrm{s}}^2$ for $0 < u \quad R_{\mathrm{s}}$ and is a uniform random variable in $(0; 2\ ]$. We assume that the SBSs are deployed at the center of user hotspots, i.e., at $f\mathbf{x}_i g$. The ABS provides wireless backhaul to these SBSs over mm-wave links. See Fig. 7.1a for an illustration. Having defined the spatial distribution of SBSs and users, we now define the *typical user* for which we will compute the rate coverage probability. The typical user is a user chosen uniformly at random from the network. The hotspot to which the typical user belongs is termed as the *representative hotspot*. We denote the center of representative hotspot as $\mathbf{x}$, where $\mathbf{x} = \mathbf{x}_n$, without loss of generality and the location of the typical user as $\mathbf{x} + \mathbf{u}$. For Type 1, the number of users in the representative cluster is $N_{\mathbf{x}} = N_{\mathbf{x}_n} = m$. For Type 2, although $N_{\mathbf{x}_i}$ is i.i.d. Poisson, $N_{\mathbf{x}}$ does not follow the same distribution since the typical user will more likely belong to a hotspot with more number of users [132]. If $n \ ! \ 1$, $N_{\mathbf{x}}$ follows a weighted Poisson distribution with PMF $\mathrm{P}(N_{\mathbf{x}} = k) = \frac{m^k \ ^1 e \ ^m}{(k \ 1)!}$, where, $k \ 2 \ \mathrm{Z}^+$. It can be easily shown that if $N_{\mathbf{x}}$ follows a weighted Poisson distribution, we have $N_{\mathbf{x}} = N_{\mathbf{x}_n} + 1$. Hence, for $n \ ! \ 1$, one can obtain the distribution of $N_{\mathbf{x}}$ by first choosing a hotspot uniformly at random and then adding one user to it. However, when n is finite, $N_{\mathbf{x}}$ will lie between $N_{\mathbf{x}_n}$ and $N_{\mathbf{x}_n} + 1$ ($N_{\mathbf{x}_n} \quad N_{\mathbf{x}} \quad N_{\mathbf{x}_n} + 1$). The lower bound on $N_{\mathbf{x}}$ is trivially achieved when $n = 1$. Since the actual distribution of $N_{\mathbf{x}}$ for finite number of hotspots ($n > 1$) is not tractable, we fix the typical user for Type 2 according to the following Remark.

Remark 7.1. For Type 2, we first choose a hotspot centered at $\mathbf{x}$ uniformly at random from n hotspots, call it the representative hotspot, and then add the typical user at $\mathbf{x} + \mathbf{u}$, where $\mathbf{u}$ follows the PDF in (7.2). Although this process of selecting the typical user is asymptotically exact when $N_{\mathbf{x}_i} \overset{i.i.d.}{\sim} \mathrm{Poisson}(m); \ 8 \ i = 1; 2; : : : ; n$, and $n \ ! \ 1$, it will have negligible impact on the analysis since our interest will be in the cases where the macrocells have moderate to high number of hotspots [2].

Propagation assumptions

All backhaul and access transmissions are assumed to be performed in mm-wave spectrum. We assume that the ABS and SBS transmit at constant power spectral densities (PSDs) P_{m}/W and P_{s}/W, respectively over a system BW W. The received power at $\mathbf{z}$ is given by $P \ hL(\mathbf{z}; \mathbf{y}) \ ^1$, where P is a generic variable denoting transmit power with $P \ 2 \ fP_{\mathrm{m}}; P_{\mathrm{s}}g$, is the combined antenna gain of the transmitter and receiver, and $L(\mathbf{z}; \mathbf{y}) = 10^{((\ +10 \ \log_{10} k\mathbf{z} \ \ \mathbf{y}k)=10)}$ is the associated pathloss. We assume that all links undergo i.i.d. Nakagami-m fading. Thus, $h \quad \mathrm{Gamma}(m; m \ ^1)$.

Blockage model

Since mm-wave signals are sensitive to physical blockages such as buildings, trees and even human bodies, the LOS and NLOS path-loss characteristics have to be explicitly included into the analysis. On similar lines of [114], we assume exponential blocking model. Each mm-wave link of distance r between the transmitter (ABS/SBS) and receiver (SBS/user) is LOS or NLOS according to an independent Bernoulli random variable with LOS probability $p(r) = \exp(\ \ r=\ )$, where $\ \ $ is the LOS range constant that depends on the geometry and density of blockages. Since the blockage environment seen by the links between the ABS and SBS, SBS to user and ABS to user may be very different, one can assume three different blocking constants $f\ _{\mathrm{b}};\ _{\mathrm{s}};\ _{\mathrm{m}}g$, respectively instead of a single blocking constant $\ $. As will be evident in the technical exposition, this does not require any major changes in the analysis. However, in order to keep our notational simple, we will assume the same $\ $ for all the links in this chapter. Also, LOS and NLOS links may likely follow different fading statistics, which is incorporated by assuming different Nakagami-m parameters for LOS and NLOS, denoted by m_L and m_{NL}, respectively.

We assume that all BSs are equipped with steerable directional antennas and the user equipments have omni-directional antenna. Let G be the directivity gain of the transmitting and receiving antennas of the BSs (ABS and SBS). Assuming perfect beam alignment, the effective gains on backhaul and access links are G^2 and G, respectively. We assume that the system is noise-limited, i.e., at any receiver, the interference is negligible compared to the thermal noise with PSD N_0. Hence, the SNR-s of a backhaul link from ABS to SBS at $\mathbf{x}$, access links from SBS at $\mathbf{x}$ to user at $\mathbf{x}+\mathbf{u}$, and ABS to user at $\mathbf{x}+\mathbf{u}$ are respectively expressed as:

$$\mathrm{SNR}_{\mathrm{b}}(\mathbf{x}) = \frac{P_{\mathrm{m}} G^2 h_{\mathrm{b}} L(\mathbf{0};\mathbf{x})\ ^{1}}{\mathrm{N}_0 W};\tag{7.3a}$$

$$\mathrm{SNR}_{\mathrm{a}}^{\mathrm{SBS}}(\mathbf{x}+\mathbf{u}) = \frac{P_{\mathrm{s}} G h_{\mathrm{s}} L(\mathbf{x};\mathbf{x}+\mathbf{u})\ ^{1}}{\mathrm{N}_0 W};\tag{7.3b}$$

$$\mathrm{SNR}_{\mathrm{a}}^{\mathrm{ABS}}(\mathbf{x}+\mathbf{u}) = \frac{P_{\mathrm{m}} G h_{\mathrm{m}} L(\mathbf{0};\mathbf{x}+\mathbf{u})\ ^{1}}{\mathrm{N}_0 W};\tag{7.3c}$$

where $fh_{\mathrm{b}};h_{\mathrm{s}};h_{\mathrm{m}}g$ are the corresponding small-scale fading gains.

User association

We assume that the SBSs operate in closed-access, i.e., users in hotspot can only connect to the SBS at the hotspot center, or the ABS. This model is inspired by the way smallcells with closed user groups, for instance the privately owned femtocells, are dropped in the HetNet models considered by 3GPP [1, Table A.2.1.1.2-1]. Given the complexity of user association in mm-wave using beam sweeping techniques, we assume a much simpler way of user association which is performed by signaling in sub-6 GHz, analogous to the current LTE standard [118]. In particular, the BSs broadcast paging signal using omni-directional

antennas in sub-6 GHz and the user associates to the candidate serving BS based on the maximum received power over the paging signals. Since the broadcast signaling is in sub-6 GHz, we assume the same power-law pathloss function for both LOS and NLOS components with path-loss exponent due to rich scattering environment. We define the association event E for the typical user as:

$$E = \begin{cases} 1 & \text{if } P_s k\mathbf{u}k \quad > P_m k\mathbf{x}+\mathbf{u}k \quad ; \\ 0; & \text{otherwise,} \end{cases} \tag{7.4}$$

where $f0;1g$ denote association to ABS and SBS, respectively. The typical user at $\mathbf{x}+\mathbf{u}$ is *under coverage* in the downlink if either of the following two events occurs:

$$\begin{aligned} &E = 1 \text{ and } \mathsf{SNR}_b(\mathbf{x}) > \ {}_1; \mathsf{SNR}_a^{\mathsf{SBS}}(\mathbf{u}) > \ {}_2; \text{ or,} \\ &E = 0 \text{ and } \mathsf{SNR}_a^{\mathsf{ABS}}(\mathbf{x}+\mathbf{u}) > \ {}_3; \end{aligned} \tag{7.5}$$

where $f \ {}_1; \ {}_2; \ {}_3g$ are the coverage thresholds for successful demodulation and decoding.

7.2.2 Resource allocation

The ABS, SBSs and users are assumed to be capable of communicating on both mm-wave and sub-6 GHz bands. The sub-6 GHz band is reserved for control channel and the mm-wave band is kept for data-channels. The total mm-wave BW W for downlink transmission is partitioned into two parts, $W_b = \ W$ for backhaul and $W_a = (1 \quad)W$ for access, where $2 \ [0;1)$ determines the access-backhaul split. Each BS is assumed to employ a simple round robin scheduling policy for serving users, under which the total access BW is shared equally among its associated users, referred to alternatively as *load* on that particular BS. On the other hand, the backhaul BW is shared amongst n SBSs by either of the three strategies as follows.

1. *Equal partition.* This is the simplest partition strategy where the ABS does not require any load information from the SBSs and divides W_b equally into n splits.
2. *Instantaneous load-based partition.* In this scheme, the SBSs regularly feed back the ABS its load information and accordingly the ABS allocates backhaul BW proportional to the instantaneous load on each small cell.
3. *Average load-based partition.* Similar to the previous strategy, the ABS allocates backhaul BW proportional to the load on each small cell. But in this scheme, the SBSs feed back the ABS its load information after sufficiently long intervals. Hence the instantaneous fluctuations in SBS load are averaged out.

If the SBS at $\mathbf{x}$ gets backhaul BW $W_s(\mathbf{x})$, then

$$W_s(\mathbf{x}) = \begin{cases} \gtrsim \frac{W_b}{n}; & \text{for equal partition;} \\ > \frac{N_{\mathbf{x}}^{\mathsf{SBS}}}{n\mathsf{P}1} W_b, & \text{for instantaneous load-based partition;} \\ \cdot \frac{N_{\mathbf{x}}^{\mathsf{SBS}}+\mathsf{E}[N_{\mathbf{x}}^{\mathsf{SBS}}]}{\mathsf{E}[N_{\mathbf{x}}^{\mathsf{SBS}}]+\sum_{i=1}^{n\mathsf{P}1}\mathsf{E}[N_{\mathbf{x}_i}^{\mathsf{SBS}}]} W_b, & \text{for average load-based partition;} \end{cases} \tag{7.6}$$

where $N_{\mathbf{x}}^{\mathrm{SBS}}$ and $N_{\mathbf{x}_i}^{\mathrm{SBS}}$ denote the load on the SBS of the representative hotspot and load on the SBS at $\mathbf{x}_i$, respectively. The BW partition is illustrated in Fig. 7.1b.

To compare the performance of these strategies, we define the network performance metric of interest next.

7.2.3 Downlink data rate

The maximum achievable downlink data rate, henceforth referred to as simply the *data rate*, on the backhaul link between the ABS and the SBS, the access link between SBS and user, and the access link between ABS and user can be expressed as:

$$R_{\mathrm{b}}^{\mathrm{ABS}} = W_{\mathrm{s}}(\mathbf{x}) \log_2(1 + \mathrm{SNR}_{\mathrm{b}}(\mathbf{x})); \tag{7.7a}$$

$$R_{\mathrm{a}}^{\mathrm{SBS}} = \min \left(\frac{W_{\mathrm{a}}}{N_{\mathbf{x}}^{\mathrm{SBS}}} \log_2(1 + \mathrm{SNR}_{\mathrm{a}}^{\mathrm{SBS}}(\mathbf{u})); \frac{R_{\mathrm{b}}^{\mathrm{ABS}}}{N_{\mathbf{x}}^{\mathrm{SBS}}} \right); \tag{7.7b}$$

$$R_{\mathrm{a}}^{\mathrm{ABS}} = \frac{W_{\mathrm{a}}}{N_{\mathbf{x}}^{\mathrm{ABS}} + \sum_{i=1}^{n} N_{\mathbf{x}_i}^{\mathrm{ABS}}} \log_2(1 + \mathrm{SNR}_{\mathrm{a}}^{\mathrm{ABS}}(\mathbf{x} + \mathbf{u})); \tag{7.7c}$$

where $W_{\mathrm{s}}(\mathbf{x})$ is defined according to backhaul BW partition strategies in (7.6) and $N_{\mathbf{x}}^{\mathrm{ABS}}$ ($N_{\mathbf{x}_i}^{\mathrm{ABS}}$) denotes the load on the ABS due to the macro users of the representative hotspot (hotspot at $\mathbf{x}_i$). In (7.7b), the first term inside the min-operation is the data rate achieved under no backhaul constraint when the access BW W_{a} is equally partitioned between $N_{\mathbf{x}}^{\mathrm{SBS}}$ users. However, due to finite backhaul, $R_{\mathrm{a}}^{\mathrm{SBS}}$ is limited by the second term.

7.3 Rate coverage probability analysis

In this Section, we derive the expression of rate coverage probability of the typical user conditioned on its location at $\mathbf{x} + \mathbf{u}$ and later decondition over them. This deconditioning step averages out all the spatial randomness of the user and hotspot locations in the given network configuration. We first partition each hotspot into SBS and ABS association regions such that the users lying in the SBS (ABS) association region connects to the SBS (ABS). Note that the formation of these mathematically tractable association regions is the basis of the distance-dependent load modeling which is one of the major contributions of this work.

7.3.1 Association region and association probability

We first define the association region in the representative user hotspot as follows. Given the representative hotspot is centered at $\mathbf{x}$, the SBS association region is defined as: $S_{\mathbf{x}} = \{\mathbf{x}+\mathbf{u} \in b(\mathbf{x}; R_{\mathrm{s}}) : P_{\mathrm{m}} k\mathbf{x}+\mathbf{u}k^{-} < P_{\mathrm{s}} u^{-}\}$ and the ABS association area is $b(\mathbf{x}; R_{\mathrm{s}}) \setminus S_{\mathbf{x}}^{c}$. In the following Proposition, we characterize the shape of $S_{\mathbf{x}}$.

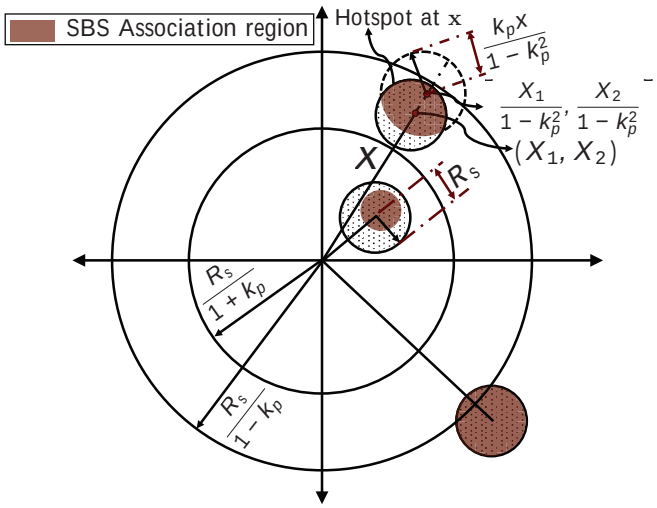

Figure 7.2: An illustration of association region.

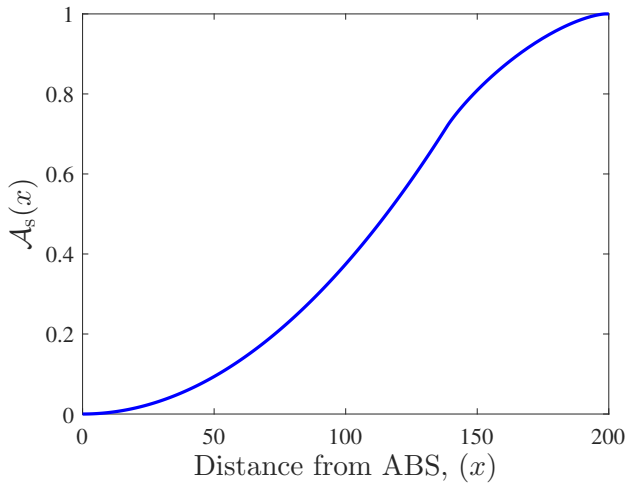

Figure 7.3: Variation of association probability to SBS with distance from ABS.

7.3. Rate coverage probability analysis

Proposition 7.2. *The SBS association region $S_{\mathbf{x}}$ for the SBS at $\mathbf{x}$ can be written as:* $S_{\mathbf{x}} =$

$$\begin{cases} b\left((1-k_p^2)^{-1}\mathbf{x}; \frac{k_p x}{1-k_p^2}\right); & 0 < x < \frac{k_p R_s}{1+k_p}; \\ b\left((1-k_p^2)^{-1}\mathbf{x}; \frac{k_p x}{1-k_p^2}\right) \setminus b(\mathbf{x}; R_s); & \frac{k_p R_s}{1+k_p} \le x \le \frac{k_p R_s}{1-k_p}; \\ b(\mathbf{x}; R_s); & x > \frac{k_p R_s}{1-k_p}; \end{cases} \tag{7.8}$$

where $k_p = \left(\frac{P_s}{P_m}\right)^{1/\alpha}$.

Proof. Let $\mathbf{x} = (X_1, X_2)$ be the Cartesian representation of $\mathbf{x}$. Let, $S_{\mathbf{x}} = \{(X_1 + t_1, X_2 + t_2)\}$. Then, following the definition of $S_{\mathbf{x}}$, $P_m(t_1^2 + t_2^2)^{-\alpha/2} \ge P_s((t_1 - X_1)^2 + (t_2 - X_2)^2)^{-\alpha/2}$ $\Rightarrow$ $t_1 - \frac{X_1}{1-k_p^2}^2 + t_2 - \frac{X_2}{1-k_p^2}^2 \le \frac{k_p x}{1-k_p^2}^2$. Thus, $\{(t_1, t_2)\} = b((1-k_p^2)^{-1}\mathbf{x}; k_p x/(1-k_p^2))$. Since, $S_{\mathbf{x}}$ can not spread beyond $b(\mathbf{x}; R_s)$, $S_{\mathbf{x}} = b\left((1-k_p^2)^{-1}\mathbf{x}; \frac{k_p x}{1-k_p^2}\right) \setminus b(\mathbf{x}; R_s)$. When $0 < x < \frac{k_p}{1+k_p} R_s$, $b\left((1-k_p^2)^{-1}\mathbf{x}; \frac{k_p x}{1-k_p^2}\right) \subset b(\mathbf{x}; R_s)$. Beyond this limit of x, a part of $b((1-k_p^2)^{-1}\mathbf{x}; k_p x/(1-k_p^2))$ lies outside of $b(\mathbf{x}; R_s)$. Finally, when $x > \frac{k_p}{1-k_p} R_s$, $b((1-k_p^2)^{-1}\mathbf{x}; k_p x/(1-k_p^2)) \not\subset b(\mathbf{x}; R_s)$. □

This formulation of $S_{\mathbf{x}}$ is illustrated in Fig. 7.2. We now compute the SBS association probability as follows.

Lemma 7.3. *Conditioned on the fact that the user belongs to the hotspot at $\mathbf{x}$, the association probability to SBS is given by:* $A_s(\mathbf{x}) =$

$$\int_0^{2\pi} \frac{\min\left(R_s; x\frac{k_p\left(\sqrt{1-k_p^2 \cdot \sin^2\theta} + k_p\cos\theta\right)}{1-k_p^2}\right)^2}{2R_s^2} d\theta \tag{7.9}$$

$$= \begin{cases} \frac{k_p^2 x^2}{(1-k_p^2)^2 R_s^2} & \text{if } 0 < x < \frac{k_p}{1+k_p} R_s; \\ \frac{C\left(R_s; \frac{k_p x}{1-k_p^2}; \frac{k_p^2 x}{1-k_p^2}\right)}{\pi R_s^2} & \text{if } \frac{k_p}{1+k_p} R_s \le x \le \frac{k_p}{1-k_p} R_s; \\ 1 & \text{if } x > \frac{k_p}{1-k_p} R_s \end{cases} \tag{7.10}$$

where

$$C(r_1; r_2; d) = r_1^2 \tan^{-1}\left(\frac{t}{d^2 + r_1^2 - r_2^2}\right) + r_2^2 \tan^{-1}\left(\frac{t}{d^2 - r_1^2 + r_2^2}\right) - \frac{t}{2}$$

is the area of intersection of two intersecting circles of radii r_1, and r_2 and distance between centers d with $t = \frac{1}{2}\sqrt{(d + r_1 + r_2)(d + r_1 - r_2)(d - r_1 + r_2)(-d + r_1 + r_2)}$. *The association probability to the ABS is given by* $A_m(x) = 1 - A_s(x)$.

Proof. Conditioned on the location of the hotspot center at $\mathbf{x}$, $A_s(\mathbf{x}) = \mathrm{P}(E = 1 | \mathbf{x}) =$

$$\begin{aligned}
&\mathrm{E}\left[\mathbf{1}(P_m \|\mathbf{x} + \mathbf{u}\|^{-} < P_s \|\mathbf{u}\|^{-})|\mathbf{x}\right] = \mathrm{P}(\mathbf{x} + \mathbf{u} \in S_x | \mathbf{x}) \\
&= \mathrm{P}(P_m(x^2 + u^2 + 2xu\cos\theta)^{-\alpha/2} < P_s u^{-\alpha}|x) \\
&= \mathrm{P}(u^2(1 - k_p^2) - 2x\cos\theta\, k_p^2 u - k_p^2 x^2 < 0 | x) \\
&\overset{(a)}{=} \mathrm{P}\left(u \in \left[0, \frac{xk_p\cos\theta + \sqrt{1 - k_p^2\sin^2\theta}}{1 - k_p^2}\right], \theta \in (0, 2\pi]\right) \\
&= \int_0^{2\pi}\int_0^{R_s} \mathbf{1}\left(0 \le u < \frac{xk_p\cos\theta + \sqrt{1 - k_p^2\sin^2\theta}}{1 - k_p^2}\right) f_U(u)\mathrm{d}u\frac{1}{2\pi}\mathrm{d}\theta,
\end{aligned}$$

where $\theta = \arg(\mathbf{u} - \mathbf{x})$ and is uniformly distributed in $(0, 2\pi]$. Here, (a) follows from solving the quadratic inequality inside the indicator function. The last step follows from deconditioning over u and θ. Finally, (7.9) is obtained by evaluating the integration over u. Note that, due to angular symmetry, $A_s(\mathbf{x}) = A_s(x)$. Alternatively,

$$A_s(x) = \int_{S_x} f_U(u)\mathrm{d}u\frac{1}{2\pi}\mathrm{d}\theta = \frac{\pi S_x}{\pi R_s^2}.$$

The final result in (7.10) is obtained by using Proposition 7.2. □

In Fig. 7.3, we plot $A_s(x)$ as a function of x. We now evaluate the coverage probability of a typical user which is the probability of the occurrence of the events defined in (7.5).

Theorem 7.4. *The coverage probability is given by:*

$$\mathrm{P_c} = \int_0^{R_s} \mathrm{P_{cs}}(\gamma_1, \gamma_2 | x) + \mathrm{P_{cm}}(\gamma_3 | x)\ f_X(x)\mathrm{d}x, \tag{7.11}$$

where

$$\begin{aligned}
\mathrm{P_{cs}}(\gamma_1, \gamma_2 | x) = \int_0^{2\pi}\int_0^{u_{\max}(x,\theta)} &p(x)F_h\left(\frac{x^{\alpha_L}\mathrm{N}_0 W(2^{\gamma_1} - 1)}{P_m G^2}; m_L\right) + (1 - p(x)) \\
&F_h\left(\frac{x^{\alpha_{NL}}\mathrm{N}_0 W(2^{\gamma_1} - 1)}{P_m G^2}; m_{NL}\right) p(u)F_h\left(\frac{u^{\alpha_L}\mathrm{N}_0 W(2^{\gamma_2} - 1)}{P_s G}; m_L\right) \\
&+ (1 - p(u))F_h\left(\frac{u^{\alpha_{NL}}\mathrm{N}_0 W(2^{\gamma_2} - 1)}{P_s G}; m_{NL}\right)\frac{f_U(u)}{2\pi}\mathrm{d}u\,\mathrm{d}\theta,
\end{aligned}$$

where $u_{\max}(x, \theta) = \min\left(R_s; xk_p\frac{\cos\theta + \sqrt{(1 - k_p^2\sin^2\theta) + k_p\cos\theta}}{1 - k_p^2}\right)$ *and* $F_h(\cdot)$ *is the complementary cumulative distribution function (CCDF) of Gamma distribution, and* $\mathrm{P_{cm}}(\gamma_3 | x) =$

$$\int_0^{2\pi}\int_{u_{\max}(x,\theta)}^{R_s} p(\ell(x,u,\theta))F_h\left(\frac{(x,u,\theta)^{-\alpha_L} N_0 W}{P_m G};m_L\right) + (1-p(\ell(x,u,\theta)))F_h\left(\frac{(x,u,\theta)^{-\alpha_{NL}} N_0 W}{P_m G};m_{NL}\right)\frac{f_U(u)\,du\,d\theta}{2\pi};$$

where $\ell(x,u,\theta) = (x^2+u^2+2xu\cos\theta)^{1/2}$.

Proof. Conditioned on the location of the typical user at $\mathbf{u} = (u,\theta)$ and its hotspot center at $\mathbf{x}$, $\mathsf{P}_{cs}(\beta_1,\beta_2|x) =$

$$\begin{aligned}
&\mathsf{P}(\mathrm{SNR}_a^{SBS}(u) > \beta_2, \mathrm{SNR}_b(x) > \beta_1, E=1|x)\\
&= \mathsf{P}(\mathrm{SNR}_a^{SBS}(u) > \beta_2, E=1|x)\mathsf{P}(\mathrm{SNR}_b(x) > \beta_1|x)\\
&\overset{(a)}{=} \mathsf{E}_u\left[p(u)\mathsf{P}\left(\frac{P_s G\, {}^1h_{s(L)} u^{-\alpha_L}}{N_0 W} > \beta_2\right) + (1-p(u))\mathsf{P}\left(\frac{P_s\, {}^1G h_{s(NL)} u^{-\alpha_{NL}}}{N_0 W} > \beta_2\right)\right]\\
&\qquad \mathbf{1}\left(u \ge 2\left(0,\frac{xk_p - \sqrt{1-k_p^2\sin^2\theta} + k_p\cos\theta}{1-k_p^2}\right)\right), \quad \theta \in (0,2\pi], \quad x\\
&\qquad p(x)\mathsf{P}\left(\frac{P_m\, {}^1G^2 h_{b(L)} x^{-\alpha_L}}{N_0 W} > \beta_1|x\right)\\
&+ (1-p(x))\mathsf{P}\left(\frac{P_m\, {}^1G^2 h_{b(NL)} x^{-\alpha_{NL}}}{N_0 W} > \beta_1|x\right).
\end{aligned}$$

Here (a) follows from step (a) in the proof of Lemma 7.3. The final form is obtained by evaluating the expectation with respect to u and θ. We can similarly obtain $\mathsf{P}_{cm}(\beta_3|\mathbf{x}) =$

$$\begin{aligned}
&\mathsf{P}(\mathrm{SNR}_a^{ABS}(\mathbf{x}+\mathbf{u}) > \beta_3, E=0|x)\\
&= \mathsf{E}_\theta\left[p\left(\sqrt{x^2+u^2+2xu\cos\theta}\right)\mathsf{P}\left(\frac{P_m G\, {}^1h_{m(L)}(x^2+u^2+2xu\cos\theta)^{-\frac{\alpha_L}{2}}}{N_0 W} > \beta_2\right)\right.\\
&\left.+ (1-p(\sqrt{x^2+u^2+2xu\cos\theta}))\mathsf{P}\left(\frac{P_m\, {}^1G h_{m(NL)}}{N_0 W}(x^2+u^2+2xu\cos\theta)^{-\frac{\alpha_{NL}}{2}} > \beta_2\right)\right]_{u=x},
\end{aligned}$$

followed by deconditioning over u and θ. □

As expected, coverage probability is the summation of two terms, each corresponding to the probability of occurrences of the two mutually exclusive events appearing in (7.5).

7.3.2 Load distributions

While the load distributions for the PPP-based models are well-understood [24, 129], they are not directly applicable to the 3GPP-inspired finite model used in this chapter.

Consequently, in this Section, we provide a novel approach to characterize the ABS and SBS load for this model. As we saw in (7.7c), the load on the ABS has two components, one is due to the contribution of the number of users of the representative hotspot connecting to the ABS (denoted by $N_{\mathbf{x}}^{\mathrm{ABS}}$) and the other is due to the macro users of the other clusters, which we lump into a single random variable, $N_0^{\mathrm{ABS}} = \sum_{i=1}^{n-1} N_{\mathbf{x}_i}^{\mathrm{ABS}}$. On the other hand, $N_{\mathbf{x}}^{\mathrm{SBS}}$ and $N_0^{\mathrm{SBS}} = \sum_{i=1}^{n-1} N_{\mathbf{x}_i}^{\mathrm{SBS}}$ respectively denote the load on the SBS at $\mathbf{x}$ and sum load of all SBSs except the one at $\mathbf{x}$. First, we obtain the PMFs of $N_{\mathbf{x}}^{\mathrm{ABS}}$ and $N_{\mathbf{x}}^{\mathrm{SBS}}$ using the fact that given the location of the representative hotspot centered at $\mathbf{x}$, each user belongings to the association regions $S_{\mathbf{x}}$ or $b(\mathbf{x}; R_{\mathrm{s}}) \setminus S_{\mathbf{x}}^{c}$ according to an i.i.d. Bernoulli random variable.

Lemma 7.5. *Given the fact that the representative hotspot is centered at $\mathbf{x}$, load on the ABS due to the macro users in the hotspot at $\mathbf{x}$ ($N_{\mathbf{x}}^{\mathrm{ABS}}$) and load on the SBS at $\mathbf{x}$ ($N_{\mathbf{x}}^{\mathrm{SBS}}$) are distributed as follows:*

Type 1 *($N_{\mathbf{x}_i} = m$, $\forall\, i = 1, \ldots, n$).*

$$\mathrm{P}(N_{\mathbf{x}}^{\mathrm{ABS}} = k | \mathbf{x}) = \binom{m-1}{k-1} A_{\mathrm{m}}(x)^{k-1} A_{\mathrm{s}}(x)^{m-k}; \tag{7.12a}$$

$$\mathrm{P}(N_{\mathbf{x}}^{\mathrm{SBS}} = k | \mathbf{x}) = \binom{m-1}{k-1} A_{\mathrm{s}}(x)^{k-1} A_{\mathrm{m}}(x)^{m-k}; \tag{7.12b}$$

where $k = 1, 2, \ldots, m$.

Type 2 *($N_{\mathbf{x}_i} \overset{i.i.d.}{\sim} \mathrm{Poisson}(m)$, $\forall\, i = 1, \ldots, n$).*

$$\mathrm{P}(N_{\mathbf{x}}^{\mathrm{ABS}} = k | \mathbf{x}) = \frac{(mA_{\mathrm{m}}(x))^{k-1}}{(k-1)!} e^{-mA_{\mathrm{m}}(x)}; \tag{7.13a}$$

$$\mathrm{P}(N_{\mathbf{x}}^{\mathrm{SBS}} = k | \mathbf{x}) = \frac{(mA_{\mathrm{s}}(x))^{k-1}}{(k-1)!} e^{-mA_{\mathrm{s}}(x)}; \tag{7.13b}$$

where $k \in \mathbb{Z}^{+}$.

Proof. Conditioned on the fact that the representative hotspot is centered at $\mathbf{x}$ and the typical user connects to the ABS, $N_{\mathbf{x}}^{\mathrm{ABS}} = 1 + N_{\mathbf{x}}^{\mathrm{ABS,o}}$, where $N_{\mathbf{x}}^{\mathrm{ABS,o}}$ is the load due to rest of the users in the representative hotspot connecting to the ABS, where, $N_{\mathbf{x}}^{\mathrm{ABS,o}} =$

$$\begin{cases} \mathrm{E}\left[\sum_{j=1}^{N_{\mathbf{x}}-1} \mathbf{1}(P_{\mathrm{m}} k\mathbf{x} + \mathbf{u}_j k^{-} > P_{\mathrm{s}} k\mathbf{u}_j k^{-}) | \mathbf{x}\right] & \text{for Type 1,} \\ \mathrm{E}\left[\sum_{j=1}^{N_{\mathbf{x}}} \mathbf{1}(P_{\mathrm{m}} k\mathbf{x} + \mathbf{u}_j k^{-} > P_{\mathrm{s}} k\mathbf{u}_j k^{-}) | \mathbf{x}\right] & \text{for Type 2.} \end{cases}$$

Note that the difference between the above two expressions is the upper bound of the summation. Recall that, $N_{\mathbf{x}} = N_{\mathbf{x}_n} = m$ for Type 1, and $N_{\mathbf{x}} = N_{\mathbf{x}_n} + 1$ for Type 2 (by Remark 7.1). Hence, the number of other users except the typical user in the representative

cluster is $N_{\mathbf{x}} - 1$ for Type 1 and $N_{\mathbf{x}}$ for Type 2. For Type 1, the conditional moment generating function (MGF) of $N_{\mathbf{x}}^{\mathrm{ABS};o}$ is:

$$\begin{aligned}
\mathrm{E}[e^{sN_{\mathbf{x}}^{\mathrm{ABS};o}} | \mathbf{x}] &= \mathrm{E}\left[\prod_{j=1}^{m-1} e^{s\mathbf{1}(P_m\|\mathbf{x}+\mathbf{u}_j\|^{-} > P_s\|\mathbf{u}_j\|^{-})} | \mathbf{x}\right] \\
&= \prod_{j=1}^{m-1} \mathrm{E}[e^{s\mathbf{1}(P_m\|\mathbf{x}+\mathbf{u}_j\|^{-} > P_s\|\mathbf{u}_j\|^{-})} | \mathbf{x}] \\
&= \prod_{j=1}^{m-1} e^{s}\mathrm{P}(P_m\|\mathbf{x}+\mathbf{u}_j\|^{-} > P_s\|\mathbf{u}_j\|^{-} | \mathbf{x}) + \mathrm{P}(P_s\|\mathbf{u}_j\|^{-} > P_m\|\mathbf{x}+\mathbf{u}_j\|^{-} | \mathbf{x}) \\
&= (A_m(x)e^{s} + (1 - A_m(x)))^{m-1};
\end{aligned}$$

which is the MGF of a Binomial distribution with $(m-1; A_m(x))$. Here, the first step follows from the fact that $\mathbf{u}_j$-s are i.i.d. Similarly for Type 2,

$$\begin{aligned}
\mathrm{E}[e^{sN_{\mathbf{x}}^{\mathrm{ABS};o}} | \mathbf{x}] &= \mathrm{E}\left[\prod_{j=1}^{N_{\mathbf{x}}} \mathrm{E}[e^{s\mathbf{1}(P_m\|\mathbf{x}+\mathbf{u}_j\|^{-} > P_s\|\mathbf{u}_j\|^{-})} | \mathbf{x}]\right] \\
&= \mathrm{E}[(A_m(x)e^{s} + (1 - A_m(x)))^{N_{\mathbf{x}}}] \\
&= \sum_{k=0}^{\infty} (A_m(x)e^{s} + (1 - A_m(x)))^{k} \frac{m^k e^{-m}}{k!} = e^{mA_m(x)(e^{s}-1)};
\end{aligned}$$

which is the MGF of a Poisson distribution with mean $mA_m(x)$. From the PMF of $N_{\mathbf{x}}^{\mathrm{ABS};o}$, one can easily obtain the PMF of $N_{\mathbf{x}}^{\mathrm{ABS}}$. The PMF of $N_{\mathbf{x}}^{\mathrm{SBS}}$ can be obtained on similar lines by altering the inequality in the first step of the above derivation. □

We present the first moments of these two load variables in the following Corollary which will be required for the evaluation of the rate coverage for the average load-based partition and the derivation of easy-to-compute approximations of rate coverage in the sequel.

Corollary 7.6. *The conditional means of $N_{\mathbf{x}}^{\mathrm{ABS}}$ and $N_{\mathbf{x}}^{\mathrm{SBS}}$ given the center of the representative hotspot at $\mathbf{x}$ are*

$$\begin{aligned}
&\text{Type 1: } \mathrm{E}[N_{\mathbf{x}}^{\mathrm{ABS}}] = (m-1)A_m(x) + 1; \mathrm{E}[N_{\mathbf{x}}^{\mathrm{SBS}}] = (m-1)A_s(x) + 1; \\
&\text{Type 2: } \mathrm{E}[N_{\mathbf{x}}^{\mathrm{ABS}}] = mA_m(x) + 1; \mathrm{E}[N_{\mathbf{x}}^{\mathrm{SBS}}] = mA_s(x) + 1.
\end{aligned}$$

We now obtain the PMFs of N_0^{ABS} and N_0^{SBS} in the following Lemma. Note that, since $\mathbf{x}_i$-s are i.i.d., N_0^{ABS} and N_0^{SBS} are independent of $\mathbf{x}$. In what follows, the exact PMF of N_0^{ABS} (N_0^{SBS}) is in the form of $(n-1)$-fold discrete convolution and hence is not computationally efficient beyond very small values of n. We present an alternate easy-to-use expression of this PMF by invoking central limit theorem (CLT). In the numerical results Section, we verify that this approximation is tight even for moderate values of n.

Lemma 7.7. *Given the fact that the typical user belongs to a hotspot at* $\mathbf{x}$*, load on the ABS due to all other* $n-1$ *hotspots is distributed as:* $\frac{N_0^{\text{ABS}} - \mu_m}{\sigma_m} \sim N(0;1)$ *(for large* n*) and sum of the loads on the other SBSs at* $\mathbf{x}_1, \mathbf{x}_2, \ldots, \mathbf{x}_{n-1}$ *is distributed as:* $\frac{N_0^{\text{SBS}} - \mu_s}{\sigma_s} \sim N(0;1)$ *(for large* n*), where* $N(0;1)$ *denotes the standard normal distribution,* $\mu_m = (n-1)m\mathrm{E}[A_m(X)]$; $\mu_s = (n-1)m\mathrm{E}[A_s(X)]$; *and*

$$\begin{aligned}
&\textit{for Type 1,} && \sigma_m^2 = (n-1)\, m\mathrm{E}[A_m(X)A_s(X)] + m^2\mathrm{Var}[A_m(X)] = \sigma_s^2;\\
&\textit{for Type 2,} && \sigma_m^2 = (n-1)\, m\mathrm{E}[A_m(X)] + m^2\mathrm{Var}[A_m(X)]\ ;\\
& && \sigma_s^2 = (n-1)\, m\mathrm{E}[A_s(X)] + m^2\mathrm{Var}[A_s(X)]\ :
\end{aligned}$$

Here,

$$\mathrm{E}[A_m(X)] = \int_0^{R-R_s} A_m(x) f_X(x)\mathrm{d}x;\ \textit{and}$$

$$\mathrm{Var}[A_m(X)] = \int_0^{R-R_s} A_m(x)^2 f_X(x)\mathrm{d}x - (\mathrm{E}[A_m(X)])^2;$$

and $\mathrm{E}[A_s(X)]$, $\mathrm{Var}[A_s(X)]$ *can be similarly obtained by replacing* $A_m(X)$ *with* $A_s(X)$ *in the above expressions.*

Proof. Following the proof of Lemma 7.5, conditioned on the location of a hotspot at $\mathbf{x}_i$, $N_{\mathbf{x}_i}^{\text{ABS}}$ becomes (i) Type 1. a Binomial random variable with $(m; A_m(x_i))$, or (ii) Type 2. a Poisson random variable with $mA_m(x_i)$. Now, $N_0^{\text{ABS}} = \sum_{i=1}^{n-1} \mathrm{E}_{\mathbf{x}_i}[N_{\mathbf{x}_i}^{\text{ABS}}]$, where $\mathrm{E}_{\mathbf{x}_i}[N_{\mathbf{x}_i}^{\text{ABS}}]$-s are i.i.d. with $\mathrm{P}(\mathrm{E}_{\mathbf{x}_i}[N_{\mathbf{x}_i}^{\text{ABS}}] = k) =$

$$\begin{cases}
\int_{R-R_s}^{R} \binom{m}{k} A_m(x_i)^k A_s(x_i)^{m-k} f_X(x_i)\mathrm{d}x_i; & \text{for Type 1}\\
\int_0^{R-R_s} e^{-mA_m(x_i)} \frac{(mA_m(x_i))^k}{k!} f_X(x_i)\mathrm{d}x_i; & \text{for Type 2}
\end{cases};$$

where $k \in \mathbb{Z}^+$. The exact PMF of N_0^{ABS} is obtained by the $(n-1)$-fold discrete convolution of this PMF. We avoid this complexity of the exact analysis by first characterizing the mean and variance of N_0^{ABS} as: $\mu_m = \mathrm{E}[N_0^{\text{ABS}}] = \sum_{i=1}^{n-1} \mathrm{E}[\mathrm{E}_{\mathbf{x}_i}[N_{\mathbf{x}_i}^{\text{ABS}}]] = (n-1)mA_m(X)$, and $\sigma_m^2 =$

$$\begin{aligned}
\mathrm{Var}[N_0^{\text{ABS}}] &\overset{(a)}{=} \sum_{i=1}^{n-1} \mathrm{Var}[\mathrm{E}_{\mathbf{x}_i}[N_{\mathbf{x}_i}^{\text{ABS}}]]\\
&= \sum_{i=1}^{n-1} \mathrm{E}[(\mathrm{E}_{\mathbf{x}_i}[N_{\mathbf{x}_i}^{\text{ABS}}])^2] - (\mathrm{E}[\mathrm{E}_{\mathbf{x}_i}[N_{\mathbf{x}_i}^{\text{ABS}}]])^2\\
&= \begin{cases}
\sum_{i=1}^{n-1} \int_0^{R-R_s} (mA_m(x_i)A_s(x_i) + (mA_m(x_i))^2) f_X(x_i)\mathrm{d}x_i - (m\mathrm{E}[A_m(X)])^2; & \text{for Type 1}\\
\sum_{i=1}^{n-1} \int_0^{R-R_s} (mA_m(x_i) + (mA_m(x_i))^2) f_X(x_i)\mathrm{d}x_i - (m\mathrm{E}[A_m(X)])^2; & \text{for Type 2}
\end{cases};
\end{aligned}$$

where (a) is due to the fact that $\mathsf{E}_{\mathbf{x}_i}[N_{\mathbf{x}_i}^{\mathsf{ABS}}]$-s are i.i.d. The final result follows from some algebraic manipulation. Having derived the mean and variance of N_0^{ABS}, we invoke CLT to approximate the distribution of N_0^{ABS} since it can be represented as a sum of i.i.d. random varables with finite mean and variance. Similar steps can be followed for the distribution of N_0^{SBS}. □

7.3.3 Rate coverage probability

We first define the downlink rate coverage probability (or simply, rate coverage) as follows.

Definition 7.8 (Rate coverage probability)**.** The rate coverage probability of a link with BW W is defined as the probability that the maximum achievable data rate (R) exceeds a certain threshold , i.e., $\mathsf{P}(R >) =$

$$\mathsf{P}\left(W \log_2(1+\mathsf{SNR}) > \right) = \mathsf{P}(\mathsf{SNR} > 2^{ /W} \quad 1). \tag{7.14}$$

Hence, we see that the rate coverage probability is the coverage probability evaluated at a modified SNR-threshold. We now evaluate the rate coverage probability for different backhaul BW partition strategies for a general distribution of $N_{\mathbf{x}_i}$ and $N_{\mathbf{x}}$ in the following Theorem. We later specialize this result for Types 1 and 2 for numerical evaluation.

Theorem 7.9. *The rate coverage probability for a target data rate is given by:*

$$\mathsf{P}_{\mathsf{r}} = \mathsf{P}_{\mathsf{rm}} + \mathsf{P}_{\mathsf{rs}}; \tag{7.15}$$

where P_{rm} (P_{rs}) denotes the ABS rate coverage (SBS rate coverage) which is the probability that the typical user is receiving data rate greater than or equal to and is served by the ABS (SBS). The ABS rate coverage is given by:

$$\mathsf{P}_{\mathsf{rm}} = \int_{1}^{\infty}\int_{0}^{R_{\mathsf{s}}} \mathsf{E}_{N_{\mathbf{x}}^{\mathsf{ABS}}}\left[\mathsf{P}_{\mathsf{cm}}\left(2^{\frac{(t+N_{\mathbf{x}}^{\mathsf{ABS}})}{W_{\mathsf{a}}}} \quad 1 | x\right)\right] f_X(x)\mathrm{d}x \frac{1}{\sigma_{\mathsf{m}}\sqrt{2}} e^{\frac{(t \quad \mu_{\mathsf{m}})^2}{2\sigma_{\mathsf{m}}^2}} \mathrm{d}t. \tag{7.16}$$

The SBS rate coverage depends on the backhaul BW partition strategy. For equal partition,

$$\mathsf{P}_{\mathsf{rs}} = \int_{0}^{R_{\mathsf{s}}} \mathsf{E}_{N_{\mathbf{x}}^{\mathsf{SBS}}}\left[\mathsf{P}_{\mathsf{cs}}\left(2^{\frac{nN_{\mathbf{x}}^{\mathsf{SBS}}}{W_{\mathsf{b}}}} \quad 1; 2^{\frac{N_{\mathbf{x}}^{\mathsf{SBS}}}{W_{\mathsf{a}}}} \quad 1 \; x\right)\right] f_X(x)\mathrm{d}x; \tag{7.17}$$

for instantaneous load-based partition,

$$\mathsf{P}_{\mathsf{rs}} = \int_{1}^{\infty}\int_{0}^{R_{\mathsf{s}}} \mathsf{E}_{N_{\mathbf{x}}^{\mathsf{SBS}}}\left[\mathsf{P}_{\mathsf{cs}}\left(2^{\frac{(N_{\mathbf{x}}^{\mathsf{SBS}}+t)}{W_{\mathsf{b}}}} \quad 1; 2^{\frac{N_{\mathbf{x}}^{\mathsf{SBS}}}{W_{\mathsf{a}}}} \quad 1 \; x\right)\right] f_X(x)\mathrm{d}x \frac{1}{\sigma_{\mathsf{s}}\sqrt{2}} e^{\frac{(t \quad \mu_{\mathsf{s}})^2}{2\sigma_{\mathsf{s}}^2}} \mathrm{d}t; \tag{7.18}$$

and for average load-based partition,

$$\mathsf{P}_{\mathrm{rs}} = \int_{1}^{\infty}\int_{0}^{R_{\mathrm{s}}} \mathsf{E}_{N_{\mathbf{x}}^{\mathrm{SBS}}}\left[\mathsf{P}_{\mathrm{cs}}\left(2^{\frac{N_{\mathbf{x}}^{\mathrm{SBS}}\left(\mathsf{E}[N_{\mathbf{x}}^{\mathrm{SBS}}]+mt\right)}{W_{\mathrm{b}}\mathsf{E}[N_{\mathbf{x}}^{\mathrm{SBS}}]}}-1\right);\right.$$

$$\left.2^{\frac{N_{\mathbf{x}}^{\mathrm{SBS}}}{W_{\mathrm{a}}}}-1\right] x \, f_X(x)\mathrm{d}x \, \frac{e^{-\frac{t-(n-1)\mathsf{E}[A_{\mathrm{s}}(X)]}{2(n-1)\mathrm{Var}[A_{\mathrm{s}}(X)]}^{2}}}{\sqrt{2\pi(n-1)\mathrm{Var}[A_{\mathrm{s}}(X)]}}\mathrm{d}t. \quad (7.19)$$

Proof. First we evaluate $\mathsf{P}_{\mathrm{rm}} = \mathsf{P}_{\mathrm{rm}} = \mathsf{P}(R_{\mathrm{a}}^{\mathrm{ABS}} > \quad) =$

$$\mathsf{P}\left[\frac{W_{\mathrm{a}}}{N_{\mathbf{x}}^{\mathrm{ABS}}+N_{0}^{\mathrm{ABS}}}\log_2(1+\mathrm{SNR}_{\mathrm{a}}^{\mathrm{ABS}}(\mathbf{x}+\mathbf{u})) >\right.$$

$$= \mathsf{P}\left[\mathrm{SNR}_{\mathrm{a}}^{\mathrm{ABS}}(\mathbf{x}+\mathbf{u}) > 2^{\frac{(N_{\mathbf{x}}^{\mathrm{ABS}}+N_{0}^{\mathrm{ABS}})}{W_{\mathrm{a}}}}-1\right.$$

$$= \mathsf{P}_{\mathrm{cm}}\left[2^{\frac{(N_{\mathbf{x}}^{\mathrm{ABS}}+N_{0}^{\mathrm{ABS}})}{W_{\mathrm{a}}}}-1\right.;$$

where, the first step follows from (7.7c). The final form is obtained by deconditioning with respect to $N_{\mathbf{x}}^{\mathrm{ABS}}$, N_{0}^{ABS} and $\mathbf{x}$. Now for equal partition, $\mathsf{P}_{\mathrm{rs}} = \mathsf{P}(R_{\mathrm{a}}^{\mathrm{SBS}} > \quad) =$

$$\mathsf{P}\left[\frac{W_{\mathrm{b}}}{N_{\mathbf{x}}^{\mathrm{SBS}}n}\log_2(1+\mathrm{SNR}_{\mathrm{b}}(\mathbf{x})) > \right] \mathsf{P}\left[\frac{W_{\mathrm{a}}}{N_{\mathbf{x}}^{\mathrm{SBS}}}\log_2(1+\mathrm{SNR}_{\mathrm{a}}^{\mathrm{SBS}}(\mathbf{u})) >\right.$$

$$= \mathsf{P}\left[\mathrm{SNR}_{\mathrm{b}}(\mathbf{x}) > 2^{\frac{nN_{\mathbf{x}}^{\mathrm{SBS}}}{W_{\mathrm{b}}}}-1\right] \mathsf{P}\left[\mathrm{SNR}_{\mathrm{a}}^{\mathrm{SBS}}(\mathbf{u}) > 2^{\frac{N_{\mathbf{x}}^{\mathrm{SBS}}}{W_{\mathrm{a}}}}-1\right]$$

$$= \mathsf{E}\left[\mathsf{P}_{\mathrm{cs}}\left[2^{\frac{nN_{\mathbf{x}}^{\mathrm{SBS}}}{W_{\mathrm{b}}}}-1;2^{\frac{N_{\mathbf{x}}^{\mathrm{SBS}}}{W_{\mathrm{a}}}}-1\right] x\right] :$$

Here step (a) follows from (7.7b) and the fact that the two rate terms appearing under the min operator are independent. The final form is obtained by deconditioning with respect to $N_{\mathbf{x}}^{\mathrm{SBS}}$ and x. For instantaneous load-based partition,

$$\mathsf{P}_{\mathrm{rs}} = \mathsf{P}\left[\frac{W_{\mathrm{b}}}{N_{\mathbf{x}}^{\mathrm{SBS}}+N_{0}^{\mathrm{SBS}}}\log_2(1+\mathrm{SNR}_{\mathrm{b}}(\mathbf{x})) > \right] \mathsf{P}\left[\frac{W_{\mathrm{a}}}{N_{\mathbf{x}}^{\mathrm{SBS}}}\log_2(1+\mathrm{SNR}_{\mathrm{a}}^{\mathrm{SBS}}(\mathbf{u})) >\right.$$

$$= \mathsf{P}\left[\mathrm{SNR}_{\mathrm{b}}(\mathbf{x}) > 2^{\frac{(N_{\mathbf{x}}^{\mathrm{SBS}}+N_{0}^{\mathrm{SBS}})}{W_{\mathrm{b}}}}-1\right] \mathsf{P}\left[\mathrm{SNR}_{\mathrm{a}}^{\mathrm{SBS}}(\mathbf{u}) > 2^{\frac{N_{\mathbf{x}}^{\mathrm{SBS}}}{W_{\mathrm{a}}}}-1\right]$$

$$= \mathsf{E}\left[\mathsf{P}_{\mathrm{cs}}\left[2^{\frac{(N_{\mathbf{x}}^{\mathrm{SBS}}+N_{0}^{\mathrm{SBS}})}{W_{\mathrm{b}}}}-1;2^{\frac{N_{\mathbf{x}}^{\mathrm{SBS}}}{W_{\mathrm{a}}}}-1\right] x\right] :$$

The final form is obtained by deconditioning with respect to $N_{\mathbf{x}}^{\mathrm{SBS}}$, N_{0}^{SBS} and x. For average load-based partition, $\mathsf{P}_{\mathrm{rs}} =$

7.3. Rate coverage probability analysis

$$\mathsf{P}\left(\frac{W_{\mathrm{b}}\mathsf{E}[N_{\mathbf{x}}^{\mathrm{SBS}}]}{N_{\mathbf{x}}^{\mathrm{SBS}}(\mathsf{E}[N_{\mathbf{x}}^{\mathrm{SBS}}]+\sum_{i=1}^{n-1}\mathsf{E}[N_{\mathbf{x}_i}^{\mathrm{SBS}}])}\log_2(1+\mathrm{SNR}_{\mathrm{b}}(\mathbf{x}))>\right.$$
$$\left.\mathsf{P}\left(\frac{W_{\mathrm{a}}}{N_{\mathbf{x}}^{\mathrm{SBS}}}\log_2(1+\mathrm{SNR}_{\mathrm{a}}^{\mathrm{SBS}}(\mathbf{u}))>\right)\right.$$
$$=\mathsf{P}\left(\frac{W_{\mathrm{b}}\mathsf{E}[N_{\mathbf{x}}^{\mathrm{SBS}}]}{N_{\mathbf{x}}^{\mathrm{SBS}}(\mathsf{E}[N_{\mathbf{x}}^{\mathrm{SBS}}]+m\sum_{i=1}^{n-1}A_{\mathrm{s}}(x_i))}\log_2(1+\mathrm{SNR}_{\mathrm{b}}(\mathbf{x}))>\right.$$
$$\left.\mathsf{P}\left(\frac{W_{\mathrm{a}}}{N_{\mathbf{x}}^{\mathrm{SBS}}}\log_2(1+\mathrm{SNR}_{\mathrm{a}}^{\mathrm{SBS}}(\mathbf{u}))>\right)\right;$$

where the last step is obtained by using the fact that $\mathsf{E}[N_{\mathbf{x}_i}^{\mathrm{SBS}}]=m\mathsf{E}[A_{\mathrm{s}}(X)]$ and $\mathsf{E}[N_{\mathbf{x}}^{\mathrm{SBS}}]$ depends on the underlying distribution of $N_{\mathbf{x}}$. Since the random variable $\sum_{i=1}^{n-1}A_{\mathrm{s}}(x_i)$ is a summation of $n-1$ i.i.d. random variables with mean $(n-1)\mathsf{E}[A_{\mathrm{s}}(X)]$ and variance $(n-1)\mathrm{Var}[A_{\mathrm{s}}(X)]$, we again invoke CLT instead of resorting to the exact expression that would have involved the $(n-1)$-fold convolution of the PDF of $A_{\mathrm{s}}(X)$. □

Note that the key enabler of the expression of P_{r} in Theorem 7.9 is the fact that the system is considered to be noise-limited. Including the SBS interference into analysis is not straightforward from this point since it would involve coupling between the coverage probability and load since both are dependent on the locations of the other $n-1$ SBSs. Having derived the exact expressions of rate coverage in Theorem 7.9, we present approximations of these expressions by replacing (i) $N_{\mathbf{x}}^{\mathrm{ABS}}$ in P_{rm} with its mean $\mathsf{E}[N_{\mathbf{x}}^{\mathrm{ABS}}]$, and (ii) $N_{\mathbf{x}}^{\mathrm{SBS}}$ in P_{rs} with its mean $\mathsf{E}[N_{\mathbf{x}}^{\mathrm{SBS}}]$ in the following Lemma.

Lemma 7.10. *The ABS rate coverage can be approximated as*

$$\mathsf{P}_{\mathrm{rm}}=\int_{1}^{\infty}\int_{0}^{R_{\mathrm{s}}}\mathsf{P}_{\mathrm{cm}}\left(2^{\frac{(t+\mathsf{E}[N_{\mathbf{x}}^{\mathrm{ABS}}])}{W_{\mathrm{a}}}}-1|x\right)f_X(x)\mathrm{d}x\frac{e^{\frac{(t-m)^2}{2\sigma_{\mathrm{m}}^2}}}{\sigma_{\mathrm{m}}\sqrt{2\pi}}\mathrm{d}t. \tag{7.20}$$

The SBS rate coverage can be approximated as follows. For equal partition,

$$\mathsf{P}_{\mathrm{rs}}=\int_{0}^{R_{\mathrm{s}}}\mathsf{P}_{\mathrm{cs}}\left(2^{\frac{n\mathsf{E}[N_{\mathbf{x}}^{\mathrm{SBS}}]}{W_{\mathrm{b}}}}-1;2^{\frac{\mathsf{E}[N_{\mathbf{x}}^{\mathrm{SBS}}]}{W_{\mathrm{a}}}}-1\,x\right)f_X(x)\mathrm{d}x; \tag{7.21}$$

for instantaneous load-based partition,

$$\mathsf{P}_{\mathrm{rs}}=\int_{1}^{\infty}\int_{0}^{R_{\mathrm{s}}}\mathsf{P}_{\mathrm{cs}}\left(2^{\frac{(\mathsf{E}[N_{\mathbf{x}}^{\mathrm{SBS}}]+t)}{W_{\mathrm{b}}}}-1;2^{\frac{\mathsf{E}[N_{\mathbf{x}}^{\mathrm{SBS}}]}{W_{\mathrm{a}}}}-1\,x\right)f_X(x)\mathrm{d}x\frac{e^{\frac{(t-s)^2}{2\sigma_{\mathrm{s}}^2}}}{\sigma_{\mathrm{s}}\sqrt{2\pi}}\mathrm{d}t; \tag{7.22}$$

Table 7.1: Key system parameters

Notation	Parameter	Value
P_m; P_s	BS transmit powers	50, 20 dBm
$_L$; $_{NL}$	Path-loss exponent	2.0, 3.3
	Path loss at 1 m	70 dB
G	Main lobe gain	18 dB
	LOS range constant	170 m
N_0W	Noise power	-174 dBm/Hz+ $10\log_{10}W$ +10 dB (noise-figure)
$m_L; m_{NL}$	Parameter of Nakagami distribution	2, 3
R, R_s	Macrocell and hotspot radius	200 m, 30 m
m	Average number of users per hotspot	5
	Rate threshold	50 Mbps

and for average load-based partition,

$$P_{rs} = \int_1^{\infty}\int_0^{R_s} P_{cs}\left(2^{\frac{\left(E[N_x^{SBS}]+mt\right)}{W_b}}-1;2^{\frac{E[N_x^{SBS}]}{W_a}}-1\right) x\, f_X(x)dx \frac{e^{\frac{t-(n-1)E[A_s(X)]}{2(n-1)Var[A_s(X)]}^2}}{\sqrt{2\pi(n-1)Var[A_s(X)]}}dt. \tag{7.23}$$

We now specialize the result of Theorem 7.9 for Types 1 and 2 in the following Corollaries.

Corollary 7.11. *For* Type 1*, i.e., when* $N_{x_i} = m$*,* $\forall\, i = 1,\ldots,n$*, the ABS rate coverage is*

$$P_{rm} = \sum_{k=1}^{m}\binom{m}{k}\int_1^{\infty}\int_0^{R_s} P_{cm}\left(2^{\frac{(t+k)}{W_a}}-1|x\right) A_m(x)^k\,{}^{-1}A_s(x)^{m-k} f_X(x)dx \frac{1}{\sqrt{2\pi}\sigma_m} e^{-\frac{(t-m)^2}{2\sigma_m^2}}dt. \tag{7.24}$$

The SBS rate coverages for the three backhaul BW parition strategies are expressed as follows.
(i) For equal partition,

$$P_{rs} = \sum_{k=1}^{m}\binom{m}{k}\int_0^{R_s} P_{cs}\left(2^{\frac{nk}{W_b}}-1;2^{\frac{k}{W_a}}-1\right) x\, A_s(x)^k\,{}^{-1}A_m(x)^{m-k} f_X(x)dx; \tag{7.25}$$

(ii) for instantaneous load-based partition,

$$P_{rs} = \sum_{k=1}^{m} \binom{m}{k} \int_{1}^{\infty} \int_{0}^{R_s} P_{cs}\left(2^{\frac{(k+t)}{W_b}} - 1; 2^{\frac{k}{W_a}} - 1, x\right) A_s(x)^k (1 - A_m(x))^{m-k} f_X(x) dx \frac{e^{-\frac{(t-\mu_s)^2}{2\sigma_s^2}}}{\sigma_s\sqrt{2\pi}} dt; \quad (7.26)$$

and (iii) for average load-based partition,

$$P_{rs} = \sum_{k=1}^{m} \binom{m}{k} \int_{1}^{\infty} \int_{0}^{R_s} P_{cs}\left(2^{\frac{k(1+(m-1)A_s(x)+mt)}{W_b(1+(m-1)A_s(x))}} - 1; 2^{\frac{k}{W_a}} - 1, x\right) A_s(x)^k (1 - A_m(x))^{m-k} f_X(x) dx \frac{e^{-\frac{t-(n-1)\mathrm{E}[A_s(X)]^2}{2(n-1)\mathrm{Var}[A_s(X)]}}}{\sqrt{2\pi(n-1)\mathrm{Var}[A_s(X)]}} dt. \quad (7.27)$$

Proof. The result can be obtained from Theorem 7.9 by using the PMFs of $N_{\mathbf{x}}^{\mathrm{ABS}}$, $N_{\mathbf{x}}^{\mathrm{SBS}}$, N_o^{ABS} and N_o^{ABS} from Lemmas 7.5 and 7.7 and substituting $\mathrm{E}[N_{\mathbf{x}}^{\mathrm{SBS}}]$ from Corollary 7.6 for Type 1. □

Corollary 7.12. *For* Type 2, *i.e., when* $N_{\mathbf{x}_i} \overset{i.i.d.}{\sim}$ Poisson(m), *$\forall$ $i = 1, \ldots, n$, the ABS rate coverage is expressed as*

$$P_{rm} = \sum_{k=1}^{\infty} \frac{m^{k-1}}{(k-1)!} \int_{1}^{\infty} \int_{0}^{R_s} (A_m(x))^{k-1} e^{-mA_m(x)} P_{cm}\left(2^{\frac{(t+k)}{W_a}} - 1 | x\right) f_X(x) dx \frac{1}{\sigma_m\sqrt{2\pi}} e^{-\frac{(t-\mu_m)^2}{2\sigma_m^2}} dt. \quad (7.28)$$

The SBS rate coverages for the three backhaul BW parition strategies are expressed as follows. (i) For equal partition,

$$P_{rs} = \sum_{k=1}^{\infty} \frac{m^{k-1}}{(k-1)!} \int_{0}^{R_s} (A_s(x))^{k-1} e^{-mA_s(x)} P_{cs}\left(2^{\frac{nk}{W_b}} - 1; 2^{\frac{k}{W_a}} - 1, x\right) f_X(x) dx; \quad (7.29)$$

(ii) for instantaneous load-based partition,

$$P_{rs} = \sum_{k=1}^{\infty} \frac{m^{k-1}}{(k-1)!} \int_{1}^{\infty} \int_{0}^{R_s} (A_s(x))^{k-1} e^{-mA_s(x)} P_{cs}\left(2^{\frac{(k+t)}{W_b}} - 1; 2^{\frac{k}{W_a}} - 1, x\right) f_X(x) dx \frac{1}{\sigma_s\sqrt{2\pi}} e^{-\frac{(t-\mu_s)^2}{2\sigma_s^2}} dt; \quad (7.30)$$

and (iii) for average load-based partition,

$$\mathsf{P}_{\mathsf{rs}} = \sum_{k=1}^{n} \frac{m^k}{(k-1)!} \int_{1}^{\infty} \int_{0}^{R_s} (A_s(x))^k e^{-mA_s(x)} \mathsf{P}_{\mathsf{cs}}\left(2^{\frac{k(1+mA_s(x)+mt)}{W_b(1+mA_s(x))}} - 1; 2^{\frac{k}{W_a}} - 1\right) f_X(x)\mathrm{d}x \, p_{\frac{1}{2}}(n-1)\mathrm{Var}[A_s(X)] \, e^{-\frac{t-(n-1)\mathrm{E}[A_s(X)]^2}{2(n-1)\mathrm{Var}[A_s(X)]}} \mathrm{d}t. \quad (7.31)$$

Proof. The result can be similarly obtained from Theorem 7.9 by using the PMFs of $N_{\mathbf{x}}^{\mathsf{ABS}}$, $N_{\mathbf{x}}^{\mathsf{SBS}}$, N_0^{ABS} and N_0^{ABS} from Lemmas 7.5 and 7.7, and substituting $\mathsf{E}[N_{\mathbf{x}}^{\mathsf{SBS}}]$ from Corollary 7.6 for Type 2. □

7.4 Results and discussion

7.4.1 Trends of rate coverage

In this Section we verify the accuracy of our analysis of rate coverage with Monte Carlo simulations of the network model delineated in Section 9.4.1 with parameters listed in Table 8.1. For each simulation, the number of iterations was set to 10^6. Since P_r fundamentally depends upon SNR, we first plot the cumulative density function (CDF) of SNRs without beamforming in Fig. 7.5, averaged over user locations. Precisely we plot $\mathsf{E}_{\mathbf{x}}\left[\mathsf{P}\left[\frac{h_m P_m k x^{-k}}{\mathsf{N}_0 W} < \tau\right]\right] = \int_0^{R_s} \mathsf{P}_{\mathsf{cm}}(\tau x) f_X(x)\mathrm{d}x$ and $\mathsf{E}_{\mathbf{u}}\left[\mathsf{P}\left[\frac{h_s P_s k u^{-k}}{\mathsf{N}_0 W} < \tau\right]\right] = \mathsf{P}_{\mathsf{cs}}(\beta_1 \tau, \beta_2 \tau)$, where P_{cm} and P_{rs} were defined in Theorem 7.4 from simulation and using our analytical results and observe a perfect match. We now plot the rate coverages for different user distributions (Types 1 and 2) for three different backhaul BW partition strategies in Figs. 7.4a-7.4c. Recall that one part of ABS and SBS load was approximated using CLT in Lemma 7.7 for efficient computation. Yet, we obtain a perfect match between simulation and analysis even for $n = 10$ for Type 1 and Type 2. Further, we observe that, (i) $\mathsf{P}_\mathsf{r} = 0$ for $\beta = 1$ since this corresponds to the extreme when no BW is given to access links, and (ii) the rate coverage is maximized for a particular access-backhaul BW split ($\beta^* = \arg\max_{\beta} \mathsf{P}_\mathsf{r}$). Also note that the rate coverage trends for Types 1 and 2 are the same, although P_r for Type 1 is slightly higher than P_r of Type 2 since the representative cluster, on average, has more number of users in Type 2 than in Type 1 (see Corollary 7.6). However, for space constraint, we only present the results of Type 1 for subsequent discussions.

Comparison of backhaul BW partition strategies

In Fig. 7.6, we overlay P_r for three different backhaul BW partition strategies. We observe that the maximum rate coverage, $\mathsf{P}_\mathsf{r}^* = \mathsf{P}_\mathsf{r}(\beta^*)$ (marked as '*' in the figures) for instantaneous load-based partition dominates P_r in average load-based partition, and P_r in

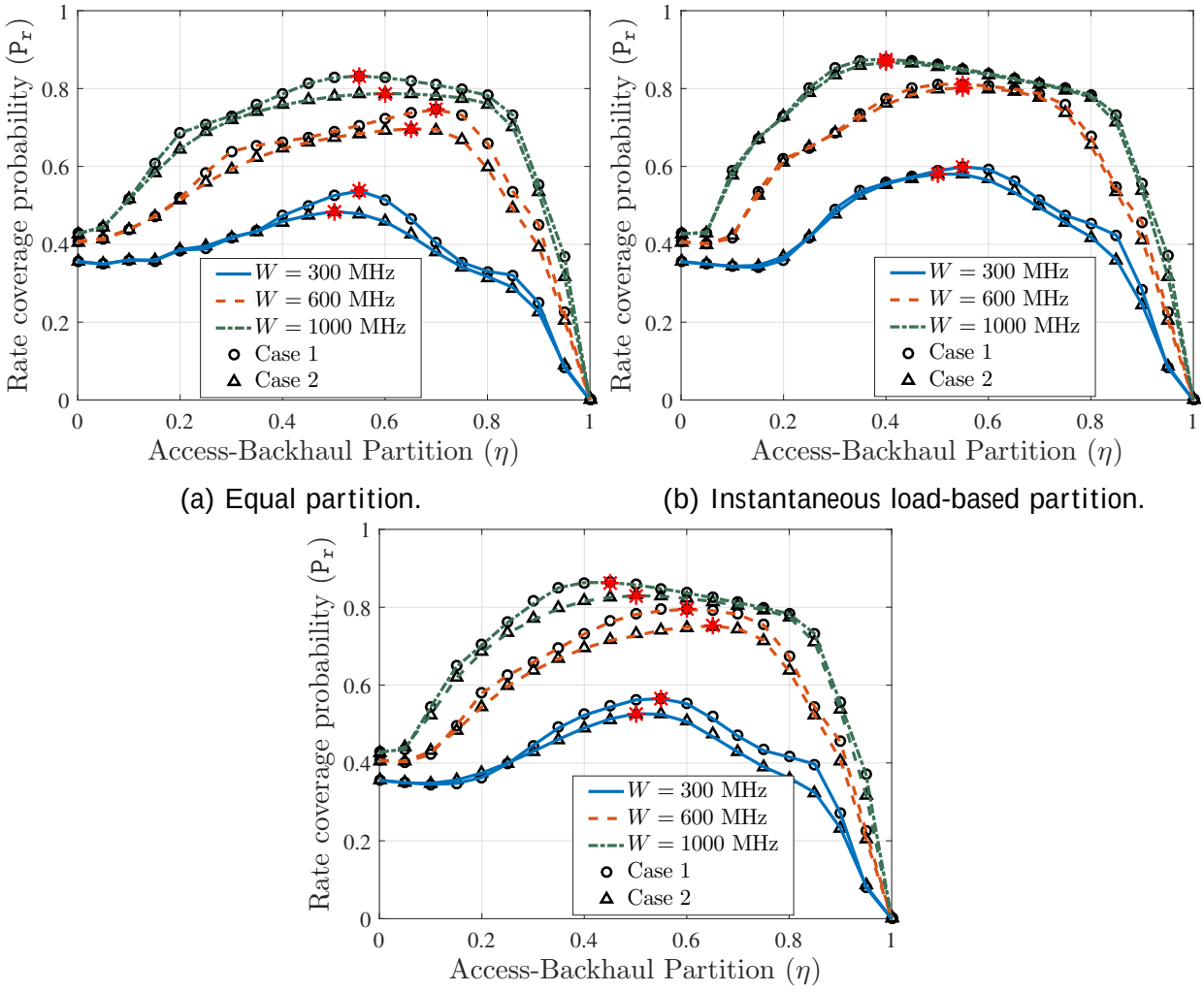

(a) Equal partition.

(b) Instantaneous load-based partition.

(c) Average load-based partition.

Figure 7.4: Rate coverage probability for different bandwidths (= 50 Mbps, n = 10) for Types 1 and 2 obtained by Corollaries 7.11 and 7.12. Lines and markers indicate theoretical and simulation results, respectively. Theoretical results for Types 1 and 2 are obtained from Corollaries 7.11 and 7.12, respectively.

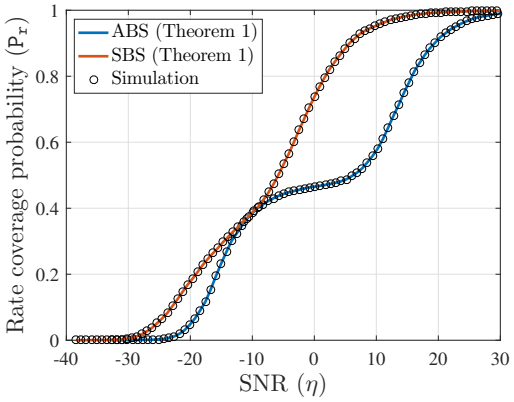

Figure 7.5: The CDF plot of SNR from the ABS and SBS (P_{m} = 50 dBm, P_{s} = 20 dBm). The markers indicate empirical CDF obtained from Monte Carlo simulations.

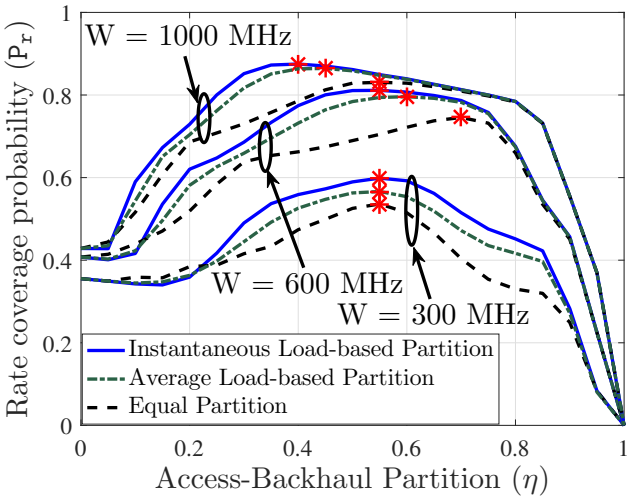

Figure 7.6: Comparison of backhaul partition strategies for Type 1 (= 50 Mbps, n = 10).

7.4. Results and discussion

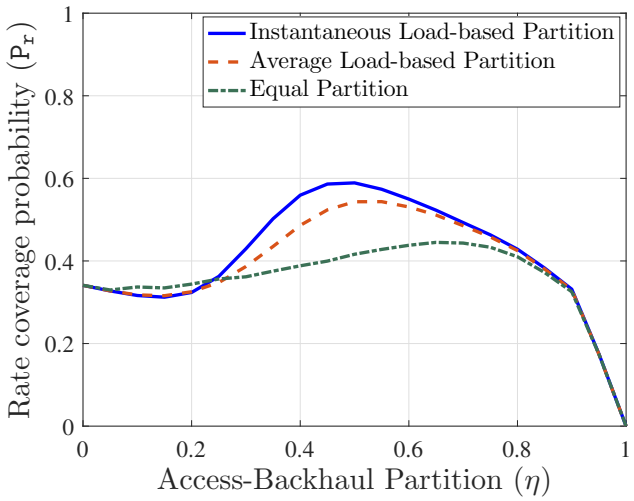

Figure 7.7: Comparision of backhaul BW parition strategies (= 50 Mbps, n = 10, W = 600 MHz) for Type 1 and = 30 m. The results are obtained from Corollary 7.11.

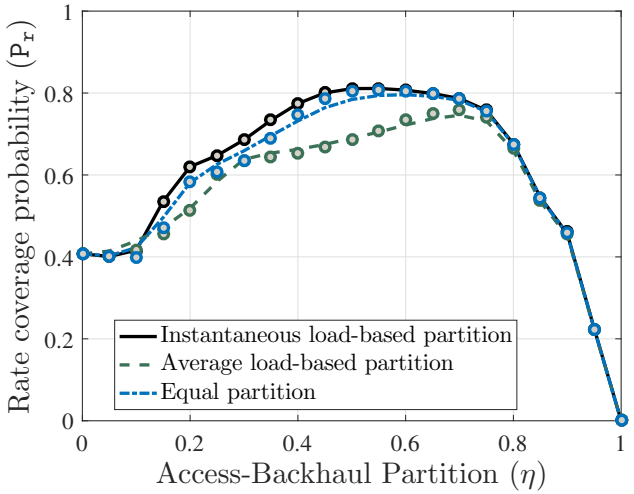

Figure 7.8: Comparison of the exact expression (Corollary 7.11) and approximate expression (Lemma 7.10) of rate coverage probability for Type 1 (= 50 Mbps, W = 600 MHz, n = 10). Lines and markers indicate exact and approximate results, respectively.

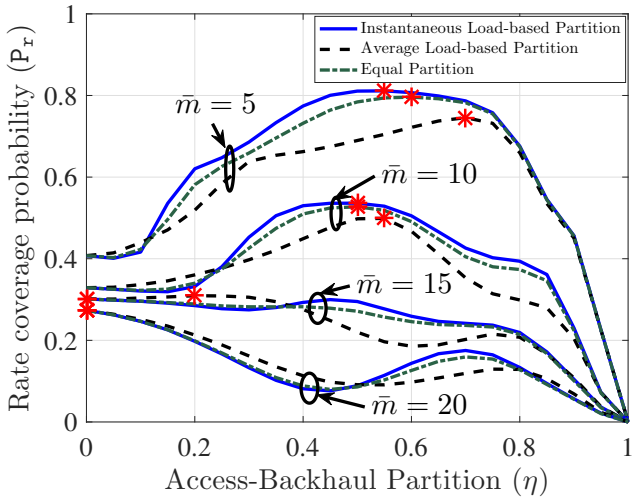

Figure 7.9: Rate coverage for different numbers of users per hotspot for Type 1 (W = 600 MHz, = 50 Mbps). The values of $\mathsf{P_r}$ are computed using Lemma 7.10.

average load-based partition dominates $\mathsf{P_r}$ in equal partition. Also note that is different for different combination of BW partition strategy and W. We further compared these three strategies in a high blocking environment in Fig. 7.7 by setting = 30 m and observe the same ordering of performance of the three strategies. As expected, $\mathsf{P_r}$ is in general lower for this case. That said, it should be kept in mind that instantaneous load-based partition requires more frequent feedback of the load information from the SBSs and hence has the highest signaling overhead among the three strategies. The average load-based partition requires comparatively less signaling overhead since it does not require frequent feedback. On the other hand, equal partition does not have this overhead at all. This motivates an interesting performance-complexity trade-off for the design of cellular networks with IAB.

Effect of system BW

We observe the effect of increasing system BW on rate coverage in Fig 7.6. As expected, $\mathsf{P_r}$ increases as W increases. However, the increment of $\mathsf{P_r}$ saturates for very high values of W since high noise power degrades the link spectral efficiency. Another interesting observation is that starting from = 0 to , $\mathsf{P_r}$ does not increase monotonically. This is due to the fact that sufficient BW needs to be steered from access to backhaul so that the network with IAB performs better than the macro-only network (corresponding to = 0).

Accuracy of approximation

We now plot $\mathsf{P_r}$ obtained by the approximations in Lemma 7.10 in Fig. 7.8. It is observed that the approximation is surprisingly close to the exact values of $\mathsf{P_r}$ obtained by Corollary 7.11. Motivated by the tightness of the approximation, we proceed with the easy-to-compute expressions of $\mathsf{P_r}$ obtained by Lemma 7.10 instead of the exact expressions

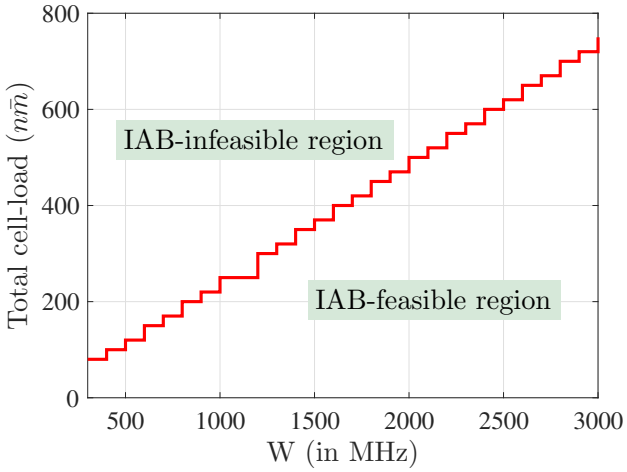

Figure 7.10: Total cell-load upto which IAB-enabled network outperforms macro-only network (for instantaneous load-based partition).

(Corollary 7.11) for the metrics evaluated in the sequel, namely, critical load, median rate, and 5^{th} percentile rate. It is important to note that each numerical evaluation of these metrics requires high number of computations of P_r and is highly inefficient if P_r is computed by simulation, which further highlights the importance of analytical expressions derived in this chapter.

7.4.2 Critical load

We plot the variation of P_r with m in Fig. 7.9. We observe that as m increases, more number of users share the BW and as a result, P_r decreases. However, the optimality of P_r completely disappears for very large value of m ($10 < m < 20$ in this case). This implies that for given BW W there exists a *critical total cell-load* (nm) beyond which the gain obtained by the IAB architecture completely disappears. Observing Fig. 7.10, we find that the critical total cell-load varies linearly with the system BW. The reason of the existence of the critical total cell-load can be intuitively explained as follows. Recall that the SBS rate R_a^{SBS} was limited by the backhaul constraint R_b^{ABS}=N_x^{SBS}. When m is high, N_x^{SBS} is also high and this puts stringent backhaul constraint on R_a^{SBS}. Hence, an ABS can serve more users by direct macro-links at the target rate instead of allocating any backhaul partition.

7.4.3 Median and 5^{th} percentile rates

We now shift our attention to two more performance metrics of interest, the median (50^{th} percentile) and 5^{th} percentile rate, which are denoted as $_{50}$ and $_{95}$, respectively. These rates are defined as the values where the rate CDF attains 0.5 and 0.05, respectively, i.e., $P_r = 0.5$ at $= _{50}$ and $P_r = 0.95$ at $= _{95}$. Figs. 7.11 and 7.12 illustrate $_{50}$ and $_{95}$

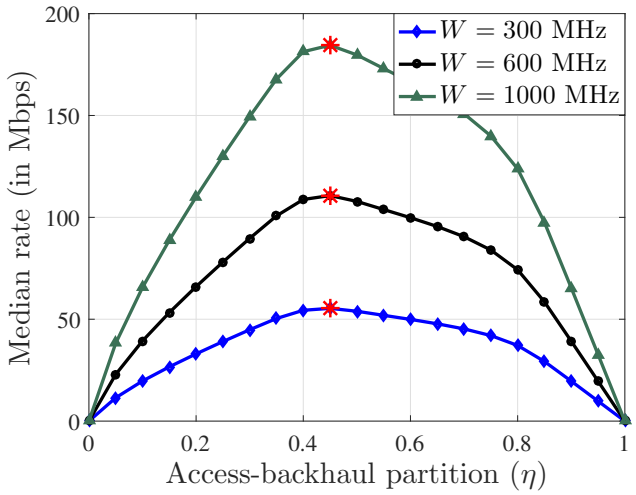

Figure 7.11: Median rate for Type 1 for instantaneous load-based partition (n = 10).

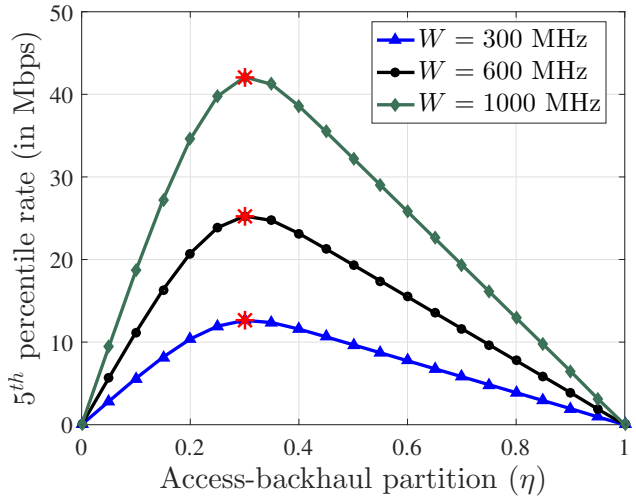

Figure 7.12: 5^{th} percentile rate for Type 1 for instantaneous load-based partition (n = 10).

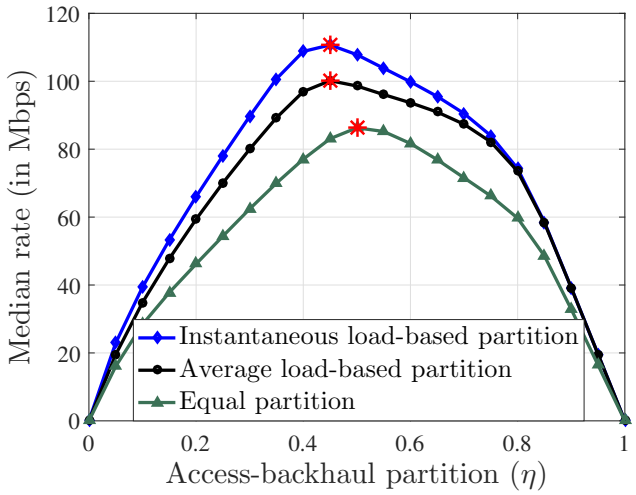

Figure 7.13: Median rate for Type 1 for different backhaul BW partition strategies (n = 10, W = 600 MHz).

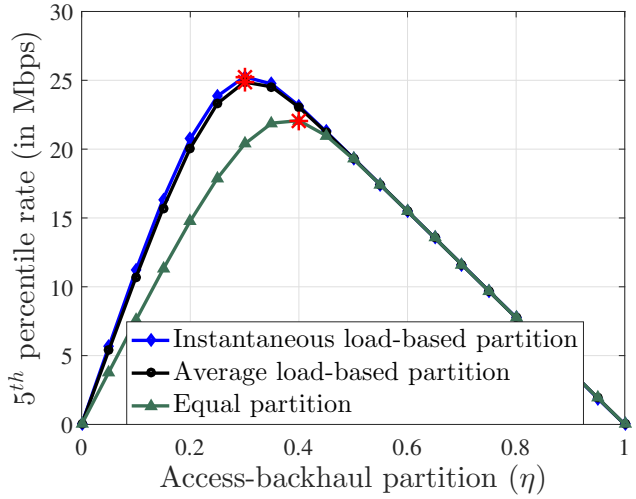

Figure 7.14: 5^{th} percentile rate for Type 1 for different backhaul BW partition strategies (n = 10, W = 600 MHz).

respectively for different W. We first observe that for a given , these rates increase linearly with W. This is because of the fact that in all the expressions of rate coverage, and W appear as a ratio ($=W$). Thus, once we find a desired rate coverage at a particular for a given W, same rate coverage will be observed for kW at target data rate k (where k is a positive constant). Further, we notice that the median rate is relatively flat around the maximum compared to the 5^{th} percentile rate. Also, the optimal does not vary significantly (stays close to 0.4 in our setup) for median and 5^{th} percentile rates. In Figs. 7.13 and 7.14, we have compared the three backhaul BW partition strategies in terms of these two rates. As expected, the ordering in performance is similar to the one observed for P_r . Interestingly, from Fig. 7.14, it appears that the average and instantaneous load-based partition policies have almost similar performance in terms of 5^{th} percentile rate. This is because of the fact that $_{95}$ is towards the tail of the rate distribution which is not significantly affected by difference between instantaneous or average load. However, the performance gap becomes prominent once median rate is considered.

7.5 Summary

In this chapter, we proposed the first 3GPP-inspired analytical framework for two-tier mm-wave HetNets with IAB and investigated three backhaul BW partition strategies. In particular, our model was inspired by the spatial configurations of the users and BSs considered in 3GPP simulation models of mm-wave IAB, where the SBSs are deployed at the centers of user hotspots. Under the assumption that the mm-wave communication is noise limited, we evaluated the downlink rate coverage probability. As a key intermediate step, we characterized the PMFs of load on the ABS and SBS for two different user distributions per hotspot. Our analysis leads to two important system-level insights: (i) for three performance metrics namely, downlink rate coverage probability, median rate, and 5^{th} percentile rate, the existence of the optimal access-backhaul bandwidth partition splits for which the metrics are maximized, and (ii) maximum total cell-load that can be supported using the IAB architecture.

8

Load Balancing in Integrated Access and Backhaul

8.1 Introduction

Aggressive frequency reuse achieved through network densification is regarded as one of the most effective ways of increasing network capacity. The introduction of low power SBSs has made it possible, in principle, to implement this at large scale in cellular networks. Despite all the promising gains, the number of SBSs actually deployed in practice has lagged the market estimates [133]. This is a direct consequence of the challenges involved in providing reliable backhaul to tens of thousands of these SBSs. While it is not viable to connect all the SBSs to the network core with the traditional fiber backhaul, the wireless backhaul solutions have not also been widely adopted due to the spectrum shortage at sub-6 GHz. However, thanks to the availability of huge spectrum in mm-wave, it is possible to achieve fiber-like performance on the MBS-SBS backhaul links while keeping sufficient bandwidth for the base station (BS)-user access links. Further, the access and backhaul networks can be tightly integrated to manage the dynamic traffic demand of the HetNet by proper resource partitioning within the access and backhaul links [21, 24, 134]. This IAB architecture introduces several new modeling aspects which were not present in the conventional HetNet models with no backhaul constraints on the SBSs. For instance, the end-user data rate is affected by the rate achievable on the wireless backhaul links and the number of users and SBSs sharing the available BW which is significantly different from the number of users served by the BSs (also known as the *load* on the BSs) in the conventional networks. In this chapter, we capture these unique IAB characteristics by designing the first stochastic geometry-based multi-cell framework for a two-tier IAB-enabled mm-wave network where the MBSs serve the users and SBSs from the same pool of spectral resources. Using this framework, we seek the answers to the following questions: (i) Should the resources be split between access and backhaul *a priori* or allocated dynamically based on the load? (ii) How do the data rates change with network densification under backhaul constraints imposed by IAB? and (iii) How effective is offloading traffic from MBSs to SBSs in an IAB setting?

8.1.1 Background and related works

Due to the availability of huge bandwidth and the use of noise-limited directional transmission in mm-wave, 5G is envisioning the integration of mm-wave wireless backhaul net-

work and RAN such that the same spectral resources and infrastructure could be used for both [112]. This emerging IAB architecture has motivated a lot of recent research activities, such as finding optimal routing and scheduling strategies in a mm-wave IAB network [135–137], end-to-end network simulator design [138], and finding optimal user association schemes for HetNets with IAB [139]. The existing works on IAB mostly ignore the effect of network topology and its interplay with user traffic, which collectively have a significant impact on the signal-to-interference-and-noise-ratios (SINRs) of access and backhaul links as well as the loads on different BSs. Such spatial interactions can be naturally captured by stochastic geometry-based models [21], where the BS and user locations are modeled as point processes, most commonly the Poisson point processes (PPPs). These models have yielded tractable expressions of network performance metrics such as coverage [55, 140], cell load [141] and rate [24, 57] for sub-6 GHz networks. However, most of the prior works in this direction focus on the access network performance without incorporating any backhaul capacity constraints. Some notable works that do include backhaul constraints are [126–128, 130, 131, 142], where [127, 128, 130, 131, 142] characterize the network performance in terms of data rate and [126] in terms of delay.

These stochastic geometry-based models, initially applied to sub-6 GHz networks, have been extended to the coverage analysis for mm-wave networks [113–115]. However, none of these works consider the impact of limited backhaul capacity (of which IAB is a special case). In fact, the stochastic geometry-based models for mm-wave IAB are quite sparse with [129, 134] being the only notable related works. While [134] focused on a single macro cell of a two-tier mm-wave IAB, [129] presents a stochastic geometry-based multi-cell model of a *single-tier* mm-wave IAB, where the BSs and users are distributed as PPPs. As will be evident in the sequel, none of these models is sufficient to analyze the rate performance of IAB in a mm-wave mutli-cell *multi-tier* network. In particular, the aspects of load balancing, which is one of the key flexibilities of HetNets [24], has never been studied in a multi-cell IAB-enabled HetNet setting.

Before we state our main contributions, it would be instructive to discuss the fundamental challenges involved in developing an analytical framework for mm-wave IAB-enabled HetNets. First, to evaluate the coverage probabilities, we need to consider the joint SINR statistics for the SBS-user access link and SBS-MBS backhaul link which is difficult to do in any stochastic geometry setup in general. Second, instead of SINR-based coverage, rate is a more meaningful metric for the performance evaluation of IAB for which one needs to take into account both the SINR and the cell loads. Now the load modeling requires the characterization of the association cells of the BSs which in mm-waves are fundamentally different from the relatively well-understood association cells in the sub-6 GHz due to the sensitivity of mm-wave propagation to blockages. The existing approach for blockage modeling is to assume that each link undergoes independent blocking. This simple assumption turns out to be reasonably accurate (especially when the blockages are not too big) for the characterization of SINR distribution of a typical receiver, or the coverage probability [29]. Since this assumption facilitates analytical tractability, the follow-up works on mm-wave

networks, including the prior arts on rate analyses in mm-wave networks [116,119,129], tend to simply accept the independent blocking as a *de facto* model for blocking. However, this assumption may not lead to a meaningful characterization of mm-wave association cells and hence the load served by different BSs. For instance, by ignoring this correlation, two adjoining points in space may be assigned to the cells of two different BSs, thus resulting in association cells that deviate significantly from reality. Therefore, for the association cells, we need to jointly consider the blocking statistics for adjacent points which is likely to have some spatial correlation. While this spatial correlation can be introduced by considering some spatial distribution of blockages [114], it induces tremendous complexity in computing the link state between any transmitter and receiver (line-of-sight (LOS) or non-LOS (NLOS)) and is neglected in all analytical and even most of the 3GPP simulation models [143]. Therefore, a tractable and reasonably accurate approach to rate analysis needs to revisit such assumptions for different components of the analysis, while making sure that the resulting constructs remain physically meaningful. Constructing such an approach is the main focus of this chapter.

8.1.2 Contributions

Tractable model for IAB-enabled mm-wave HetNet. A tractable and realistic model is developed for the study of the rate performances in IAB-enabled HetNet operating in mm-wave. We assume that only the MBSs are provided with fiber backhaul and the SBSs are wirelessly backhauled by the MBSs over mm-wave links. For this IAB setting, we derive the rate coverage, or equivalently, the CCDF of the downlink data rate perceived by a user equipment (UE) for two resource partition strategies at the MBS: (a) *IRA:* where the total BW is dynamically split between access and backhaul, and (b) *ORA:* where a static partition is defined for the access and backhaul communications. Since this chapter deals with the rate analysis, we start with a germ-grain model of blockages and apply the well-accepted assumption of independent exponential blocking for deriving the SINR distributions. Under this assumption, we are able to characterize the joint distribution of the SINRs of the access and backhaul link when the typical UE associates to the SBS. We then leverage the property of the stationarity of the BS, UE and the blockage distributions to characterize the association cells. In particular, the association cells in our two-tier HetNet model are stationary partitions which enable the characterization of their mean areas. Using these results, we then characterize the loads served by the BSs of two tiers for IRA and ORA, which lead to tractable expressions of rate coverage for the two strategies.

System design insights. Using this model, we obtain the following insights.

(i) As expected, the BW split between access and backhaul links has a significant impact on the performance of ORA. Our numerical results indicate that there exists an optimum BW split for which the rate coverage is maximized. As SBS density increases, the optimal split claims more BW to be dedicated to the backhaul links.

(ii) The two-tier IAB network performs better than the single-tier macro-only network but significantly worse than a two-tier network with fiber-backhauled SBSs. Moreover, offloading users from MBSs to SBSs does not yield significant rate improvement as observed in a two-tier HetNet with fiber-backhauled SBSs. This is because the UEs offloaded to SBSs are actually coming back to the MBS through the increased backhaul load due to self-backhauling.

(iii) While the rate coverages and median rates improve steadily with SBS density for a two-tier HetNet with fiber-backhauled SBSs, these metrics quickly saturate with increasing SBS density for an IAB setting because of the capacity bottleneck of the wireless backhaul links. This result indicates that the capacity gains of HetNets are significantly overestimated if no constraint on the SBS backhaul is considered.

8.2 System model

In this Section, we describe the two-tier HetNet setup and define the rate coverage probability.

8.2.1 BS and user locations

We consider a two-tier HetNet where the MBSs and SBSs are distributed in R^2 according to independent homogeneous PPPs $_m$ and $_s$ with densities $_m$ and $_s$, respectively. All BSs are assumed to operate in mm-wave regime. The UEs are assumed to be distributed according to a homogeneous PPP $_u$ with intensity $_u$.

The analysis is done for a *typical* UE which is sampled from $_u$ uniformly at random. We shift the origin of our coordinate system to the location of the typical user. The BS that serves this user is known as the *tagged BS*. We assume that the MBSs are equipped with high capacity wired backhaul, i.e., they are connected to the network core by high speed fibers. On the other hand, the SBSs are wirelessly backhauled by the MBSs over mm-wave links. All BSs operate in open access, i.e., a UE may either connect to an MBS or an SBS depending on the max power-based association strategy (details in Section 8.2.3). Thus the UEs are served by one-hop links if they are connected to the MBS and two-hop links if they are connected to the SBS. We refer to the link between a user and BS as an *access link* and to the link between an MBS and SBS as a *backhaul link*.

Notation. We will denote a point process and its associated counting measure by the same notation. Thus, if denotes a point process, then (A) denotes the number of points of falling in $A \in B(\mathsf{R}^2)$, where $B(\mathsf{R}^2)$ denotes the Borel- algebra in R^2. Also $j \ j$ denotes the Lebesgue measure in R^2 (i.e., for a set $B \ \mathsf{R}^2$, jBj denotes the area of B).

8.2.2 Propagation model

Blockage model

Since mm-wave signals are sensitive to physical blockages such as buildings and trees, the LOS and NLOS pathloss characteristics of mm-wave signals are significantly different. Since blockage models are highly context specific, both deterministic [143] and stochastic models [114, 144, 145] have been used in the literature. Similar to [144, 145], we will use a well-known stochastic model known as the germ-grain model for modeling blockages. In particular, the blockages are assumed to be a sequence of line segments $_{\text{bl}} = f\mathbf{p}; L_{\text{bl}}; g$ where $\mathbf{p}$, L_{bl}, and $$ denote the location of midpoint, length, and orientation of each segment, respectively. The sequence $f\mathbf{p}g$ is distributed as a PPP density $_{\text{bl}}$ in R^2 and $f\ g$ is a sequence of independently and identically distributed (i.i.d.) uniform random variables in $(0; 2\ ]$. A link between a transmitter at $\mathbf{x}$ and a receiver at $\mathbf{y}$ is in LOS ($s(\mathbf{x}; \mathbf{y}) = \grave{}$) if there is no intersection between the line segment connecting $\mathbf{x}$ and $\mathbf{y}$, denoted as $\overline{\mathbf{x}; \mathbf{y}}$, and the elements in $_{\text{bl}}$. We denote the state of a link as $s\ 2\ f\grave{}; \mathsf{n}g$ in accordance with the link being in LOS or NLOS state. For a link of type k, the pathloss is defined as

$$L_{k_i}(z) = \begin{cases} z^{\,k_{i;\grave{}}}; & \text{if } s = \grave{};\ i.e.:\ \#(\ _{\text{bl}} \setminus \overline{\mathbf{x}; \mathbf{y}}) = 0; \\ z^{\,k_{i;\mathsf{n}}}; & \text{if } s = \mathsf{n};\ \text{i.e.:}\ \#(\ _{\text{bl}} \setminus \overline{\mathbf{x}; \mathbf{y}}) > 0; \end{cases} k\ 2\ f\mathsf{a}; \mathsf{b}g;\ i = f\mathsf{m}; \mathsf{s}g; \tag{8.1}$$

where $f\ _{k_{i;s}}g$ denote the pathloss exponents and $\#(\ _{\text{bl}} \setminus \overline{\mathbf{x}; \mathbf{y}})$ gives the number of line segments from $_{\text{bl}}$ that intersect with $\overline{\mathbf{x}; \mathbf{y}}$. In Fig. 8.1, we illustrate a realization of the network. In addition to its relevance from the systems perspective (as justified in [145]), there are two reasons for choosing this particular blocking distribution. First, it reduces to the well-known independent exponential blocking if L_{bl} is not large enough [145], which will be useful for the SINR analysis in Section 8.3.1. Second, it is a stationary distribution which will facilitate the characterization of cell load in Section 8.3.2.

Effective antenna gain

The propagation loss in mm-wave frequencies can be overcome by beamformed directional transmission. To this end, all mm-wave BSs and UEs are assumed to be equipped with antenna arrays. For the analytical tractability, the BS antenna gains are approximated with sectorized gain patterns, in which the array gains are assumed to be G_i for all the angles within the main lobe of beam width $_{b_i}$ and another smaller constant g_i for the rest of the angles ($i\ 2\ f\mathsf{m}; \mathsf{s}g$). The configuration of UE antenna patterns are also assumed to be sectorized with gains G_{u} and g_{u} in the main and side lobes, respectively and beamwidth $_{\mathsf{u}}$[1]. Hence, if $_{k_i}$ denotes the effective antenna gain for a link of type k between a BS in $_i$ and a reference point (a UE for $k = \mathsf{a}$ and SBS for $k = \mathsf{b}$), then under perfect beam

[1] For notational simplicity, we are assuming that the antenna units for access and backhaul communications at the SBS and MBS have similar gain patterns. However, different antenna patterns for access and backhaul communications can be easily incorporated without any significant change in the analysis.

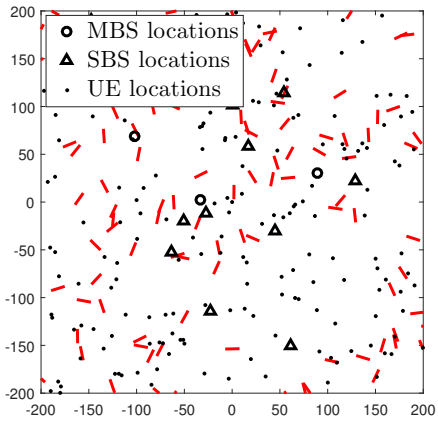

Figure 8.1: A realization of the two-tier network. The blockages are indicated by red lines.

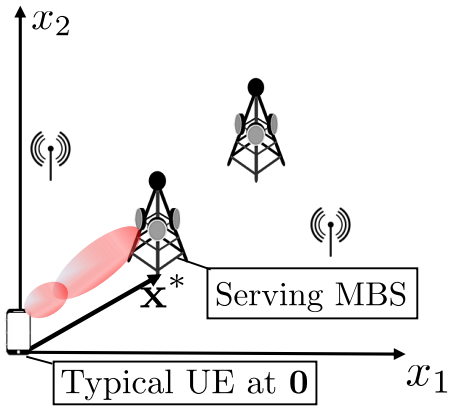

(a) Association to SBS.

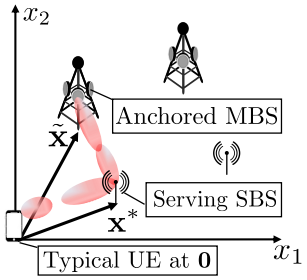

(b) Association cells to SBS.

Figure 8.2: Illustration of $\mathbf{x}$ and $\tilde{\mathbf{x}}$.

alignment between the transmit and receive antennas, $_{a_i} = G_i G_u$ and $_{b_i} = G_i G_s$. We assume that the BSs are transmitting at constant power spectral density P_i/W ($i \in \{m, s\}$) over the system BW W. Hence, the received power over a bandwidth W^0 in the downlink at a reference point located at $\mathbf{y}$ from a BS at $\mathbf{x} \in \_{i}$ is given by

$$P(\mathbf{x}, \mathbf{y}) = \frac{P_i}{W} W^0 h_{\mathbf{x},\mathbf{y}} \_{k_i} \_{k_i} L_{k_i}(k\mathbf{x} \quad \mathbf{y}k)^{-1}, \qquad i \in \{m, s\}, \tag{8.2}$$

where $k \in \{a, b\}$ refer to the access and backhaul links, respectively, and $_{k_i}$ is the propagation loss at a reference distance (1 m). We assume each link undergoes Rayleigh fading, i.e., $\{h_{\mathbf{x},\mathbf{y}}\}$ is a sequence of i.i.d. random variables with $h_{\mathbf{x},\mathbf{y}} \quad \exp(1)$. Note that while one can, in principle, include more general fading distributions, such as Nakagami [29], the additional complexity of the analytical expressions will significantly outweigh any additional design insights. This is primarily because the performance *trends* are somewhat robust to the choice of fading distribution as long as the distance-dependent channel components are included. The well-known tractability of Rayleigh distribution has therefore led to its use in the analysis of mm-wave systems as well [119, 129].

8.2.3 Association policy

The typical UE connects to the BS at $\mathbf{x}$ providing maximum biased average received power,

$$\mathbf{x} = \arg \max_{\substack{\mathbf{x} \in \_{i} \\ i \in \{s,m\}}} P_i T_i \_{a_i} G_i G_u L_{a_i}(k\mathbf{x}k)^{-1}, \tag{8.3}$$

where T_i denotes the bias factor for association to the i^{th} BS-tier [24]. As it will be demonstrated in the sequel, bias factors play pivotal role to offload users (traffic) from one tier to another [24]. If the serving BS is an SBS, i.e. $\mathbf{x} \in \_{s}$, then this SBS is wirelessly backhauled to an MBS in $_{m}$ offering maximum power at the serving SBS location. We call this MBS the *anchor MBS* of the serving SBS. Thus, if $\mathbf{x}$ is the location of the anchor MBS of the SBS at $\mathbf{x}$, then,

$$\mathbf{x} = \arg \max_{\mathbf{x} \in \_{m}} P_m \_{b_m} G_m G_s L_{b_m}(k\mathbf{x} \quad \mathbf{x}k)^{-1}. \tag{8.4}$$

Fig. 8.2 gives an illustration of $\mathbf{x}$ and $\mathbf{x}$. Following the association policy, this typical access link will be associated to either an MBS or an SBS with an association probability which is formally defined as follows.

Definition 8.1 (Association Probability)**.** The association probability A_i is defined as the probability of the following association event: $A_i = P(\mathbf{x} \in \_{i}), \forall\, i \in \{m, s\}$.

Since the spatial distribution of the network is stationary, A_i denotes the fraction of users of $_{u}$ being served by the BSs of $_{i}$ [24]. We now define the association cells as follows.

Definition 8.2 (Association Cell)**.** The association cell of a BS located at $\mathbf{x}$ refers to a closed subset in $\mathbb{R}^2$ where the received power from $\mathbf{x}$ is greater than the received powers

(a) Association cells for RAN (b) Association cells for backhaul network

Figure 8.3: Association cells formed by the BSs of the two-tier HetNet under correlated blocking. Circles represent the MBSs, and triangles represent the SBSs.

from all other BSs in the network. For the access links, an association cell of the i^{th} tier can be expressed as

$$C_{\mathrm{a}_i}(\mathbf{x}) = \{\mathbf{z} \in \mathbb{R}^2 : P_i T_i \, {}_{\mathrm{a}_i} G_i L_{\mathrm{a}_i}(\|\mathbf{z} - \mathbf{x}\|)^{-1} \geq P_j T_j \, {}_{\mathrm{a}_j} G_j L_{\mathrm{a}_j}(\|\mathbf{z} - \mathbf{y}\|)^{-1}; \quad \forall \mathbf{y} \in \Phi_j, j \in \{\mathrm{m}, \mathrm{s}\}, \mathbf{x} \in \Phi_i\}, \tag{8.5}$$

and for backhaul links,

$$C_{\mathrm{b}}(\mathbf{x}) = \{\mathbf{z} \in \mathbb{R}^2 : L_{\mathrm{b}_m}(\|\mathbf{z} - \mathbf{x}\|)^{-1} \geq L_{\mathrm{b}_m}(\|\mathbf{z} - \mathbf{y}\|)^{-1}; \forall \mathbf{y} \in \Phi_{\mathrm{m}}, \mathbf{x} \in \Phi_{\mathrm{m}}\}. \tag{8.6}$$

These association cells are depicted in Fig. 8.3.

8.2.4 Interference modeling

We now elaborate on the aggregate interference I_{a_j} from Φ_j ($j \in \{\mathrm{m}, \mathrm{s}\}$) experienced by the typical access link, which can be written as

$$I_{\mathrm{a}_j} = \sum_{\mathbf{x} \in \Phi_j \setminus \{\mathbf{x}_0\}} \frac{P_j}{W} W' h_{0,\mathbf{x}} \, {}_{\mathrm{a}_j} \, {}_{\mathrm{a}_j} L_{\mathrm{a}_j}(\|\mathbf{x}\|)^{-1}, \tag{8.7}$$

where ${}_{\mathrm{a}_j}$ denotes the effective antenna gain of an interfering link seen by the typical UE. Similar to [114, 115, 129], we model beam directions of the interfering BSs as uniform random variables in $(0, 2\pi]$. Then, $\{{}_{\mathrm{a}_j}\}$ becomes a sequence of i.i.d. discrete random variables taking values from the set $M_{\mathrm{a}_j} = \{G_j G_{\mathrm{u}}, G_j g_{\mathrm{u}}, g_j G_{\mathrm{u}}, g_j g_{\mathrm{u}}\}$ with probabilities $\{\frac{\theta_j}{2\pi}\frac{\theta_{\mathrm{u}}}{2\pi}, \frac{(2\pi-\theta_j)}{2\pi}\frac{\theta_{\mathrm{u}}}{2\pi}, \frac{\theta_j}{2\pi}\frac{(2\pi-\theta_{\mathrm{u}})}{2\pi}, \frac{(2\pi-\theta_j)}{2\pi}\frac{(2\pi-\theta_{\mathrm{u}})}{2\pi}\}$, respectively, where $j \in \{\mathrm{m}, \mathrm{s}\}$. In general,

8.2. System model

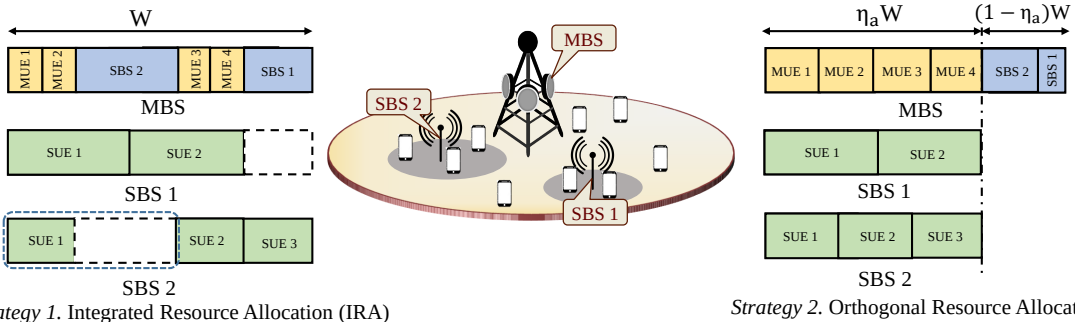

Strategy 1. Integrated Resource Allocation (IRA)

Strategy 2. Orthogonal Resource Allocation (ORA)

Figure 8.4: Resource partition strategies for a toy example: MBS with two SBSs and four macro users (MUEs), SBS 1 has two users (denoted as SUEs) and SBS 2 has three users.

we will denote $G \in M_{a_j}$ as an element occurring with probability p_G.We now shift our attention to the interference experienced by the tagged backhaul link. Similar to the access links, $_{b_j}$ can be modeled as a discrete random variable taking values from the set $M_{b_j} = \{G_j G_s; g_j G_s; G_j g_s; g_j g_s\}$ with probabilities

$$\left\{\frac{b_j\ b_s}{4^{\ 2}}; \frac{(2\quad b_j)\ b_s}{4^{\ 2}}; \frac{b_j(2\quad b_s)}{4^{\ 2}}; \frac{(2\quad b_j)(2\quad b_s)}{4^{\ 2}}\right\}$$

, respectively, where $j \in \{m; s\}$. Using this, the interference experienced by the tagged backhaul link from all BSs in $_j$ conditioned on $\mathbf{x} \in {}_s$ can be expressed as

$$I_{b_j} = \begin{cases} \sum\limits_{x \in \Phi_m \setminus x} \frac{P_m}{W} W^{\prime} h_{x,x\ b_m\ b_m} L_{b_m}(\|x\quad x\|)^{-1}; & j = m; \\ \sum\limits_{x \in \Phi_s \setminus x} \frac{P_s}{W} W^{\prime} h_{x,x\ b_s\ b_s} L_{b_s}(\|x\quad x\|)^{-1}; & j = s. \end{cases} \tag{8.8}$$

We also assume that all BSs are active in the downlink (*full buffer* assumption). This means that there is at least one user in an access association cell and one SBS in a backhaul association cell. This assumption is justified since $_m << {}_s << {}_u$.

8.2.5 Resource allocation and data rate

In this Section, we introduce two resource allocation strategies.

Integrated resource allocation (IRA)

We assume that the access and backhaul links share the same pool of radio resources through orthogonal resource allocation (such as time and frequency division multiple access) and at any BS the total pool of available resources is equally divided among the number of UEs served by each BS (i.e. the BS load) by a simple round robin scheduling. By this resource allocation scheme, if the typical UE connects to the MBS ($\mathbf{x} \in {}_m$), the resource

fraction allocated for the typical UE by the tagged MBS is the inverse of the total load on the tagged MBS which is $(\ _{\mathrm{u}}(C_{\mathrm{a_m}}(\mathbf{x}\ )) + \sum_{\mathbf{x}2\ _{\mathrm{s}}\setminus C_{\mathrm{b}}(\mathbf{x}\ )}\ _{\mathrm{u}}(C_{\mathrm{a_s}}(\mathbf{x})))$. Here the first term is the load due to the users connected to the tagged MBS over access links and the second terms is due to the users connected to the tagged MBS via SBSs (two hop links). If the typical UE connects to the SBS ($\mathbf{x}\ 2\ _{\mathrm{s}}$), the fraction of total resources allocated for the tagged SBS for backhaul by the anchor MBS is

$$! = \frac{\ _{\mathrm{u}}(C_{\mathrm{a_s}}(\mathbf{x}\ ))}{\ _{\mathrm{u}}(C_{\mathrm{a_m}}(\mathbf{x})) + \sum_{\mathbf{x}2\ _{\mathrm{s}}\setminus C_{\mathrm{b}}(\mathbf{x})}\ _{\mathrm{u}}(C_{\mathrm{a_s}}(\mathbf{x}))}. \tag{8.9}$$

At the tagged SBS, the resources not occupied by the backhaul link can be further split equally between the access links of the associated UEs. Thus the rate of a UE is given by

$$\mathrm{Rate}_{\mathrm{IRA}} = \begin{cases} \frac{W}{\ _{\mathrm{u}}(C_{\mathrm{a_m}}(\mathbf{x}\ ))+\sum_{\mathbf{x}2\ _{\mathrm{s}}\setminus C_{\mathrm{b}}(\mathbf{x}\ )}\ _{\mathrm{u}}(C_{\mathrm{a_s}}(\mathbf{x}))}\log\left(1+\mathrm{SINR}_{\mathrm{a}}(\mathbf{0})\right); & \text{if } \mathbf{x}\ 2\ _{\mathrm{m}}; \\ \frac{W}{\ _{\mathrm{u}}(C_{\mathrm{a_s}}(\mathbf{x}\ ))}\min\left(!\log\left(1+\mathrm{SINR}_{\mathrm{b}}(\mathbf{x}\ )\right);(1\quad !)\log\left(1+\mathrm{SINR}_{\mathrm{a}}(\mathbf{0})\right)\right); & \text{if } \mathbf{x}\ 2\ _{\mathrm{s}}. \end{cases} \tag{8.10}$$

Here the SINR on the access link experienced by the typical UE conditioned on the fact that it connects to a BS of $\ _i$ (i.e. $\mathbf{x}\ 2\ _i$) is expressed as

$$\mathrm{SINR}_{\mathrm{a}}(\mathbf{0}) = \frac{P_i G_i G_{\mathrm{u}\ \mathrm{a}_i} h_{0;\mathbf{x}}\ L_{\mathrm{a}_i}(k\mathbf{x}\ k)^{\ 1}}{\sum_{j2\{s;m\}g\mathbf{x}2\ _j nf\mathbf{x}\ g} P_j h_{0;\mathbf{x}\ \mathrm{a}_j\ \mathrm{a}_j} L_{\mathrm{a}_j}(k\mathbf{x}k)^{\ 1} + \mathrm{N}_0 W}; \tag{8.11}$$

and the SINR on the backhaul link experienced by the serving SBS conditioned on $\mathbf{x}\ 2\ _{\mathrm{s}}$ is expressed as

$$\mathrm{SINR}_{\mathrm{b}}(\mathbf{x}\ ) = \frac{P_{\mathrm{m}} G_{\mathrm{m}} G_{\mathrm{s}\ \mathrm{b_m}} h_{\mathbf{x}\ ;\mathbf{x}} L_{\mathrm{b_m}}(k\mathbf{x}\quad \mathbf{x}k)^{\ 1}}{\sum_{j2\{m;s\}g\mathbf{x}2\ _j nf\mathbf{x}g} P_j h_{\mathbf{x}\ ;\mathbf{x}\ \mathrm{b}_j\ \mathrm{b}_j} L_{\mathrm{b}_j}(k\mathbf{x}\quad \mathbf{x}\ k)^{\ 1} + \mathrm{N}_0 W}. \tag{8.12}$$

Orthogonal resource allocation (ORA)

In the ORA scheme, we assume that a fraction $\ _{\mathrm{a}}$ of resources is reserved for access links and the rest is allocated to the backhaul links. The share of the total backhaul BW $(1\quad _{\mathrm{a}})W$ obtained by an SBS at $\mathbf{x}$ is proportional to its load ($\ _{\mathrm{s}}(C_{\mathrm{a_s}}(\mathbf{x}))$). Then the rate of a UE is given by

$$\mathrm{Rate}_{\mathrm{ORA}} = \begin{cases} \frac{\ _{\mathrm{a}}W}{\ _{\mathrm{u}}(C_{\mathrm{a_m}}(\mathbf{x}\ ))}\log\left(1+\mathrm{SINR}_{\mathrm{a}}(\mathbf{0})\right); & \text{if } \mathbf{x}\ 2\ _{\mathrm{m}}; \\ \min\left(\frac{\ _{\mathrm{a}}W}{\ _{\mathrm{u}}(C_{\mathrm{a_s}}(\mathbf{x}\ ))}\log\left(1+\mathrm{SINR}_{\mathrm{a}}(\mathbf{0})\right); \frac{(1\quad _{\mathrm{a}})W}{\sum_{\mathbf{x}2C_{\mathrm{b}}(\mathbf{x})}\ _{\mathrm{u}}(C_{\mathrm{a_s}}(\mathbf{x}))}\log\left(1+\mathrm{SINR}_{\mathrm{b}}(\mathbf{x}\ )\right)\right); & \\ \qquad \text{if } \mathbf{x}\ 2\ _{\mathrm{s}}; & \end{cases} \tag{8.13}$$

where $\mathtt{SINR}_a(\mathbf{0})$ is given by (8.11) and $\mathtt{SINR}_b(\mathbf{x})$ is given by

$$\mathtt{SINR}_b(\mathbf{x}) = \frac{P_m G_m G_s h_{\mathbf{x}} \; ; \mathbf{x} \; b_m L_{b_m}(k\mathbf{x} \quad \mathbf{x}k)^{\;1}}{\sum_{\mathbf{x}2 \;\; m n f \mathbf{x} g} P_m h_{\mathbf{x}} \; ; \mathbf{x} \;\; b_m \;\; b_m \; L_{b_m}(k\mathbf{x} \quad \mathbf{x}\; k)^{\;1} + N_0 W}. \tag{8.14}$$

Note that $\mathtt{SINR}_b(\mathbf{x})$ for ORA is greater than $\mathtt{SINR}_b(\mathbf{x})$ for IRA, since in ORA, the tagged backhaul link operating in backhaul BW will not experience the interference from SBSs operating in access BW. However, it will be shown in the sequel that this interference difference does not affect the rate since the backhaul links are mostly noise limited. Under the *full bu er* assumption, $\mathtt{SINR}_a(\mathbf{0})$-s for IRA and ORA are the same. We define the rate coverage probability (or simply rate coverage) as the complementary cumulative density function (CCDF) of rate, i.e., $\mathtt{P}_r = \mathtt{P}(\mathtt{Rate} > \;\;)$, where $\;\;$ is the target rate threshold. The two resource allocation strategies are illustrated in Fig. 8.4.

8.2.6 Two-tier HetNet with fiber-backhauled SBSs

To compare and contrast the rate characteristics of the two-tier HetNet with IAB, we define another two-tier network where the SBSs have access to fiber backhaul similar to the MBSs. This setup is also known as HetNets with *ideal SBS backhaul* and has been thoroughly analyzed in the literature [115, 119]. The user perceived rate in this setup can be expressed as:

$$\mathtt{Rate}_{\mathtt{Wb}} = \begin{cases} \frac{W}{u(C_m(\mathbf{x}))} \log\left(1 + \mathtt{SINR}_a(\mathbf{0})\right); & \text{if } \mathbf{x} \;\; 2 \;\;\; _m; \\ \frac{W}{u(C_s(\mathbf{x}))} \log\left(1 + \mathtt{SINR}_a(\mathbf{0})\right); & \text{if } \mathbf{x} \;\; 2 \;\;\; _s; \end{cases}. \tag{8.15}$$

Clearly it can be seen that $\mathtt{Rate}_{\mathtt{Wb}}$ stochastically dominates $\mathtt{Rate}_{\mathtt{IRA}}$ and $\mathtt{Rate}_{\mathtt{ORA}}$, i.e., $\mathtt{P}(\mathtt{Rate}_{\mathtt{Wb}} > \;\;) \;\; \mathtt{P}(\mathtt{Rate} > \;\;)$ for $\;\; 2 \; f\mathtt{IRA}; \mathtt{ORA}g$.

8.3 Rate distribution

In this Section, we evaluate the rate coverage probability defined in the previous Section. Note that the random variables appearing in the $\mathtt{Rate}$ expressions are of two main types, $\mathtt{SINR}$s of the access and backhaul links and loads on different BSs. While these $\mathtt{SINR}$ and load variables are correlated due to the same underlying point processes, this correlation is typically ignored for analytical tractability in this stationary setup without incurring any significant loss in accuray [57, 128, 129, 141].

8.3.1 SINR distributions

In this Section, we are going to evaluate the following CDFs: (i) *MBS coverage:* $\mathtt{P}(\mathtt{SINR}_a(\mathbf{0}) > \; j\mathbf{x} \;\; 2 \;\;\; _m)$, and (ii) *joint SBS and backhaul coverage:* $\mathtt{P}(\mathtt{SINR}_a(\mathbf{0}) > \;\; _1; \mathtt{SINR}_b(\mathbf{x}) > \;\; _2 j\mathbf{x} \;\; 2 \;\; _s)$. As noted earlier, the germ-grain model for blockages introduced in Section 8.2 is not

conductive for the SINR analysis [114]. However, if L_{bl} is not large enough, we can characterize the SINR distributions by assuming the *independent blocking model* [145] which is stated as follows.

Assumption 2. Each link state is assumed to be in LOS independently with probability $p(r) = \exp(-r/\beta)$, where $r > 0$ is the link distance and β is the LOS range constant.

As evident in the sequel, the independent exponential blocking model closely approximates the germ-grain model of blocking in terms of the SINR distributions. The connection between β and bl will be established in Remark 8.7. In addition, recall that the germ-grain model will provide the underlying correlation necessary to construct meaningful association cells for load and rate analysis in Section 8.3.2. For preserving the simplicity of analysis, we now make another reasonable assumption on the SINR.

Assumption 3. (a) For the typical access link, interference from the MBSs is neglected, i.e.,

$$\mathrm{SINR}_{\mathrm{a}}(\mathbf{0}) = \frac{P_i G_i G_{\mathrm{u}\ \mathrm{a}_i} h_{0;\mathbf{x}}\ L_{\mathrm{a}_i}(k\mathbf{x}\ k)^{-1}}{\sum\limits_{\mathbf{x}2\ _s nf\mathbf{x}\ g} P_s h_{0;\mathbf{x}\ \mathrm{as}\ \mathrm{as}} L_{\mathrm{as}}(k\mathbf{x}k)^{-1} + \mathrm{N}_0 W}; \tag{8.16}$$

and (b) the tagged backhaul link is assumed to be noise-limited, i.e.,

$$\mathrm{SINR}_{\mathrm{b}} = \mathrm{SNR}_{\mathrm{b}} = \mathrm{SINR}_{\mathrm{b}}(\mathbf{x}\ ) = \frac{P_{\mathrm{m}} G_{\mathrm{m}} G_{\mathrm{s}\ \mathrm{bm}} h_{\mathbf{x}\ ;\mathbf{x}} L_{\mathrm{bm}}(k\mathbf{x}\quad \mathbf{x}k)^{-1}}{\mathrm{N}_0 W}. \tag{8.17}$$

The intuition behind the above simplification is as follows. The SBSs, equipped with large antenna arrays, are able to beamform towards the direction of the ABS antenna to establish the backhaul link. On the other hand, the UEs, with lower beamforming capabilities compared to the BSs, are likely to experience SBS interference due to the dense deployments alongside thermal noise. As will be clear in the sequel, this reasonable assumption allows us to compute the joint distribution of $\mathrm{SINR}_{\mathrm{a}}(\mathbf{0})$ and $\mathrm{SINR}_{\mathrm{b}}(\mathbf{x}\ )$, which is currently an open problem in the literature.

As a first step towards the coverage and rate analyses, we define the pathloss point process on similar lines of [113, 115, 129]. However note that due to the exponential blocking model considered in this chapter, the properties of this process are different than those of the LOS-ball model used in the prior arts (see [29, Section III-C] for details on the LOS-ball model).

Definition 8.3 (Pathloss process)**.** We define the sequence $\{L_{k_i} = L_{k_i}(k\mathbf{x}k) : \mathbf{x} \in \Phi_i\}$ as a pathloss process associated with Φ_i $(i \in \{\mathrm{m}, \mathrm{s}\})$ where the reference point at the origin is the typical UE for $k = \mathrm{a}$ (corresponding to the typical access link) and typical SBS for $k = \mathrm{b}$ (corresponding to the typical backhaul link).

8.3. Rate distribution

Lemma 8.4. *The pathloss process L_{k_i} ($k \in \{a, b\}$, $i \in \{m, s\}$) is a PPP in $\mathbb{R}^+$ with intensity measure:* $\Lambda_{k_i}([0, l)) =$

$$2\pi\lambda_i \left(e^{-\beta_{i,k}^{\frac{1}{\alpha_{i,k}}}} l^{\frac{1}{\alpha_{i,k}}} + \cdots + \frac{l^{\frac{2}{\alpha_{i,n}}}}{2} e^{-\beta_{i,n}^{\frac{1}{\alpha_{i,n}}}} l^{\frac{1}{\alpha_{i,n}}} + \cdots \right); \quad (8.18)$$

and density:

$$\Lambda_{k_i}(l) = 2\pi\lambda_i \left(\frac{1}{\alpha_{i,k}} l^{\frac{2}{\alpha_{i,k}}-1} e^{-\beta_{i,k} l} + \frac{1}{\alpha_{i,n}} l^{\frac{2}{\alpha_{i,n}}-1} \left(1 - e^{-\beta_{i,n} l}\right) \right); \text{ for } l > 0. \quad (8.19)$$

Proof. Since the link state (i.e. LOS or NLOS) can be considered as independent mark on each BS in Φ_i, the LOS and NLOS BSs with respect to the typical UE (typical SBS) are inhomogeneous PPPs with densities $\Phi_i e^{-\beta_k \|x\|^{\alpha_k}}$ and $\Phi_i(1 - e^{-\beta_k \|x\|^{\alpha_k}})$, respectively [17]. These PPPs under mapping $L_{k_i}(\|x\|)$ are PPPs in $\mathbb{R}^+$. Superposition of these PPPs gives us L_{k_i}, which is again a PPP with intensity measure:

$$\Lambda_{k_i}([0, l)) = 2\pi\lambda_i \int_0^{\infty} \mathbb{P}(L_{k_i}(r) < l) r dr = 2\pi\lambda_i \int_0^{\infty} e^{-\beta_k r^{\alpha_{i,k}}} \mathbb{1}(r^{\alpha_{i,k}} < l) + \left(1 - e^{-\beta_k r^{\alpha_{i,k}}}\right) \mathbb{1}(r^{\alpha_{i,n}} < l) \, r dr = 2\pi\lambda_i \int_0^{l^{\frac{1}{\alpha_{i,k}}}} e^{-\beta_k r^{\alpha_{i,k}}} r dr + 2\pi\lambda_i \int_0^{l^{\frac{1}{\alpha_{i,n}}}} \left(1 - e^{-\beta_n r^{\alpha_{i,n}}}\right) r dr.$$

The final expression in (8.18) follows from algebraic simplifications. Differentiating with respect to l using Leibniz integral rule, we obtain the density function in (8.19). □

In the following Corollary, we provide the expressions of the intensity measures and densities of the PPPs formed by the LOS and NLOS BSs of Φ_s with respect to the typical UE, to be later used for the derivation of the joint SBS and backhaul coverage.

Corollary 8.5. *The pathloss processes of the LOS and NLOS links from the BSs in Φ_s to the typical UE are PPPs with intensity measures*

$$\Lambda_{s,k}([0, l)) = 2\pi\lambda_s \left(e^{-\beta_{s,k}^{\frac{1}{\alpha_{s,k}}}} l^{\frac{1}{\alpha_{s,k}}} + \cdots \right); \quad (8.20)$$

$$\Lambda_{s,n}([0, l)) = 2\pi\lambda_s \left(\frac{l^{\frac{2}{\alpha_{s,n}}}}{2} e^{-\beta_{s,n}^{\frac{1}{\alpha_{s,n}}}} l^{\frac{1}{\alpha_{s,n}}} + \cdots \right); \quad (8.21)$$

and density functions

$$\Lambda_{s,k}(l) = \frac{2\pi\lambda_s}{\alpha_{s,k}} l^{\frac{2}{\alpha_{s,k}}-1} e^{-\beta_{s,k} l}; \quad \Lambda_{s,n}(l) = \frac{2\pi\lambda_s}{\alpha_{s,n}} l^{\frac{2}{\alpha_{s,n}}-1} \left(1 - e^{-\beta_{s,n} l}\right); \quad l > 0. \quad (8.22)$$

Note that $_{a_s;`}((0;l]) + _{a_s;n}((0;l]) = _{a_s}((0;l])$ and $_{a_s;`}(l) + _{a_s;n}(l) = _{a_s}(l)$. Since the user association directly depends on the pathloss (see (8.5)), we are now in a position to characterize the association probabilities to $_m$ and $_s$ for the typical access link defined in Definition 8.1.

Lemma 8.6. *The association probability of the typical access link to a BS of $_i$ is expressed as*

$$A_i = \int_0^{Z^1} e^{\sum_{j2\{m;s\}} {}_{a_j}((0;\ {}_{j;i}l])} \ {}_{a_i}(l)\mathrm{d}l; \tag{8.23}$$

where $_{a_j}(\ )$ and $_{a_j}(\ )$ are given by (8.18) and (8.19), respectively, and $_{j;i} = \frac{P_j T_j\ {}_{a_j} G_j}{P_i T_i\ {}_{a_i} G_i}$.

Proof. First we denote the location of candidate serving BS of $_i$ as

$$\mathbf{x}_i = \arg\max_{\mathbf{x}2\ {}_i} P_i T_i\ {}_{a_i} G_i G_u L_{a_i}(k\mathbf{x}k)^{\ 1} = \arg\min_{\mathbf{x}2\ {}_i} L_{a_i}(\mathbf{x}):$$

The CDF of $L_{a_i} := L_{a_i}(\mathbf{x}_i)$ can be obtained from the CDF of the contact distance of L_{a_i} as $\mathrm{P}(L_{a_i}\quad l) = 1\quad e^{\ {}_{a_i}((0;l])}$: Differentiating with respect to l, we obtain the PDF of L_{a_i} as: $f_{L_{a_i}}(l) = e^{\ {}_{a_i}((0;l])}\ {}_{a_i}(l); l > 0$: Now, $A_i = \mathrm{P}(\mathbf{x}\quad 2\quad {}_i) = \mathrm{P}\ P_i T_i\ {}_{a_i} G_i L_{a_i}^{\ 1}$ $P_j T_j\ {}_{a_j} G_j L_{a_j}^{\ 1} = \mathrm{P}\ L_{a_j}\quad {}_{j;i} L_{a_i} = \mathrm{E}\ e^{\ {}_{a_j}((0;\ {}_{j;i}L_{a_i}])} = \int_0^{R^1} e^{\ {}_{a_j}((0;\ {}_{j;i}l])} f_{L_{a_i}}(l)\mathrm{d}l$. The final expression is obtained by substituting $f_{L_{a_i}}(l)$. □

We remind that the results derived in this Section are functions of , which appears in the expression for the blocking probability given in Assumption 2. While characterizing for the germ-grain blockage model of Section 8.2 is known to be hard, we propose one reasonable way of choosing given a particular blockage configuration ($_{bl}$, L_{bl}) in the following remark.

Remark 8.7. We choose such that A_i in (8.23) evaluated as a function of is equal to the empirical value of A_i computed as Definition 8.1. Since we have a two-tier network, it is sufficient to match only one quantity, say, A_m (since $A_s = 1\quad A_m$) for the calibration of . A simple Matlab script to empirically obtain the value of is provided by the authors at [146].

While one can of course use other ways to calibrate with the blockage parameters [29], the reason of this particular way of calibration will be clarified in the next Section. We now derive the distribution of pathloss of the serving link, i.e., the link between the typical UE and its serving BS.

Lemma 8.8. *Conditioned on $\mathbf{x}\ \ 2\ \ {}_i$, the PDF of $L_a := L_{a_i}(k\mathbf{x}\ k)$ is given by*

$$f_{L_a}(l|\mathbf{x}\ \ 2\ \ {}_i) = \frac{1}{A_i} e^{\sum_{j2\{m;s\}} {}_{a_j}((0;\ {}_{j;i}l])}\ {}_{a_i}(l); \qquad l > 0; \tag{8.24}$$

where $_{a_j}(\ )$, $_{a_j}(\ )$, and A_i are given by (8.18), (8.19), and (8.23), respectively.

Proof. The conditional CCDF of L_{a} given $\mathbf{x} \in \mathcal{A}_i$ is $F_{L_{\mathrm{a}}}(l|\mathbf{x} \in \mathcal{A}_i) =$

$$\mathrm{P}\left[L_{\mathrm{a}_i} > l|\mathbf{x} \in \mathcal{A}_i\right] = \frac{\mathrm{P}\left[L_{\mathrm{a}_i} > l, \mathbf{x} \in \mathcal{A}_i\right]}{\mathrm{P}(\mathbf{x} \in \mathcal{A}_i)} = \frac{1}{A_i} \int_l^{\infty} e^{-\sum_{j \in \mathcal{B}_{\mathrm{m}}} \mathcal{A}_j((0, \mathcal{R}_j, \mathcal{R}_i, l])} \mathcal{A}_i(l)\mathrm{d}l.$$

The desired PDF can be obtained by differentiating with respect to l. □

In Lemmas 8.6-8.8, we derived the association probability and pathloss PDFs of the serving link for the two-tier HetNet. One can further interpret this network as a three-tier HetNet by splitting $\mathcal{B}_{\mathrm{s}}$ into $\mathcal{B}_{\mathrm{s},\ell}$ and $\mathcal{B}_{\mathrm{s},\mathrm{n}}$ which are the sets of SBSs at LOS and NLOS of the typical UE, respectively. In the following Corollary, we provide the association probabilities to $\mathcal{B}_{\mathrm{s},\ell}$ and $\mathcal{B}_{\mathrm{s},\mathrm{n}}$ and the corresponding PDFs of pathloss of the serving link.

Corollary 8.9. *The SBS association event can split into two events based on the state of the link between the typical UE and serving SBS:*

$$A_{\mathrm{s}} = \underbrace{\mathrm{P}(\mathbf{x} \in \mathcal{B}_{\mathrm{s}}, s(\mathbf{x}, 0) = \ell)}_{A_{\mathrm{s}_\ell}} + \underbrace{\mathrm{P}(\mathbf{x} \in \mathcal{B}_{\mathrm{s}}, s(\mathbf{x}, 0) = \mathrm{n})}_{A_{\mathrm{s}_\mathrm{n}}},$$

where the association probabilities to LOS SBS and NLOS SBS are given by

$$A_{\mathrm{s}_t} = \int_0^{\infty} e^{-\sum_{j \in \mathcal{B}_{\mathrm{m}}} \mathcal{A}_j((0, \mathcal{R}_j, \mathcal{R}_{\mathrm{s}}, l])} \mathcal{A}_{\mathrm{s},t}(l)\mathrm{d}l, \qquad t \in \{\ell, \mathrm{n}\},$$

and the corresponding pathlosses of the serving links are denoted as $L_{\mathrm{a}}|s(\mathbf{x}, 0) = \ell$ and $L_{\mathrm{a}}|s(\mathbf{x}, 0) = \mathrm{n}$, respectively whose PDFs are given as

$$f_{L_{\mathrm{a}}}(l|\mathbf{x} \in \mathcal{B}_{\mathrm{s}}, s(\mathbf{x}, 0) = t) = \frac{1}{A_{\mathrm{s}_t}} e^{-\sum_{j \in \mathcal{B}_{\mathrm{m}}} \mathcal{A}_j((0, \mathcal{R}_j, \mathcal{R}_{\mathrm{s}}, l])} \mathcal{A}_{\mathrm{s},t}(l), \qquad l > 0, t \in \{\ell, \mathrm{n}\}, \tag{8.25}$$

where $\mathcal{A}_{\mathrm{s},\ell}$, $\mathcal{A}_{\mathrm{s},\mathrm{n}}$, $\mathcal{A}_{\mathrm{s},\ell}$, and $\mathcal{A}_{\mathrm{s},\mathrm{n}}$ are given by Corollary 8.5.

Proof. The SBS PPP can be treated as a superposition of LOS and NLOS SBS PPPs. Considering these two PPPs instead of $\mathcal{B}_{\mathrm{s}}$, the proof follows on similar lines of Lemmas 8.6 and 8.8 for a three-tier HetNet. □

We now characterize the pathloss process of MBSs for the *tagged* backhaul link which is not the same as that of the *typical* backhaul link since it is conditioned on the pathloss of the typical access link (L_{a}) and the fact that $\mathbf{x} \in \mathcal{B}_{\mathrm{s}}$. Note that this pathloss characterization is required to derive the joint SBS and backhaul coverage.

Lemma 8.10. *The pathloss process formed by the MBSs perceived by the tagged SBS at* $\mathbf{x}$ *conditioned on the pathloss and state of the typical access link i.e.* L_a, $s(\mathbf{x};0)$, *the location of the serving SBS at* $\mathbf{x}$ $(L_a^{1=\ a;s(\mathbf{x};0)};\ )$, *and the association to SBS* $(\mathbf{x}\ 2\ _s)$, *denoted as* $L_{b_m}js(\mathbf{x};0);\mathbf{x}\ 2\ _s;\mathbf{x}\ (L_a^{1=\ a;s(\mathbf{x};0)};\ )$ *are PPPs in* R^+ *with intensity measure*

$$\tilde{}_{b_t}((0;I];L_a;\ ) = \int_0^{\ 2}\left(\int_0^{I^{1=\ b_{m;\grave{}}}} \tilde{}_m(r;\ ;L_a^{1=\ a_{s;t}};\ )e^{\ r=}\ r\,dr\right.$$
$$\left. + \int_0^{I^{1=\ b_{m;n}}} \tilde{}_m(r;\ ;L_a^{1=\ a_{s;t}};\ )(1\ \ e^{\ r=})r\,dr\right)\ \ d\ ;\quad \textit{for } t = s(\mathbf{x};0)\ 2\ f\grave{};ng; \tag{8.26}$$

and intensity function

$$\tilde{}_{b_t}(I;L_a;\ ) = \int_0^{\ 2} \tilde{}_m(I^{1=\ b_{m;\grave{}}};\ ;L_a^{1=\ a_{s;t}};\ )\frac{1}{b_{m;\grave{}}}I^{\frac{2}{b_{m;\grave{}}}\ 1}e^{\ \frac{I}{}} + \tilde{}_m(I^{1=\ b_{m;n}};\ ;L_a^{1=\ a_{s;t}};\ )$$
$$\frac{1}{b_{m;n}}I^{\frac{2}{b_{m;n}}\ 1}\ 1\ \ e^{\ \frac{I}{}}\ \ d\ ;\ \textit{for } t = s(\mathbf{x};0)\ 2\ f\grave{};ng; \tag{8.27}$$

where

$$\tilde{}_m(r;\ ;x;\ ) = \tilde{}^{\emptyset}_m(r^2 + x^2\ \ 2rx\cos(\ \ ))^{\frac{1}{2}};$$

with

$$\tilde{}^{\emptyset}_m(r) = \ _m e^{\ r=}\mathbf{1}\ \ r > (\ _{s;m}L_a)^{\frac{1}{a_{m;\grave{}}}}\ \ +\ _m(1\ \ e^{\ r=})\mathbf{1}\ \ r > (\ _{s;m}L_a)^{\frac{1}{a_{m;n}}}\ :$$

Proof. The point process $_m jfL_a;\mathbf{x}\ 2\ _s;s(\mathbf{x};0) = \grave{}g$ is a PPP in R^2 with density:

$$\tilde{}^{\emptyset}_m(r) = \ _m e^{\ r=}\mathbf{1}\ \ r > {}^{\frac{1}{a_{m;\grave{}}}}_{s;m}L_a^{\frac{1}{a_{m;\grave{}}}}\ \ +\ _m(1\ \ e^{\ r=})\mathbf{1}\ \ r > {}^{\frac{1}{a_{m;n}}}_{s;m}L_a^{\frac{1}{a_{m;n}}}\ :$$

When this point process is seen from the tagged SBS at $\mathbf{x}\ = (L_a^{\frac{1}{s;\grave{}}};\ )$, the density becomes $\tilde{}_m(r;\ ;\mathbf{x}\ ) = \tilde{}^{\emptyset}_m((r^2 + L_a^{\frac{2}{s;\grave{}}}\ \ 2rL_a^{\frac{1}{s;\grave{}}}\cos(\ \ ))^{\frac{1}{2}})$. Now the pathloss process on R^+ for this conditional version of $_m$ perceived by the tagged SBS will be a PPP with intensity function: $\tilde{}_{b_\cdot}((0;I]j\mathbf{x}\ ) = \int_0^{R_1}\int_0^{R_2} \tilde{}_m(r;\ ;\mathbf{x}\ )\mathsf{P}(L_{b_m}(r) < I)\mathrm{d}\ \ r\,dr =$

$$\int_0^{\ 1}\int_0^{\ 2} \tilde{}_m(r;\ ;\mathbf{x}\ )\ \ e^{\ r=}\mathbf{1}(r^{\ b_{m;\grave{}}} < I) + (1\ \ e^{\ r=})\mathbf{1}(r^{\ b_{m;n}} < I)\ \ \mathrm{d}\ \ r\,dr:$$

Differentiating with respect to I, we obtain the intensity function. Similar steps can be followed when $s(\mathbf{x};0) = n$. □

We now obtain the SINR CCDFs required for the rate analysis as follows.

8.3. Rate distribution

Lemma 8.11. *The MBS and the joint SBS and backhaul coverages under Assumption 3 is given by*

$$\mathrm{P}(\mathrm{SINR_a}(0) > \; jx \;\; 2 \;\; {}_{\mathrm{m}}) = \frac{1}{A_{\mathrm{m}}} \int_0^{Z^1} \exp\Bigg(- \sum_{G 2 M_{\mathrm{as}}} \int_{{}_{\mathrm{s;m}} I}^{Z^1} 1 - \frac{1}{1 + \frac{P_{\mathrm{s}} \; {}_{\mathrm{as}} G I}{P_{\mathrm{m}} \; {}_{\mathrm{am}} G_{\mathrm{m}} G_{\mathrm{u}} z}} \; p_G \; {}_{\mathrm{as}}(z) \mathrm{d}z \Bigg)$$

$$\frac{\mathrm{N}_0 W I}{P_{\mathrm{m}} \; {}_{\mathrm{am}} G_{\mathrm{m}} G_{\mathrm{u}}} \sum_{j 2 \mathrm{fm;sg}} {}_{\mathrm{a}_j}((0; \;\; {}_{j;\mathrm{m}} I]) \mathrm{A} \; {}_{\mathrm{am}}(I) \mathrm{d}I; \tag{8.28}$$

$$\mathrm{P}(\mathrm{SINR_a}(\mathbf{0}) > \; {}_1; \mathrm{SNR_b}(\mathbf{x}) > \; {}_2 jx \;\; 2 \;\; {}_{\mathrm{s}}) = \frac{1}{A_{\mathrm{s}}} \sum_{t 2 \mathrm{fl;ng}} \int_0^{Z^1} \int_0^{Z^1} \exp\Bigg(- \sum_{G 2 M_{\mathrm{as}}} \int_{I_1}^{Z^1} 1 - \frac{1}{1 + \frac{{}_1 G I_1}{G_{\mathrm{s}} G_{\mathrm{u}} z}} \; 1$$

$$p_G \; {}_{\mathrm{as}}(z) \mathrm{d}z \;\; \frac{{}_1 \mathrm{N}_0 W I_1}{P_{\mathrm{s}} \; {}_{\mathrm{as}} G_{\mathrm{s}} G_{\mathrm{u}}} \;\; \frac{{}_2 \mathrm{N}_0 W I_2}{P_{\mathrm{m}} \; {}_{\mathrm{bm}} G_{\mathrm{m}} G_{\mathrm{s}}} \;\; \tilde{}_{\mathrm{b}_t}((0; I_2]; I_1; 0) \sum_{j 2 \mathrm{fm;sg}} {}_{\mathrm{a}_j}((0; \;\; {}_{j;\mathrm{s}} I_1]) \mathrm{A}$$

$$\tilde{}_{\mathrm{b}_{s;t}}(I_2; I_1; 0) \;\; {}_{\mathrm{a}_{s;t}}(I_1) \; \mathrm{d}I_2 \; \mathrm{d}I_1: \tag{8.29}$$

Proof. The MBS coverage can be written as $\mathrm{P}(\mathrm{SINR_a}(\mathbf{0}) > \; jx \;\; 2 \;\; {}_{\mathrm{m}}) =$

$$\mathrm{P} \;\; \frac{P_{\mathrm{m}} \; {}_{\mathrm{am}} G_{\mathrm{m}} G_{\mathrm{u}} h_{0;\mathbf{x}} \; L_{\mathrm{am}}(k\mathbf{x} \; k)^{\;\; 1}}{I_{\mathrm{as}} + \mathrm{N}_0 W} > \;\; \mathbf{x} \;\; 2 \;\; {}_{\mathrm{m}} \;\; = \mathrm{P} \;\; h_{0;\mathbf{x}} > \frac{I_{\mathrm{as}} + \mathrm{N}_0 W}{P_{\mathrm{m}} \; {}_{\mathrm{am}} G_{\mathrm{m}} G_{\mathrm{u}} L_{\mathrm{a}}^{\;\; 1}} \mathbf{x} \;\; 2 \;\; {}_{\mathrm{m}}$$

$$= \mathrm{E} \;\; e^{\;\; \frac{I_{\mathrm{s}} + \mathrm{N}_0 W}{P_{\mathrm{m}} \; {}_{\mathrm{am}} G_{\mathrm{m}} G_{\mathrm{u}} L_{\mathrm{a}}^{\;\; 1}}} \mathbf{x} \;\; 2 \;\; {}_{\mathrm{m}} \;\; = \mathrm{E} \;\; \mathrm{E} \;\; e^{\;\; \frac{L_{\mathrm{a}}}{P_{\mathrm{m}} \; {}_{\mathrm{am}} G_{\mathrm{m}} G_{\mathrm{u}}} I_{\mathrm{as}}} \;\; e^{\;\; \frac{\mathrm{N}_0 W L_{\mathrm{a}}}{P_{\mathrm{m}} \; {}_{\mathrm{am}} G_{\mathrm{m}} G_{\mathrm{u}}}} \mathbf{x} \;\; 2 \;\; {}_{\mathrm{m}} \; :$$

The first step follows from Assumption 3-a. In the last step, the expectations inside the product are conditional expectations given L_{a} while the outer expectation is with respect to L_{a}. Now focusing on the first term of the product, which can be also viewed as the Laplace transform of I_{as} evaluated at $\frac{L_{\mathrm{a}}}{P_{\mathrm{m}} \; {}_{\mathrm{am}} G_{\mathrm{m}} G_{\mathrm{u}}}$, $\mathrm{E} \;\; e^{\;\; \frac{L_{\mathrm{a}}}{P_{\mathrm{m}} \; {}_{\mathrm{am}} G_{\mathrm{m}} G_{\mathrm{u}}} I_{\mathrm{as}}} \;\; =$

$$\mathrm{E} \;\; \exp \;\; \frac{L_{\mathrm{a}}}{P_{\mathrm{m}} \; {}_{\mathrm{am}} G_{\mathrm{m}} G_{\mathrm{u}}} \sum_{\substack{z 2 L_{\mathrm{as}}; \\ z > \; {}_{\mathrm{s;m}} L_{\mathrm{a}}}} P_{\mathrm{s}} h_{0;\mathbf{x}} \; {}_{\mathrm{as}} \; {}_{\mathrm{as}} z^{\;\; 1} \overset{(a)}{=} \mathrm{E} \prod_{\substack{z 2 L_{\mathrm{as}}; \\ z > \; {}_{\mathrm{s;m}} L_{\mathrm{a}}}} \mathrm{E} \;\; e^{\;\; \frac{P_{\mathrm{s}} h_{0;\mathbf{x}} \; {}_{\mathrm{as}} \; {}_{\mathrm{as}} L_{\mathrm{a}}}{P_{\mathrm{m}} \; {}_{\mathrm{am}} G_{\mathrm{m}} G_{\mathrm{u}} z}} \;\; L_{\mathrm{a}}$$

$$= \mathrm{E} \prod_{\substack{z 2 L_{\mathrm{as}}; \\ z > \; {}_{\mathrm{s;m}} L_{\mathrm{a}}}} \mathrm{E} \; \frac{1}{1 + \frac{P_{\mathrm{s}} \; {}_{\mathrm{as}} \; {}_{\mathrm{as}} L_{\mathrm{a}}}{P_{\mathrm{m}} \; {}_{\mathrm{am}} G_{\mathrm{m}} G_{\mathrm{u}} z}} \;\; L_{\mathrm{a}} = \prod_{G 2 M_{\mathrm{as}}} e^{\;\; \int_{{}_{\mathrm{s;m}} L_{\mathrm{a}}}^{\infty} 1 - \frac{1}{1 + \frac{P_{\mathrm{s}} \; {}_{\mathrm{as}} G L_{\mathrm{a}}}{P_{\mathrm{m}} \; {}_{\mathrm{am}} G_{\mathrm{m}} G_{\mathrm{u}} z}} \;\; p_G \; {}_{\mathrm{as}}(z) \, \mathrm{d}z} \; :$$

Step (a) follows from the assumption that $fh_{0;\mathbf{x}}g$ is an i.i.d. sequence of exponential random variables. The last step follows from the fact that conditioned on L_{a} , the pathloss process of the BSs of $\;\; {}_{\mathrm{s}}$ with effective antenna gain G is a thinned version of the PPP $L_{\mathrm{as}} \setminus [0; \;\; {}_{\mathrm{s;m}} L_{\mathrm{a}}]^c$ with thinning probability p_G [114]. Hence we apply the probability generating functional

of PPP [17] to compute the product over the point process. The final expression in (8.28) is obtained by deconditioning over the distribution of L_a whose PDF is given by (8.24). Now, the conditional joint SBS and backhaul coverage can be expressed as: $\mathrm{P}(\mathrm{SINR_a}(\mathbf{0}) > {}_1; \mathrm{SNR_b}(\mathbf{x}) > {}_2 | \mathbf{x} \; 2 \; {}_s) =$

$$\sum_{s(\mathbf{x}) \in \{\mathbf{x}, \mathbf{n}\}} \mathrm{P}(\mathrm{SINR_a}(\mathbf{0}) > {}_1; \mathrm{SNR_b}(\mathbf{x}) > {}_2 | \mathbf{x} \; 2 \; {}_s; s(\mathbf{x}; \mathbf{0})) \mathrm{P}(s(\mathbf{x}; \mathbf{0}) | \mathbf{x} \; 2 \; {}_s)$$

$$= \sum_{s(\mathbf{x}) \in \{\mathbf{x}, \mathbf{n}\}} \mathrm{P}(\mathrm{SINR_a}(\mathbf{0}) > {}_1; \mathrm{SNR_b}(\mathbf{x}) > {}_2 | \mathbf{x}; \mathbf{x} \; 2 \; {}_s; s(\mathbf{x}; \mathbf{0})) \frac{\mathrm{P}(s(\mathbf{x}; \mathbf{0}); \mathbf{x} \; 2 \; {}_s)}{\mathrm{P}(\mathbf{x} \; 2 \; {}_s)}.$$

The second term under the summation is equal to A_{s_k}/A_s and the first term can be simplified as: $\mathrm{P}(\mathrm{SINR_a}(\mathbf{0}) > {}_1; \mathrm{SNR_b}(\mathbf{x}) > {}_2 | \mathbf{x} \; 2 \; {}_s; s(\mathbf{x}; \mathbf{0})) =$

$$\mathrm{P}\left(\frac{P_s \; {}_{a_s} G_s G_u h_{0;\mathbf{x}} \; L_a \; {}^{-1}}{I_{a_s} + \mathrm{N}_0 W} > {}_1; \frac{P_m \; {}_{a_m} G_m G_s h_{\mathbf{x};\mathbf{x}} \; \tilde{L}_b \; {}^{-1}}{\mathrm{N}_0 W} > {}_2 \mathbf{x} \; 2 \; {}_s; s(\mathbf{x}; \mathbf{0}) \right)$$

$$= \mathrm{P}\left(h_{0;\mathbf{x}} > \frac{{}_1 (I_{a_s} + \mathrm{N}_0 W) L_a}{P_s \; {}_{a_s} G_s G_u}; h_{\mathbf{x};\mathbf{x}} > \frac{{}_2 \mathrm{N}_0 W \tilde{L}_b}{P_m \; {}_{a_m} G_m G_s} \mathbf{x} \; 2 \; {}_s; s(\mathbf{x}; \mathbf{0}) \right)$$

$$= \mathrm{E}\left[e^{-\frac{{}_1 (I_{a_s} + \mathrm{N}_0 W) L_a}{P_s \; {}_{a_s} G_s G_u}} \right] \mathrm{E}\left[e^{-\frac{{}_2 \mathrm{N}_0 W \tilde{L}_b}{P_m \; {}_{a_m} G_m G_s}} | L_a; s(\mathbf{x}; \mathbf{0}); \mathbf{x} \; 2 \; {}_s \; \mathbf{x} \; 2 \; {}_s; s(\mathbf{x}; \mathbf{0}) \right].$$

The first step follows from Assumption 3-a. Here $\tilde{L}_b = \min(L_{b_m} | \mathbf{x} \; 2 \; {}_s; s(\mathbf{x}; \mathbf{0}))$. Note that the outer expectation is with respect to $L_a | \mathbf{x} \; 2 \; {}_s; s(\mathbf{x}; \mathbf{0})$ whose PDF is given by Corollary 8.9. The first exponential term can be handled exactly as the MBS coverage. The inner expectation is with respect to $\tilde{L}_b | \mathbf{x} \; 2 \; {}_s; s(\mathbf{x}; \mathbf{0}); L_a$ whose PDF is given by: $f_{\tilde{L}_b}(l | \mathbf{x} \; 2 \; {}_s; s(\mathbf{x}; \mathbf{0}) = t; L_a) = \mathrm{E}[\tilde{}_{b_t}(I; L_a; \;)e^{-\tilde{}_{b_t}((0;I];L_a;\;)}] = \tilde{}_{b_t}(I; L_a; 0)e^{-\tilde{}_{b_t}((0;I];L_a;0)}; \; I > 0;$ where $\tilde{}_{b_t}(I; L_a; \;)$ and $\tilde{}_{b_t}((0; I]; L_a; \;)$ are obtained from Lemma 8.10. Note that the expectation with respect to (which is a uniform random variable within $(0; 2 \;]$) can be simplified since it can be shown that the function under the exception is invariant to . □

Note that the summation appearing in the expression of joint SBS and backhaul coverage in (8.29) is over the link states of the access link between the typical user and the serving SBS.

Remark 8.12. It is worth mentioning that one of the key contributions of this chapter is the characterization of the joint SBS and backhaul coverage in mm-wave HetNets. This is enabled by the exponential path-loss assumption and can facilitate the analysis of joint coverage in other similar settings such as [147], some of which may yield much simpler forms for the expression.

However, for our case, since (8.29) contains (8.26) and (8.27) which have integrals over discontinuous functions that are prone to numerical errors, we simplify the expression of

joint SBS and backhaul coverage with the following Assumption. As will be evident in the sequel, this facilitates further analysis without compromising the accuracy of the results and design insights.

Assumption 4. The joint SBS and backhaul coverage is approximated as the product of the coverages of a typical access and typical backhaul link:

$$\mathsf{P}(\mathsf{SINR}_{\mathsf{a}}(\mathbf{0}) > {}_1; \mathsf{SNR}_{\mathsf{b}}(\mathbf{x}) > {}_2 | \mathbf{x} \;\; 2 \;\; {}_{\mathsf{s}}) = \mathsf{P}(\mathsf{SINR}_{\mathsf{a}}(\mathbf{0}) > {}_1 | \mathbf{x} \;\; 2 \;\; {}_{\mathsf{s}}) \mathsf{P}(\mathsf{SNR}_{\mathsf{b}}(\mathbf{0}) > {}_2); \tag{8.30}$$

where $\mathsf{SNR}_{\mathsf{b}}(\mathbf{0})$ is the SNR of a typical backhaul link.

The main reason for the expression of (8.29) to be complex is the correlation of $\mathsf{SINR}_{\mathsf{a}}(\mathbf{x})$ and $\mathsf{SNR}_{\mathsf{b}}(\mathbf{x})$. Since we ignore this correlation in the above assumption, we obtain a simpler expression for the joint SBS and backhaul coverage in the following Corollary.

Corollary 8.13. *Under Assumption 4, the joint SBS and backhaul coverage is given by:*

$$\mathsf{P}(\mathsf{SINR}_{\mathsf{a}}(\mathbf{0}) > {}_1 | \mathbf{x} \;\; 2 \;\; {}_{\mathsf{s}}) \mathsf{P}(\mathsf{SNR}_{\mathsf{b}}(\mathbf{0}) > {}_2) = \frac{1}{A_{\mathsf{s}}} \int_0^{\infty} \exp\left(- \sum_{G 2 M_{\mathsf{a}_{\mathsf{s}}} l_1} 1 - \frac{1}{1 + \frac{{}_1 G l_1}{G_{\mathsf{s}} z}} \right)^{!}$$
$$p_{G \;\; \mathsf{a}_{\mathsf{s}}}(z) \mathrm{d}z \;\; \frac{{}_1 \mathsf{N}_0 W l_1}{P_{\mathsf{m}} \;\; \mathsf{a}_{\mathsf{m}} G_{\mathsf{m}}} \sum_{j 2 \{\mathsf{m};\mathsf{s}\}} \mathsf{a}_j((0; \;\; {}_{j;\mathsf{s}} l_1]) \;\; \mathsf{a}_{\mathsf{s}}(l_1) \, \mathrm{d}l_1$$
$$\int_0^{\infty} \exp\left(- \frac{{}_2 \mathsf{N}_0 W l_2}{P_{\mathsf{m}} \;\; \mathsf{b}_{\mathsf{m}} G_{\mathsf{m}} G_{\mathsf{s}}} \;\; \mathsf{b}_{\mathsf{m}}((0; l_2]) \right) \;\; \mathsf{b}_{\mathsf{m}}(l_2) \, \mathrm{d}l_2 \tag{8.31}$$

Proof. The two probability terms appearing in the product can be handled separately. The first term can be simplified by following the same steps used to derive the MBS coverage. For the second term, $\mathsf{P}(\mathsf{SNR}_{\mathsf{b}}(\mathbf{0}) > {}_2) =$

$$\mathsf{P}\left(\frac{P_{\mathsf{m}} \;\; \mathsf{a}_{\mathsf{m}} G_{\mathsf{m}} G_{\mathsf{s}} h_{\mathbf{0};\mathbf{x}} L_{\mathsf{b}_{\mathsf{m}}}(k\mathbf{x}k)^{\;\; 1}}{\mathsf{N}_0 W} > {}_2 \right) = \mathsf{P}\left(h_{\mathbf{0};\mathbf{x}} > \frac{{}_2 \mathcal{L}_{\mathsf{b}_{\mathsf{m}}} \mathsf{N}_0 W}{P_{\mathsf{m}} \;\; \mathsf{a}_{\mathsf{m}} G_{\mathsf{m}} G_{\mathsf{s}}} \right) = \mathsf{E}\left[e^{\; \frac{{}_2 \mathcal{L}_{\mathsf{b}_{\mathsf{m}}} \mathsf{N}_0 W}{P_{\mathsf{m}} \;\; \mathsf{a}_{\mathsf{m}} G_{\mathsf{m}} G_{\mathsf{s}}}} \right];$$

where $\mathbf{x}$ denotes the location of the MBS serving the typical SBS and $\mathcal{L}_{\mathsf{b}_{\mathsf{m}}} = \min(L_{\mathsf{b}_{\mathsf{m}}})$, where the PPP $L_{\mathsf{b}_{\mathsf{m}}}$ is defined in Definition 8.3. Thus, the PDF of $\mathcal{L}_{\mathsf{b}_{\mathsf{m}}}$ is given by $f_{\mathcal{L}_{\mathsf{b}_{\mathsf{m}}}}(l) = {}_{\mathsf{b}_{\mathsf{m}}}(l) e^{\; {}_{\mathsf{b}_{\mathsf{m}}}((0;l])}; \; l > 0$. The final expression is obtained by deconditioning with respect to $\mathcal{L}_{\mathsf{b}_{\mathsf{m}}}$. Hence, $\mathsf{P}(\mathsf{SNR}_{\mathsf{b}}(\mathbf{0}) > {}_2) = \int_0^{\infty} e^{\; \frac{{}_2 l_2 \mathsf{N}_0 W}{P_{\mathsf{m}} \;\; \mathsf{a}_{\mathsf{m}} G_{\mathsf{m}} G_{\mathsf{s}}}} \;\; {}_{\mathsf{b}_{\mathsf{m}}}(l_2) e^{\; {}_{\mathsf{b}_{\mathsf{m}}}((0;l_2])} \mathrm{d}l_2;$ □

8.3.2 Load distribution

We now focus on the distributions of loads on the serving BS and the anchor MBS which appeared in the expression of rates in (8.10), (8.13), and (8.15). Note that although we relied

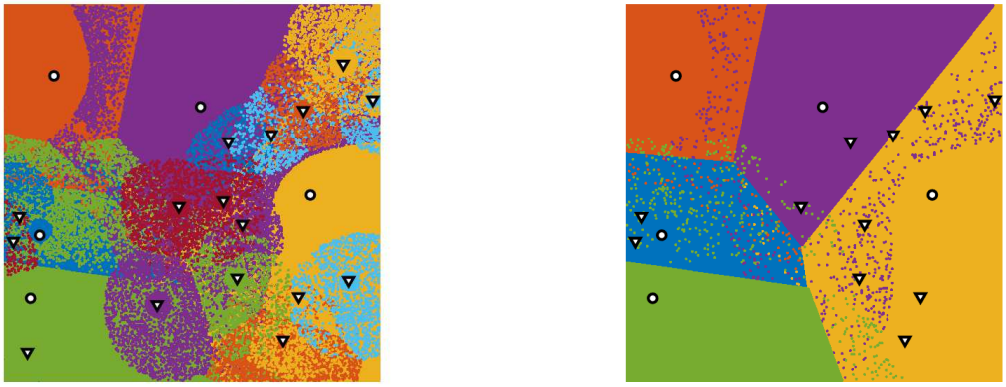

(a) Association cells for RAN (b) Association cells for backhaul network

Figure 8.5: Association cells formed by the BSs of the two-tier HetNet under independent blocking. Circles represent the MBSs, and triangles represent the SBSs.

on Assumption 2 for the SINR analysis (for which it is well-accepted and reasonable), it is not quite meaningful for load analysis where it is imperative to consider spatial correlation of the link states to make sure that two adjoining points in space are not assigned to two different association cells. That said, the existing works on the load characterization in a PPP-network (such as [129]) completely ignore this spatial correlation and simply assume that the link states seen by any two points are completely independent. This assumption leads to the association cells (a key component of the load analysis) that have no physical significance (such as the ones shown in in Figs. 8.5a and 8.5b). On the contrary, the association cells have much regular shape (see Figs. 8.3a and 8.3b) if we consider spatial correlation of link states which is induced by the germ-grain model. However, the exact characterization of the association cells in our current setup is extremely difficult. Note that for a PPP-modeled HetNet in sub-6 GHz, the association cell areas can be analyzed under very simple propagation environment with no blockage-effects which reduces to the formation of weighted Poisson Voronoi (PV) tessellation [24, 128, 141]. While the weighted PV cells may not appear to be directly applicable to the setting considered in this chapter, one can discover some useful connections in order to obtain a tractable characterization of load. The key enabling argument is provided next.

Remark 8.14. Since the spatial distribution of blockages is stationary [145], the association cells generated by $_{\mathsf{m}}$ and $_{\mathsf{s}}$ according to the association rules given by (8.3) and (8.4) are stationary partition of R^2 [141]. Hence it is possible to characterize the mean area of a typical association cell (denoted by $\mathsf{C}_{\mathsf{a}_i}(\mathbf{0})$ and $\mathsf{C}_{\mathsf{b}}(\mathbf{0})$).

This helps us to formulate the following proposition.

Proposition 8.15. *The mean area of a typical backhaul association cell is* $\mathsf{E}[|C_{\mathsf{b}}(\mathbf{0})|] = \frac{1}{\lambda_{\mathsf{m}}}$ *and mean area of a typical access association cell is* $\mathsf{E}[|C_{\mathsf{a}_i}(\mathbf{0})|] = \frac{A_i}{\lambda_i}$ *(*$i \in \{\mathsf{m}, \mathsf{s}\}$*).*

Proof. Following Remark 8.14, (8.4) is a stationary association strategy, for which $\mathsf{E}[|C_{\mathsf{b}}(\mathbf{0})|] = \frac{1}{\lambda_{\mathsf{m}}}$ [141]. For the access association cells, a typical cell belongs to Φ_i with probability $\mathsf{P}(\mathbf{0} \in \Phi_i) = A_i$ (according to Definition 8.1). Hence, $\mathsf{E}[|C_{\mathsf{a}_i}(\mathbf{0})|] = \frac{A_i}{\lambda_i}$. □

We now explain the reason of calibrating λ_{u} according to Remark 8.7.

Remark 8.16. According to Proposition 8.15, we need A_i to characterize the mean access association cell areas. While A_i can be evaluated analytically for simpler blockage models [129], its analytical characterization does not seem straightforward for the germ grain-model considered in Section 8.2. However, since λ_{u} was chosen in a way that always ensures that A_i obtained by (8.23) is equal to the empirically obtained A_i, we are able to accurately capture the mean association cell areas into our analysis.

We now compute the load distributions as follows.

Lemma 8.17. *Under Proposition 8.15, the PMFs of* $\Phi_{\mathsf{u}}(C_{\mathsf{a}_{\mathsf{m}}}(\mathbf{x}))$ *and* $\Phi_{\mathsf{u}}(C_{\mathsf{a}_{\mathsf{s}}}(\mathbf{x}))$ *are given as:*

$$\mathsf{P}(\Phi_{\mathsf{u}}(C_{\mathsf{a}_i}(\mathbf{x})) = n) = \mathsf{K}_t(n; \tfrac{i}{A_i}; \lambda_{\mathsf{u}}); \mathsf{P}(\Phi_{\mathsf{u}}(C_{\mathsf{a}_{\mathsf{m}}}(\mathbf{x})) = n) = \mathsf{K}(n; \tfrac{i}{A_{\mathsf{m}}}; \lambda_{\mathsf{u}}); i \in \{\mathsf{m}, \mathsf{s}\}; \tag{8.32}$$

where

$$\mathsf{K}_t(n; ; \lambda_{\mathsf{u}}) = \frac{3.5^{3.5}}{(n-1)!} \frac{(n+3.5)}{(3.5)} \left(\frac{\lambda_{\mathsf{u}}}{}\right)^{n-1} \left(3.5 + \frac{\lambda_{\mathsf{u}}}{}\right)^{-n-3.5}; n \geq 1; \tag{8.33}$$

$$\mathsf{P}(\Phi_{\mathsf{s}}(C_{\mathsf{b}}(\mathbf{x})) = n) \quad \mathsf{P}(\Phi_{\mathsf{s}}(C_{\mathsf{b}}(\mathbf{x}) = n) = \mathsf{K}(n; \lambda_{\mathsf{m}}; \lambda_{\mathsf{s}}); n \geq 0; \tag{8.34}$$

and

$$\mathsf{K}(n; ; \lambda_{\mathsf{u}}) = \frac{3.5^{3.5}}{n!} \frac{(n+3.5)}{(3.5)} \left(\frac{\lambda_{\mathsf{u}}}{}\right)^{n} \left(3.5 + \frac{\lambda_{\mathsf{u}}}{}\right)^{-n-3.5}; n \geq 0. \tag{8.35}$$

Note that a random variable following the PMF $\mathsf{K}(\ ; \lambda_1; \lambda_2)$ has mean $\lambda_2 = \lambda_1$.

8.3.3 Rate coverage probability

We are now in position to evaluate the rate coverage.

Theorem 8.18. *Rate coverage for a typical UE in the two-tier HetNet with IAB introduced in Section 8.2 for a target rate-threshold is expressed as follows.*

$$\mathrm{P_r}^{\mathrm{IRA}}(\ ) = A_{\mathrm{m}} \sum_{n=1}^{\infty} \mathrm{P}\left[\mathrm{SINR_a}(0) > 2^{\overline{w}\left(n+\frac{A_{\mathrm{s}}\ \mathrm{u}}{\mathrm{m}}\right)} \quad 1\right] \mathrm{K}_t\ \ n; \frac{\mathrm{m}}{A_{\mathrm{m}}};\ \mathrm{u}$$
$$+ A_{\mathrm{s}} \sum_{n=1}^{\infty} \mathrm{P}\left[\mathrm{SINR_a}(0) > 2^{\frac{n}{\overline{w}}\left(1+\frac{\mathrm{m}\,n}{\mathrm{u}}\right)} \quad 1\right] \mathrm{P}\left[\mathrm{SNR_b}(0) > 2^{\frac{\left(n+\frac{\mathrm{u}}{\mathrm{m}}\right)}{w}} \quad 1\right] \mathrm{K}_t\ \ n; \frac{\mathrm{s}}{A_{\mathrm{s}}};\ \mathrm{u}\ : \tag{8.36}$$

$$\mathrm{P_r}^{\mathrm{ORA}}(\ ) = A_{\mathrm{m}} \sum_{n=1}^{\infty} \mathrm{P}\left[\mathrm{SINR_a}(0) > 2^{\frac{n}{\mathrm{a}\overline{W}}} \quad 1\right] \mathrm{K}_t\ \ n; \frac{\mathrm{m}}{A_{\mathrm{m}}};\ \mathrm{u}$$
$$+ A_{\mathrm{s}} \sum_{n=1}^{\infty} \mathrm{P}(\mathrm{SINR_a}(0) > 2^{\frac{n}{\overline{W}\ \mathrm{a}}} \quad 1)\mathrm{P}(\mathrm{SNR_b}(0) > 2^{\frac{\left(n+\frac{A_{\mathrm{s}}\ \mathrm{u}}{\mathrm{m}}\right)}{\overline{W}(1\ \ \mathrm{a})}} \quad 1)\mathrm{K}_t\ \ n; \frac{\mathrm{s}}{A_{\mathrm{s}}};\ \mathrm{u}\ ; \tag{8.37}$$

where the MBS coverage, joint SBS and backhaul coverage, and $\mathrm{K}_t(\ )$ *are given by* (8.28), (8.31), *and* (8.33), *respectively.*

Proof. For IRA, following (8.10), the CCDF of $\mathtt{Rate}^{\mathrm{IRA}}$ is given by

$$\mathrm{P}(\mathrm{Rate_{IRA}}) = A_{\mathrm{m}}\mathrm{P}\left[\frac{W}{\mathrm{u}(C_{\mathrm{a_m}}(\mathbf{x}\ )) + \sum_{\mathbf{x}2\ \ \mathrm{s}\,|\,C_{\mathrm{b}}(\mathbf{x}\ )} \mathrm{u}(C_{\mathrm{a_s}}(\mathbf{x}))} \log\left(1+\mathrm{SINR_a}(0)\right) >\right.$$
$$\left. + A_{\mathrm{s}}\mathrm{P}\left[\frac{W}{\mathrm{u}(C_{\mathrm{a_s}}(\mathbf{x}\ ))} \min\left(!\log\left(1+\mathrm{SINR_b}(\mathbf{x}\ )\right); (1 \quad !)\log\left(1+\mathrm{SINR_a}(0)\right)\right) > \right.\right. : \tag{8.38}$$

The first term of the summation, i.e., the conditional rate coverage when the typical UE connects to an MBS can be simplified as

$$A_{\mathrm{m}}\mathrm{P}\left[\mathrm{SINR_a}(0) > 2^{\overline{w}\left(\mathrm{u}(C_{\mathrm{a_m}}(\mathbf{x}\ ))+\sum_{\mathbf{x}2\ \ \mathrm{a_s}\,|\,C_{\mathrm{b}}(\mathbf{x}\ )} \mathrm{u}(C_{\mathrm{a_s}}(\mathbf{x}))\right)^{!}} \quad 1\right] :$$

The PMF of $\mathrm{u}(C_{\mathrm{m}}(\mathbf{x}\ ))$ is given by Lemma 8.17. The second term can be approximated as the average number of UEs per SBS (i.e. $A_{\mathrm{s}}\ \mathrm{u}=\ \mathrm{s}$) times the number of SBSs falling in $C_{\mathrm{b}}(\mathbf{x}\ )$: $\sum_{\mathbf{x}2\ \ \mathrm{s}\,|\,C_{\mathrm{b}}(\mathbf{x}\ )} \mathrm{u}(C_{\mathrm{a_s}}(\mathbf{x}))\ \ \frac{A_{\mathrm{s}}\ \mathrm{u}}{\mathrm{s}}\mathrm{E}[\ \mathrm{s}(C_{\mathrm{b}}(\mathbf{x}\ ))] = \frac{A_{\mathrm{s}}\ \mathrm{u}}{\mathrm{s}}\ \ \frac{\mathrm{s}}{\mathrm{m}} = \frac{A_{\mathrm{s}}\ \mathrm{u}}{\mathrm{m}}$: The PMF of $\mathrm{s}(C_{\mathrm{b}}(\mathbf{x}\ ))$ is given by Lemma 8.17. We now focus on the second term in (8.38) which can be simplified as:

$$A_{\mathrm{s}}\mathrm{P}\left[\mathrm{SINR_a}(0) > 2^{\overline{w}\ \ \mathrm{u}(C_{\mathrm{a_s}}(\mathbf{x}\ ))\ 1+\frac{\sum \mathrm{u}(C_{\mathrm{a_s}}(\mathbf{x}\ ))}{\mathrm{u}(C_{\mathrm{a_m}}(\mathbf{x}))+\sum_{\mathbf{x}2\ \ \mathrm{s}\,|\,C_{\mathrm{b}}(\mathbf{x})\cap f\mathbf{x}\ \ g} \mathrm{u}(C_{\mathrm{a_s}}(\mathbf{x}))}} \quad 1\right]$$

$$\mathsf{P}\left(\mathsf{SNR}_{\mathsf{b}}(\mathbf{0}) > 2^{\overline{w}\left(\ _{\mathsf{u}}(C_{\mathsf{a}_{\mathsf{m}}}(\mathbf{x}))+\ _{\mathsf{u}}(C_{\mathsf{a}_{\mathsf{s}}}(\mathbf{x}\ ))+\sum_{\mathbf{x}2\ _{\mathsf{s}}\setminus C_{\mathsf{b}}(\mathbf{x})nf\mathbf{x}\ g}\ _{\mathsf{u}}(C_{\mathsf{a}_{\mathsf{s}}}(\mathbf{x}))\right)}\right)\quad 1\ :$$

To obtain the final expression, the following approximations on the load variables is applied: $\sum_{\mathbf{x}2\ _{\mathsf{s}}\setminus C_{\mathsf{b}}(\mathbf{x})nf\mathbf{x}\ g}\ _{\mathsf{u}}(C_{\mathsf{a}_{\mathsf{s}}}(\mathbf{x}))\quad \frac{A_{\mathsf{s}}\ _{\mathsf{u}}}{_{\mathsf{s}}}\mathsf{E}[\ _{\mathsf{s}}(C_{\mathsf{b}}(\mathbf{x}))] = \frac{A_{\mathsf{s}}\ _{\mathsf{u}}}{_{\mathsf{s}}}\ \frac{_{\mathsf{s}}}{_{\mathsf{m}}} = \frac{A_{\mathsf{s}}\ _{\mathsf{u}}}{_{\mathsf{m}}}$; and $_{\mathsf{u}}(C_{\mathsf{a}_{\mathsf{m}}}(\mathbf{x}))\ \mathsf{E}[\ _{\mathsf{u}}(C_{\mathsf{a}_{\mathsf{m}}}(\mathbf{x}))] = \frac{A_{\mathsf{m}}\ _{\mathsf{u}}}{_{\mathsf{m}}}$.

For ORA, following (8.13), $\mathsf{P}_{\mathsf{r}}{}^{\mathsf{ORA}} =$

$$A_{\mathsf{m}}\mathsf{P}\left(\mathsf{SINR}_{\mathsf{a}}(\mathbf{0}) > 2^{\frac{_{\mathsf{u}}(C_{\mathsf{a}_{\mathsf{m}}}(\mathbf{x}\ ))}{_{\mathsf{a}}\overline{w}}}\quad 1\right) + A_{\mathsf{s}}\mathsf{P}\left(\mathsf{SINR}_{\mathsf{a}}(\mathbf{0}) > 2^{\frac{_{\mathsf{u}}(C_{\mathsf{a}_{\mathsf{s}}}(\mathbf{x}\ ))}{_{\mathsf{a}}\overline{w}}}\quad 1\right)$$
$$\mathsf{P}\left(\mathsf{SNR}_{\mathsf{b}}(\mathbf{0}) > 2^{\frac{\sum_{\mathbf{x}2C_{\mathsf{b}}(\mathbf{x})nf\mathbf{x}\ g}\ _{\mathsf{u}}(C_{\mathsf{a}_{\mathsf{s}}}(\mathbf{x}))+\ _{\mathsf{u}}(C_{\mathsf{a}_{\mathsf{s}}}(\mathbf{x}))}{\overline{w}(1\quad _{\mathsf{a}})}}\right)\quad 1\ :$$

From this step, the final expression of rate coverage for ORA can be derived on similar lines of the derivation for IRA. □

We conclude this Section with the rate coverages of a single-tier macro-only network and a two-tier HetNet with fiber-backhauled SBSs which will be used for comparing the performances of IRA and ORA in Section 9.5.3. The former can be obtained from (8.36) by setting $_{\mathsf{s}} = 0$ and the later can be obtained from (8.15) following the steps outlined in the proof of Theorem 8.18.

Corollary 8.19. *For a single tier macro-only network,* P_{r} *is given by:*

$$\mathsf{P}_{\mathsf{r}}(\ ) = \sum_{n=1}^{\infty}\mathsf{P}\left(\mathsf{SINR}_{\mathsf{a}}(\mathbf{0}) > 2^{\frac{n}{\overline{w}}}\quad 1\right)\ \mathsf{K}_t\ \left(n; \frac{_{\mathsf{m}}}{A_{\mathsf{m}}};\ _{\mathsf{u}}\right)\ : \tag{8.39}$$

For a two-tier HetNet with fiber-backhauled SBSs, P_{r} *is given by:*

$$\mathsf{P}_{\mathsf{r}}(\ ) = A_{\mathsf{m}}\sum_{n=1}^{\infty}\mathsf{P}\left(\mathsf{SINR}_{\mathsf{a}}(\mathbf{0}) > 2^{\frac{n}{\overline{w}}}\quad 1\right)\ \mathsf{K}_t\ \left(n; \frac{_{\mathsf{m}}}{A_{\mathsf{m}}};\ _{\mathsf{u}}\right)$$
$$+ A_{\mathsf{s}}\sum_{n=1}^{\infty}\mathsf{P}\left(\mathsf{SINR}_{\mathsf{a}}(\mathbf{0}) > 2^{\frac{n}{\overline{w}}}\quad 1\right)\ \mathsf{K}_t\ \left(n; \frac{_{\mathsf{s}}}{A_{\mathsf{s}}};\ _{\mathsf{u}}\right)\ : \tag{8.40}$$

8.4 Results and Discussions

8.4.1 Verification of Accuracy

We now verify the accuracy of our analysis by comparing our analytical results with Monte Carlo simulations of the network defined in Section 8.2. We further emphasize that the simulation of the network is a "true" simulation in the sense that it accounts for the

Table 8.1: Key system parameters and default values

Notation	Parameter	Value
P_m; P_s	BS transmit powers	40, 20 dBm
$_{k_i;\cdot}$; $_{k_i;n}$ $(8\ k\ 2\ fa; bg, i\ 2\ fm; sg)$	Path-loss exponent	3.0, 4.0
$_{k_i}$ $(8\ k\ 2\ fa; bg, i\ 2\ fm; sg)$	Path loss at 1 m	70 dB
G_m, G_s	BS antenna main lobe gain	18 dB
g_m, g_s	BS antenna side lobe gain	2 dB
G_u, g_u	UE antenna main and side lobe gains	0 dB
$_{k_i}$ $(8\ k\ 2\ fa; bg, i\ 2\ fm; sg)$	LOS range constant	200 m
N_0W	Noise power	174 dBm/Hz+ $10\log_{10}W$ +10 dB (noise-figure)
$f\ _m$; $_s$; $_u g$	Density of MBS, SBS, and user PPP	$f10; 50; 1000g$ km ^{2}
$T_m; T_s$	Bias factors	1,1
$_u$	UE density	1000 km ^{2}
L_{bl}; $_{bl}$	Blockage parameters	5 m, 1500 km ^{2}

spatial correlation of blocking while a lot of the existing works (including 3GPP) consider the independent blocking assumption in simulation. The values of the key system parameters are listed in Table 8.1. For each simulation, the number of iterations was set to $1 \quad 10^3$. The number of iterations is kept low because, as noted in Remark 8.16, the system-level simulation is extremely time consuming. The primary reason is the computation of every link state for which it is required to compute the intersection of each link with all the line segments of $_{bl}$. Following Remark 8.7, we obtain $= 200$ m by matching A_m given by (8.23) with its empirical value obtained by running the simulation scripts provided in [146]. In Fig. 8.6, we plot the MBS and the joint SBS and backhaul coverages. The close match between theory and simulation validates our assumptions for the coverage analysis. We now plot P_r for IRA and ORA obtained from simulation and analysis (see Theorem 8.18). For both strategies, we observe that P_r obtained from our analysis closely follows P_r obtained from simulation. This further highlights the utility of our analytical expressions of P_r which are considerably faster to evaluate than its computation by brute-force simulations.

8.4.2 Optimal bandwidth partition for ORA

In Fig. 8.8, we plot the variation of P_r^{ORA} with $_a$ for ORA. Note that $_a$ defines the BW split for ORA and is hence a crucial system parameter [134]. While it is expected that P_r^{ORA} is quite sensitive to the choice of $_a$, we observe that there is an optimal access-backhaul BW split ($_a$) for which P_r^{ORA} is maximized, i.e., $_a = \arg\max\ P_r^{ORA}(\ ;\ _a)$. We also find that $_a$ decreases with increasing $_s$ which is further evident from Fig. 8.9. This is because as $_s$ increases, sufficient backhaul BW has to be reserved to support a given target data rate. Since this reduces the available access BW, it is clear that SBS densification provides diminishing returns for the overall rate performance of the network. We revisit this observation in Section 8.4.4.

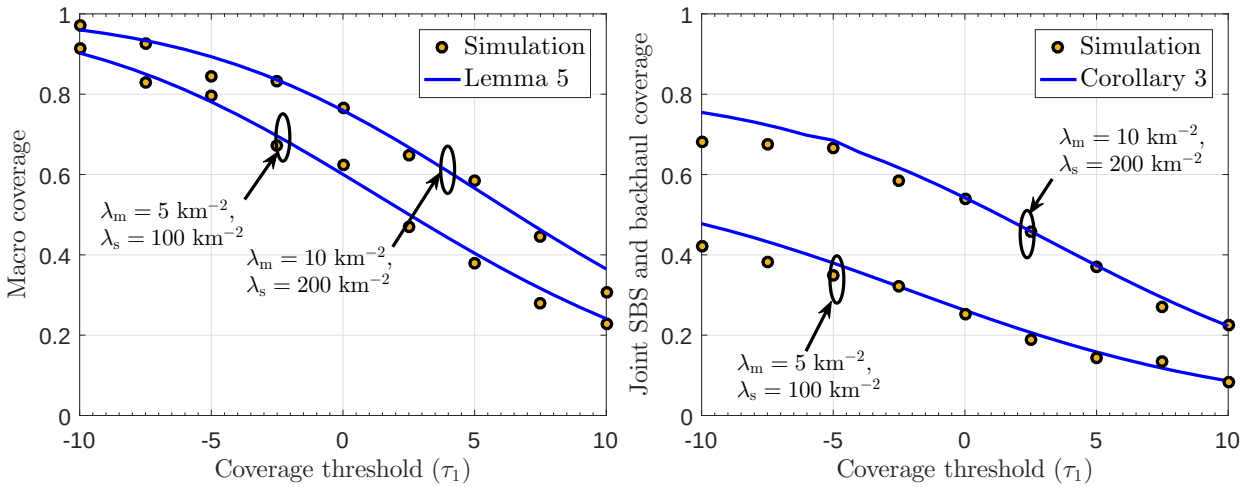

(a) MBS coverage

(b) Joint SBS and backhaul coverage at $_2$ = 5 dB

Figure 8.6: CCDFs of SINR distributions obtained from Monte Carlo simulation and analysis.

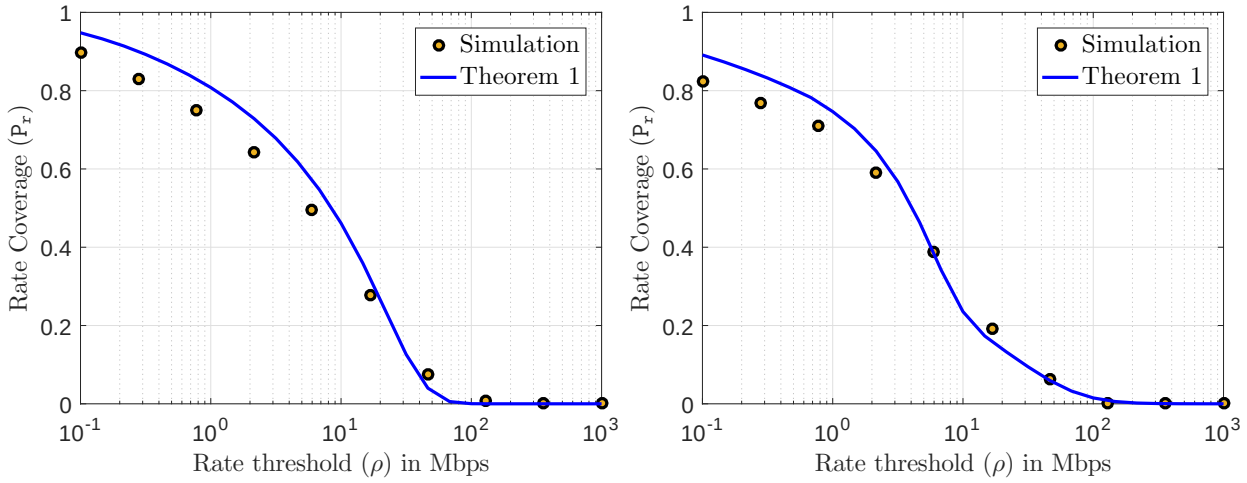

(a) IRA

(b) ORA ($_a$ = 0:8)

Figure 8.7: Rate CCDF for IRA and ORA for the two-tier HetNet with IAB ($_m$ = 5 km ^{2} and $_s$ = 100 km ^{2}).

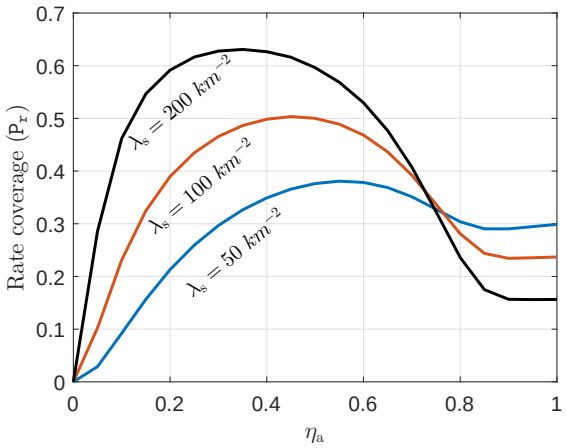

Figure 8.8: Rate coverage versus bandwidth partition factor for ORA (= 20 Mbps).

8.4.3 User offloading and Rate Coverage

We now offload more traffic to SBSs by increasing T_s ($T_m = 1$) and plot P_r and the median rate ($_{50}$ where $P_r(\ _{50}) = 0.5$) for IRA and ORA in Figs. 8.10 and 8.11. For comparison, we also plot P_r and $_{50}$ of a two-tier HetNet with fiber-backhauled SBSs (see Corollary 8.19). We observe that P_r and $_{50}$ are maximized at certain values of T_s. Also, $P_r^{IRA} > P_r^{ORA}$ and $^{IRA}_{50} > {}^{ORA}_{50}$, which are expected because of the system design of ORA, i.e. fixed $_a$ cannot cope up with the increase in backhaul load due to increasing T_s. What is interesting is that the improvement in P_r and $_{50}$ with T_s is much less prominent for IAB than P_r for the HetNet with fiber-backhauled SBSs. This is because the offloaded UEs from $_m$ to $_s$ are not completely disappearing from the MBS load, i.e., they are coming back to the MBS load in the form of increased backhaul load. Note that this phenomena is quite unique to the IAB design and does not occur for the HetNet with fiber-backhauled SBSs. Thus, traffic offloading in IAB-enabled HetNets is not as effective as in HetNets with fiber-backhauled SBSs. However, as indicated by Fig. 8.13, the two-tier network with IAB still performs better than a single-tier macro-only network.

8.4.4 SBS density and Rate coverage

We plot the the variation of P_r with $_s$ in Fig. 8.12. As expected, P_r increases with $_s$. However, while P_r steadily increases with $_s$ for the fiber-backhauled SBSs, P_r tends to saturate for IAB. This effect is more prominent in Fig. 8.13, where we plot $_{50}$ versus $_s$. Figs. 8.12 and 8.13 clearly illustrate the realistic gain of SBS densification in HetNets. Although the two-tier HetNet is prominently advantageous over a single tier macro-only network, the assumption of fiber backhaul for all SBSs leads to an overestimation of the rate improvement of HetNets with increasing $_s$. Since the overall rate is limited by the rate on the backhaul link, increasing $_s$ decreases the rate supported by the wireless backhual as the

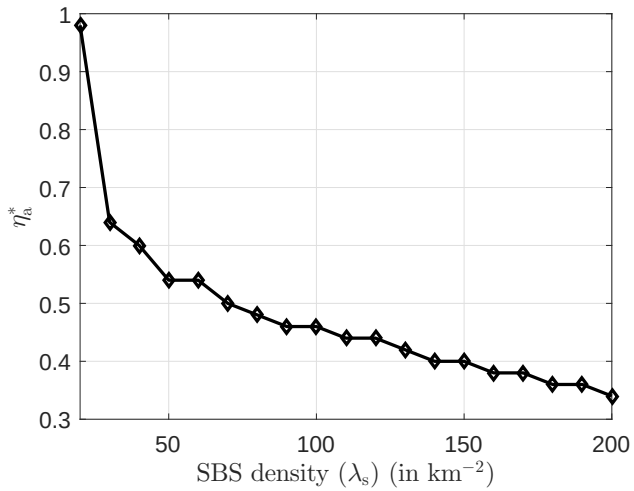

Figure 8.9: Optimum BW partition versus SBS density for ORA (= 20 Mbps).

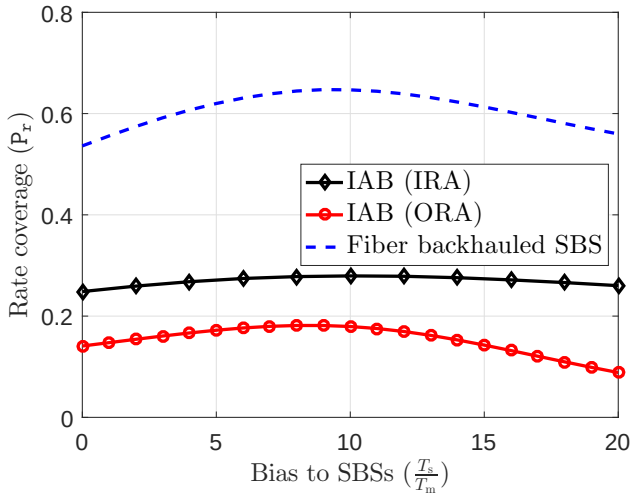

Figure 8.10: Rate coverage versus bias factor (= 50 Mbps).

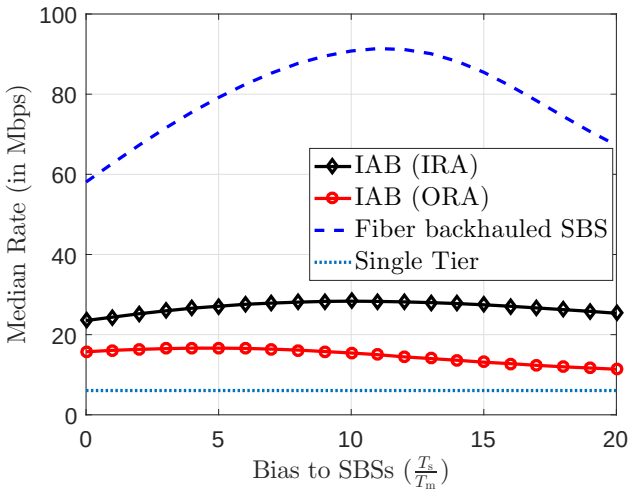

Figure 8.11: Median rate versus bias factor.

BW is shared by more number of SBSs.

8.5 Summary

In this chapter, we proposed a tractable model of an IAB-enabled mm-wave two-tier HetNet where all MBSs have access to fiber backhaul and the SBSs are wirelessly backhauled by the MBSs. For this network, we derived the CCDF of downlink end-user data rate assuming that the total BW at the MBS is split between access and backhaul links by dynamic or static partitions. While the blockages in mm-wave communication and the two hop links from MBS to UE over SBS due to the IAB setup impose analytical challenges for the exact characterization of the rate distributions, we propose reasonable approximations that allow us to obtain easy-to-compute expressions of rate coverage. Using these expressions, we obtain some useful system insights of the multi-tier IAB design such as the impact of traffic offloading and SBS density on data rate.

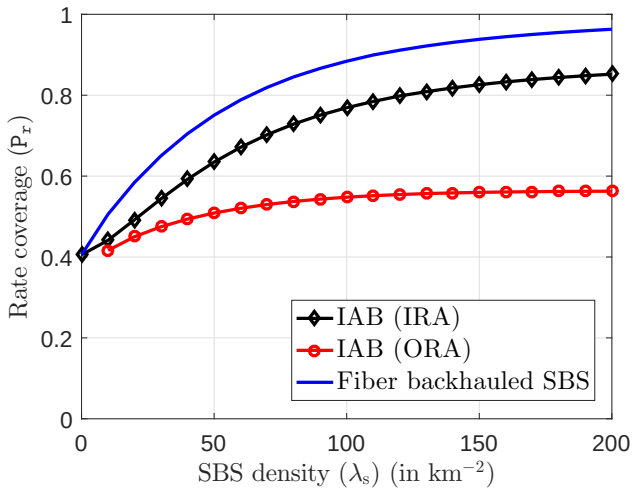

Figure 8.12: Rate coverage versus SBS density (= 10 Mbps, $\frac{T_s}{T_s}$ = 10 dB, a = 0:8).

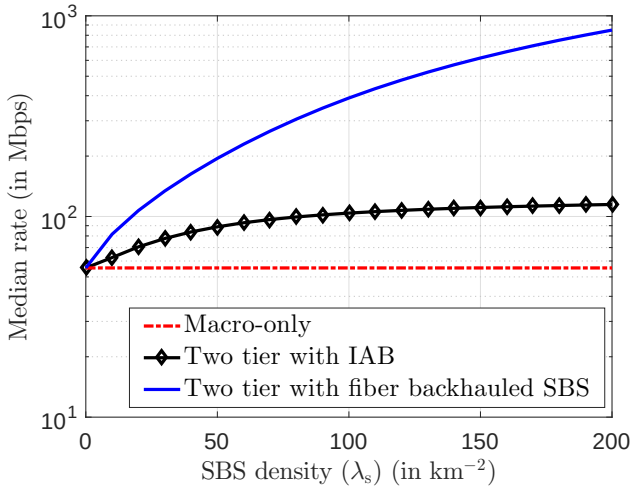

Figure 8.13: Median rate versus SBS density ($\frac{T_s}{T_s}$ = 10 dB).

9

Determinantal Subset Selection for Wireless Networks

9.1 Introduction

ML and SG have recently found many applications in the design and analysis of wireless networks. However, since the nature of the problems studied with these tools are so fundamentally different, it is rare to find a common ground where the strength of these tools can be jointly leveraged. While the foundation of wireless networks is built on traditional probabilistic models (such as channel, noise, interference, queuing models), ML is changing this *model-driven* approach to a more *data-driven* simulation-based approach by *learning* the models from extensive datasets available from real networks or field trials [148]. On the other hand, the basic premise of SG is to enhance the *model-driven* approach by endowing distributions on the locations of the transmitters (Tx-s) and receivers (Rx-s) so that one can derive the exact and tractable expressions for key performance metrics such as interference, coverage, and rate. In this chapter, we concretely demonstrate that these two mathematical tools can be jointly applied to a class of problems known as the *subset selection problems*, which have numerous applications in wireless networks.

9.1.1 Subset selection problems

In wireless networks, a wide class of resource management problems such as power/rate control, link scheduling, network utility maximization, and beamformer design fall into the category of *subset selection problems* where a subset from a ground set needs to be chosen to optimize a given objective function. For most of the cases, finding the optimal subset is NP-hard. The common practice in the literature is to design some heuristic algorithms, which find a local optimum under reasonable complexity. Even most of these heuristic approaches are NP-complete and are hence difficult to implement when the network size grows large.

In ML, subset selection problems appear in a slightly different context where the primary objective is to preserve the balance between *quality* and *diversity* of the items in the subset, i.e., to select good quality items from a ground set which are also non-overlapping in terms of their features. For example, assume that a user is searching the images of New York in a web-browser. The image search engine will pick a subset of stock images related to New York from the image library which contains the popular landmarks (*quality*) as well as

ensure that one particular landmark does not occur repeatedly the search result (*diversity*). Few more examples of subset selection with diversity are text summarization [149], citation management [150], and sensor placement [151]. The attempt to model diversity among the items in a subset selection problem brings us to the probabilistic models constructed by DPPs, which lie at the intersection of ML and SG. Initially formulated as a repulsive point process in SG [66], DPPs are natural choice for inducing diversity or negative correlation between the items in a subset. Although the traditional theoretical development of DPPs has been focused on continuous spaces, the finite version of the DPPs have recently emerged as useful probabilistic models for the subset selection problems with *quality-diversity trade-o* in ML. This is due to the fact that the finite DPPs are amenable to the data-driven learning and inference framework of ML [150].

9.1.2 Relevant prior art on DPPs

In wireless networks, DPPs have mostly been used in the SG-based modeling and analysis of cellular networks. In these models, DPPs are used to capture spatial repulsion in the BS locations, which cannot be modeled using more popular Poisson point process (PPP) [66]. For some specific DPPs, for instance the Ginibre point process, it is possible to analytically characterize the performance metrics of the network such as the coverage probability [84]. However, the finite DPPs and the associated data-driven learning framework, which is under rapid development in the ML community has not found any notable application in wireless networks. The only existing work is [152], where the authors have introduced a new class of *data-driven SG models* using DPP and have trained them to mimic the properties of some hard-core point processes used for wireless network modeling (such as the Matérn type-II process) in a finite window.

9.1.3 Contributions

The key technical contribution of this chapter is the novel *DPPL framework* for solving general subset selection problems in wireless networks.

Application to the link scheduling problem. In order to concretely demonstrate the proposed DPPL framework, we apply it to solve the link scheduling problem which is a classical subset selection problem in wireless networks. The objective is to assign optimal binary power levels to Tx-Rx pairs so as to maximize the sum-rate [153]. The links transmitting at a higher (lower) power level will be termed active (inactive) links. Therefore, the objective is to determine the optimal subset of *simultaneously active links*. Similar to the subset selection problems in ML, the simultaneously active links will be selected by balancing between the quality and diversity. The links which will be naturally favored are the ones with better link quality in terms of signal-to-interference-and-noise-ratio (SINR) so that the rates on these links contribute more to the sum-rate (*quality*). On the other hand, the simultaneously active links will have some degree of spatial repulsion to avoid mutual interference (*diversity*).

With this insight, it is reasonable to treat the set of active links in the optimal solution as a DPP over the set of links in a given network. The DPP is trained by a sequence of networks and their optimal subsets which are generated by using an optimization algorithm based on geometric programming (GP). We observe that the sum-rates of the estimated optimal subsets generated by the trained DPP closely approach the optimal sum-rates. Moreover, we show that the subset selection using DPP is significantly more computationally efficient than the optimization based subset selection methods.

Interference Analysis Assuming that the transmitters are distributed as a DPP, we analytically characterize the characteristic function of interference at an arbitrary point in the network. Using this Laplace transform (LT), we then characterize the cumulative density function (CDF) of interference using the Gil Pelaez inversion formula [97]. Our numerical results demonstrate that even with the aid of simple formulation of quality and diversity metrics in the DPPL, the trained DPP yields near-perfect match with the test data in terms of the interference distribution.

9.2 Determinantal point process: Preliminaries

In this Section, we provide a concise introduction to DPP on finite sets. The interested readers may refer to [150] for a more pedagogical treatment of the topic as well as extensive surveys of the prior art. In general, DPPs are probabilistic models that quantify the likelihood of selecting a subset of items as the determinant of a kernel matrix (K). More formally, if $Y = f1;:::;Ng$ is a discrete set of N items, a DPP is a probability measure on the power set 2^Y which is defined as:

$$P(A \quad \mathbf{Y}) = \det(K_A); \tag{9.1}$$

where $\mathbf{Y}$ P is a random subset of Y and K_A $[K_{i;j}]_{i;j2A}$ denotes the restriction on K 2 $\mathsf{R}^{N \ N}$ to the indices of the elements of A Y ($K_? = 1$). We denote K as the marginal kernel which is a positive semidefinite matrix such that K I (I is an N N identity matrix), i.e. all eigenvalues of K are less than or equal to 1. For learning purposes, it is more useful to define DPP with another formalism known as the *L-ensemble*. A DPP can be alternatively defined in terms of a matrix L (L I) indexed by Y Y:

$$P_L(Y) \quad P_L(\mathbf{Y} = Y) = \frac{\det(L_Y)}{\sum_{Y^0 22^Y} \det(L_{Y^0})} = \frac{\det(L_Y)}{\det(L + I)}; \tag{9.2}$$

where $L_Y = [L_{i;j}]_{i;j2Y}$. The last step follows from the identity $\sum_{Y^0 22^Y} \det(L_{Y^0}) = \det(L + I)$ (see [150, Theorem 2.1] for proof). Following [150, Theorem 2.2], K and L are related by the following equation:

$$K = (L + I) \ ^1 L: \tag{9.3}$$

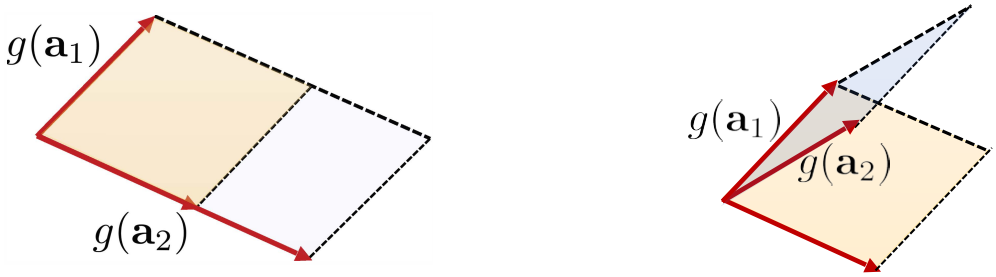

(a) $g(\mathbf{a}_1)$ increases. (b) $S_{1;2}$ increases.

Figure 9.1: In DPP, the probability of occurrence of a set Y depends on the volume of the parallelopiped with sides $g(\mathbf{a}_i)$ and angles proportional to $\arccos(S_{i;j})$: (a) as $g(\mathbf{a}_i)$ increases, the volume increases, (b) as $S_{i;j}$ increases, the volume decreases.

Since, L is real and symmetric by definition, its eigendecomposition is $L = \sum_{n=1}^{N} {}_n \mathbf{v}_n \mathbf{v}_n^{>}$, where $f\mathbf{v}_n g$ is the orthonormal sequence of eigenvectors corresponding to the eigenvalues $f\ {}_n g$. Using (9.3), K can also be obtained by rescaling the eigenvalues of L as:

$$K = \sum_{n=1}^{N} \frac{{}_n}{1 + {}_n} \mathbf{v}_n \mathbf{v}_n^{>}: \tag{9.4}$$

In the ML formalism, if $\mathbf{a}_i \ 2 \ \mathsf{R}^N$ is some vector representation of the i^{th} item of Y, then $L \ 2 \ \mathsf{R}^{N \ N}$ can be interpreted as a kernel matrix, i.e., $L_{i;j} = k(\mathbf{a}_i; \mathbf{a}_j) \quad (\mathbf{a}_i)^{>} \ (\mathbf{a}_j)$; where $k(\ ;\ )$ is a kernel function and $\quad$ is the corresponding feature map. The kernel $k(\mathbf{a}_i; \mathbf{a}_j)$ can be further decomposed according to the quality-diversity decomposition [150] as:

$$L_{i;j} = k(\mathbf{a}_i; \mathbf{a}_j) = g(\mathbf{a}_i) S_{i;j} g(\mathbf{a}_j); \tag{9.5}$$

where $g(\mathbf{a}_i)$ denotes the quality of $\mathbf{a}_i$ $(8i \ 2 \ Y)$ and $S_{i;j} = L_{i;j} = \sqrt{L_{i;i} L_{j;j}}$ denotes the similarity of $\mathbf{a}_i$ and $\mathbf{a}_j$ $(8i; j \ 2 \ Y; i \ 6 \ j)$. Using (9.5), we can write (9.2) after some manipulation as: $P_L(\mathbf{Y} = Y) \ / \ \det(L_Y) = \det(S_Y) \prod_{i2Y} g(\mathbf{a}_i)^2$; where the first term denotes the diversity and second term denotes the quality of the items in Y. We now provide a geometric interpretation of $P_L(\mathbf{Y} = Y)$ as follows.

Remark 9.1. We can intuitively interpret $\det(L_Y)$ as the squared volume of the parallelepiped spanned by the vectors $f \ (\mathbf{a}_i) g_{i2Y}$, where $k \ (\mathbf{a}_i) k = g(\mathbf{a}_i)$ and $\backslash f \ (\mathbf{a}_i); \ (\mathbf{a}_j) g = \arccos(S_{i;j})$. Thus, items with higher $g(\mathbf{a}_i)$ are more probable since the corresponding $(\mathbf{a}_i)$-s span larger volumes. Also diverse items are more probable than the similar items since more orthogonal collection of $(\mathbf{a}_i)$-s span larger volume (see Fig. 9.1 for an illustration). Thus DPP naturally balances the quality and diversity of items in a subset.

9.3 The proposed DPPL framework

9.3.1 Conditional DPPs

Most of the learning applications are *input-driven*. For instance, recalling the image search example, a user input will be required to show the search results. To model these input-driven problems, we require conditional DPPs. In this framework, let X be an external input. Let $Y(X)$ be the collection of all possible candidate subsets given X. The conditional DPP assigns probability to every possible subset $Y \quad Y(X)$ as:

$$P(\mathbf{Y} = Y | X) \; / \; \det(L_Y(X)); \tag{9.6}$$

where $L_Y(X) \; 2 \; (\mathbb{R}^+)^{|Y(X)| \; |Y(X)|}$ is a positive semidefinite kernel matrix. Following (9.2), the normalization constant is $\det(I + L(X))$. Now, similar to the decomposition technique in (9.5),

$$L_{i;j}(X) = g(\mathbf{a}_i | X) S_{i;j}(X) g(\mathbf{a}_j | X); \tag{9.7}$$

where $g(\mathbf{a}_i | X)$ denotes the quality measure of link i and $S_{i;j}(X)$ denotes the diversity measure of the links i and j ($i \neq j$) given X. In [150], the authors proposed a log-linear model for the quality measure as follows:

$$g(\mathbf{a}_i | X) = \exp \quad ^{>} \mathbf{f}(\mathbf{a}_i | X) \;\; ; \tag{9.8}$$

where $\mathbf{f}$ assigns m feature values to $\mathbf{a}_i$. We will discuss the specifics of $\mathbf{f}(j)$ in the next Section. For $S_{i;j}(X)$, we choose the Gaussian kernel: $S_{i;j}(X) = e^{\frac{k\mathbf{a}_i \;\; \mathbf{a}_j k^2}{2}}$:

9.3.2 Learning DPP model

We now formulate the learning framework of the conditional DPP as follows. We denote the *training set* as a sequence of ordered pairs $T := (X_1; Y_1); : : : ; (X_K; Y_K)$, where X_k is the input and $Y_k \quad Y(X_k)$ is the output. Then the learning problem is the maximization of the log-likelihood of T:

$$(\quad ; \quad) = \arg \max_{(\; ; \;)} L(T; \quad ; \quad); \tag{9.9}$$

where $L(T; \quad ; \quad) =$

$$\log \quad \overset{\forall}{\underset{k=1}{}} P_{\; ;} \; (Y_k | X_k) = \quad \overset{\not\exists}{\underset{k=1}{}} \log P_{\; ;} \; (Y_k | X_k); \tag{9.10}$$

where $P_{\; ;} \quad P_L$ parameterized by and . The reason for choosing the log-linear model for quality measure and Gaussian kernel is the fact that under these models, $L(T; \quad ; \quad)$ becomes a concave function of and [150, Proposition 4.2].

9.3.3 Inference

We now estimate $\hat{Y}$ given X using the trained conditional DPP. This phase is known as the *testing* or inference phase. In what follows, we present two methods for choosing $\hat{Y}$.

Sampling from DPP

The first option is to draw random sample from the DPP, i.e., $\mathbf{Y} \sim P_{\_}(\cdot|X)$ and set $\hat{Y} = \mathbf{Y}$. We now discuss the sampling scheme for a general DPP which naturally extends to sampling from conditional DPP. We start with drawing a random sample from a special class of DPP, known as the *elementary* DPP and will use this method to draw samples from a general DPP. A DPP on Y is called *elementary* if every eigenvalue of its marginal kernel

Algorithm 1 Sampling from a DPP

procedure SampleDPP(L)
  Eigen decomposition of L: $L = \sum_{n=1}^{N} {}_n\mathbf{v}_n\mathbf{v}_n^{>}$
  $J = ?$
  for $n = 1;:::;N$ **do**
    $J \leftarrow J \cup \{n\}$ with probability $\frac{n}{n+1}$
  $V \leftarrow \{\mathbf{v}_n\}_{n2J}$
  $Y \leftarrow ?$
  $B = [\mathbf{b}_1;:::;\mathbf{b}_n \leftarrow V^{>}]$
  for 1 to $|V|$ **do**
    select i from Y with probability $\propto \|\mathbf{b}_i\|^2$
    $Y \leftarrow Y \cup \{i\}$
    $\mathbf{b}_j \leftarrow \mathrm{Proj}_{?\mathbf{b}_i}\mathbf{b}_j$
  return Y

lies in $\{0;1\}$. Thus an elementary DPP can be denoted as P^V where $V = \{\mathbf{v}_1;:::;\mathbf{v}_k\}$ is the set of k orthonormal vectors such that $K^V = \sum_{\mathbf{v}2V} \mathbf{v}\mathbf{v}^{>}$. We now establish that the samples drawn according to P^V always have fixed size.

Lemma 9.2. *If $\mathbf{Y} \sim P^V$, then $|\mathbf{Y}| = |V|$ almost surely.*

Proof. If $|Y| > |V|$, $P^V(Y = \mathbf{Y}) = 0$ since $\mathrm{rank}(K_Y^V) = |V|$. Hence $|\mathbf{Y}| \le |V|$. Now, $\mathrm{E}[|\mathbf{Y}|] = \mathrm{E}[\sum_{n=1}^{N} \mathbf{1}(\mathbf{a}_n \in \mathbf{Y})] = \mathrm{E}\sum_{n=1}^{N}[\mathbf{1}(\mathbf{a}_n \in \mathbf{Y})] = \sum_{n=1}^{N} K_{n;n} = \mathrm{trace}(K) = |V|$. □

Our objective is to find a method to draw a $k = |V|$ length sample $Y \sim Y$. Using Lemma 9.2, $P^V(Y) = P^V(Y = \mathbf{Y}) = \det(K_Y^V)$. In what follows, we present an iterated sampling scheme that samples k elements of Y from Y without replacement such that the joint probability of obtaining Y is $\det(K_Y^V)$. Without loss of generality, we assume $Y = \{1;2;:::;k\}$. Let $B = [\mathbf{v}_1^{>};:::;\mathbf{v}_k^{>}]^{>}$ be the matrix whose rows contain the eigenvectors of V. Then, $K^V = BB^{>}$ and $\det(K_Y^V) = (\mathrm{Vol}(\{\mathbf{b}_i\}_{i2Y}))^2$, where $\mathrm{Vol}(\{\mathbf{b}_i\}_{i2Y})$ is the volume of the parallelepiped spanned by the column vectors ($\mathbf{b}_i$-s) of B. Now, $\mathrm{Vol}(\{\mathbf{b}_i\}_{i2Y}) = \|\mathbf{b}_1\|\mathrm{Vol}(\{\mathbf{b}_i^{(1)}\}_{i=2}^{k})$, where $\mathbf{b}_i^{(1)} = \mathrm{Proj}_{?\mathbf{b}_1}\mathbf{b}_i$ denotes the projection of $\{\mathbf{b}_i\}$ onto the subspace orthogonal to $\mathbf{b}_1$. Proceeding in the same way,

$$\det(K_Y^V) = (\mathrm{Vol}(\{\mathbf{b}_i\}_{i2Y}))^2 = \|\mathbf{b}_1\|^2\|\mathbf{b}_2^{(1)}\|^2 ::: \|\mathbf{b}_k^{(1;:::;k\ 1)}\|^2: \tag{9.11}$$

Thus, the j^{th} step ($j > 1$) of the sampling scheme assuming $y_1 = 1; : : : ; y_{j-1} = j-1$ is to select $y_j = j$ with probability proportional to $\|\mathbf{b}_j^{(1;:::;j-1)}\|^2$ and project $\{\mathbf{b}_i^{(1;:::;j-1)}\}$ to the subspace orthogonal to $\mathbf{b}_j^{(1;:::;j-1)}$. By (9.11), it can be guaranteed that $P^V(Y) = \det(K_Y^V)$.

Having derived the sampling scheme for an elementary DPP, we are in a position to draw samples from a DPP. The sampling scheme is enabled by the fact that a DPP can be expressed as a mixture of elementary DPPs. The result is formally stated in the following Lemma.

Lemma 9.3. *A DPP with kernel* $L = \sum_{n=1}^{N} {}_n\mathbf{v}_n\mathbf{v}_n^{>}$ *is a mixture of elementary DPPs:*

$$P_L = \sum_{J \subseteq \{1;:::;N\}} P^{V_J} \prod_{n \in J} \frac{n}{1 + {}_n}; \tag{9.12}$$

where $V^J = \{\mathbf{v}_n\}_{n \in J}$.

Proof. Please refer to [150, Lemma 2.6]. □

Thus, given an eigendecomposition of L, the DPP sampling algorithm can be separated into two main steps: (i) sample an elementary DPP P^{V_J} with probability proportional to $\prod_{n \in J} {}_n$, and (ii) sample a sequence of length $|J|$ from the elementary DPP P^{V_J}. The steps discussed thus far are summarized in Alg. 1.

MAP inference

A more formal technique is to obtain the maximum *a posteriori* (MAP) set, i.e.,

$$\hat{Y} = \arg \max_{Y \subseteq Y(X)} P_{\;;\;}(Y|X):$$

But, finding $\hat{Y}$ is an NP-hard problem because of the exponential order search space $|Y \subseteq Y(X)|$. However, one can construct computationally efficient MAP inference algorithm which has similar complexity as random sampling. Due to space limitations, more formal discussions of these approximation techniques are outside the scope of the chapter. We refer to [154] for one possible near-optimal MAP inference scheme for DPPs which will be used in the numerical simulations.

9.4 Case study: Link scheduling

We will now introduce the link scheduling problem where we will apply the DPPL discussed in the previous section.

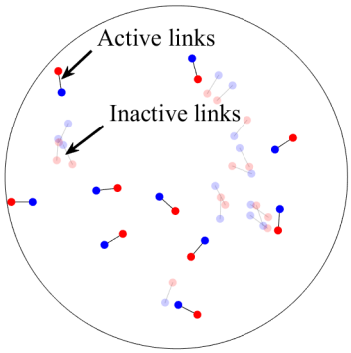

Figure 9.2: Illustration of link scheduling as a subset selection problem. A realization of the network ($M = 24$) with the active link subset (E). Details of the network model are mentioned in Section 9.4.5.

9.4.1 System model

We consider a wireless network with M Tx-Rx pairs with fixed link distance d. The network can be represented as a directed bipartite graph $G := fN_t; N_r; Eg$, where N_t and N_r are the independent sets of vertices denoting the set of Tx-s and Rx-s, respectively and $E := f(t; r)g$ is the set of directed edges where $t \ 2 \ N_t$ and $r \ 2 \ N_r$. Since each Tx has its dedicated Rx, the in-degree and out-degree of each node in N_t and N_r are one. Also $jN_tj = jN_rj = jEj = M$. An illustration of the network topology is presented in Fig 9.2. Let $K^W_{N_t;N_r}$ be the complete weighted bipartite graph on $N_t; N_r$ with $W(i; j) = \ _{ij}$ for all $i \ 2 \ N_t; j \ 2 \ N_r$. Here $\ _{ij}$ denotes the channel gain between Tx i and Rx j.

9.4.2 Problem formulation

We assume that each link can be either in *active* or *inactive* state. A link is active when the Tx transmits at a power level p_h and is inactive when the Tx transmits at a power level $p_\cdot$ (with $0 \quad p_\cdot < p_h$). Each link transmits over the same frequency band whose bandwidth is assumed to be unity. Then the sum-rate on the l^{th} link is given by $\log_2(1 + \ _l)$, where $\ _l$ is the SINR at the l^{th} Rx: $\ _l = \frac{\ _{ll}p_l}{\ ^2 + \sum_{e_j \in E, j \neq l} \ _{jl}p_j}$. Here $\ ^2$ is thermal noise power. The sum-rate maximization problem can be expressed as follows.

$$\text{maximize} \quad \sum_{e_l \in E} \log_2(1 + \ _l); \tag{9.13a}$$

$$\text{subjected to } p_l \ 2 \ fp_\cdot; p_h g; \tag{9.13b}$$

where the variables are $fp_l g_{e_l \in E}$. An optimal subset of simultaneously active links denoted as $E \quad E$ is the solution of (9.13b). Thus, $p_l = p_h; \ 8 \ e_l \ 2 \ E$ and $p_l = p_\cdot; \ 8 \ e_l \ 2 \ E \ n \ E$.

9.4.3 Optimal solution

The optimization problem in (9.13) is NP hard [153]. However, for bipartitle networks the problem can be solved by a low-complexity heuristic algorithm based on GP (see Alg. 2). For completeness, we provide the rationale behind its formulation as follows.

Since (9.13) is an integer programming problem, the first step is to solve the relaxed version of the problem assuming continuous power allocations. In particular, we modify the integer constraint (9.13b) as $0 \quad p_l \quad p_{\max}$. Since $\log_2(\,)$ is an increasing function, the problem can be restated as:

$$\min_{\{p_l\}_{e_l \in E}} \prod_{e_l \in E} (1 + \gamma_l)^{-1} \tag{9.14a}$$

$$\text{s.t.} \quad \gamma_l = \frac{h_{ll} p_l}{\sigma^2 + \sum_{j \neq l} h_{jl} p_j}; e_l \in E \tag{9.14b}$$

$$0 \quad p_l \quad p_{\max} \ \forall e_l \in E. \tag{9.14c}$$

Since the objective function is decreasing in γ_l, we can replace the equality in (9.14b) with inequality. Using the auxiliary variables $v_l \quad 1 + \gamma_l$, (9.14) can be formulated as:

$$\min_{\{p_l, \gamma_l, v_l\}} \prod_{e_l \in E} v_l^{-1} \tag{9.15a}$$

$$\text{s.t. } v_l \quad 1 + \gamma_l; \forall e_l \in E \tag{9.15b}$$

$$\sigma^2 h_{ll}^{-1} p_l^{-1} \gamma_l + \sum_{j \neq l} h_{ll}^{-1} h_{jl} p_j p_l^{-1} \gamma_l \quad 1; e_l \in E; \tag{9.15c}$$

$$0 \quad p_l p_{\max}^{-1} \quad 1. \tag{9.15d}$$

Now in (9.15), we observe that (9.15a) is a monomial function, (9.15b) contains posynomial function in the right hand side (RHS), and all the constraints contain either monomial or posynomial functions. Hence, (9.15) is a complementary GP [155]. If the posynomial in (9.15b) can be replaced by a monomial, (9.15) will be a standard GP. Since GPs can be reformulated as convex optimization problems, they can be solved efficiently irrespective of the scale of the problem. One way of approximating (9.15) with a GP at a given point $\{\gamma_l\} = \{\hat{\gamma}_l\}$ is to replace the posynomial $1 + \gamma_l$ by a monomial $k_l \gamma_l^{\prime}$. From $1 + \hat{\gamma}_l = k_l \hat{\gamma}_l^{\prime}$, we get

$$\gamma_l = \hat{\gamma}_l (1 + \hat{\gamma}_l)^{-1}; \quad k_l = \hat{\gamma}_l^{\prime} (1 + \hat{\gamma}_l). \tag{9.16}$$

Also note that $1 + \gamma_l \quad k_l \gamma_l^{\prime}, \ \forall \gamma_l > 0$ for $k_l > 0$ and $0 < \gamma_l < 1$. Thus the local approximation of (9.15) will still satisfy the original constraint (9.15b). The modified inequality constraint becomes

$$v_l \quad k_l \gamma_l^{\prime}; \ \forall e_l \in E; \tag{9.17}$$

where k_l and γ_l are obtained by (9.16).

Since (9.15a) is a decreasing function of v_l, we can substitute v_l with its maximum value $k_{l\ l'}$, which satisfies the other inequality constraints. Thus, v_l can be eliminated as:

$$\prod_{e_l \in E} v_l^{\ 1} = \prod_{e_l \in E} k_{l\ l'}^{\ 1} = K \prod_{e_l \in E} \ ^{\frac{\hat{}_l}{1+\hat{}_l}}; \tag{9.18}$$

where K is some constant which does not affect the minimization problem. Thus, the i^{th} iteration of the heuristic runs as follows. Let $\hat{}_l^{(i)}$ be the current guess of SINR values. The GP will provide a better solution $\hat{}_l$ around the current guess which is set as the initial guess in the next iteration, i.e., $\hat{}_l^{(i+1)} = \ _l$ unless a termination criterion is satisfied. These steps are summarized in Alg. 2. To ensure that the GP does not drift away from the initial guess $\hat{}_l^{(i)}$, a new constraint (9.19b) is added so that $\ _l$ remains in the local neighborhood of $\ _l^{(i)}$. Here $\ > 1$ is the control parameter. The smaller the value of $\ $, the higher is the accuracy of the monomial approximation, but the slower is the convergence speed. For a reasonable tradeoff between accuracy and speed, $\ $ is set to 1.1. The algorithm terminates with the quantization step which assigns discrete power levels $p_{\cdot}$ and p_{h}. Once we obtain the optimal power allocation $p_l \in [0; p_{\max}]$, we quantize it into two quantization levels $p_{\cdot}$ and p_{h} by setting $p_l = p_{\cdot}$ whenever its value lies below some threshold level p_{th} or otherwise $p_l = p_{\mathsf{h}}$.

For further details on solving the general class of link scheduling problems, the reader is referred to [153]. Fig. 9.2 demonstrates a realization of the network and $E\ $ chosen by Alg. 2.

9.4.4 Estimation of optimal subset with DPPL

We will now model the problem of optimal subset selection $E\ \ E$ with DPPL. We train the DPP with a sequence of networks and the optimal subsets obtained by Alg. 2. For the training phase, we set $X_k = (K^{W}_{N_t;N_r}; E; E\ )_k$ as the k^{th} realization of the network and its optimal subset. The quality and diversity measures are set as: $g(\mathbf{a}_i | X) := \exp(\ _1\ _{II} p_{\mathsf{h}} + \ _2 I_1 + \ _3 I_2)$; where $I_1 = p_{\mathsf{h}}\ _{j^0 i}$ with $j^0 = \arg\max_{j=1;\ldots;L \in i;j^0} f\ _{j i} g$ and $I_2 = p_{\mathsf{h}}\ _{j^{00} i}$ with $j^{00} = \arg\max_{j=1;\ldots;L \in i;j^0} f\ _{j i} g$ are the two strongest interfering powers, and $S_{i;j}(X) = \exp\ (k\mathbf{x}(t_i)\ \ \mathbf{x}(r_j)k^2 + k\mathbf{x}(t_j)\ \ \mathbf{x}(r_i)k^2) = \ ^2$; where $\mathbf{x}(t_i)$ and $\mathbf{x}(r_j)$ denote the locations of Tx $t_i \in N_t$ and Rx $r_j \in N_r$, respectively. The ground set of the DPP $Y(X) = E$. We denote the subset estimated by DPPL in the testing phase as $\hat{E}$. The block diagram of the DPPL is illustrated in Fig. 9.3. In order to ensure the reproducibility of the results, we provide the Matlab implementation of the DPPL for this case study in [156].

9.4.5 Results and discussions

We now demonstrate the performance of DPPL through numerical simulations. We construct the network by distributing M links with $d = 1$ m within a disc of radius 10 m uniformly at random. We assume channel gain is dominated by the power law path loss,

Algorithm 2 Optimization algorithm for (9.13)

procedure SumRateMax($K_N^W; E$)
  Initialization: given tolerance > 0, set $\mathbf{P}_0 = \{p_{l;0}\}$. Set $i = 1$. Compute the initial SINR guess $\gamma^{(i)} = \{\gamma_l^{(i)}\}$.
  repeat
    Solve the GP:

$$\text{minimize} \quad K^{(i)} \prod_l \frac{\gamma_l^{(i)}}{1+\gamma_l^{(i)}} \tag{9.19a}$$

$$\text{subject to} \quad \frac{1}{\gamma_l^{(i)}} \, I_l \le \gamma_l^{(i)}; e_l \in E; \tag{9.19b}$$

$$\frac{2}{|h_{ll}|^2 p_l} \le I_l + \sum_{j \ne l} |h_{jl}|^2 p_j \le \frac{1}{|h_{ll}|^2 p_l} I_l, \quad 1; e_l \in E; \tag{9.19c}$$

$$p_l \le p_{\max}; \ \forall e_l \in E: \tag{9.19d}$$

    with the variables $\{p_l; I_l\}_{e_l \in E}$. Denote the solution by $\{p_l^*; I_l^*\}_{e_l \in E}$.
  until $\max_{e_l \in E} |I_l - \gamma_l^{(i)}| \le$
  if $p_l \le p_{\text{th}}$ **then**
    $p_l = p_{\text{h}}$
  else
    $p_l = p_{\text{`}}$
  return E

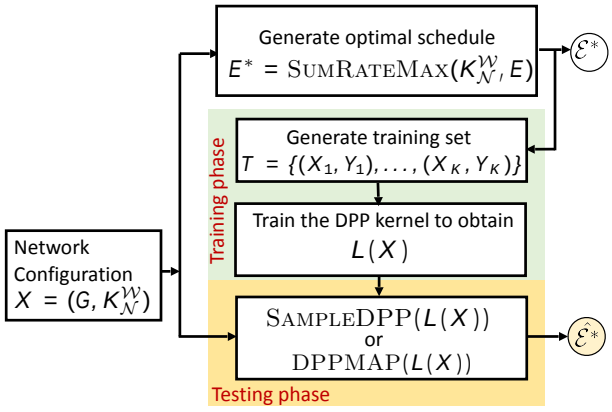

Figure 9.3: Block diagram of DPPL for the link scheduling problem.

i.e., $_{ij} = k\mathbf{x}(t_i) \quad \mathbf{x}(r_j)k \quad$, where $t_i \ 2 \ N_t$, $r_j \ 2 \ N_r$, and $\quad = 2$ is the pathloss exponent. The network during training and testing phases was generated by setting $M \quad \texttt{Poisson}(M)$ with $M = 20$. The instances where $M = 0$ were discarded. We set $p_{\text{h}} = {}^2 = p_{\max} = {}^2 = 33$ dB, $p = {}^2 = 13$ dB, and $p_{\text{th}} = 23$ dB. The training set T was constructed by $K = 200$ independent realizations of the network. Note that changing K from 20 to 200 did not change the values of and ($= 0{:}266; \quad = [996; 675; 593]$) significantly. In Fig. 9.4, we plot the empirical cumulative distribution functions (CDFs) of the sum-rates obtained by Alg. 2 and DPPL. We observe that the sum-rate obtained by DPPL framework closely approximates the max-sum-rate. We also notice that DPP MAP inference gives better sum-rate estimates than DPP sampling. We further compare the performance with the well-known SG-based model where the simultaneously active links are modeled as *independent thinning* of the actual network [152]. In particular, each link is assigned p_{h} according to an independent and identically distributed (i.i.d.) Bernoulli random variable with probability . We estimate by averaging the activation of a randomly selected link which is equivalent to: $= \sum_{k=1}^{K} \mathbf{1}(e_i \ 2 \ E_k)/K$ for a fixed i. We see that the sum-rate under independent thinning is significantly lower than the one predicted by DPP. The reason is the fact that the independent thinning scheme is not rich enough to capture spatial repulsion which exists across the links of E .

Run-time comparison

Another key strength of the proposed DPPL appears when we compare its run-time in the testing phase and Alg. 2 applied on a network $(K^{W}_{N_t;N_r}; E)$. In Fig. 9.5, we plot the run-times of different subset selection schemes for different network sizes. The absolute values of run-times were obtained averaging the run-times of all the schemes over 1000 iterations in the same computation environment. In order to obtain a unit-free measure, we normalize these absolute values by dividing them with the average absolute run-time of Alg. 2 for $M = 5$. We observe that DPPL is at least 10^5 times faster than Alg. 2. The run-time of Alg. 2 increases exponentially with M whereas run-times of the DPPL scale as some polynomial order of M. Note that DPPL is not just a sum-rate estimator of the network, but it estimates the optimal subset of links $\hat{E}$ significantly faster than the optimization algorithms. Thus, DPPL can be implemented in real networks to determine E even when the network size is large. In Fig. 9.6, we plot the sum-rates averaged over 10^3 network realizations for a given value of M. Note that evaluating max-sum-rates for higher values of M using Alg. 2 is nearly impossible due to its exponentially increasing run-time. Quite interestingly, DPPL, thanks to its fast computation, provides some crisp insights on the network behavior: as more number of links are added, the estimated max-sum-rate tends to saturate (see Fig. 9.6). This is expected because as long as the resources are fixed, there will be a limit on the number of simultaneously active links (irrespective of M) that would maximize the sum-rate. If the number of active links is more than this limit, sum-rate may decrease because of the increased interference. Also we observe that the performance difference between MAP-inference and DPP-sampling increases significantly at higher values of M.

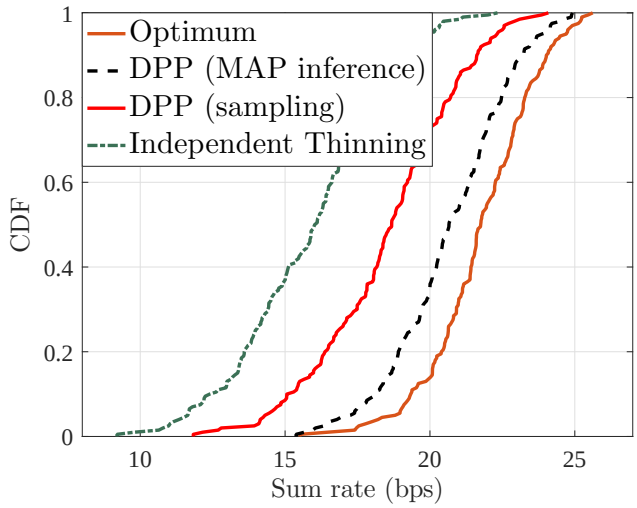

Figure 9.4: CDF of sum-rate obtained by different subset selection schemes.

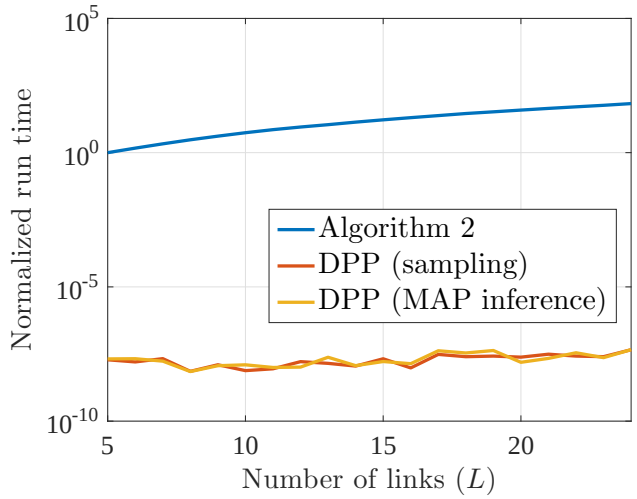

Figure 9.5: Comparison of run-times of Alg. 2 and DPPL in testing phase.

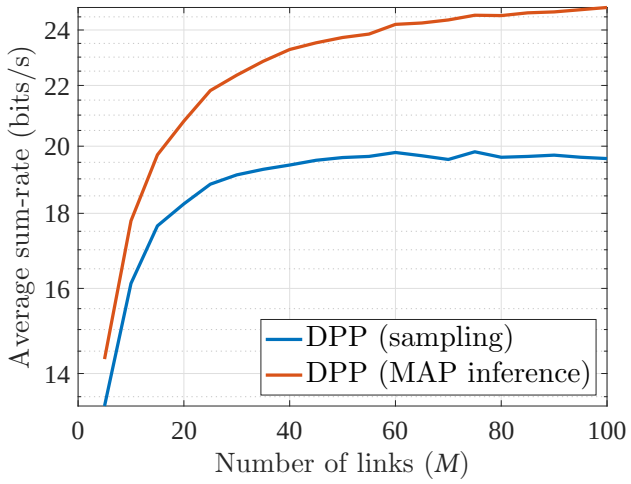

Figure 9.6: Average rates obtained for different network sizes using DPPL.

9.5 Interference analysis

Having discussed the utility of DPP in learning the spatial distribution of the set of active Tx-s in a WLAN, we now focus on the analytical tractability of the DPP-based network model. For this purpose, we characterize the distribution of interference at the origin assuming that the Tx-s are distributed as a DPP. The kernel of the DPP may be learned by using the framework proposed in the previous section.

9.5.1 Spatial model

We consider a bipolar setting for WLAN in which a base set of Tx-s are assumed to be distributed as a homogeneous PPP R^2 with intensity > 0. Each Tx is assumed to have a dedicated Rx at a fixed distance R in a uniformly random orientation independently from the rest of the network. Due to the MAC scheme (like the channel access scheme described in Section 9.4), we assume a subset of these Tx-s are simultaneously active at any given instance. We denote the set of the simultaneously active Tx-s by . We assume that conditional distribution of given follows a DPP. In particular, is obtained by a determinantal thinning of . In other words, each realization of (denoted as 2) is a DPP over each realization of (denoted as 2).

9.5.2 Signal model

We denote the small scale fading (power) between a node pair $\mathbf{x}; \mathbf{y}$ 2 as $h_{\mathbf{x};\mathbf{y}}$, where $fh_{\mathbf{x};\mathbf{y}}g$ as the sequence of independently and identically distributed (i.i.d.) random variables with the characteristic function $\mathsf{CF}_h(s) = \mathsf{E}[\exp(sh)]$: The path-loss associated with a link with distance $r > 0$ is given by $l(r) = r$, where > 2 is the path-loss coefficient. Then

the interference at a point $\mathbf{x}$ can be denoted as:

$$I(\mathbf{x}; \quad) = P \sum_{\mathbf{y} 2 \quad nf\mathbf{x}g} h_{\mathbf{y};r(\mathbf{y})} l(k\mathbf{y} \quad r(\mathbf{y})k); \tag{9.20}$$

where P is the constant transmit power. Because of the stationarity of the network, it is sufficient to characterize the distribution of interference at the origin, i.e. $I(\mathbf{0}; \quad) \quad I$. Before we provide the main result, we will discuss a few useful properties of determiantally thinned point process which will be instrumental in the derivation of the interference distributions. Note that is a doubly stochastic point process and all the expressions evaluated in this section are conditioned on the realization of the base process: = . We now define the probability generating functional (PGFL) of .

Definition 9.4 (PGFL)**.** The conditional PGFL of given is the following:

$$E\left[\prod_{\mathbf{x}2} v(\mathbf{x}) \quad\right] = E\left[E\left[\prod_{\mathbf{x}2} v(\mathbf{x}) \quad\right] \quad\right]; \tag{9.21}$$

where $v : R^2 \not\to [0; 1]$ is a measurable map.

The PGFL of is given by the following Lemma.

Lemma 9.5. *The conditional PGFL of given is expressed as:*

$$E\left[\prod_{\mathbf{x}2} v(\mathbf{x}) \quad\right] = E\left[\det(I \quad A(\ )K(\ )A^{>}(\ ))\right] = \quad; \tag{9.22}$$

where $A(\ ) = \mathrm{diag}(f(1 \quad v(\mathbf{x}))^{\frac{1}{2}}; \mathbf{x} \; 2 \quad g)$.

Proof. See [157] for detailed proof. □

We now evaluate the characteristic function of I in the following Lemma.

Lemma 9.6. *The conditional characteristic function of I given , denoted as $\mathrm{CF}_I(sj \ )$ is given by the right hand side (RHS) of (9.22) where*

$$v(\mathbf{x}) = \mathrm{CF}_h \quad sPk\mathbf{x}k \quad : \tag{9.23}$$

Proof. The characteristic function is given as:

$$E[\exp(sI)j \ ] = E\left[\exp\left(s \sum_{\mathbf{x}2} Ph_{\mathbf{x};\mathbf{0}} k\mathbf{x}k \quad\right)\right]$$

$$= \mathsf{E}\left[\prod_{x \in \Phi} \exp\left(sPh_{x;0}kxk\right)\right]$$
$$\stackrel{(a)}{=} \mathsf{E}_{\Phi}\left[\prod_{x \in \Phi} \mathsf{E}_{h}\left[\exp\left(sPh_{x;0}kxk\right)\right]\right]$$
$$= \mathsf{E}_{\Phi}\left[\prod_{x \in \Phi} \mathrm{CF}_{h}(sPkxk^{\alpha})\right]: \quad (9.23)$$

Here step (a) follows from the fact that $\{h_{x;y}\}$ is an i.i.d. sequence. The final step is nothing but the PGFL of Φ evaluated at $\mathrm{CF}_h(sPkxk^{\alpha})$, which can be computed using Lemma 9.5. □

We now characterize the distributions of I as follows.

Theorem 9.7. *The CDF of I is given as:*

$$F_I(t) = \frac{1}{2} - \frac{1}{\pi}\mathsf{E}_{\Phi}\left[\int_0^{\infty} \mathrm{Imag}(\exp(-its\mathrm{CF}_I(sj^{\alpha})))ds\right]; \quad (9.24)$$

where the expectation is taken over Φ.

Proof. The results follow directly by applying Gil-Pelaez inversion formulae [97] on the characteristic function of I. □

Remark 9.8. Note that the final expression of the CDF of I is conditioned on Φ which implies that in order to obtain the final results, the expression needs to be averaged out over the realizations of Φ. The existence of the results even in the semi-analytical form demonstrate the synergy between SG and ML in DPPL: while ML handles the fitting of the DPPL to the samples drawn from a blackbox spatial model with spatial repulsion (which in our case is the set of locations of the active Tx-s in the WLAN), SG provides analytical handle to the characterization of key performance metrics of this network (such as the characteristic function of interference) which can be expressed as some functionals of DPP.

9.5.3 Results and discussions

In this section, we demonstrate the performance of DPPL in estimating the interference distribution of the WLAN. For the generation of the training set, we chose a Matérn hard core process (MHCP) with hard core radius 2 m. In future work, we intend to replace the MHCP with more realistic spatial distributions of the active nodes in a WLAN with carrier sense multiple access (CSMA). However, since the DPPL is not aware of the actual distribution of the nodes in the training set, it is sufficient to use MHCP for the training set generation

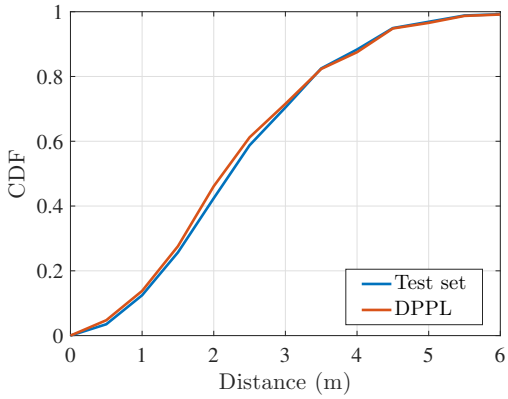

Figure 9.7: Contact distance CDF (= 5 10 ^{2} m ^{2}, retention distance 2 m).

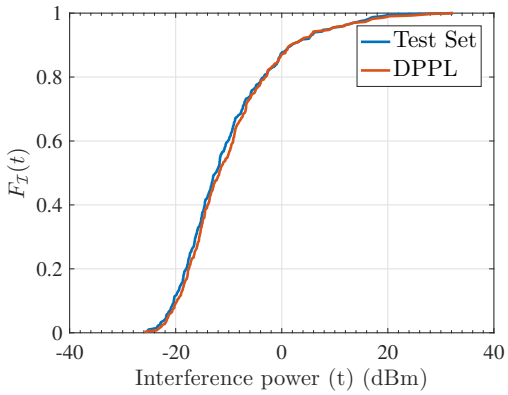

Figure 9.8: CDF of interference (P = 1 mW, = 4, Rayleigh fading).

to demonstrate the analytical tractability of the proposed framework. The MHCP (type-II) was generated by thinning a homogeneous PPP with = 5 10 ^{2} m ^{2} simulated within a 70 m 70 m square window. For the DPPL, we chose the quality function as follows. For a point $\mathbf{x}$ 2 , $\mathbf{f}(\mathbf{x}j)$ = 1; $d_1(\mathbf{x})$; $d_2(\mathbf{x})$ $^{>}$, where $d_i(\mathbf{x})$ denotes the distance of the i^{th} nearest neighbor of $\mathbf{x}$ in . The size of the training set (K) was chosen to be 100 and the size of the test set was 900. For a sanity check of the learning performance of the DPPL, we first plot the contact distance distribution (i.e. the CDF of the distance between the origin and the closest point of the point process to it) of the MHCP computed empirically from the samples in the test set in Fig. 9.7. For the analytical result, we computed the contact distance distribution of the DPP with L ; using the semi-analytical expression derived in [152]. Since contact distance distribution (or equivalently) completely characterizes the distribution of a point process, a significant match in contact distance demonstrates the capability of DPP to learn the distribution of an unknown spatial point pattern with spatial repulsion.

We now provide the CDF of interference in Fig. 9.8. We obtain significant match with

the actual distribution of the interference in MHCP. It is to be noted that the analytical characterization of the repulsive point processes is in general difficult and specific to the distribution under consideration. Thanks to the DPPL, it is now possible to develop a general analytical framework for these networks after fitting the DPP to the sampling distributions of the active Tx-s.

9.6 Summary

In this chapter, we identified a general class of subset selection problems in wireless networks which can be solved by jointly leveraging ML and SG, two fundamentally different mathematical tools used in communications and networking. To solve these problems, we developed the DPPL framework, where the DPP orginiates from SG and its learning applications have been fine-tuned by the ML community. As a case study, we considered the wireless link scheduling problem where we found that the DPP is able to *learn* the underlying quality-diversity tradeoff in the locations of the simultaneously active links. After exploring the learning capability of this framework, we demonstrated its analytical tractability enabled by the connection of DPP with SG. We derived the semi-analytical expression of the distribution of interference at the origin from the active Tx-s which are distributed as a DPP.

10

Conclusion

In this chapter, we will discuss some key take-aways of this dissertation and a few promising future works.

10.1 Summary

Over the last decade, stochastic geometry has played a major role in the mathematical performance analysis of cellular networks. This line of work has been enriched in different directions, such as the characterization of coverage and rate of HetNets, analyzing the performance of MIMO networks, mm-wave and energy-harvesting networks, co-existence of different networks (e.g. cellular and WiFi), and many more. Despite the plethora of applications of the stochastic geometry based models, there is one principle assumption of these models which mostly remains unmodified. This assumption is the complete spatial randomness of the network topology which means that the BSs and users are distributed as independent and homogeneous PPPs. This assumption, although yields mathematical tractability, is becoming outdated with the increasing network complexity. The key aspect of network topology that cannot be captured in the PPP based model of the network is the spatial coupling between the users and BSs. Such couplings may not be very crucial in yesteryear's cellular network with the coverage-centric deployment of the macrocells. But as the networks are becoming more and more heterogeneous with one layer of macrocells and other layers of small cells targetting coverage dead-zones or user hotspots, the spatial coupling between BS and user locations are being too prominent to be considered in the spatial models of the networks. While the state-of-the-art analytical network models are becoming outdated, in this dissertation, we developed new stochastic geometry based models for the cellular networks.

One of the main outcomes of this dissertation is the PCP based model of cellular network. In particular, we have proposed that PCP can be used as an alternative of the homogeneous PPP for spatial distribution for the BSs and users in a HetNet. This proposition enables us to construct a handful of possible spatial models for the HetNet, for instance, (a) users PCP with SBSs at the cluster center, and (b) users and SBSs both are PCP sharing the same cluster center. These scenarios essentially capture a wide set of user-BS couplings which are considered in the 3GPP-compliant network simulators. Moreover, the HetNet model based on the combination of PPP and PCP generalizes the state-of-the-art PPP-based network model. In other words, as the cluster size of the PCPs tend to infinity,

the spatial coupling in the HetNet model disappears and the network converges to the PPP-based model. Different aspects of the PCP-based general HetNet models have been studied in Chapters 2-6.

In Chapter 2, we considered a K tier HetNet where the user locations as PCPs with the SBSs at the cluster centers. For such spatial setup, we derived the downlink coverage probability. Our results demonstrated that the coverage probability is strongly affected by the spatial coupling between the user and BS locations: coverage decreases as the size of user clusters around BSs increases. We also showed that if the cluster size tends to infinity, the coverage in this setup converges to the coverage obtained under the assumption of PPP distribution of users independent of the BS locations.

In Chapter 3, we further enriched the PCP-based HetNet model proposed in Chapter 2 by adding another way to model user-BS coupling using PCP. Here we assumed that the BSs (especially the SBSs) can be also distributed as PCP. The coupling between the user and BS locations in this scenario can be modeled by setting same parent point process (set of cluster centers) for the user and BS PCPs. Although we have different choices for modeling the BS and user distributions by now, we showed that all these configurations can be unified under a general K-tier HetNet model. We demonstrated that the special cases of this general HetNet model closely resemble the point patterns of the user and BS locations used in 3GPP-compliant system-level simulation of HetNets. For this general HetNet model, we derived the downlink coverage probability assuming that the typical user connects to the BS providing maximum instantaneous SIR. As a part of the analysis, we characterized the sum product functional of the PCP under its original and Palm distribution. Our numerical results reveal the strong connection of coverage with the spatial coupling in the network topology which was so far ignored in the PPP-based models. For instance, when we consider user-BS coupling, we have two types of users in the network: Type 1: users whose locations are independent of the BS locations, and Type 2: users whose locations are coupled with the BS locations. As example, in our general HetNet model, the users are of Type 1 if their locations are modeled as homogeneous PPP. If the user locations are modeled as PCP coupled with the BS locations (PCP), then we call them Type 2 users. Our analysis showed an interesting trend of coverage for the Type 1 and Type 2 users: as the cluster size of the BS PCP increases, the coverage of the Type 2 users decreases and the coverage of Type 1 users increases. As the cluster size tends to infinity, the coverage of both the users converges to the coverage of a typical user in a PPP-based HetNet.

In Chapter 4, we focus on further enhancing the analytical tractability of the general HetNet model developed in Chapter 3 by considering a more realistic user association rule. Here we assume that the typical user connects to the BS providing the maximum received power averaged over fading. This association rule is very similar to the maximum reference signal received power (RSRP) based association considered in 3GPP-compliant network simulations. We showed that the coverage probability can be expressed as a product of sum-product and probability generating functionals (PGFLs) of the parent point processes of the BS PCPs.

In Chapter 5, we characterized the SIR received at the typical user of the general HetNet model under the max-power based association. The SIR meta distribution, or the distribution of the conditional success probability (also known as the link reliability) of the typical user, is considered as a more fine grained coverage analysis of cellular networks with coverage probability appearing as the first moment of the meta distribution.

In Chapter 6, we focus on another fundamental metric related to the performance characterization of cellular networks which is the distribution of the load on a BS in a network. The load characterization in a stochastic geometric setting is a very complicated problem involving the understanding of the intersection of the user point process and the random tessellation generated by the BS point processes. The load distribution in a PPP-based network is quite well-known. The reason the load distribution remains tractable in a PPP setting is because the moments of the BS load only depends on the volume of the Poisson Voronoi cell whose distribution is a standard result in stochastic geometry. However, the problem becomes complicated even with the slightest departure from the PPP assumption of the BS and user distributions. In fact, load distributions for any non-Poisson network models have remained open problems in literature. In Chapter 6, we made the first attempt towards this direction by characterizing the distribution of the typical cell load where the BSs are distributed as a homogeneous PPP and the users are distributed as an independent PCP. We also demonstrated the utility of this result by using it to characterize the user rate for a representative user in the typical cell.

After we studied the PCP-based modeling of the spatial couplings in the network topology due to the user-centric deployment of small cells, we shifted our attention to the IAB networks which is the key architecture associated with the small cell driven network densification. While the idea of network densification with low power small cells has been matured since the 4G era, the actual deployment of the small cells has not picked up as expected despite the theoretical guarantees of the rate improvement provided by the existing HetNet models. One main reason for the disparity in the analysis and reality is the backhaul network which needs to be scaled equally as the small cells. The existing spatial models of the HetNets assume no capacity constraints on the backahul links for all the BSs in the network. While this assumption is reasonable for the macrocells since they are connected to the network core with high capacity optical fiber, it is questionable for the small cells since it not possible to reach every SBS with fiber. This problem of the *last mile fiber* has been simplified with the possibility of establishing high capacity *fiber-like* wireless backhaul links between the MBS and SBS using directional mm-wave transmission. Since the mm-wave can be also used for the access networks, the access and backhaul networks are further integrated leading to a new network architecture known as IAB. As expected, the existing networks need to be redesigned to accommodate this integrated architecture. For instance, an important question pertaining IAB is how the available resources in at the MBS will be split between the SBSs served over backhaul and users served over access links. Using the stochastic geometry based models, we attempted to answer these questions in Chapters 7 and 8. In Chapter 7, we modeled the user hotspots and smallcells within a single macrocell

of a two tier IAB network. We assumed that the MBS is anchored to the core network and provides mm-wave backhaul to the SBSs. For this network, we characterized its downlink rate coverage probability. We studied the performance of three backhaul bandwidth (BW) partition strategies: 1) equal partition: when all SBSs obtain equal share of the backhaul BW; 2) instantaneous load-based partition: when the backhaul BW share of an SBS is proportional to its instantaneous load; and 3) average load-based partition: when the backhaul BW share of an SBS is proportional to its average load. We found that depending on the choice of the partition strategy, there exists an optimal split of access and backhaul BW for which the rate coverage is maximized. Further, we showed the existence of a critical volume of cell-load (total number of users) beyond which the gains provided by the IAB-enabled network disappear and its performance converges to that of the traditional macro-only network with no SBSs.

In Chapter 8, we considered a multi-cell (more precisely, multiple macrocells) spatial model of IAB. The main challenge in the rate analysis in the multi-cell setting is the characterization of the access load on SBS and access and backhaul loads on the MBSs which are highly correlated with each other. As noted earlier, the load analysis in any coupled setting is highly complicated, we ignored any spatial coupling in the network by resorting to the baseline PPP-based model. We derived the downlink rate coverage probability for two types of resource allocations at the MBS: 1) IRA: where the total bandwidth is dynamically split between access and backhaul, and 2) ORA: where a static partition is defined for the access and backhaul communications. Our analysis also showed that it is not possible to improve the user rate in an IAB setting by simply densifying the SBSs due to the bottleneck on the rate of wireless backhaul links between MBS and SBS.

Finally in Chapter 9, we proposed a new class of machine learning inspired stochastic geometry-based models which are fundamentally different from the modeling approach followed in the previous chapters. The general approach towards the stochastic geometry based modeling of wireless networks is to assume some spatial distributions (like PPP or PCP) of BSs and users. Then the properties of these distributions (e.g. the PGFL or the sum product functional) are leveraged to derive the analytical expressions of the network performance metrics (e.g. coverage and rate). The downside of this model-driven approach is the dependence on the choice of models (in particular, the spatial models) of network. If the spatial distribution of the network is available in form of data (e.g. a sequence of locations), the existing approach is not equipped to fit a distribution to the data and still carry out the analysis. In order to develop the data-driven analytical models of network, we looked at the intersection of stochastic geometry and machine learning, the two powerful yet very different tools used for modeling and design of wireless networks. The basis of the proposed framework is DPP which has been used in machine learning as a model for subset selection problems and stochastic geometry to model repulsive point patterns. While subset selection problems occur frequently in any recommendation system, they can be also identified in wireless networks. One such example is wireless link scheduling, where the goal is to determine the subset of simultaneously active links which maximizes the network-wide

sum-rate. We showed that the DPP is able to learn the spatial pattern of the active Tx-s from a training set generated by running a GP based optimization over the ground set of Tx-locations. We then demonstrated the analytical tractability of this model by characterizing the distribution of interference from the active Tx-s at the origin.

10.2 Future works

There are numerous extensions of the works presented in this dissertation. Few of the prominent directions are listed below.

10.2.1 Extension of the PCP-based network models.

The PCP-based network model developed in Chapters 2-6 has already been extended in multiple directions, such as mm-wave HetNets [158], IoT networks [159] and unmanned areal vehicles (UAV) networks [160, 161]. Here we will focus on two relatively less-explored extensions of this line of work.

Downlink rate analysis. The analytical framework of the PCP-based models developed in this dissertation has mostly focused on the characterization of downlink coverage probability or the distribution of the SINR experienced by a user. However, often times we need to characterize more sophisticated performance metric like the data rate. For instance, we heavily relied on the downlink rate distributions for the performance characterization of the backhaul limited networks in Chapters 6-8. As we have already discussed, for the rate characterization of a network, we need the distribution of BS load. However, the BS load is difficult to analyze for any non-Poisson spatial model. In Chapter 6 and 7, we characterized the cell load when the user point process had clustering behavior. Except a few special configurations, the load characterization for the general HetNet model is still an open problem. For instance, let us consider a simple single tier cellular network as follows. Let be the point process of the BSs which is a PCP with parameters $(\ _{\mathrm{p}}; m; f)$ and $\ _{\mathrm{u}}$ be the user point process, which is either an independent homogeneous PPP (Type 1) or a PCP that shares the same parent points with (Type 2). For either of the cases, let us consider the random variables $\ _{\mathrm{u}}(C_0)$ and $\ _{\mathrm{u}}(C(0))$, where C_0 and $C(0)$ denote the zero cell and typical cell of . When is a PCP, these distributions are not known. The first step towards this direction will be to understand the volume distributions of the typical and zero cells of PCP which have not been investigated extensively in the stochastic geometry literature.

Uplink coverage analysis. The second important direction is the analysis of uplink coverage of the PCP-based network model. The main challenge of the uplink analysis is the characterization of the point process for the interfering users. Let us assume that each BS schedules one user at a given time-frequency resource block. Then there will be one active user per in each cell of the BS point process. Following the notations of the single tier network

introduced above, the set of interfering users (call it $\Phi_{u(a)}$) will be a thinned version of Φ_u that lie outside the typical cell C_0. When Φ_u is distributed as a PCP, the distribution of $\Phi_{u(a)}$ for Type 1 and Type 2 users and henceforth the interference have not been characterized yet.

10.2.2 Extension of DPPL

The next promising future work is the extension of DPPL that was introduced in Chapter 9. During the time of writing this dissertation, the DPPL framework has been explored as a proof-of-concept in a couple of scenarios, (1) learning the distribution of the active transmitters in a wireless link scheduling problem, and (2) learning the distribution of a MHCP and deriving the semi-analytical expression of interference at the origin. While the results obtained in both these scenarios are certainly promising, we need to further enhance the DPPL framework in the following directions.

- *Enhancement of the learning objective.* Recall that the learning framework proposed in Section 9.3.2 was to maximize the conditional probability of the occurrence of the subset (Y) from the ground set (X). Instead of the original probability measure, one can use the Palm measure of DPP which will condition that X will always have a point in the origin [162, Section 5.7.4]. From the analysis point of view, learning the Palm measure will lead us to more accurate characterization of the metrics like interference distribution and outage which depend on the Palm distribution of the point process.
- *Enhancement of the learning model.* The main component of the DPPL was the quality diversity decomposition given by (9.5). For the quality functions and diversity kernel, we used simple log-linear model and Gaussian kernel, respectively. While these choices are inspired from the classical *shallow* learning, one can use artificial neural networks as the quality function and diversity kernels following the works like [163] used for multi-label classification of images.

Bibliography

[1] 3GPP TR 36.814, "Further advancements for E-UTRA physical layer aspects," Tech. Rep., 2010.

[2] 3GPP TR 36.872 V12.1.0 , "3rd generation partnership project; technical specification group radio access network; small cell enhancements for E-UTRA and E-UTRAN - physical layer aspects (release 12)," Tech. Rep., Dec. 2013.

[3] 3GPP TR 36.932 V13.0.0 , "3rd generation partnership project; technical specification group radio access network; scenarios and requirements for small cell enhancements for E-UTRA and E-UTRAN (release 13)," Tech. Rep., Dec. 2015.

[4] J. G. Proakis and M. Salehi, *Fundamentals of communication systems*. Pearson Education, 2007.

[5] A. Goldsmith, *Wireless communications*. Cambridge university press, 2005.

[6] V. H. MacDonald, "Advanced mobile phone service: The cellular concept," *The bell system technical Journal*, vol. 58, no. 1, pp. 15–41, Jan. 1979.

[7] L. Chenand, W. Chen, B. Wang, X. Zhang, H. Chen, and D. Yang, "System-level simulation methodology and platform for mobile cellular systems," *IEEE Commun. Magazine*, vol. 49, no. 7, pp. 148–155, Jul. 2011.

[8] H. S. Dhillon, "Fundamentals of heterogeneous cellular networks," Ph.D. dissertation, UT Austin, 2013.

[9] H. P. Keeler, N. Ross, and A. Xia, "When do wireless network signals appear Poisson?" 2014, available online: arXiv.org/abs/1411.3757.

[10] D. J. Daley and D. Vere-Jones, *An introduction to the theory of point processes: volume II: general theory and structure*. Springer Science & Business Media, 2007.

[11] A. Baddeley *et al.*, "Analysing spatial point patterns in R," 2008.

[12] R. Schneider and W. Weil, *Stochastic and integral geometry*. Springer Science & Business Media, 2008.

[13] S. N. Chiu, D. Stoyan, W. S. Kendall, and J. Mecke, *Stochastic Geometry and its Applications*, 3rd ed. New York: John Wiley and Sons, 2013.

[14] M. Haenggi, J. G. Andrews, F. Baccelli, O. Dousse, and M. Franceschetti, "Stochastic geometry and random graphs for the analysis and design of wireless networks," *IEEE journal on selected areas in commun.*, vol. 27, no. 7, pp. 1029–1046, Aug. 2009.

[15] S. Weber and J. G. Andrews, "Transmission capacity of wireless networks," *Foundations and Trends in Networking*, vol. 5, no. 2-3, pp. 109–281, 2012.

[16] M. Haenggi and R. K. Ganti, "Interference in large wireless networks," *Foundations and Trends in Networking*, vol. 3, no. 2, pp. 127–248, 2009.

[17] F. Baccelli and B. Blaszczyszyn, *Stochastic Geometry and Wireless networks, Volume 1- Theory*. NOW: Foundations and Trends in Networking, 2009.

[18] F. Baccelli and S. Zuyev, "Stochastic geometry models of mobile communication networks," *Frontiers in queueing*, pp. 227–243, Jan. 1997.

[19] F. Baccelli, M. Klein, M. Lebourges, and S. Zuyev, "Stochastic geometry and architecture of communication networks," *Telecommunication Systems*, vol. 7, no. 1-3, pp. 209–227, Jun. 1997.

[20] J. G. Andrews, F. Baccelli, and R. K. Ganti, "A tractable approach to coverage and rate in cellular networks," *IEEE Trans. on Commun.*, vol. 59, no. 11, pp. 3122–3134, Nov. 2011.

[21] H. S. Dhillon, R. K. Ganti, F. Baccelli, and J. G. Andrews, "Modeling and analysis of K-tier downlink heterogeneous cellular networks," *IEEE Journal on Sel. Areas in Commun.*, vol. 30, no. 3, pp. 550–560, Apr. 2012.

[22] H. S. Jo, Y. J. Sang, P. Xia, and J. G. Andrews, "Heterogeneous cellular networks with flexible cell association: A comprehensive downlink SINR analysis," *IEEE Trans. on Wireless Commun.*, vol. 11, no. 10, pp. 3484–3495, Oct. 2012.

[23] S. Mukherjee, *Analytical Modeling of Heterogeneous Cellular Networks*. Cambridge University Press, 2014.

[24] S. Singh, H. S. Dhillon, and J. G. Andrews, "Offloading in heterogeneous networks: Modeling, analysis, and design insights," *IEEE Trans. on Wireless Commun.*, vol. 12, no. 5, pp. 2484–2497, May. 2013.

[25] H. S. Dhillon, Y. Li, P. Nuggehalli, Z. Pi, and J. G. Andrews, "Fundamentals of heterogeneous cellular networks with energy harvesting," *IEEE Trans. on Wireless Commun.*, vol. 13, no. 5, pp. 2782–2797, May 2014.

[26] H. S. Dhillon, M. Kountouris, and J. G. Andrews, "Downlink MIMO HetNets: Modeling, ordering results and performance analysis," *IEEE Trans. on Wireless Commun.*, vol. 12, no. 10, pp. 5208–5222, Oct. 2013.

[27] Z. Gao, L. Dai, D. Mi, Z. Wang, M. A. Imran, and M. Z. Shakir, "MmWave massive-MIMO-based wireless backhaul for the 5G ultra-dense network," *IEEE Wireless Commun.*, vol. 22, no. 5, pp. 13–21, Oct. 2015.

[28] J. Schloemann, H. S. Dhillon, and R. M. Buehrer, "A tractable analysis of the improvement in unique localizability through collaboration," *IEEE Trans. on Wireless Commun.*, vol. 15, no. 6, pp. 3934–3948, Feb. 2016.

[29] J. G. Andrews, T. Bai, M. N. Kulkarni, A. Alkhateeb, A. K. Gupta, and R. W. Heath, "Modeling and analyzing millimeter wave cellular systems," *IEEE Trans. Commun.*, vol. 65, no. 1, pp. 403–430, Jan. 2017.

[30] H. ElSawy, E. Hossain, and M. Haenggi, "Stochastic geometry for modeling, analysis, and design of multi-tier and cognitive cellular wireless networks: A survey," *IEEE Commun. Surveys Tutorials*, vol. 15, no. 3, pp. 996–1019, 2013.

[31] H. ElSawy, A. Sultan-Salem, M. S. Alouini, and M. Z. Win, "Modeling and analysis of cellular networks using stochastic geometry: A tutorial," *IEEE Commun. Surveys and Tutorials*, vol. 19, no. 1, pp. 167–203, Firstquarter 2017.

[32] J. G. Andrews, A. K. Gupta, and H. S. Dhillon, "A primer on cellular network analysis using stochastic geometry," 2016, available online: arxiv.org/abs/1604.03183.

[33] H. Elsawy, E. Hossain, and M. Haenggi, "Stochastic geometry for modeling, analysis, and design of multi-tier and cognitive cellular wireless networks: A survey," *IEEE Commun. Surveys and Tutorials*, vol. 15, no. 3, pp. 996–1019, 3th quarter 2013.

[34] H. S. Dhillon, R. K. Ganti, and J. G. Andrews, "A tractable framework for coverage and outage in heterogeneous cellular networks," in *Proc., Info. Theory and Applications (ITA) Workshop*, Feb. 2011.

[35] S. Mukherjee, "Distribution of downlink SINR in heterogeneous cellular networks," *IEEE Journal on Sel. Areas in Commun.*, vol. 30, no. 3, pp. 575–585, Apr. 2012.

[36] P. Madhusudhanan, J. G. Restrepo, Y. Liu, and T. X. Brown, "Analysis of downlink connectivity models in a heterogeneous cellular network via stochastic geometry," *IEEE Trans. on Wireless Commun.*, vol. 15, no. 6, pp. 3895–3907, Jun. 2016.

[37] H. Dhillon, R. Ganti, and J. Andrews, "Load-aware modeling and analysis of heterogeneous cellular networks," *IEEE Trans. Wireless Commun.*, vol. 12, no. 4, pp. 1666–1677, Apr. 2013.

[38] W. C. Cheung, T. Quek, and M. Kountouris, "Throughput optimization, spectrum allocation, and access control in two-tier femtocell networks," *IEEE Journal on Sel. Areas Commun.*, vol. 30, no. 3, pp. 561–574, Apr. 2012.

[39] A. Jaziri, R. Nasri, and T. Chahed, "System level analysis of heterogeneous networks under imperfect traffic hotspot localization," *IEEE Trans. on Vehicular Technology*, vol. 65, no. 12, pp. 9862–9872, Dec. 2016.

[40] F. Boccardi, R. W. Heath, A. Lozano, T. L. Marzetta, and P. Popovski, "Five disruptive technology directions for 5G," *IEEE Commun. Magazine*, vol. 52, no. 2, pp. 74–80, Feb. 2014.

[41] M. Taranetz and M. Rupp, "Performance of femtocell access point deployments in user hot-spot scenarios," in *Proc., Telecommunication Networks and Applications Conference (ATNAC)*, Nov. 2012.

[42] Q. Ying, Z. Zhao, Y. Zhou, R. Li, X. Zhou, and H. Zhang, "Characterizing spatial patterns of base stations in cellular networks," in *IEEE Int. Conf. on Commun. in China (ICCC)*, Oct. 2014, pp. 490–495.

[43] C. Chen, R. C. Elliott, and W. A. Krzymien, "Downlink coverage analysis of *n*-tier heterogeneous cellular networks based on clustered stochastic geometry," in *Proc., IEEE Asilomar*, Nov. 2013, pp. 1577–1581.

[44] Y. Zhong and W. Zhang, "Multi-channel hybrid access femtocells: A stochastic geometric analysis," *IEEE Transa. Commun.*, vol. 61, no. 7, pp. 3016–3026, Jul. 2013.

[45] Y. J. Chun, M. O. Hasna, and A. Ghrayeb, "Modeling heterogeneous cellular networks interference using Poisson cluster processes," *IEEE Journal on Sel. Areas in Commun.*, vol. 33, no. 10, pp. 2182–2195, Oct. 2015.

[46] Qualcomm Incorporated, "A Comparison of LTE Advanced HetNets and Wi-Fi," Tech. Rep., Oct. 2011.

[47] D. Lee, S. Zhou, X. Zhong, Z. Niu, X. Zhou, and H. Zhang, "Spatial modeling of the traffic density in cellular networks," *IEEE Wireless Commun.*, vol. 21, no. 1, pp. 80–88, Feb. 2014.

[48] M. Mirahsan, R. Schoenen, and H. Yanikomeroglu, "HetHetNets: Heterogeneous traffic distribution in heterogeneous wireless cellular networks," *IEEE J. Sel. Areas Commun.*, vol. 33, no. 10, pp. 2252–2265, Oct. 2015.

[49] Z. Wang, R. Schoenen, H. Yanikomeroglu, and M. St-Hilaire, "The impact of user spatial heterogeneity in heterogeneous cellular networks," in *Proc., IEEE Globecom Workshops*, Dec. 2014, pp. 1278–1283.

[50] H. S. Dhillon, R. K. Ganti, and J. G. Andrews, "Modeling non-uniform UE distributions in downlink cellular networks," *IEEE Wireless Commun. Letters*, vol. 2, no. 3, pp. 339–342, Jun. 2013.

[51] C. Li, A. Yongacoglu, and C. D'Amours, "Mixed spatial traffic modeling of heterogeneous cellular networks," in *2015 IEEE Int. Conf. on Ubiquitous Wireless Broadband (ICUWB)*, Oct. 2015.

[52] M. Taranetz, T. Bai, R. Heath, and M. Rupp, "Analysis of small cell partitioning in urban two-tier heterogeneous cellular networks," in *Proc., Int. Symp. on Wireless Commun. Systems (ISWCS)*, Aug. 2014, pp. 739–743.

[53] M. Afshang, H. S. Dhillon, and P. H. J. Chong, "Fundamentals of cluster-centric content placement in cache-enabled device-to-device networks," *IEEE Trans. on Commun.*, vol. 64, no. 6, pp. 2511–2526, Jun. 2016.

[54] M. Haenggi, *Stochastic Geometry for Wireless Networks*. Cambridge University Press, 2012.

[55] P. Madhusudhanan, J. G. Restrepo, Y. Liu, T. X. Brown, and K. R. Baker, "Downlink performance analysis for a generalized shotgun cellular system," *IEEE Trans. on Wireless Commun.*, vol. 13, no. 12, pp. 6684–6696, Dec. 2014.

[56] M. Di Renzo, A. Guidotti, and G. Corazza, "Average rate of downlink heterogeneous cellular networks over generalized fading channels: A stochastic geometry approach," *IEEE Trans. Commun.*, vol. 61, no. 7, pp. 3050–3071, Jul. 2013.

[57] H. S. Dhillon and J. G. Andrews, "Downlink rate distribution in heterogeneous cellular networks under generalized cell selection," *IEEE Wireless Commun. Letters*, vol. 3, no. 1, pp. 42–45, Feb. 2014.

[58] H. P. Keeler, B. Blaszczyszyn, and M. K. Karray, "SINR-based k-coverage probability in cellular networks with arbitrary shadowing," in *Proc., IEEE International Symposium on Information Theory Proceedings (ISIT)*, Jul. 2013, pp. 1167–1171.

[59] M. Afshang, H. S. Dhillon, and P. H. J. Chong, "Modeling and performance analysis of clustered device-to-device networks," *IEEE Trans. on Wireless Commun.*, vol. 15, no. 7, pp. 4957–4972, Jul. 2016.

[60] C. Saha and H. S. Dhillon, "Downlink coverage probability of K-Tier HetNets with general non-uniform user distributions," in *Proc., IEEE Int. Conf. on Commun. (ICC)*, May 2016.

[61] P. D. Mankar, G. Das, and S. S. Pathak, "Modeling and coverage analysis of BS-centric clustered users in a random wireless network," *IEEE Wireless Commun. Lett.*, vol. 5, no. 2, pp. 208–211, Apr. 2016.

[62] D. Zwillinger, *Table of integrals, series, and products*. Elsevier, 2014.

[63] Y. Li, F. Baccelli, J. G. Andrews, T. D. Novlan, and J. C. Zhang, "Modeling and analyzing the coexistence of Wi-Fi and LTE in unlicensed spectrum," *IEEE Trans. on Wireless Commun.*, vol. 15, no. 9, pp. 6310–6326, Sep. 2016.

[64] A. Guo, Y. Zhong, W. Zhang, and M. Haenggi, "The Gauss-Poisson process for wireless networks and the benefits of cooperation," *IEEE Trans. on Commun.*, vol. 64, no. 5, pp. 1916–1929, May 2016.

[65] N. Deng, W. Zhou, and M. Haenggi, "The Ginibre point process as a model for wireless networks with repulsion," *IEEE Trans. on Wireless Commun.*, vol. 14, no. 1, pp. 107–121, Jan. 2015.

[66] Y. Li, F. Baccelli, H. S. Dhillon, and J. G. Andrews, "Statistical modeling and probabilistic analysis of cellular networks with determinantal point processes," *IEEE Trans. on Commun.*, vol. 63, no. 9, pp. 3405–3422, Sep. 2015.

[67] B. Blaszczyszyn, M. K. Karray, and H.-P. Keeler, "Using Poisson processes to model lattice cellular networks," in *Proc., IEEE INFOCOM*, Turin, Italy, Apr. 2013.

[68] Z. Yazdanshenasan, H. S. Dhillon, M. Afshang, and P. H. J. Chong, "Poisson hole process: Theory and applications to wireless networks," *IEEE Trans. on Wireless Commun.*, vol. 15, no. 11, pp. 7531–7546, Nov. 2016.

[69] N. Deng, W. Zhou, and M. Haenggi, "Heterogeneous cellular network models with dependence," *IEEE Journal on Sel. Areas in Commun.*, vol. 33, no. 10, pp. 2167–2181, Oct. 2015.

[70] P. Parida, H. Dhillon, and P. Nuggehalli, "Stochastic geometry-based modeling and analysis of citizens broadband radio service system," *IEEE Access*, vol. 5, pp. 7326–7349, 2017.

[71] C. Saha, M. Afshang, and H. S. Dhillon, "Enriched K-tier HetNet model to enable the analysis of user-centric small cell deployments," *IEEE Trans. on Wireless Commun.*, vol. 16, no. 3, pp. 1593–1608, Mar. 2017.

[72] M. Afshang and H. S. Dhillon, "Poisson cluster process based analysis of hetnets with correlated user and base station locations," *IEEE Trans. on Wireless Commun.*, vol. 17, no. 4, pp. 2417–2431, Apr. 2018.

[73] M. Afshang, C. Saha, and H. S. Dhillon, "Nearest-neighbor and contact distance distributions for Thomas cluster process," *IEEE Wireless Commun. Letters*, vol. 6, no. 1, pp. 130–133, Feb. 2017.

[74] ——, "Nearest-neighbor and contact distance distributions for Matern cluster process," *IEEE Commun. Letters*, vol. 21, no. 12, pp. 2686–2689, Dec. 2017.

[75] U. Schilcher, S. Toumpis, M. Haenggi, A. Crismani, G. Brandner, and C. Bettstetter, "Interference functionals in Poisson networks," *IEEE Trans. on Info. Theory*, vol. 62, no. 1, pp. 370–383, Jan, 2016.

[76] R. K. Ganti and M. Haenggi, "Interference and outage in clustered wireless ad hoc networks," *IEEE Trans. on Info. Theory*, vol. 55, no. 9, pp. 4067–4086, Sep. 2009.

[77] T. Mikosch, *Weak Convergence of Point Processes*. Berlin, Heidelberg: Springer Berlin Heidelberg, 2009, pp. 1–41.

[78] J. Zhu, S. Govindasamy, and J. Hwang, "Performance of Multiantenna linear MMSE receivers in doubly stochastic networks," *IEEE Trans. on Commun.*, vol. 62, no. 8, pp. 2825–2839, Aug. 2014.

[79] C. Saha, M. Afshang, and H. S. Dhillon, "3GPP-inspired HetNet model using Poisson cluster process: Sum-product functionals and downlink coverage," *IEEE Trans. on Commun.*, vol. 66, no. 5, pp. 2219–2234, May 2018.

[80] B. Blaszczyszyn, M. Haenggi, P. Keeler, and S. Mukherjee, *Stochastic geometry analysis of cellular networks*. Cambridge University Press, 2018.

[81] E. Turgut and M. C. Gursoy, "Downlink analysis in unmanned aerial vehicle (UAV) assisted cellular networks with clustered users," *IEEE Access*, vol. 6, pp. 36 313–36 324, May 2018.

[82] Y. Li, F. Baccelli, J. G. Andrews, T. D. Novlan, and J. C. Zhang, "Modeling and analyzing the coexistence of Wi-Fi and LTE in unlicensed spectrum," *IEEE Trans. on Wireless Commun.*, vol. 15, no. 9, pp. 6310–6326, 2016.

[83] D. B. Taylor, H. S. Dhillon, T. D. Novlan, and J. G. Andrews, "Pairwise interaction processes for modeling cellular network topology," in *Proc., IEEE Global Commun. Conf. (GLOBECOM)*, Dec. 2012, pp. 4524–4529.

[84] N. Miyoshi and T. Shirai, "A cellular network model with Ginibre configured base stations," *Advances in Applied Probability*, vol. 46, no. 3, pp. 832–845, 2014.

[85] I. Nakata and N. Miyoshi, "Spatial stochastic models for analysis of heterogeneous cellular networks with repulsively deployed base stations," *Performance Evaluation*, vol. 78, pp. 7–17, 2014.

[86] C. Saha, M. Afshang, and H. S. Dhillon, "Poisson cluster process: Bridging the gap between PPP and 3GPP HetNet models," in *Proc., Information Theory and Applications (ITA)*, 2017.

[87] V. Suryaprakash, J.Møller, and G. Fettweis, "On the modeling and analysis of heterogeneous radio access networks using a Poisson cluster process," *IEEE Trans. on Wireless Commun.*, vol. 14, no. 2, pp. 1035–1047, Feb. 2015.

[88] W. Bao and B. Liang, "Handoff rate analysis in heterogeneous wireless networks with Poisson and Poisson cluster patterns," in *Proc. 16th ACM International Symposium on Mobile Ad Hoc Networking and Computing*, ser. MobiHoc '15. New York, NY, USA: ACM, 2015, pp. 77–86.

[89] S. M. Azimi-Abarghouyi, B. Makki, M. Haenggi, M. Nasiri-Kenari, and T. Svensson, "Stochastic geometry modeling and analysis of single- and multi-cluster wireless networks," *IEEE Trans. on Commun.*, vol. 66, no. 10, pp. 4981–4996, Oct. 2018.

[90] N. Miyoshi, "Downlink coverage probability in cellular networks with Poisson-Poisson cluster deployed base stations," *IEEE Wireless Commun. Letters*, vol. 8, no. 1, pp. 5–8, Feb. 2019.

[91] C. Saha and H. S. Dhillon, "Matlab code for the computation of coverage probability in the unified HetNet model with PPP and PCP," 2019, available at: github.com/stochastic-geometry/PCP-HetNet-Max-Power-Association.

[92] M. Afshang, C. Saha, and H. S. Dhillon, "Equi-coverage contours in cellular networks," *IEEE Wireless Commun. Letters*, vol. 7, no. 5, pp. 700–703, Oct. 2018.

[93] C. Saha, H. S. Dhillon, N. Miyoshi, and J. G. Andrews, "Unified analysis of HetNets using Poisson cluster processes under max-power association," *IEEE Trans. on Wireless Commun.*, vol. 18, no. 8, pp. 3797–3812, Aug. 2019.

[94] M. Haenggi, "The Meta distribution of the SIR in Poisson bipolar and cellular networks," *IEEE Trans. on Wireless Commun.*, vol. 15, no. 4, pp. 2577–2589, Apr. 2016.

[95] Y. Wang, M. Haenggi, and Z. Tan, "SIR meta distribution of k-tier downlink heterogeneous cellular networks with cell range expansion," *IEEE Trans. on Commun.*, vol. 67, no. 4, pp. 3069–3081, Apr. 2018.

[96] N. Deng and M. Haenggi, "SINR and rate meta distributions for HCNs with joint spectrum allocation and offloading," *IEEE Trans. on Commun,*, vol. 67, no. 5, pp. 3709–3722, May 2019.

[97] J. Gil-Pelaez, "Note on the inversion theorem," *Biometrika*, vol. 38, no. 3-4, pp. 481–482, 1951.

[98] Y. Wang, M. Haenggi, and Z. Tan, "The meta distribution of the SIR for cellular networks with power control," *IEEE Trans. on Commun.*, vol. 66, no. 4, pp. 1745–1757, Apr. 2018.

[99] G. George, A. Lozano, and M. Haenggi, "Distribution of the number of users per base station in cellular networks," *IEEE Wireless Commun. Letters*, vol. 8, no. 2, pp. 520–523, 2018.

[100] V. V. Chetlur and H. S. Dhillon, "Coverage and rate analysis of downlink cellular vehicle-to-everything (C-V2X) communication," *IEEE Trans. on Wireless Commun.*, 2019, to appear.

[101] P. D. Mankar, P. Parida, H. S. Dhillon, and M. Haenggi, "Distance from the nucleus to a uniformly random point in the 0-cell and the typical cell of the Poisson-Voronoi tessellation," 2019, available online: arXiv/abs/1907.03635.

[102] J.-S. Ferenc and Z. Néda, "On the size distribution of Poisson Voronoi cells," *Physica A: Statistical Mechanics and its Applications*, vol. 385, no. 2, pp. 518–526, 2007.

[103] J. Cavers, "On the fast fourier transform inversion of probability generating functions," *IMA Journal of Applied Mathematics*, vol. 22, no. 3, pp. 275–282, 1978.

[104] P. D. Mankar, P. Parida, H. S. Dhillon, and M. Haenggi, "Downlink analysis for the typical cell in Poisson cellular networks," *IEEE Wireless Commun. Letters*, 2019, to appear.

[105] C. Dehos, J. L. González, A. De Domenico, D. Ktenas, and L. Dussopt, "Millimeter-wave access and backhauling: the solution to the exponential data traffic increase in 5G mobile communications systems?" *IEEE Commun. Magazine*, vol. 52, no. 9, pp. 88–95, 2014.

[106] T. Q. S. Quek, G. de la Roche, I. Gven, and M. Kountouris, *Small Cell Networks: Deployment, PHY Techniques, and Resource Management*. New York, NY, USA: Cambridge University Press, 2013.

[107] O. Tipmongkolsilp, S. Zaghloul, and A. Jukan, "The evolution of cellular backhaul technologies: Current issues and future trends," *IEEE Commun. Surveys Tuts.*, vol. 13, no. 1, pp. 97–113, 2011.

[108] H. S. Dhillon and G. Caire, "Wireless backhaul networks: Capacity bound, scalability analysis and design guidelines," *IEEE Trans. on Wireless Commun.*, vol. 14, no. 11, pp. 6043–6056, Nov. 2015.

[109] S. Rangan, T. S. Rappaport, and E. Erkip, "Millimeter-wave cellular wireless networks: Potentials and challenges," *Proc. IEEE*, vol. 102, no. 3, pp. 366–385, Mar. 2014.

[110] A. Ghosh, T. A. Thomas, M. C. Cudak, R. Ratasuk, P. Moorut, F. W. Vook, T. S. Rappaport, G. R. MacCartney, S. Sun, and S. Nie, "Millimeter-wave enhanced local area systems: A high-data-rate approach for future wireless networks," *IEEE Journal on Sel. Areas Commun.*, vol. 32, no. 6, pp. 1152–1163, Jun. 2014.

[111] E. Dahlman, G. Mildh, S. Parkvall, J. Peisa, J. Sachs, Y. Selén, and J. Sköld, "5G wireless access: requirements and realization," *IEEE Commun. Magazine*, vol. 52, no. 12, pp. 42–47, Dec. 2014.

[112] 3GPP TR 38.874, "NR; Study on integrated access and backhaul," Tech. Rep., 2017.

[113] M. D. Renzo, "Stochastic geometry modeling and analysis of multi-tier millimeter wave cellular networks," *IEEE Trans. on Wireless Commun.*, vol. 14, no. 9, pp. 5038–5057, Sep. 2015.

[114] T. Bai, R. Vaze, and R. W. Heath, "Analysis of blockage effects on urban cellular networks," *IEEE Trans. on Wireless Commun.*, vol. 13, no. 9, pp. 5070–5083, Sep. 2014.

[115] E. Turgut and M. C. Gursoy, "Coverage in heterogeneous downlink millimeter wave cellular networks," *IEEE Trans. on Commun.*, vol. 65, no. 10, pp. 4463–4477, Oct. 2017.

[116] S. Singh, M. N. Kulkarni, and J. G. Andrews, "A tractable model for rate in noise limited mmwave cellular networks," in *Proc. IEEE Asilomar*, Nov. 2014, pp. 1911–1915.

[117] Y. Li, F. Baccelli, J. G. Andrews, and J. C. Zhang, "Directional cell search delay analysis for cellular networks with static users," *IEEE Trans. on Commun.*, vol. 66, no. 9, pp. 4318–4332, 2018.

[118] A. Alkhateeb, Y. H. Nam, M. S. Rahman, J. Zhang, and R. W. Heath, "Initial beam association in millimeter wave cellular systems: Analysis and design insights," *IEEE Trans. Wireless Commun.*, vol. 16, no. 5, pp. 2807–2821, May 2017.

[119] H. Elshaer, M. N. Kulkarni, F. Boccardi, J. G. Andrews, and M. Dohler, "Downlink and uplink cell association with traditional macrocells and millimeter wave small cells," *IEEE Trans. on Wireless Commun.*, vol. 15, no. 9, pp. 6244–6258, Sep. 2016.

[120] H. Raza, "A brief survey of radio access network backhaul evolution: part I," *IEEE Commun. Magazine*, vol. 49, no. 6, pp. 164–171, Jun. 2011.

[121] 3GPP TR 36.116, "Evolved universal terrestrial radio access (E-UTRA); Relay radio transmission and reception," Tech. Rep., Mar. 2017.

[122] 3GPP TR 36.117, "Evolved universal terrestrial radio access (E-UTRA); Relay conformance testing," Tech. Rep., Mar. 2017.

[123] N. Johansson, J. Lundsjö, G. Mildh, A. Ràcz, and C. Hoymann, "Self-backhauling in LTE," U.S. Patent 8 797 952, Aug. 5, 2014.

[124] MiWaveS White Paper, "Heterogeneous wireless network with millimetre wave small cell access and backhauling," Tech. Rep., Jan. 2016.

[125] A. D. La Oliva, X. C. Perez, A. Azcorra, A. D. Giglio, F. Cavaliere, D. Tiegelbekkers, J. Lessmann, T. Haustein, A. Mourad, and P. Iovanna, "Xhaul: toward an integrated fronthaul/backhaul architecture in 5G networks," *IEEE Wireless Commun.*, vol. 22, no. 5, pp. 32–40, Oct. 2015.

[126] G. Zhang, T. Q. S. Quek, M. Kountouris, A. Huang, and H. Shan, "Fundamentals of heterogeneous backhaul design–Analysis and optimization," *IEEE Trans. on Commun.*, vol. 64, no. 2, pp. 876–889, Feb. 2016.

[127] V. Suryaprakash and G. P. Fettweis, "An analysis of backhaul costs of radio access networks using stochastic geometry," in *Proc. IEEE Int. Conf. Commun. (ICC)*, Jun. 2014, pp. 1035–1041.

[128] S. Singh and J. G. Andrews, "Joint resource partitioning and offloading in heterogeneous cellular networks," *IEEE Trans. on Wireless Commun.*, vol. 13, no. 2, pp. 888–901, Feb. 2014.

[129] S. Singh, M. N. Kulkarni, A. Ghosh, and J. G. Andrews, "Tractable model for rate in self-backhauled millimeter wave cellular networks," *IEEE Journal on Sel. Areas in Commun.*, vol. 33, no. 10, pp. 2196–2211, Oct. 2015.

[130] A. Sharma, R. K. Ganti, and J. K. Milleth, "Joint backhaul-access analysis of full duplex self-backhauling heterogeneous networks," *IEEE Trans. on Wireless Commun.*, vol. 16, no. 3, pp. 1727–1740, Mar. 2017.

[131] H. Tabassum, A. H. Sakr, and E. Hossain, "Analysis of massive MIMO-enabled downlink wireless backhauling for full-duplex small cells," *IEEE Trans. on Commun.*, vol. 64, no. 6, pp. 2354–2369, Jun. 2016.

[132] J. Qin, *Examples and Basic Theories for Length Biased Sampling Problems*. Springer Singapore, 2017, pp. 1–9.

[133] J. Thompson, X. Ge, H.-C. Wu, R. Irmer, H. Jiang, G. Fettweis, and S. Alamouti, "5G wireless communication systems: Prospects and challenges," *IEEE Commun. Mag*, vol. 52, no. 2, pp. 62–64, 2014.

[134] C. Saha, M. Afshang, and H. S. Dhillon, "Bandwidth partitioning and downlink analysis in millimeter wave integrated access and backhaul for 5G," *IEEE Trans. on Wireless Commun.*, vol. 17, no. 12, pp. 8195–8210, Dec. 2018.

[135] M. Polese, M. Giordani, A. Roy, D. Castor, and M. Zorzi, "Distributed path selection strategies for integrated access and backhaul at mmWaves," 2018, available online: arxiv.org/abs/1805.04351.

[136] M. N. Kulkarni, A. Ghosh, and J. G. Andrews, "Max-min rates in self-backhauled millimeter wave cellular networks," 2018, available online: arxiv.org/abs/1805.01040.

[137] J. Garcia-Rois, R. Banirazi, F. J. Gonzalez-Castano, B. Lorenzo, and J. C. Burguillo, "Delay-aware optimization framework for proportional flow delay differentiation in millimeter-wave backhaul cellular networks," *IEEE Trans. on Commun.*, vol. 66, no. 5, pp. 2037–2051, May 2018.

[138] M. Polese, M. Giordani, A. Roy, S. Goyal, D. Castor, and M. Zorzi, "End-to-end simulation of integrated access and backhaul at mmWaves," in *2018 IEEE 23rd International Workshop on Computer Aided Modeling and Design of Communication Links and Networks (CAMAD)*, Sep. 2018, pp. 1–7.

[139] A. Mesodiakaki, F. Adelantado, L. Alonso, M. D. Renzo, and C. Verikoukis, "Energy- and spectrum-efficient user association in millimeter-wave backhaul small-cell networks," *IEEE Trans. on Vehicular Technology*, vol. 66, no. 2, pp. 1810–1821, Feb. 2017.

[140] M. D. Renzo and P. Guan, "Stochastic geometry modeling and system-level analysis of uplink heterogeneous cellular networks with multi-antenna base stations," *IEEE Trans. on Commun.*, vol. 64, no. 6, pp. 2453–2476, Jun. 2016.

[141] S. Singh, F. Baccelli, and J. G. Andrews, "On association cells in random heterogeneous networks," *IEEE Wireless Commun. Lett.*, vol. 3, no. 1, pp. 70–73, Feb. 2014.

[142] F. J. Martin-Vega, M. D. Renzo, M. C. Aguayo-Torres, G. Gomez, and T. Q. Duong, "Stochastic geometry modeling and analysis of backhaul-constrained hyper-dense heterogeneous cellular networks," in *17th International Conference on Transparent Optical Networks (ICTON)*, Jul. 2015, pp. 1–4.

[143] 3GPP TR 38.901, "Study on channel model for frequencies from 0.5 to 100 GHz," Tech. Rep., 2017.

[144] S. Aditya, H. S. Dhillon, A. F. Molisch, and H. Behairy, "Asymptotic blind-spot analysis of localization networks under correlated blocking using a Poisson line process," *IEEE Wireless Commun. Letters*, vol. 6, no. 5, pp. 654–657, Oct. 2017.

[145] S. Aditya, H. S. Dhillon, A. F. Molisch, and H. M. Behairy, "A tractable analysis of the blind spot probability in localization networks under correlated blocking," *IEEE Trans. on Wireless Commun.*, vol. 17, no. 12, pp. 8150–8164, Dec. 2018.

[146] C. Saha and H. S. Dhillon, "Matlab code for the computation of association probability in 5G mm-wave HetNet with integrated access and backhaul," 2019, available at: github.com/stochastic-geometry/Load-balancing-5G-mmwave.

[147] S. Krishnan and H. S. Dhillon, "Spatio-temporal interference correlation and joint coverage in cellular networks," *IEEE Trans. on Wireless Commun.*, vol. 16, no. 9, pp. 5659–5672, Sep. 2017.

[148] O. Simeone, "A very brief introduction to machine learning with applications to communication systems," *IEEE Trans. on Cognitive Commun. and Networking*, vol. 4, no. 4, pp. 648–664, Dec. 2018.

[149] A. Nenkova, L. Vanderwende, and K. McKeown, "A compositional context sensitive multi-document summarizer: exploring the factors that influence summarization," in *Proc. SIGIR*. ACM, 2006, pp. 573–580.

[150] A. Kulesza, B. Taskar *et al.*, "Determinantal point processes for machine learning," *Foundations and Trends in Machine Learning*, vol. 5, no. 2–3, pp. 123–286, 2012.

[151] A. Krause, A. Singh, and C. Guestrin, "Near-optimal sensor placements in Gaussian processes: Theory, efficient algorithms and empirical studies," *Journal of Machine Learning Research*, vol. 9, no. Feb, pp. 235–284, 2008.

[152] B. Blaszczyszyn and P. Keeler, "Determinantal thinning of point processes with network learning applications," 2018, available online: arXiv/abs/1810.08672.

[153] P. C. Weeraddana, M. Codreanu, M. Latva-aho, A. Ephremides, C. Fischione *et al.*, "Weighted sum-rate maximization in wireless networks: A review," *Foundations and Trends in Networking*, vol. 6, no. 1–2, pp. 1–163, 2012.

[154] J. Gillenwater, A. Kulesza, and B. Taskar, "Near-optimal MAP inference for determinantal point processes," in *Advances in Neural Information Processing Systems 25*. Curran Associates, Inc., 2012, pp. 2735–2743.

[155] S. Boyd, S.-J. Kim, L. Vandenberghe, and A. Hassibi, "A tutorial on geometric programming," *Optimization and Engineering*, vol. 8, no. 1, p. 67, Apr 2007.

[156] C. Saha and H. S. Dhillon, "Matlab code for determinantal point process learning," 2019, available at: github.com/stochastic-geometry/DPPL.

[157] F. Lavancier, J. Møller, and E. Rubak, "Determinantal point process models and statistical inference," *Journal of the Royal Statistical Society: Series B (Statistical Methodology)*, vol. 77, no. 4, pp. 853–877, 2015.

[158] E. Turgut and M. C. Gursoy, "Uplink performance analysis in d2d-enabled millimeter-wave cellular networks with clustered users," *IEEE Trans. on Wireless Commun.*, vol. 18, no. 2, pp. 1085–1100, Jan. 2019.

[159] A. M. A., K. M. A., and D. H. S., "Joint energy and `sinr` coverage in spatially clustered rf-powered IoT network," *IEEE Trans. on Green Commun. and Networking*, vol. 3, no. 1, pp. 132–146, Oct. 2019.

[160] G. B., K. H., and D. L. A., "A stochastic model for UAV networks positioned above demand hotspots in urban environments," *IEEE Trans. on Vehicular Tech.*, vol. 68, no. 7, pp. 6985–6996, 2019.

[161] E. Turgut and M. C. Gursoy, "Downlink analysis in unmanned aerial vehicle (UAV) assisted cellular networks with clustered users," *IEEE Access*, vol. 6, pp. 36 313–36 324, May 2018.

[162] F. Baccelli, B. Blaszczyszyn, and M. Karray, *Random Measures, Point Processes, and Stochastic Geometry*, Jan. 2020.

[163] P. Xie, R. Salakhutdinov, L. Mou, and E. P. Xing, "Deep determinantal point process for large-scale multi-label classification," in *Proc. IEEE Int. Conf. on Computer Vision (CVPR)*, 2017, pp. 473–482.